VISUAL STRESS AND READING IN SPECIAL POPULATIONS; UNDERSTANDING THE UNDERPINNINGS OF CORTICAL HYPEREXCITABILITY

by

AUSTYN JOSEPH TEMPESTA

A thesis submitted to the University of Birmingham for the degree of

DOCTOR OF PHILOSOPHY

School of Psychology

College of Life and Environmental Sciences

University of Birmingham

December 2020

UNIVERSITY OF BIRMINGHAM

University of Birmingham Research Archive
e-theses repository

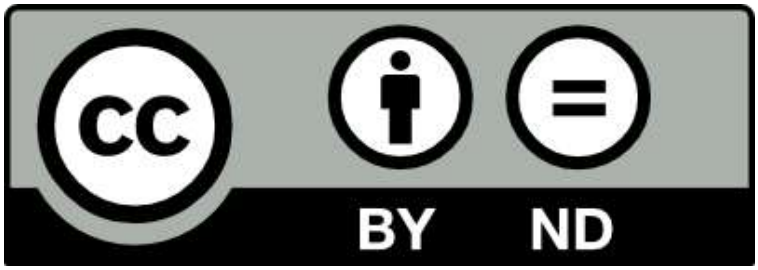

This unpublished thesis/dissertation is under a Creative Commons Attribution- NoDerivatives 4.0 International (CC BY-ND 4.0) licence.

You are free to:

Share — copy and redistribute the material in any medium or format for any purpose, even commercially.

The licensor cannot revoke these freedoms as long as you follow the license terms.

Under the following terms:

Attribution — You must give appropriate credit, provide a link to the license, and indicate if changes were made. You may do so in any reasonable manner, but not in any way that suggests the licensor endorses you or your use.

NoDerivatives — If you remix, transform, or build upon the material, you may not distribute the modified material.

No additional restrictions — You may not apply legal terms or technological measures that legally restrict others from doing anything the license permits.

Notices:

You do not have to comply with the license for elements of the material in the public domain or where your use is permitted by an applicable exception or limitation.

No warranties are given. The license may not give you all of the permissions necessary for your intended use. For example, other rights such as publicity, privacy, or moral rights may limit how you use the material.

Unless otherwise stated, any material in this thesis/dissertation that is cited to a third party source is not included in the terms of this licence. Please refer to the original source(s) for licencing conditions of any quotes, images or other material cited to a third party.

ABSTRACT

It has been shown that migraines can be triggered by Pattern-Glare stimuli. The epidemic of migraine in the UK, and indeed, the world, is significant. Migraine is the third most common disease in the world. The overarching theme of the PhD thesis is how Pattern-Glare gives rise to behavioural symptoms of Visual Stress and associated electrophysiological correlates in the occipital lobe. This thesis explores this by investigating abnormal (scalp-recorded) EEG responses to clinically relevant pattern-glare gratings (.37, 3, and 12 c/deg, where 3 c/deg is known to be visually aggravating) by undertaking three separate analyses on the same EEG data set. Additionally, we split the data apart between the first presentations of a particular stimulus and its further repetitions, enabling us to explore and distinguish surprise and habituation effects. In Chapter 2, we looked at evoked responses in the time domain, whilst in Chapters 3 and 4, we looked at evoked/induced responses in the frequency domain.

Additionally, Chapter 2 and Chapter 3 investigated questionnaires that were used to assess participants' headache history (Headache and General Health Questionnaire, HGHQ) and tendency to suffer visual stress (Cortical Hyper-Excitability index (Chi); Visual Discomfort Scale (VDS)). We regressed our EEG data onto these state and trait measures of condition susceptibility, enabling us to identify electrophysiological correlates of these measures. Chapters 2 and 3 found EEG effects that were significant on the headache and discomfort factors, whilst Chapter 4 found significant effects in the theta band. This thesis provides supporting evidence that visual stress (and by extension, migraine, and perhaps epilepsy) is driven by a failure to habituate, with this failure observable in the time-domain (missing N1) and the frequency domain (theta and gamma effects). These findings add to the body of existing knowledge and ultimately may contribute to the further development of clinical interventions in this area.

ACKNOWLEDGEMENTS

I want to extend my deepest gratitude foremost to my supervisors, Howard Bowman and Andrew Schofield, without whose help I would not have been able to finish my PhD Thesis. When I first joined the PhD, I was not as confident in my abilities as I would have hoped, being a first-generation university student with a learning disability in reading and writing. I had significant challenges to overcome to be successful. Howard and Andrew showed great dedication to my growth as a scholar and my abilities as a researcher and gave me the support I needed to succeed in my endeavours.

Additionally, I want to personally express my thanks to Claire Miller, who was there every step of the way for guidance whenever I got caught up with coding or writing, or needed general emotional support.

Furthermore, when I entered the PhD, I had never done programming in my entire life. I'm incredibly indebted to Sara Assecondi and Vladimir Litvak. Sara mainly supported me in learning to program and getting through my initial hardships at the beginning of the PhD. Vladimir was extremely helpful in getting me up to speed with SPM difficulties and some MATLAB details that were initially lost on me.

I want to also thank Jay Brophy, who was my undergraduate supervisor, who I now consider a friend. He has supported me ever since I was an undergraduate and is the reason I did a PhD in the first place. I never thought I would be able to do a PhD until I had his support. Additionally, I want to thank him for taking my calls in America and helping me not give up on myself at times when I was facing extreme hardship with my work.

I also want to thank Ann-Marie McNicholas, who was my disability support tutor. Thank you for spending so much time with me, helping me succeed and being a supporter of my work, even when I wanted to give up.

Apart from Andrew Schofield's dedication as a supervisor, he also went above and beyond with my coding training. In particular, he wrote a book for me and his students about Matlab coding, that was incredibly well-written and helpful. Finally, I am incredibly grateful for Howard Bowman’s tireless work with me; we had many late nights working through the research together and grappling with ideas and figures. At times it may have been heated, but in the end I think I’m better for it. He was an outstanding supporter of my work, and I think he took the time to understand my shortcomings and help me succeed.

TABLE OF CONTENTS

List of Figures

List of Tables

CHAPTER 1: INTRODUCTION

Imagine a clear day, and you decide that you want to take a trip to the shopping centre. As you are walking, you see a department store that you really like. You take a trip into the store and begin to feel nauseous. You remember that you have been here before and also felt nauseous then. This may be linked to different types of patterns or shapes that we see in everyday life. The brain is not really set up to contend with the modern world in the way that we intuitively think. Figure 1 (Rees et al., 2020, unpublished; Monger et al., 2016) shows typical scenes we would see every day; the left image is a natural scene that has a broad Fourier power spectrum however, the image on the right is an unnatural image that we see in everyday life and contains a spatial frequency close to that to which the visual system is most sensitive. Images such as this can be particularly aggravating for a minority of people that experience visual illusions of colour, shape and motion (Wilkins et al., 1984). Some even report migraines and, in severe cases, epilepsy. These symptoms of perception are sometimes called visual stress, which is caused by sensitivity to pattern-glare (PG) (Monger et al., 2015).

Figure 1-1 Natural Scene and Unnatural Scene.

Shown left is the natural environment and right is a man-made environment that may cause pattern glare issues resulting in visual stress symptoms (taken from Rees, 2020, unpublished; Monger et al., 2016).

1.1 An introduction to the problem

It has been shown that migraines can be triggered by PG. The epidemic of migraine in the UK, and indeed, the world, is significant. Migraine is the third most common disease in the world (Steiner et al., 2013). Severe migraines are considered by the World Health Organization (WHO) (2016) as the leading cause of disability among all neurological disorders, affecting 1 in 7 people (House of Commons, 2010), consisting of 3000 attacks each day in the UK alone with an estimated 190,000 episodes occurring annually (Steiner et al., 2003). Missed work from migraines is estimated to cause £250 million in lost revenue in the UK each year (Clarke et al., 1996). Migraine is also the least funded of all neurological illnesses in the world (House of Commons, 2014; Shapiro & Goadsby, 2007).

This issue has been investigated using fMRI (Huang et al., 2011), MEG and EEG (Adjamian et al., 2004). Of interest to this PhD thesis are biomarkers that may be specific to visual stress symptoms, occurring on the posterior of the scalp, as revealed through EEG methodologies, which are measurable indicators of a biological state or condition (Atkinson et al., 2001). This will help the field to better understand the neurological underpinnings of visual stress (VS) arising from PG, as well as providing an objective means to diagnose and stratify patients. VS has been argued to contribute to migraine and also to reading difficulties (such as the speed of reading) in children and adults with abnormal responses to PG (Irlen, 1991; Cornelissen et al., 1994). This is important to understand in order to inform treatment-based clinical work. There are many explanations for what might cause migraine and other adverse symptoms, which are covered more in detail below. For example, VS (as a potential trigger for migraine) may be caused by cortical hyperexcitability (Welch et al., 1990). This theory

proposes spontaneous depolarisation, followed by a spreading suppression of neuronal function (cortical spreading depression, CSD). Another explanation may be habituation, suggesting that those with migraines fail to habituate to repeated stimulation with the same stimulus (Schoenen et al., 1995; Afra et al., 1998; Wang et al., 1999). Few studies have recorded brain activation in response to pattern glare stimuli. Huang et al. (2003) applied such stimuli to a visual stress population showing increased fMRI activity in the occipital cortex, consistent with the cortical hyperexcitability theory in migraine. To our knowledge, only Haigh et al. (2019) and Fong et al. (2020) have previously measured event-related potentials (ERPs) in a headache prone population using the PG stimuli. Fong et al. (2020) found differences between migraine sufferers and controls at around 200ms and 400ms post-stimulus onset. The migraine group showed significantly greater negativity at 200ms for high-frequency gratings (13 c/deg). Note that 13 c/deg stimuli are not thought to induce PG symptoms via neural factors, so this effect is not the same as the classic pattern-glare response.

Overall, this thesis explores abnormal (scalp-recorded) EEG responses to clinically relevant pattern-glare gratings by undertaking three separate analyses on the same EEG data set. Each analysis investigates different domains in an effort to understand the underlying neurophysiological processes.

1.2 Empirical Chapters

Analysis one (Chapter 2) is concerned with responses to PG in the time domain, primarily looking at ERPs, which are time-locked to the onset of the stimulus (Luck, 2005), while analyses two (Chapter 3) and three (Chapter 4) relate to the frequency domain. Analyses one and two fit parametric regressors, which are extracted from a factor analysis of self-reported state and trait characteristics, e.g. sense of discomfort and headache susceptibility. The factors were 1) visual stress (a combination of the CHi, VDS, aura measures and Cortical Hyper-Excitability index (Chi), Braithwaite et al., 2015; Visual Discomfort Scale (VDS), Conlon et al., 1999), 2) headache (frequency, intensity and duration) and 3)

discomfort. Both analyses one and two utilise the same short time window following stimulus presentation. Analysis three extends the window in time to include a D/C shift period (i.e. a sustained change in the baseline response) in the frequency domain but does not analyse parametric regressors. Importantly, the frequency domain allows the researcher to see induced responses, which are increases in amplitude without a resetting of the phase of ongoing oscillations (Adjamian, 2014). ERPs are blind to such effects. Further discussion on the literature that informs this thesis is outlined below.

1.3 Visual Perception

Human visual perception operates in dynamic networks to understand and represent the environment. The cells in these networks work together through mechanisms of excitation and inhibition to process exogenous stimuli. It does this in multiple ways, such as ascending feedforward projections, descending feedback projections, and lateral connections within layers (Kafaligonul et al., 2015; Lamme et al., 1998). The role of feedforward connections is relatively well understood: each layer of processing identifies features in the image and passes that information onto the next layer: progressive layers detect ever more complex feature combinations. Lateral connections are thought to modify neuronal responses according to the context in which stimuli are placed and are of two forms: short-range connections are inhibitory and have a role in both gain-control (limiting local responsiveness) and fine-tuning the receptive field properties of each cell. These connections most likely lead to inhibitory after-effects, such as the tilt-after effect (Clifford et al., 2000). Longer-range lateral connections are excitatory and may have a role in promoting the activities of cells tuned to similar image properties at different spatial locations (Field et al., 1993). Feedback connections between processing layers and brain regions are less well understood. Some appear excitatory, inducing responses to imagined stimuli or helping the brain to resolve sensory ambiguity; others seem to have an inhibitory effect, perhaps controlling attention by

attenuating the sensory input (Lamme et al., 1998). Regardless of this pattern, feed-forward and feed-back connections create a dynamical, recurrent network of cells whose activity is held in delicate balance by excitatory and inhibitory processes. Additionally, researchers observed lower performance for migraine groups versus controls on orientation discrimination tasks (Tibber et al., 2006) and contrast sensitivity tasks (Shepherd et al., 2012).

One tenet of sensory processing is that activity in a given neuron increases the likelihood of activity in other neurons with which it has excitatory connections. For the feed-forward path in the sensory systems, the resultant chain of activity is likely to result in the organism perceiving the stimulus feature that is usually detected by the neuron(s) at the start of the chain. Even when there is no physical stimulus present, this outcome can be adaptive, as contours and surfaces that are present in the world but absent in the retinal image are nonetheless reconstructed in the cortical representation and thus perceived (modal and amodal completion; Nakayama & Shimojo, 1995). However, in other circumstances, such activity is unwanted and results in positive, illusory perceptions or hallucinations. For example, Isia Leviant's (1981; 1996) Enigma image (Figure 1.2) contains only static radial stripes and purple disks but is widely reported to induce a sensation of motion within the rings in most but not all people.

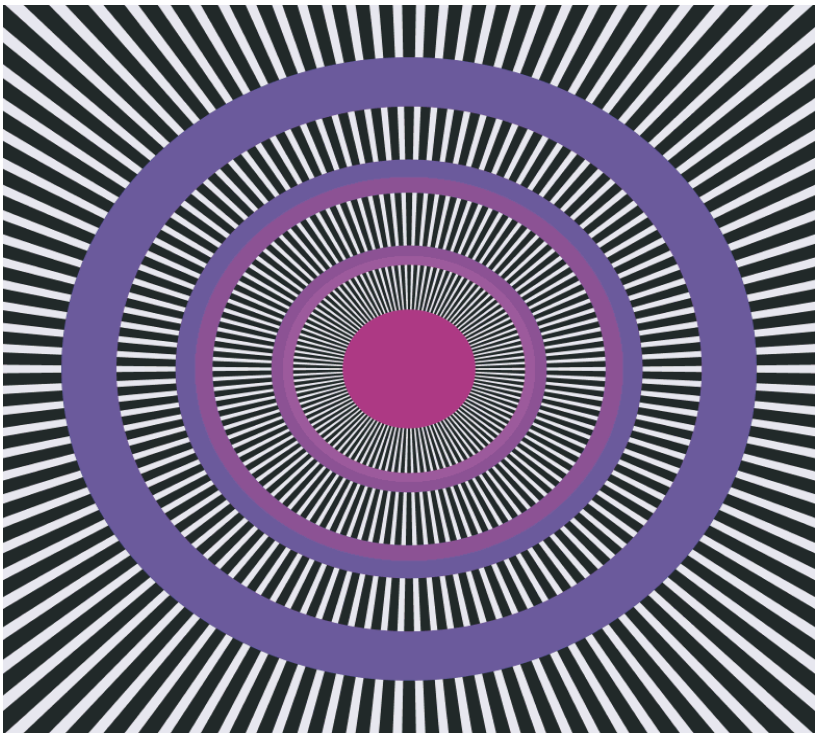

Figure 1-2 Enigma by Isia Leviant (1981; 1996).

This stimulus has been shown to elicit activity in the motion-sensitive area MT/V5 (Zeki,1993); despite the absence of motion in the stimulus, this may be caused by micro-saccadic eye movements (Zanker & Walker, 2004) being miss-interpreted as object motion. The fact that motion is perceived in the rings (where there are no features whose displacement by such eye movements could be interpreted as motion) suggests that the neural activity spreads out of the inducing striped areas into the rings. Excess inhibition can result in illusions, such as in the many after-effect illusions (for example, the motion-after effect, Kohn & Movshon, 2003), where lingering inhibition, most likely mediated by lateral connections, biases the perception of the opposite stimulus from a previously viewed stimulus (e.g., viewing motion to the left produces the sensation of rightward motion in a subsequently static stimulus). There is additional evidence for greater susceptibility in migraine groups for multisensory illusions in sound-induced flash illusions (Yang et al., 2014). This

is important because the sound-induced flash illusion is thought to be determined by the integration of visual and auditory signals.

1.3.1 Visual Stress

VS forms the foundation and experimental basis of this thesis. VS is a variety of abnormal responses to specific visual stimuli when the visual cortex is exposed to certain types of patterns of light and dark stripes (Wilkins, 1995). These abnormal responses are characterised by illusions of colour, shape, and motion. In some cases, people experience migraines and, more severely epileptic attacks (Wilkins et al., 1979,1980). Using magnetoencephalography (MEG), Adjamian et al. (2004) have shown that gamma oscillations underlie hyperexcitability in area V1 peaking for stimuli with 3 cycles per spatial degree (c/deg). They hypothesise that such visual stress is caused by hyper-excitability of the visual cortex, which results in an increase in a spreading activity among neurons usually associated with sensory input, thus producing hallucinations. The somatic effect sometimes found in visual stress may be due to activity spreading outside of the visual cortex. In some cases, these effects may not be appropriately regulated by GABAergic inhibitory mechanisms. Visual symptoms might thus be the precursor to a photo-paroxysmal response. This, if not sufficiently controlled by inhibitory mechanisms, may lead to epileptic seizures and migraines. However, the mechanism underlying this activation has not been explored; this Ph.D thesis will examine this missing component in the literature.

The stimuli that are most likely to induce such anomalies, typically 3 c/deg high-contrast stripes, are precisely those most likely to induce attacks of migraine and epilepsy in those with a visual trigger (Wilkins, 1986, 1995; Wilkins et al., 1979, 1980). Most importantly, a minority report seeing such visual distortions when viewing printed text (Meares-Irlen syndrome or VS; Mears, 1980). While such distortions could be due to poor ocular accommodation and binocular convergence, they are found even when such abnormalities are excluded (Evans et al., 1995).

The fact that a minority sees such distortions in the text suggests that some populations are more prone to VS than others. Indeed, some evidence points towards this idea that VS may be co-morbid with dyslexia, migraine (with aura), and autism (Ludlow et al., 2006; Wilkins et al., 1994; Wilkins et al., 2002).

1.3.2 Visual Stress and its Connection with Dyslexia

During the 1980s and 1990s, researchers discovered that the use of coloured acetates (sheet, filter) overlays could be used to help people suffering from eye strain and visual perception distortions when reading. This gave rise to a new syndrome known as Meares-Irlen (Mears, 1980; Irlen, 1983). In this thesis, this condition is described as VS as it is commonly known in the UK. VS produces somatic symptoms such as distortions of text, illusions, sore eyes, and tiredness (Conlon, 2000). The stimuli that induce these effects are also aversive to migraineurs, trigger headaches in those with photosensitive migraine and trigger seizures in those with photosensitive epilepsy. Interestingly, VS occurs more frequently in people with dyslexia than other patient populations (Irlen, 1991). Irlen (1991) had observed these somatic symptoms in 12% of the general population but noticed that people with dyslexia had an incidence of 65%. She later observed that VS was found in 46% of the people with dyslexia and other neurophysiological disorders (autism, ADD, & other non-specified learning disabilities (Irlen, 1997)).

A theoretical explanation of the benefits of using coloured filters in patients that suffer from visual stress (specifically those with concurrent dyslexia), named ‘the magnocellular theory of dyslexia’ was proposed by a number of researchers (Stein & Walsh, 1997; Livingstone et al., 1991; Lovegrove, 1991; Lovegrove et al., 1986, Ramus et al., 2003). In the visual system, signals travel from the retina to the lateral geniculate nucleus (LGN) of the thalamus and then to the visual cortex. In this system (Figure 1.3), the LGN is described as having six distinctive layers. The inner two layers, (1 and 2) are magnocellular cell (M cell) layers, while the outer four layers (3,4,5 and 6) are

parvocellular cell (P cell) layers (Wallace et al., 2016; Brodal, 2004; Carlson, 2007). The magnocellular visual system comprises a fast pathway that processes rapid changes in the visual scene, while its counterpart, the parvocellular system, is a slower pathway responsible for more detailed, stable visual perception (Stein & Walsh, 1997).

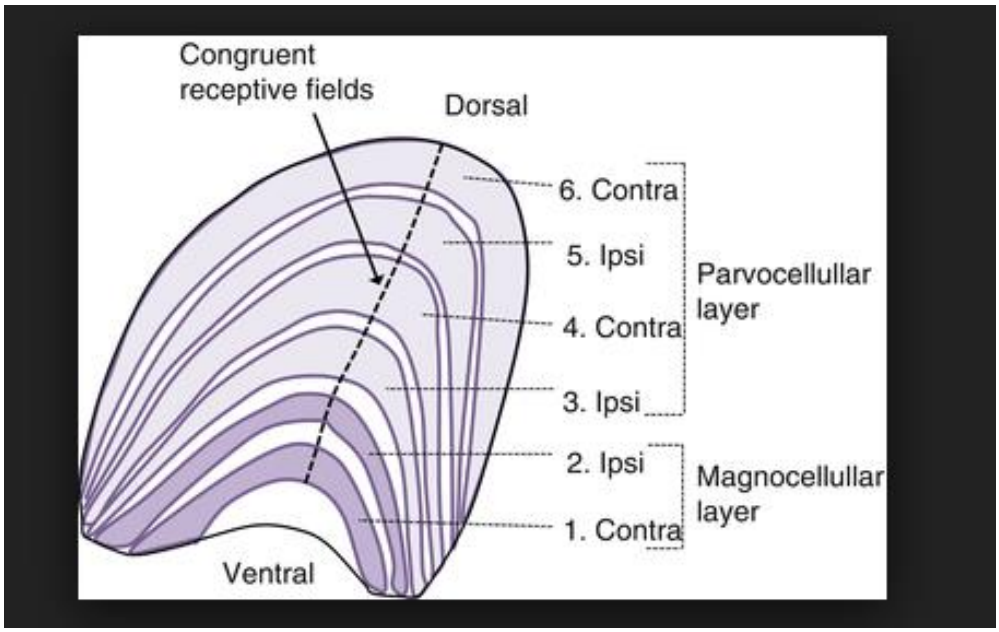

Figure 1-3. Diagram of the Lateral Geniculate Nucleus (Skalicky, 2016).

These systems work together across eye saccades, continuously facilitating and updating the visual image on the retina. When there are abnormalities in eye movement, they can lead to issues in processing text (Evans et al., 1996; Stein, 2001; Stein & Talcott, 1999; Stein & Walsh, 1997). More recent research has suggested that defective eye movements driven by the magnocellular system may be a cause of dyslexia (Vidyasagar, 2004). Researchers have used this as a basis to connect visual stress and dyslexia (Irlen, 1994; Lehmkuhle, 1993; Livingstone et al., 1991; Solman et al, 1991; Solman et al., 1995; Williams et al., 1992).

However, Wilkins and colleagues (2003) challenged this as a theory of VS. They stated that whilst the visual effects may be caused by deficits in the magnocellular system, this system, the theory, does not account for individual differences found when specific colours are optimal for

some patients, but not sufficient for other patients (people tend to have a preferred colour). Wilkins further asserted that people without dyslexia had been observed to benefit from colour filters, leading to the conclusion that VS is a condition in its own right, related to cortical hyperexcitability, and is independent from dyslexia (Wilkins, 2003). Nevertheless, there may be a connection between magnocellular deficits and PG caused by cortical hyperexcitability (Evans, 2001).

1.3.3 Reading

Reading involves many cognitive processes to extract meaning from print; this encompasses eye saccades, cognitive load, reading fluency, and deriving text meaning from print. Data taken from research evaluating the relationship between printed word identification and written and oral language comprehension processing shows that reading comprehension is impaired in a person who has not developed accuracy and fluency, even if that person is competent in oral language comprehension skills (Gough & Tunmer, 1986; Perfetti, 1985; Snowling, 2000; Stanovich, 1991; Vellutino, 1979, 1987; Vellutino et al., 1994; Vellutino et al., 1995; Vellutino et al., 1996). Developmental dyslexia has been observed to have biological foundations that affect the individual (Evans et al., 1996; Stein, 2001; Stein & Talcott, 1999; Stein & Walsh, 1997). However, aside from typical reading delays due to issues with fluency, visual stress has also been observed to affect these populations causing migraines and, more severely, seizures. These neurological events prevent fluent reading and affect the ability to comprehend text. VS comprises a variety of issues that relate to visual processing in the brain. This thesis proposes to understand different physiological processes that underlie these abnormal difficulties. It will explore such physiological processes for VS in its own right, instead of just as an oddity of dyslexia.

Additionally, this thesis will seek to make progress towards a biomarker for VS, which might make better-targeted interventions for headache or patients with other pathology related to VS. Notably, the same stimuli that elicit migraine in clinical populations are also the types of

stimuli that can cause migraines and epilepsy in people whilst they read (Wilkins, 1995). Reading contributes to a person's wellbeing in many ways: it is fundamental to education (Mitchell, 2014); it promotes economic growth (Naudé, 2004; Coulombe et al., 2004); it improves the ability of a person to interact in a social community (Stromquist, 2005) and finally, it is essential for employability. This line of research leads to the conclusion that many struggling readers that have issues with dyslexia may have additional problems that originate from abnormalities in visual information processing.

1.3.4 Visual Stress and Connections with Autism

Autism is composed of a variety of issues dealing with language, social-cognitive processing in social situations, and repetitive behavioural mannerisms (Frith, 1989). Specifically, important to this thesis is the integration of sensory information: researchers have observed abnormalities in hypersensitivity to sensory stimuli in patients with autism (Kientz & Dunn, 1997). Furthermore, there have been some abnormalities in the way people with autism perceive specific colours. Some children with autism refuse to eat certain types of food or may be averse to riding a bike because of the colour (White & White, 1987). Coloured filters have been seen to improve the reading performance of people with autism (Ludlow et al, 2006). People have reported that they were able to see the world more clearly with coloured filters, stating that their vision diverged from the everyday piecemeal visual scene usually reported in people with autism (Williams, 1998).

According to this research, patients that have shown improvements whilst using coloured filters are likely to have cortical hyperexcitability. In this vein, it is important to note that individuals with autism are more likely to have epileptic seizures than normal controls (Bryson et al., 1988; Cialdella & Mamelle, 1989; Deykin & MacMahon, 1979; Ornitz, 1973; Rutter, 1970; Steffenburg & Gillberg, 1986; Tanoue et al., 1988; Wing & Gould, 1979). Given that they benefit

from coloured filters, it is possible that the cause of the epileptic attacks observed in this patient population is due to an increased level of excitable neurons in the visual cortex.

1.4 Migraine

1.4.1 Migraine & Coloured Filters

Maclachlan et al. (1993) found that children who find colour filters helpful are twice as likely to have migraine in the family as those who show no benefit. Wilkins (1995; 2003) asserts that since the wavelength of light is known to affect neuronal sensitivity (Zeki, 1983), the use of colour could reduce hyperexcitation, thus reducing perceptual distortions and headaches when reading. Research has suggested that people with migraines had significantly more hallucinations than those without migraines when viewing striped patterns, and these people are more prone to be sensitive to pattern-glare (Harle et al., 2006). This is discussed later in this chapter. In one experiment, two groups (migraineurs and controls) had stimuli presented on a monitor with different coloured backgrounds. A target was briefly introduced to measure colour accuracy; migraineurs were observed to have alterations in colour perception. Specifically, vision in migraine deficits occurred in S-cone discriminants, and there was no difference between controls and migraineurs for L and M cones (Figure 1.5) (Shepherd, 2005). For an overview of different colour spectra for specific cones, see Figure 1.4.

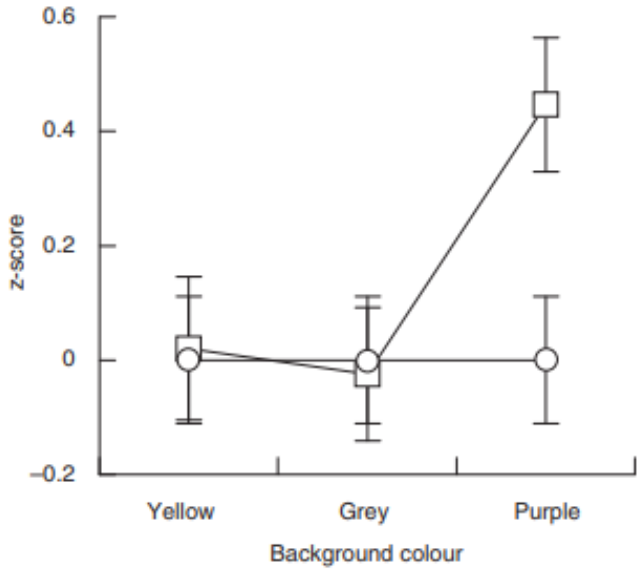

Figure 1-4. Results for threshold detection.

Circles represent the control group, and squares represent the migraine group. The average percentage errors are turned into z-scores relative to the group's performance. When objects are presented on a purple background, migraine groups make more errors (taken from Shepherd, 2005).

As mentioned previously, the link to migraine and epilepsy triggers suggests that those suffering from VS may exhibit cortical hyperexcitability (Huang et al., 2011).

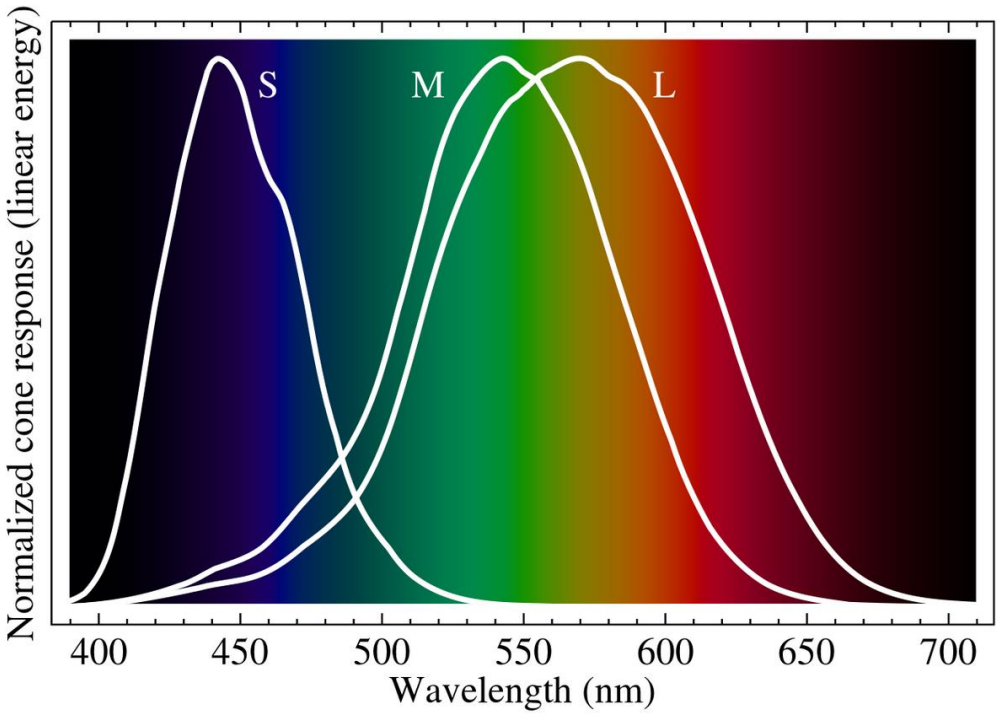

Figure 1-5. Normalised responsivity spectra of human cone cells, S, M, and L types (taken from Stockman & Sharpe, 2000).

1.4.2 Cortical Hyperexcitability and Migraine

There are several independent observations of cortical hyper-excitability found in migraineurs (Aurora & Wilkinson, 2007). Such excitation results in distortions of the visual image, which can be disruptive for reading and cause discomfort when viewing certain visual stimuli or under certain lighting conditions. In extreme cases, it can be temporarily debilitating, leading to workplace absences (e.g., migraine) or can adversely affect individual life opportunities. Cortical hyper-excitation has been observed in the NIRS responses of those who have heightened sensitivity to striped patterns, but the mechanism by which such excitation forms and spreads are unclear (Haigh et al., 2015).

Additionally, EEG and ERP studies have provided evidence that migraines with and without aura are characterised by habituation abnormalities related to aggravating sensory stimulation; this results in hyper-activation in the visual cortex (Ambrosini & Schoenen, 2006). Recall that it has

also been posited earlier in the chapter that the patterns that induce the most illusions and visual discomfort have the same physical attributes as those that trigger seizures in patients with photosensitive epilepsy (Adjamian et al., 2004; Wilkins et al., 1984). This suggests that the underlying neuronal mechanism for both abnormalities could be, at least to some extent, the same (Wilkins et al., 1979; Wilkins, 1995).

Of the variety of neuro-pathologies mentioned above, pattern-sensitive epilepsy is of interest; it is a rare disorder in which seizures are triggered by viewing specific stripped patterns. It was first discussed by Bickford and his colleagues in 1953, and many cases have been reported since (Bickford et al., 1953; Millichap et al., 1962; Bickford & Klass, 1964, 1969; Gastaut et al., 1966; Wilkins et al., 1975). Individuals asked to look at patterns of alternating light, for example light and dark stripes, report many anomalies (i.e., visual discomfort, eyestrain, headaches, blurring, motion, and diagonal coloured bands (Wilkins, 1995)).

1.4.3 Shape of the Hemodynamic Response and Cortical Hyper-Excitability

The relationship between hemodynamic changes and neural excitation is related to local field potentials (LFP). This is the electrophysiological signal generated by the summed electric current flowing from multiple nearby neurons within a small volume of nervous system tissue (Logothetis et al., 2001). It is useful to use the hemodynamic response as a substitute measure of neural activation. This is because the same visual stimuli that can evoke a strong neural response in the visual cortex will also cause a large reaction in the hemodynamic response (Olman et al., 2004; Vazquez & Noll, 1988).

Coutts et al. (2012), using NIRS, found evidence that patients with migraine had shorter oxyhaemoglobin responses compared to healthy controls. This posits that the shape of the hemodynamic response can also be related to cortical excitability. This is in line with other findings that suggest that patients with lower concentrations of GABA produce taller and thinner BOLD

responses in the visual cortex (Muthukumaraswamy et al., 2012). This directly supports the hypothesis that GABAergic mechanisms affect local cortical excitability (Semyanov et al., 2003). A study looked to explore this relationship (Haigh et al., 2015); the researchers found that the average amplitude and slope of the response to chromatic gratings were correlated with the average amplitude and slope of the responses to the moving gratings for everyone. Gratings with large chromaticity separation have been reported to be seen as uncomfortable to view, suggesting a relationship between discomfort and the amplitude of the cortical response (Haigh et al., 2013).

This means that the shape of the hemodynamic response appears to reflect the strength of the stimulus: the stimuli that evoke the most discomfort and are potentially epileptogenic, producing the largest amplitude and the steepest slope in the oxyhaemoglobin response and deoxyhaemoglobin response. Additionally, patients with migraine showed larger BOLD responses to grating stimuli than controls (Huang et al. 2003). As mentioned above, neurochemicals such as GABA also play a role in influencing patients suffering from migraines. GABA affects BOLD responses in the visual cortex and works to inhibit the hyperexcitation seen in migraine, whilst glutamate is involved in exciting the network (Gasparini & Griffiths, 2013).

1.4.4 Neurochemicals Influencing Migraine

There is some data in the fMRI literature surrounding patterns of activity in the visual cortex in response to stimuli that were around 1.2 cycles per degree. Welch et al. (1990) proposed the general hyperexcitability theory of the pathophysiology of migraine. This theory suggests spontaneous neuron depolarisation, followed by a spreading suppression of neuronal function. This chain of neuronal events is possibly mediated by the release of the excitatory amino acid glutamate or the increase in extracellular K+. Also, glutamatergic neurons are most likely responsible for neuronal hyperexcitability, particularly in the occipital cortex. Clearance of K+ is also heavily dependent upon the capacity of glial cells (Van Gelder, 1987; Wright et al., 2001).

1.5 The Pattern Glare Test

The pattern glare test (Figure 1.6) was published in 2001 by Wilkins and Evans (2001) as a standardised way for physicians to examine whether a patient had some proclivity to experiencing VS. The test is intended to induce visual stress in susceptible patients; patterns are also presented horizontally to appear like text and at different spatial frequencies (SF) (.37, 3, and 12) (Evans & Stevenson, 2008). For the purpose of this thesis we call .37 c/deg thick, 3 c/deg medium and 12 c/deg thin.

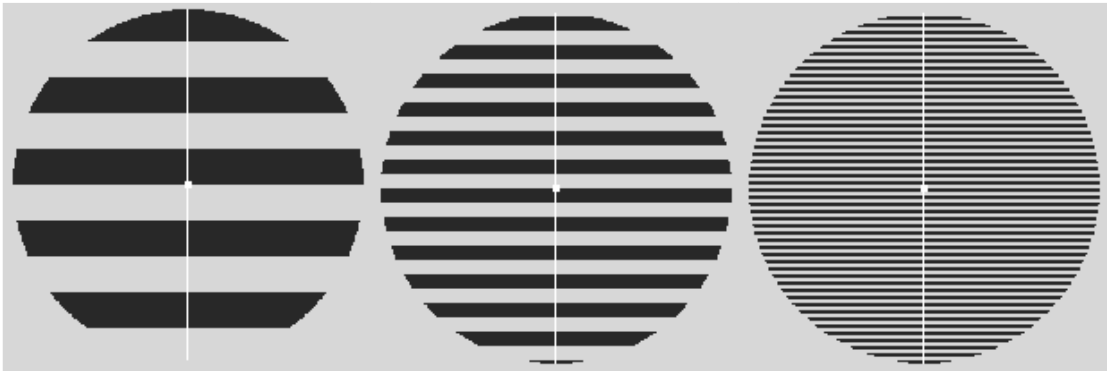

Figure 1-6 Pattern-glare Stimuli:
Left to right, thick (.37 c/deg), medium (3 c/deg) and thin (12 c/deg) gratings with a central fixation and vertical dividing line. The images shown here are representative of the stimuli but have been rendered to aid visibility in print.

Pattern 1 (thick) is meant to be a control for low SF and is not supposed to trigger distortions in most participants. However, it is useful in detecting 'which patients may be highly suggestible and may respond yes to any question about visual perception distortions' (Evans & Stevenson, 2008). Pattern 2 (medium) is the only relevant clinical stimulus falling between SF's 1-4, which are known to elicit migraines and epileptic seizures (Braithwaite et al., 2013; Wilkins, 2016). Pattern 3 (thin) is a control for poor convergence and accommodation. Those with poor convergence and/or

accommodation will see distortions in this stimulus reflecting optical rather than neurological factors (Conlon et al., 2001).

1.6 Neural oscillations

1.6.1 Background

In 1929, Berger observed neural oscillations in the brain waves as rhythmic repeating patterns of neuronal activity (Berger, 1929). Since then, more research has been undertaken on other oscillatory patterns in clinical and basic research (Buzsaki & Draguhn, 2004). Research in biophysics at the single cellular level has revealed that brain oscillations cycle at multiple frequencies and have an essential role to play in information delivery and communication between neurons (Llinás, 1988; Hutcheon & Yarom, 2000). In signal processing, time-frequency analysis is a vast array of techniques and methods used to study the signals of the time and frequency domains simultaneously (Meyer & Flandrin, 1999, see Figure 1.7).

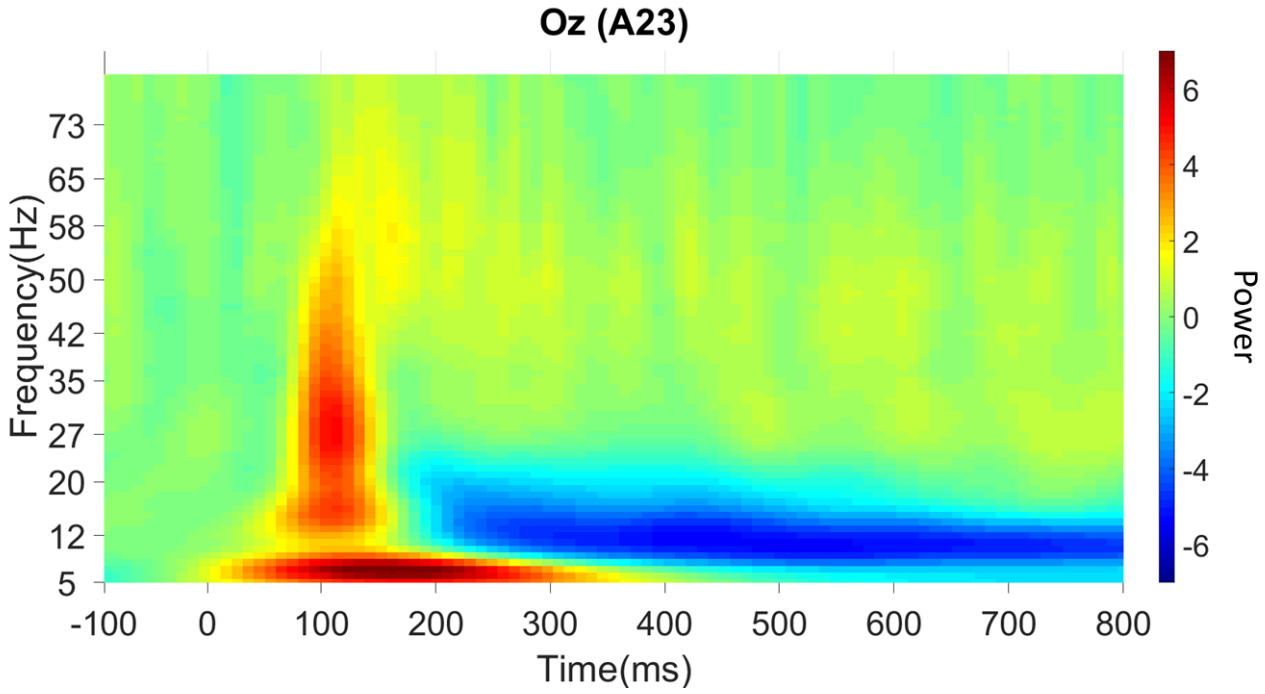

Figure 1-7. Example of a Time-Frequency plot at electrode Oz, generated by spm 12. Zero is the onset time of a visual stimulus. Colour bar represents dB power -6.5 to 6.5.

1.6.2 Oscillations in Migraine Research

Alpha-band oscillations 8-12hz (Figure 1.8) are believed to have a role in the visual system from controlling the timing of perceptual processes (Jensen et al., 2014; Klimesch et al., 2007; Klimesch et al., 2012), to playing a role in inhibiting part of the cortex (Cole & Ray, 1985; Klimesch, 1996; Klimesch, 2006; Pfurtscheller, 2001; 2003). These oscillations may also play a role in communication (Palva & Palva, 2007) and have been attributed the title the 'window of excitability' (Dugué et al., 2011). Previous studies suggest that alpha differs between migraine and healthy controls; specifically, there is activity in alpha 72 hours before an attack (Bjørk et al., 2009). There are two characteristics of alpha-band activity: peak frequency (defined as the frequency at which the maximum amplitude occurs within the band) and magnitude (variation in amplitude of the oscillation at the given frequency band) of an oscillation. Tonic alpha-band oscillations have been researched in migraine patient populations. Increased pre-attack occipital-parietal alpha asymmetry has been found before attacks (Nyrke et al., 1990); however, the cause and origin of hypersensitivity to visual stimuli in migraineurs are unknown.

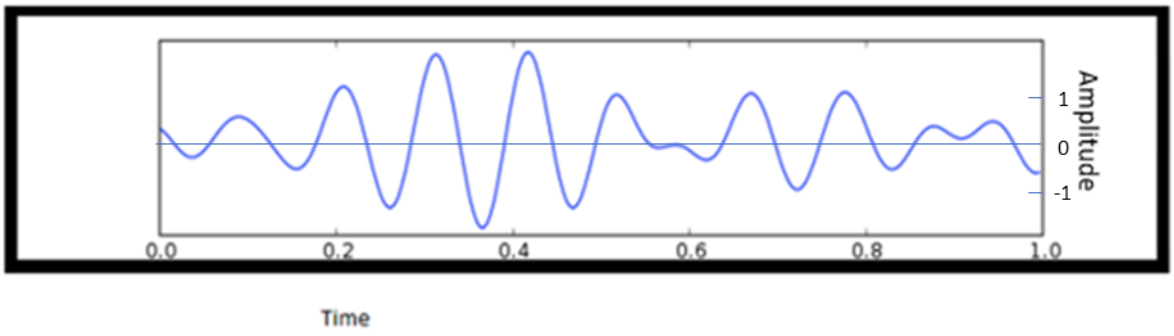

Figure 1-8. Example of an alpha wave.
The X-axis represents time, and the Y-axis represents amplitude.

It is suggested that differences in performance from migraineurs to controls are due to internal noise in the processing of visual stimuli (Wagner et al., 2010). One study showed

differences in lower alpha power in migraineurs versus control groups (Figure 1.9) (O'Hare et al., 2018). Participants were given a contrast detection task, whilst alpha-band activity was recorded before and after the psychophysics task. The visual tasks consisted of two alternative forced-choice contrast discrimination. Participants viewed two gratings of 1 c/deg presented side by side. These were presented on both sides of a small red fixation cross. The targets consisted of a one-level contrast (-10dB) and a jittered contrast. The presentation was in random order, and this randomisation was different for each person. The task of the observer was to declare using arrow keys, whether the stimulus on the left or right had higher contrast. This went on for 100 repetitions for 45 minutes. The researchers found that lower-band resting-state power was increased in migraine groups compared to control groups. This supported previous research where fluctuations in alpha-band oscillations may explain differences in tasks relating to temporal integration.

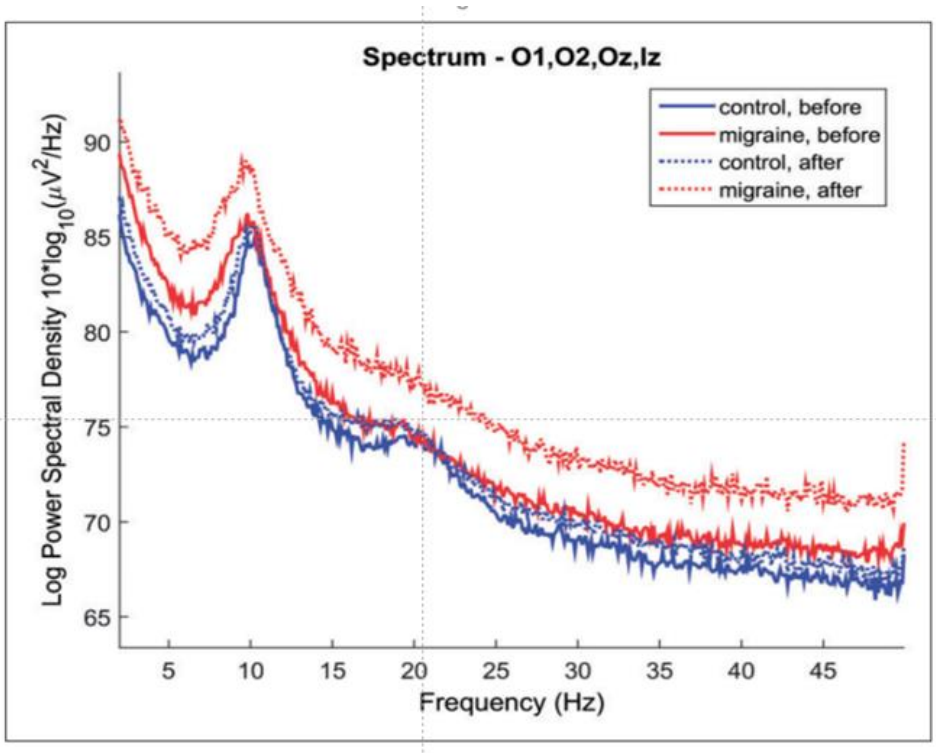

Figure 1-9. Average power spectra for migraine and control groups before and after the task. Spectral power in 10 × log_{10} (μV^2/Hz) averaged over electrodes O1, O2, Oz, and Iz. There is a bigger difference in *low alpha (8-10hz) compared with high (10-12 Hz) and overall alpha band (8 to 12 Hz) (O'Hare et al., 2018).*

Bjørk et al. (2009) studied alpha using 41 migraine patients and 32 healthy controls who had completed headache diaries and questionnaires about headaches, with recorded EEG using a 10/20 cap and an eye blink measurement. The researchers found migraine with and without aura showed a negative correlation between disease duration and alpha peak frequency (p=.001) and that correlation results indicate long-lasting attacks are associated with reduced peak frequency (p=.04) (Figure 1.10).

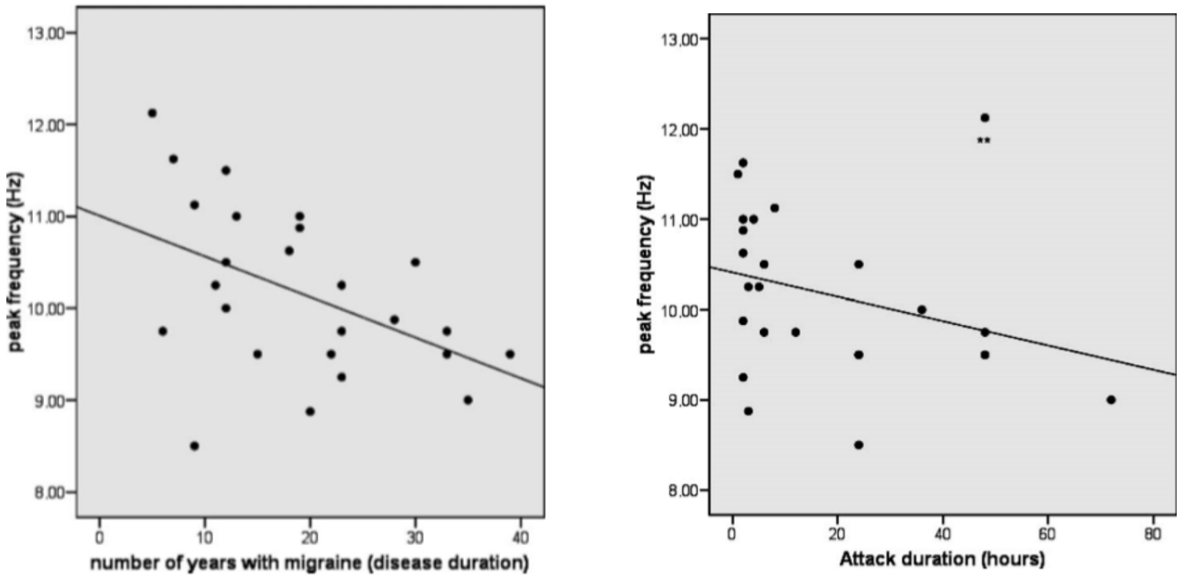

Figure 1-10. Shows a Spearman's correlation of number of years with migraine disease and attack duration in hours with peak frequency (Bjørk et al., 2009).

Gamma frequency (30-100hz) is an important signal in the brain; there is evidence that gamma is related to engaged networks, such as attention (Fries et al., 2001) and learning (Bauer et al., 2007). Gamma activity has also been connected to neurological disorders such as Alzheimer's, Parkinson's,

schizophrenia and epilepsy (Uhlhaas & Singer, 2006). Wu et al. (2018) showed that migraineurs had abnormal gamma-band activity after viewing emotional stimuli between attacks.

Of importance to this thesis is a paper by Adjamian et al. (2004), where they analysed PG stimuli between 1-6 c/deg in .5 cycle steps. The stimuli were presented to participants for 5 seconds and repeated in separate MEG recordings for sessions over 2-3 days. These recordings were source localised to visual area V1. Subjects were asked to report if they felt discomfort and/or illusions. The results showed an oscillatory synchronising response between 20-60 Hz in the gamma range, for SFs of 2-4 CPD. This gamma response was sustained throughout the 5s of stimulus viewing (see Figure 1.11 for results breakdown). Additionally, these aggravating PG stimuli (between 2-4 c/deg) induced (subjectively reported) high levels of discomfort and a number of illusions. However, Adjamian et al. (2004) did not directly relate their subjective report measures to their brain data, as we do in our mass-univariate analysis, allowing us to assess how specific parts of the data volume vary with subjective report.

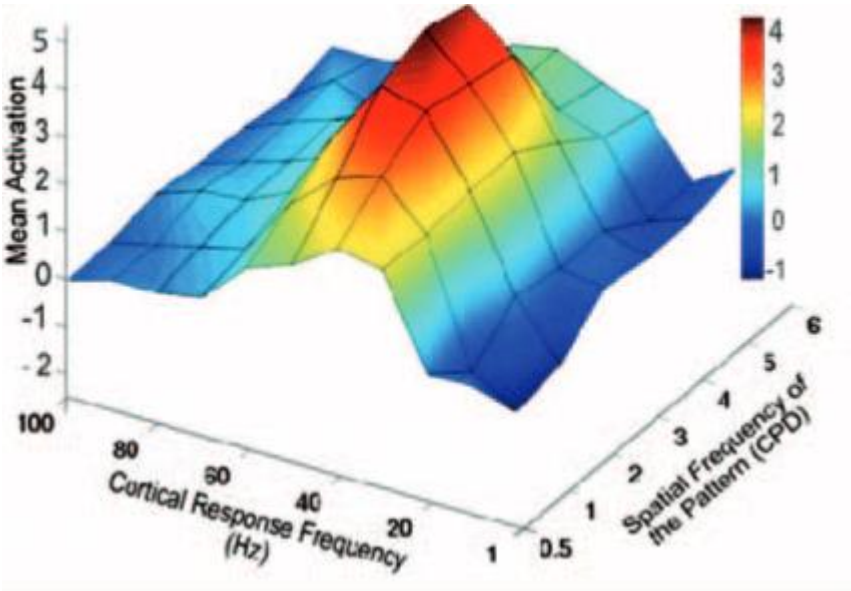

Figure 1-11. Cortical results for Adjamian et al. (2004).

The group-average (n=7) magnitude of oscillatory power in the primary visual cortex as a function of stimulus-response frequency (taken from Adjamian et al., 2004).

Additionally, Muthukumaraswamy and colleagues (2009) performed an analysis with stimulus-induced sustained gamma oscillations, using 3 c/deg gratings. They recorded data using magnetic resonance spectroscopy (MRS), fMRI and MEG over several days. Each stimulus was presented for 1.5-2s followed by 2s of fixation at cross only. Their goal was to quantify resting GABA concentrations in the visual cortex. They discovered that individuals' gamma oscillation frequency was positively correlated with resting GABA concentration.

1.7 Overarching Hypotheses

The key hypotheses that this thesis assesses are as follows.

1. There will be a response in the posterior part of the scalp, as revealed by EEG, that exhibits a more extreme difference from zero in the medium as opposed to thick and thin stimuli (i.e., the medium will be the most extreme of the three responses, either more positive with positive-going effects or more negative with negative-going effects). These will be present in both the time and frequency domains.
2. We will find effects on some factors, whereby participants higher on a factor will have more extreme pattern glare index (PGI) responses, and participants low on a factor will have less extreme PGI responses. These may be particularly found for the discomfort factor. This factor is at least partially a state measure, which may be easier to correlate with the EEG, since measure and EEG are collected in the same session.
3. There will be a different induced response in onset 1 and onset 2:8 for the oscillation pattern, i.e., desynchronisation to synchronisation versus synchronisation to desynchronisation versus sustained

synchronisation, which is not consistent in both. Onset 1 may reflect a failure to predict, or be affected by stimulus novelty effects, and onsets 2:8 represent a failure to habituate.

1.8 Experimental strategy

1.8.1 Outline

The tools outlined here will form the basis for the experiments reported in this Thesis. I will focus on utilising EEG to measure and understand brain activity. EEG studies for both event-related and steady-state methodologies will be discussed. Event-related EEG will be used to compare the amplitude of neural responses specific to striped patterns in the healthy population and groups with known or suspected cortical hyperexcitability. Tonic EEG will be used to assess the strength of the various oscillatory patterns that are associated with relatively active or inactive brain regions.

1.8.2 EEG Overview

Signaling among neurons within the brain is principally electrical and chemical. Cells send action potentials along their axons, resulting in a release of neurotransmitters at synapses with receiving cells. These neurotransmitters attach to the membrane of the receiving cells and alter the flow of chloride, calcium, potassium, and sodium ions across the cell membrane, setting up currents that are aggregated by the cell until it eventually releases its own action potential. This ion exchange process also produces ‘volume conduction’ whereby ion movements and currents, propagate to the scalp and can be recorded with electrodes. The nature of the volume conduction process means that signals recorded at the scalp are necessarily the aggregate of activity in many neurons over a wide area of the brain; thus, EEGs have low spatial resolution. Conversely, the temporal resolution of EEG is excellent. Further, by comparing the activity of multiple electrodes, it is possible to derive the approximate location of the activity driving a given EEG waveform.

1.9 Event-related EEG & Event-related potentials (ERP)

Event-related EEG (arguably the more common EEG technique) and time-frequency analysis involves the presentation of some stimulus (here visual) while recording brain activity. The activity associated with many similar presentations is then time-locked to the stimulus onset and averaged. This procedure reduces the impact of random fluctuations and reveals the results of reliable processing events and peaks and troughs in the waveform at each electrode. Activity associated with early visual processing typically occurs early in the waveform and at occipital electrode locations. The amplitude and, to some extent, the precise timing of such features is thought to correlate with the degree of processing dedicated to it. Thus, if an individual is especially sensitive to a specific stimulus, we might expect higher amplitude signals than in a control participant. In contrast, if they are less sensitive or are actively ignoring the cue, a lower amplitude might be expected.

By recoding event-related potentials (ERPs) in relation to striped stimuli of various spatial frequencies presented to those who are thought to suffer from cortical hyperexcitability and control, I hope to establish that certain stimuli do elicit higher amplitude ERPs in the patient groups relative to control. As the stimuli are very simple, differences in the N1-P1 complex recorded at the most posterior electrodes would be expected, as demonstrated in Figure 1.12, which shows variations in the N1, P1 complex when processing negative emotional words (Van Hooff et al., 2008).

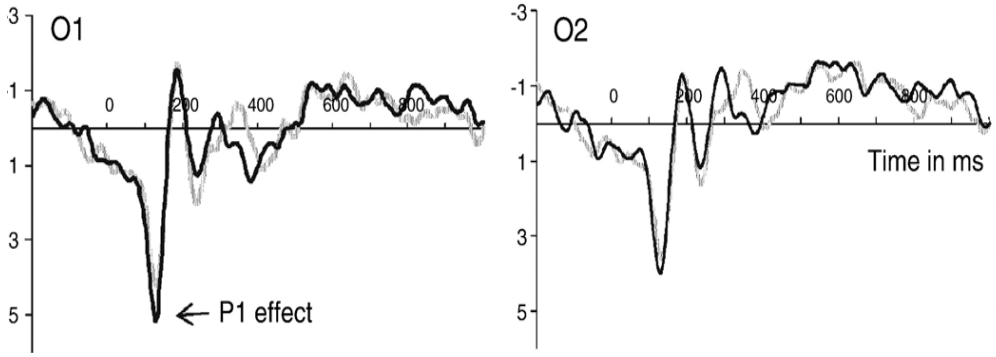

Figure 1-12. ERPs recorded at scalp locations O1 and O2 in response to neutral words (grey line) and negative affect words that produced reaction time facilitation (dark line).

The negative effect words made enlarged P1 responses. The figure was adapted from Van Hooff et al. (2008) with the permission of an author.

1.9.1 Tonic EEG

In Tonic EEG, waveforms are recorded over a period (of time) while the participant is either resting or looking at some stimulus, but signals are not explicitly time-referenced to stimulus onset. Further analysis is then used to isolate oscillations in the waveform, and power spectral analysis can identify the energy in different oscillatory bands, which are associated with different kinds of brain activity. Of specific interest to this project are the alpha (7.5–12.5Hz+ (Gerrard & Malcolm, 2007)), beta (14-30 Hz +(Berger, 1929)), and gamma (32Hz +) bands (Hughes, 1964). Some have associated alpha band with inhibition of sensory input, whilst beta and gamma-band activity have been related to active processing. I expect individuals with cortical hyper-excitability to have increased gamma and beta-band activity and or reduced alpha-band activity when viewing an aggravating stimulus (Adjamian et al., 2004). A similar difference may also be found at rest if the affected cortical area is generally excitable rather than hyper-excited only by specific stimuli.

1.10 Experimental methods

In order to investigate this, we used stimuli similar to those used in the Pattern-Glare Test (PGT) (Wilkins, 2001) (See Figure 1.6, Chapter 1). Stimuli comprised horizontal square-wave gratings (contrast = 75%) at 3 different spatial frequencies (.37, 3, and 12 c/deg: described as thick, medium, and thin respectively) displayed at 75% contrast in a circular window with diameter 15.2 deg at a viewing distance of 86 cm.

We measured EEG (using the Biosemi 128 electrode cap, Figure 1.13) responses to visual stimuli based on those used in the PGT in a novel paradigm where stimuli were repeated (flicked on and off) at a low temporal frequency, allowing the recording of both ERPs and steady-state EEG, while also allowing us to consider habituation effects. Thus, we compared stimuli known to be aggravating in migraine with those that are less aggravating, in a paradigm that allows the separation of initial and habituated responses. In all analyses, participants were not selected based on their migraine or headache status; rather ERP and EEG results were correlated with scores on a range of headache and hyper-excitation measures within a single group drawn from the general population. State measures of discomfort in response to the PGT stimuli were also taken.

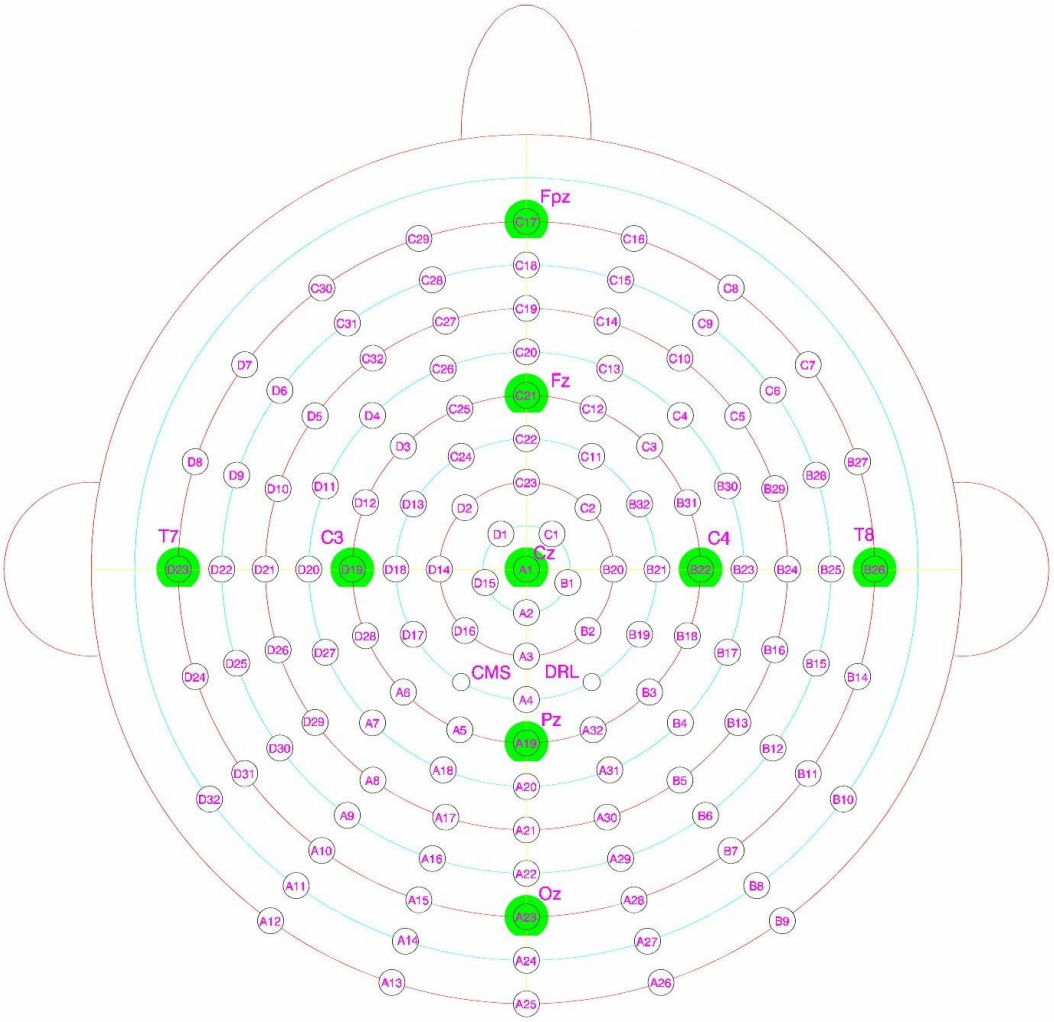

Figure 1-13 Biosemi cap used in the Experiment

Biosemi (BioSemi , Amsterdam, Netherlands) 128 cap used in the experiment.

In analyses 1 and 2, questionnaires were used to assess participants' headache history (Headache and General Health Questionnaire, HGHQ) and tendency to suffer visual stress (Cortical Hyper-Excitability index (Chi), Braithwaite et al., 2015; Visual Discomfort Scale (VDS), Conlon et al., 1999). We performed a factor analysis in which three orthogonal factors emerged in the data: 1) visual stress (a combination of the CHi, VDS and aura measures), 2) headache (frequency, intensity and duration) and 3) discomfort. Analysis 3 did not use a questionnaire or factor data.

Additionally, a contrast image was created based on what we call the PGI. This is the output file type that is used in the SPM data matrices in order to perform models or statistical tests.

> Statistical analyses of M/EEG data in SPM use the same mechanisms as all other data types (PET, fMRI, and structural MRI in VBM). This simply requires transforming data from SPM M/EEG format to image files (see NIfTI format, http://nifti.nimh.nih.gov/nifti-1/). A summary statistic image is just a technical term for the data feature summarising treatment effects that one wants to make an inference about. More formally, when this summary statistic is itself a maximum likelihood estimate based on within-subject data, the analysis is called a summary-statistic procedure for random effect models (Litvak et al., 2011).

This index enables us to focus our analysis on regions of the data volume where the clinically relevant, medium stimulus exhibits an extreme response relative to the thick and thin stimuli. Note that the images are the EEG/ERP responses to the medium, thick or thin stimulus. The PGI is defined as follows,

PGI = (medium image – average (thick image, thin image)).

1.11 Procedure

Each trial contained between seven and nine onsets of the same stimulus, which were presented on grey backgrounds with the same space-averaged luminance. After each trial, the participant was asked to rate how discomforting they found each stimulus on a 5-point scale and to indicate how many onsets they saw. This additional task was designed to ensure attention to the stimuli. At the end of each block, participants were shown the three stimuli in turn and asked to rate the extent to which they had experienced a range of possible pattern glare symptoms (Wilkins & Nimmo-Smith, 1984) (See Figure 1.14 for experimental sequence breakdown). We also split the onsets from 1 to 8 to onset 1 and onsets 2:8; this allows us to distinguish between surprise effects and habituation effects.

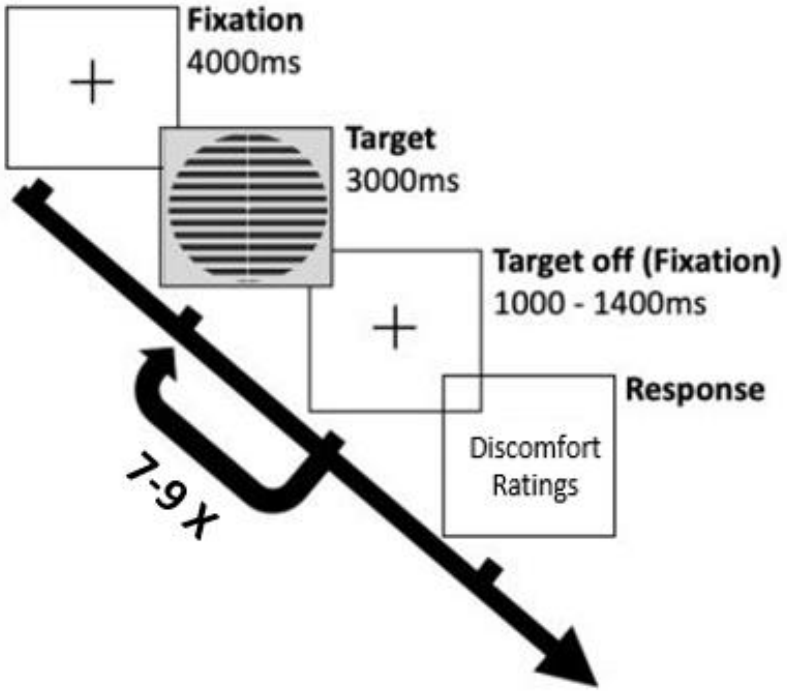

Figure 1-14 Experimental Sequence.

The experimental sequence of the experiment.

1.12 Author contributions

When writing a thesis by publication, it is understood that the analysis chapters are a collaborative effort by the authors. Listed below are the individual author contributions. Overall, each author contributed to each analysis: Schofield conducted the factor analysis used in the experiment and wrote the experimental code. Miller edited the code to add labjack commands and the range of discomfort measures. Miller and Tempesta worked on collecting most data in the study. However, some data was collected by a previous student, before Tempesta joined the lab. Tempesta wrote the code to edit plots in Matlab, binning the data, preprocessing the EEG, and the batch files for the time-frequency analysis. Litvak wrote the code to transfer the ERP/EEG data from ERPlab to SPM. Bowman assisted Tempesta with statistical analysis of the entire experiment, interpretation of the

results, manuscript supervision of analysis 2 and 3, Bowman and Tempesta also worked together with the creation of the graphics used in the analysis papers of 2 and 3.

Analysis One

For analysis one, Tempesta wrote the main manuscript, analysed the data and collected part of the data. Miller reviewed drafts of the manuscript and collected the other portion of the data. Schofield, Tempesta and Miller worked together on writing the introduction and discussion. Schofield also looked over the final draft revisions; specifically some of the introduction was re-written. Litvak helped assisted with the processing of the data in SPM and helped with the associated technical challenges. Bowman helped with all aspects of the manuscript preparation. All authors contributed to the discussion conversations, including interpretation of the results.

Analysis Two

For analysis two, Tempesta wrote the main manuscript, analysed the data and collected part of the data. Schofield reviewed final draft revisions. Bowman helped with all aspects of the manuscript preparation, including clarity of the writing. All authors contributed to the discussion conversations, including interpretation of the results.

Analysis Three

For analysis three, Tempesta wrote the main manuscript, analysed the data and collected part of the data. Schofield reviewed final draft revisions. Bowman helped with all aspects of the manuscript preparation, including clarity of the writing. All authors contributed to the discussion conversations, including interpretation of the results.

The superscript numbers next to the authors' names in the following chapters are associated with the universities below:

1. School of Psychology, College of Life and Environmental Sciences, University of Birmingham, Edgbaston, B15 2TT.

2.Wellcome Centre for Human Neuroimaging, University College London, 12, Queen Square, London, WC1N 3AR

3.School of Computing, University of Kent, Canterbury, Kent, CT2 7NF.

4.Department of Psychology, Life and Health Sciences, Aston University, Birmingham, UK, B4 7ET.

CHAPTER 2: THE MISSING N1: ELECTROPHYSIOLOGICAL CORRELATES OF PATTERN-GLARE IN THE TIME AND FREQUENCY DOMAINS

Austyn J. Tempesta[1], Claire E. Miller[1], Vladimir Litvak[2], Howard Bowman[1,3], & Andrew J. Schofield[4,1]

2.1 Abstract

Headaches, including migraine, are a major contributor to workplace absences. Many headache prone individuals also show sensitivity to certain visual stimuli (visual stress), which can extend to discomfort. We analysed event-related potentials (ERPs) in response to square-wave gratings of thick (.37 c/deg), medium (3 c/deg) and thin (12 c/deg) gratings, using mass univariate analysis, considering three factors in the normal population: headache proneness, visual stress and discomfort. We found significant relationships between ERP features and the headache and discomfort factors. Stimulus main effects were driven by the medium stimulus regardless of participant characteristics. Participants with high discomfort ratings had larger P1 components for medium stimuli suggesting cortical hyperexcitability. The participants with high headache ratings showed abnormal N1-P2 components for medium stripes relative to the other stimuli, indicating an effect of habituation. These effects were also explored in the frequency domain suggesting variations in inter-trial theta band phase coherence. Our results suggest that discomfort-and headache in response to striped stimuli are related to different neural processes; however, more exploration is needed to determine whether the results translate to a clinical migraine population.

Keywords: Headache, migraine, visual stress, pattern glare, EEG.

2.2 Introduction

Tension type headaches (TTH) and migraine are the second and third most common diseases in the world respectively (Steiner et al., 2013). Headache disorders are ranked second among causes of disability worldwide; mostly due to migraine (Institute for Health Metrics and Evaluation, 2018). Severe migraines are considered by the World Health Organization (WHO, 2016) as the leading cause of disability among neurological disorders, affecting 1 in 7 people (House of Commons, 2010), consisting of 3000 attacks each day in the UK alone with an estimated 190,000 occurring annually (Steiner et al., 2003). Missed work from migraine is estimated to cause £250 million in lost revenue in the UK each year (Clarke et al., 1996). Nonetheless, migraine is also the least funded of all neurological illnesses in the world (House of Commons, 2014; Shapiro & Goadsby, 2007). Migraine has been associated with the hyper-excitability of neurons in the visual cortex (Welch et al., 1990) and increased sensitivity to certain stimuli, both during and between episodes; even in the absence of a specific visual trigger (Friedman & De Ver Dye, 2009; Ambrosini & Schoenen, 2006; Spierings et al., 2001). Migraine has also been associated with atypical EEG patterns (Marks & Ehrenberg, 1993) and an increased fMRI blood-oxygen level dependent (BOLD) response to certain visual stimuli (Hougaard et al., 2014). These stimuli also elicit an atypical haemodynamic response function (Olman et al., 2004; Vazquez & Noll, 1988). Here, we consider a broader range of headache causes and consider differences in event related potentials (ERPs). We consider EEG frequency components in response to visually aggravating versus control stimuli and the relationship between such differences. Finally, we examine a range of state and trait measures of cortical hyper-excitability and headache proneness.

2.2.1 General Hyperexcitability Theory of Pathophysiology of Migraine

Welch and colleagues (1990) proposed the general hyper-excitability theory of the pathophysiology of migraine. This theory proposes spontaneous depolarization, followed by a spreading suppression of neuronal function (cortical spreading depression, CSD). This chain of neuronal events is possibly mediated by the release of the excitatory neurotransmitter glutamate or the increase in extracellular potassium (K+). Clearance of K+ is also heavily dependent upon the capacity of glial cells (Van Gelder, 1987; Wright et al., 2001), which may be defective in migraine. This account is broadly consistent with the genetic account of migraine, which implicates genes that affect the glutamatergic system. These genes lead to both dysfunctional sensory processing and a cortical imbalance between excitation and inhibition leading in turn to hyperactive cortical circuits (Ambrosini, & Schoenen, 2006), CSD, sensory aura and activation of the trigeminovascular pain pathway (Buzzi, 2001; see Vecchia & Pietrobon, 2012 for a review). There is some dissociation between these outcomes in that not all migraineurs experience aura and some experience aura without headache (suggesting a common trigger for aura and headache, which then proceed in parallel but with further modulation (Datta et al., 2013; Denuelle et al., 2008)).

Excitation via the glutamate system would normally be held in balance by inhibition mediated by gamma-aminobutyric acid (GABA). Bigal et al. (2008) used magnetic resonance spectroscopy to measure in vivo GABA in a migraine population and controls, finding that migraineurs with low to moderate headaches had elevated GABA, whereas those with the most severe headaches had GABA concentrations similar to controls. This result suggests that migraine sufferers may counter excess excitation through increased GABAergic inhibition but that those suffering the most severe headaches cannot bring this inhibition to bear. Alternatively, increased GABA could be associated with a pain response which is deficient in those with severe headaches (Enna & McCarson, 2006). However,

others have found only a positive association between migraine and GABA concentrations (Aguila et al., 2015; 2016). Although the GABA system is complex and elevated levels may be a result rather than cause of migraine, these results would certainly suggest that migraine sufferers do not lack this key inhibitory neurotransmitter. The suggestion that migraine results from excess excitation rather than poor inhibition is supported by psychophysical evidence showing stronger inhibitory illusions such as the motion after-effect in migraine (Shepherd & Joly-Mascheroni, 2016), suggesting greater excitation during the adaptation phase, which then produces greater inhibition. Increased after-effects would be unlikely if neural inhibition were compromised.

2.2.2 Effects of Cortical Hyper-Excitability in Migraine

Cortical hyper-excitability may make those with migraine and other headache disorders more sensitive to visual stimulation such as flickering lights (Wilkins et al., 1989) and striped patterns (Harle et al., 2006). Such stimuli induce visual distortions and eye strain and are also trigger stimuli for some individuals (Wilkins, 1986, 1995; Wilkins et al., 1979, 1980). Flickering light sources up to around 100Hz are problematic and those working under flickering fluorescent lighting experience more headaches and other symptoms than those working in natural light or under high frequency fluorescent tubes (Wilkins, et al., 1989). Of greater interest here are the visual distortions and discomfort resulting from striped stimuli. Most people have a tendency to see distortions when viewing high-contrast square-wave gratings (stripes) and this tendency increases somewhat with spatial frequency. However, migraineurs tend to see more distortions, especially when viewing mid-range spatial frequencies around 3c/deg (Harle, et al, 2006), such that the difference in the number of distortions seen between 3c/deg and 12c/deg patterns is seen as diagnostic of interictal visual stress (Evans & Stevenson, 2008). This comparison is the basis for the pattern glare test (PGT) developed by Wilkins and Evans (2001).

2.2.3 EEG Findings

If cortical hyper-excitability is responsible for heightened sensitivity to simple visual patterns, we might expect to find increased neural activity associated with early visual processing in response to such patterns. A few early studies measured ERPs in response to non-patterned flashes of light, finding these have greater amplitude than pattern flashes in the early components of the ERP waveform (Lehtonen, 1974; MacLean et al., 1975; Connolly et al., 1982; Brinciotti et al., 1986; but see also Richey et al., 1966). However, EEG studies have more typically measured pattern-reversal visual evoked potentials (PR-VEPs) in response to chequerboard stimuli and have provided mixed results for the amplitude and latency of early visual components: some studies show increased amplitude and latency and others found a reduction; however most found that PR-VEPs in migraine were similar to those in controls (see Ambrosini & Schoenen, 2006, for a review). The evidence for habituation abnormalities is more consistent, suggesting that those with migraine fail to habituate to repeated stimulation with the same stimulus (Schoenen et al., 1995; Afra et al., 1998; Wang, Wang, et al., 1999). EEG waveforms also vary with migraine phase, paradoxically being closer to that of typical non-sufferers just prior to migraine onset (Shahaf, 2015), which may explain the somewhat contradictory results for PR-VEP amplitudes. The common use of un-patterned flashes and chequerboard stimuli to test VEP responses in migraine may be sub-optimal since stripes of a mid-range frequency, rather than cheques are thought to be more aggravating for migraine sufferers and others with visual stress or pattern glare symptoms (Wilkins, 1995). It is possible then that VEP studies have not explored the strongest or most pertinent EEG responses in this population.

Few studies have recorded brain activation in response to pattern glare stimuli. Huang et al. (2003) applied such stimuli to a visual stress population showing increased fMRI activity in the occipital cortex, consistent with the cortical hyper-excitability theory in migraine. To our knowledge

only Haigh et al (2019) and Fong et al., (2020) have previously measured ERPs in a headache prone population using the pattern glare stimuli. Fong et al. (2020) found differences between migraine sufferers and controls at around 200ms and 400ms post stimulus onset. The migraine group shows significantly greater negativity at 200ms for high frequency gratings (13 c/deg). Indeed, their main findings were on the high-frequency grating, while, in contrast, the findings we report here will be on the clinically relevant, medium frequency grating (3 c/deg).

2.2.4 Implication of Cortical Hyper-Excitability to Different Brain Regions

Cortical hyper-excitability has also been observed in the fMRI BOLD responses of those who have heightened sensitivity to striped patterns. Elevated BOLD signals have been found in the primary (striate) visual cortex as well as extra-striate visual cortex, pre-cortical structures and areas of the frontal cortex (See Schwedt et al., 2015, for a review). In one study, heightened BOLD responses to striped stimuli in cortical area V3 were found to reduce when the migraine patients wore glasses with a prescribed colour tint versus a similar tint or grey filters (Huang et al., 2011). Indeed, similar coloured filters have been found to reduce distortions on the PGT (Harle et al., 2006).

Studies using near infra-red spectroscopy (NIRS) have found evidence that patients with migraine have shorter oxyhaemoglobin responses than healthy controls (Coutts et al., 2012). This result is in line with other findings suggesting that patients with lower concentrations of GABA produce higher amplitude, but shorter, BOLD responses in the visual cortex (Muthukumaraswamy et al., 2012). The result also supports the hypothesis that GABAergic mechanisms affect local cortical excitability (Semyanov et al., 2003), although, as noted above, the glutamatergic system seems to be the primary focus for hyper-excitability in migraine. Haigh et al. (2015) explored the link between pattern glare and the haemodynamic response in the normal population, comparing stimuli known to be aggravating in migraine with those that are not. The amplitude of the haemodynamic response was

largest for stripes with high chromatic contrast; these being more aggravating. Moving striped stimuli showed a steeper decline in the haemodynamic response at stimulus offset compared to static gratings. This result suggests that, even in the normal population, the shape of the haemodynamic response appears to reflect stimulus potency: the stimuli that evoke the most discomfort in migraine produce the largest amplitude and the steepest slope in oxyhaemoglobin and deoxyhaemoglobin responses in the general population.

2.2.5 State-Dependent Measures

The neurophysiological tests described above tend to be costly and difficult to administer as a diagnostic test. The PGT is an easy to use clinical tool but, like some of the physiological measures, it may be state dependent – varying with migraine phase (Wilkins et al., 1984). Such state measures are useful for judging if an individual is suffering from visual hypersensitivity at a particular moment in time but may be poor measures of their general tendency to suffer hyper-perception. Hypersensitivity results in distortions of the visual image, which can be disruptive for everyday tasks such as reading and can cause discomfort in everyday environments. Based on these and other symptoms, Conlon and colleagues developed a 23 item questionnaire (Visual Discomfort Scale - VDS; Conlon, Lovegrove & Pattison, 2010) for which scores correlate positively with headache severity and visual distortions when viewing square wave gratings (similar to the pattern-glare (PG) stimuli) and letter stimuli; and negatively with reading speed and performance on the digit symbol sub-test from the revised Wechsler Intelligence Scale for Children (WISC-R). In an attempt to address cortical hyper-excitability more broadly, if still indirectly, Braithwaite et al. (2015) developed the Cortical Hyper-Excitability index (CHi), a 27-item questionnaire in which symptoms are rated for both intensity and frequency of occurrence; although these scores can be merged. Both the VDS and CHi can be regarded as trait

measures of cortical hyper-excitability in that they measure the proneness of the participant to episodes of hyper-excitability based on their previous experience.

Cortical hyper-excitability is not limited to those who experience migraines. Stimuli that are disruptive for migraine sufferers are also triggers for those with photosensitive epilepsy (Adjamian et al., 2004; Wilkins et al., 1984). Further, visual hypersensitivity as observed with the PGT or similar metrics is co-morbid with a range of conditions including multiple sclerosis (Wright et al., 2007), stroke (Beasley & Davies, 2012), autism (Kientz & Dunn, 1997), and dyslexia (Saksida et al., 2016). In many of these conditions, visual distortions in text inhibit reading but can be alleviated using coloured filters. Some have disrupted reading and high scores on measures of visual discomfort, hyper-excitability and PGT but few other symptoms. Wilkins and colleagues describe such individuals as suffering from *visual stress* and posit that this condition is separate from but co-morbid with other conditions – especially where there is no obvious brain injury (Wilkins, 2003). This overlap of symptoms may increase the generality of findings from the migraine literature; however, it does also suggest that when comparing patient and control groups to assess cortical hyper-excitability, some members of the control group may have some degree of latent hyper-excitability. This possibility can be countered by recording several measures of hyper-excitability as possible covariates for analysis, rather than relying on whether or not the participant is in the control or experimental group as the sole predictor of atypical neural activity.

In this study, participants were not selected based on their migraine or headache status; rather ERP and EEG results were correlated with scores on a range of headache and hyper-excitation measures within a single group drawn from the general population. We measured EEG responses to visual stimuli based on those used in the PGT in a novel paradigm where stimuli were repeated (flicked on and off) at a low temporal frequency allowing the recording of both ERPs and steady state

EEG, while also allowing us to consider habituation effects. Thus, we compared stimuli known to be aggravating in migraine with those that are less aggravating, in a paradigm that allows the separation of initial and habituated responses. State measures of discomfort in response to the PGT stimuli were also taken. We hypothesised that symptoms of headache, visual discomfort, cortical hyper-excitability and pattern glare would correlate with increased amplitude and abnormal timing of early ERP components at occipital electrodes and that this would manifest in part as a lack of habituation to repeated stimulation.

2.3 Materials and Methods

2.3.1 Participants

Forty undergraduate and postgraduate participants, recruited at the University of Birmingham, gave their informed consent and were compensated with £24 for participating. Participants with a history of psychiatric, psychological, and neurological conditions, or a history of unconsciousness, convulsions or epilepsy were excluded from the study. Migraineurs were included in the study. However, migraineurs were excluded if they experienced migraine with aura and smoked, if they used the contraceptive pill or if they experienced aura that lasted more than an hour. If aura lasted less than an hour, they were included.

One participant chose to leave the experiment, one was removed due to an equipment malfunction, one due to an artefact that could not be removed and three were removed during data pre-processing due to a lack of usable trials (fewer than 20% per condition). There were thus 34 usable datasets (male=13, female=21, mean age= 22.5y, range=18-32y, standard deviation=2.86). This study was approved by The Science Technology Engineering and Maths Ethics Committee at the University of Birmingham in adherence with The Declaration of Helsinki.

2.3.2 Stimuli and Equipment

We used stimuli similar to those used in PGT (Wilkins, 2001). Stimuli comprised horizontal square-wave gratings (contrast = 75%) at 3 different spatial frequencies (.37, 3, and 12 c/deg: described as thick, medium, and thin, respectively, see Figure 2.1) displayed in a circular window with diameter (15.2 deg). These stimuli were created in MATLAB using the Psychophysics Toolbox (Brainard, 1997; Pelli, 1997; Kleiner et al., 2007) and displayed on a Samsung 932BF LCD monitor (Samsung Electronics, Suwon, South Korea).

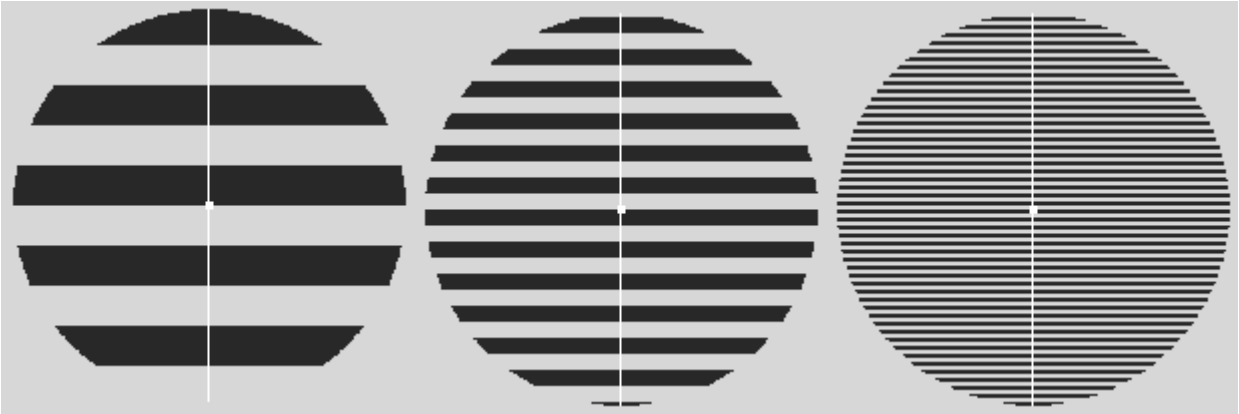

Figure 2-1. Pattern-glare stimuli
Left to right, thick (.37 c/deg), medium (3 c/deg) and thin (12 c/deg) gratings with a central fixation and vertical dividing line. The images shown here are representative of the stimuli but have been rendered to aid visibility in print.

Questionnaires were used to assess participants' headache history (Headache and General Health Questionnaire, HGHQ) and tendency to suffer visual stress (Cortical Hyper-Excitability index (Chi), Braithwaite et al., 2015; Visual Discomfort Scale (VDS), Conlon et al., 1999). EEG recordings were made using a 128-channel BioSemi (University of Amsterdam) EEG system in a dark, quiet room.

2.3.3 Procedure

After the EEG electrodes had been applied, participants began the experiment with a 5-minute resting period and then were presented with three blocks, each containing six trials for each of the three stimuli. Thus, each participant observed 18 trials per stimulus type. Each trial contained between seven and nine onsets of the same stimulus each lasting three-seconds followed by a variable interval of 1 – 1.4 seconds. We later averaged across onsets 2-8 thus increasing the effective trial count in that analysis. After each trial, the participant was asked to rate how discomforting they found each stimulus on a 5-point scale (1 = no discomfort, 5 = extreme discomfort) and to indicate how many onsets they saw. This additional task was designed to ensure attention to the stimuli. Due to ethical concerns, participants had the option to turn off stimuli by pressing a key; only three did so, and then only once each. At the end of each block, participants were shown the three stimuli in turn and asked to rate the extent to which they had experienced a range of possible pattern glare symptoms (Wilkins et al, 1984). After each block and at the end of the experiment, participants had a further resting period of 5 minutes, during which they were requested to close their eyes and relax. They were also asked if they were willing to continue at each break. Stimulus order and number of onsets per trial were counterbalanced (subjecting them to variation, increasing interval validity) (Allen, 2017).

2.3.4 Discomfort ratings and questionnaires

Working with the 39 participants who completed the study, we computed mean discomfort ratings for each participant and stimulus type across the three blocks. Discomfort ratings tend to co-vary across the stimulus types, so we computed a discomfort index for each participant by dividing discomfort ratings for the medium stimulus by the mean of the thick and thin ratings. High scores on this index identify those participants who find the medium stimulus relatively discomforting compared to the two control stimuli. Overall scores for the CHi and VDS were computed according to the instructions for

those tools. Finally, data for headache frequency, intensity and duration and the experience of sensory aura were extracted from the headache and general health questionnaire (HGHQ). These seven measures have very different ranges, so we standardized each variable before entering them, which identified 3 factors based on a Scree plot analysis. Following a Varimax rotation, the three factors were identified as visual stress (predominantly a combination of the CHi, VDS and aura), headache (frequency, intensity and duration) and discomfort (discomfort index). This factor structure is not surprising given the nature of the variables included, but the analysis also served to provide uncorrelated factors to aid the subsequent mass univariate analysis (MUA). Factor scores were computed using the regression method from coefficients shown in Section 2.9.1 of the Supplementary Materials, where we also describe the factor analysis in more detail.

2.3.5 ERP pre-processing

We decimated the EEG data from a sampling rate of 2048Hz to 512Hz using the BioSemi toolbox. EEGs were then band-pass filtered using a second-order Butterworth filter with a pass band of 0.1 to 30 Hz (½ power -3dB, fall-off at 12 dB per octave; for prior precedent for this choice, see Luck, 2014; Tanner et al., 2015). Data for each onset were epoched between -200 and 1200ms relative to stimulus onset, referenced to the average of all electrodes and baseline corrected based on the 200ms period prior to stimulus onset. Eye-blink artefacts were removed using independent component analysis (ICA), with ICA components associated with eye blinks removed and the dataset reconstructed. The crown electrodes were removed to further reduce the presence of muscle and eye-movement artefacts (Chennu et al., 2013), in line with previous work (Shirazibeheshti et al., 2018) who argue that this additional noise may confound mass univariate analysis (MUA) (explained in the next section) (electrodes removed = A11, A12, A13, A14, A24, A25, A26, A27, B8, B9) and the data referenced to the new electrode set (see figure 1-13 for full electrode cap). Data for individual onsets

were then deleted if any channel exceeded a +/-100 μV threshold, thus removing large artefacts such as movement. The data for each participant were split into 27 bins, one for each stimulus type (thick, medium or thin) and Onset number (1 to 9). Finally, we discarded data from Onset 9 - the number of onsets varied between 7 and 9 on each trial, so the occurrence of the 9th Onset was rare, making these data unreliable. Tallying across onset number, three participants who did not have at least 20% of usable stimulus repeats per stimulus type were removed (decided a priori, based on Luck, 2014). In addition, one participant was removed because an artefact could not be removed, and a further participant was removed because they had EEGs that were flat (i.e. equipment malfunction). For interpolation, approximate values between electrodes from biosemi and the internal SPM grid were mapped together, when the electrode locations from EEGLAB were combined with the SPM software. This enabled the interrogation of positions on the scalp beyond the electrode locations. In order to compare stimulus onset with habituation-effects, we divided the repeated onsets into two groups. We drew a logical distinction between the first stimulus onset in each trial (where the observer was unaware of the stimuli to be presented) and the remaining onsets (where the participant was able to anticipate the stimulus) and thus analysed Onset 1 separately from Onsets 2-8; the latter being combined so as to aggregate over the maximum number of onsets.

2.3.6 Mass Univariate Analysis

A mass univariate analysis (MUA) is the analysis of a large number of simultaneously measured dependent variables (e.g. voxels or samples) via the performance of the same univariate hypothesis tests (e.g., t-tests) across all of those dependent variables. This method allows for powerful error corrections for multiple comparisons.

An MUA was conducted in SPM-12 (Wellcome Trust Centre for Neuroimaging, London, England) on three dimensional images (two of space, one of time) derived from the ERP data. To

control for multiple comparisons, we use a family-wise error (FWE) correction. Images were created using the data for each stimulus type (thick, medium, and thin), which is a response to EEG. Images are the file type used in the SPM data matrices in order to perform analysis of models or statistical tests. Statistical analyses of M/EEG data in SPM use the same mechanisms as all other data types (PET, fMRI, and structural MRI in voxel-based morphometry ((VBM)).

This simply requires transforming data from SPM M/EEG format to image files (see NIfTI format, http://nifti.nimh.nih.gov/nifti-1/). The result of statistical inference is a summary statistic image, an image representing the data feature summarising treatment effects that one wants to make an inference about. More formally, when this summary statistic is itself a maximum likelihood estimate based on within-subject data, the analysis is called a summary-statistic procedure for random-effects models (Litvak et al., 2011).

In the context of this paper, we will be regressing the dependent variable (the EEG data) onto parametric regressors (the factors). Consequently, our summary statistic images reflect the extent to which the dependent variable correlates with the factor, as reflected in beta coefficients and one-sample t-tests exhibiting a difference from zero.

A contrast image was created based on what we call the pattern glare index (PGI). This index enables us to focus our analysis on regions of the data volume where the clinically relevant, medium stimulus exhibits an extreme response relative to the thick and thin stimuli.

PGI = (medium image – average (thick image, thin image)).

Then, we used the factor scores derived from the factor analysis as parametric regressors in the MUA, excluding factor scores from the five participants whose ERP data failed our screening tests.

This analysis focused on the evoked response generated by a stimulus onset, which will be strongest at posterior regions of the scalp. To do this, we limited our analysis in two ways. First, we calculated an overall window of analysis in time considering only that portion of the grand average ERP waveform that deviated from baseline. This window was used to seed the subsequent region of interest (ROI) analysis. Second, we calculated two 3D ROIs in order to capture the P1 and subsequent ERP features that are central to our hypotheses.

The initial window of analysis was calculated as follows. ERPs are typically characterised by a series of positive and negative excursions from baseline, which correspond to the stimulus-evoked onset transients before the time series settles back and we wanted to capture only this period. To do this, we focused on the aggregated average (Brooks et al., 2017) across the three stimulus conditions (for Onsets 2-8). ROIs can be identified on the aggregated average, without inflating false-positive rates, since it does not reflect condition (i.e. stimulus) differences, which for us amounts to the PGI (Brooks et al., 2017)[1]. However, an initial inspection of our data revealed that the aggregated average did not settle back to baseline but rather fell to a constant, positive direct current (DC) level (a stable baseline shift). Thus, working with the aggregated average at electrode A23 (Oz), we captured the period from the first significant deviation from baseline (zero) until the aggregated average finally fell to below significance compared to the DC level. We first calculated the DC level from a period of 400ms duration taken well after the end of the evoked transients. We took the mean value of all participants over this period. The window of analysis was then found by calculating confidence

[1] Indeed, it is straightforward to show that the aggregated average and the PGI are orthogonal: the dot product of the corresponding contrast vectors, [1/3,1/3,1/3] for the aggregated average and [1,-1/2,-1/2] for the PCI, is equal to zero.

intervals across participants at each time point weighted by the number of valid trials[2]. We used the following equations for the weighted confidence interval (CI) at each time point:

$$\mu_\omega = \frac{\sum_{i=1}^{n} x_i . m_i}{\sum_{i=1}^{n} m_i}$$

$$\bar{m} = \frac{\sum_{i=1}^{n} m_i}{n}$$

$$\sigma_\omega = \sqrt{\frac{\sum_{i=1}^{n} \frac{x_i^2 . m_i}{\bar{m}} - n\mu_\omega^2}{n-1}}$$

$$C_{95} = \mu_\omega - \frac{t_{95,n-1}\ \sigma_\omega}{\sqrt{n}}$$

where μ_ω is the weighted mean, σ_ω is the weighted standard deviation, C_{95} is the confidence interval, n is the number of participants, $t_{95,n-1} = 1.7$ is the critical t value for a one-tailed 95% confidence interval, x_i is the value of the ERP for the *ith* participant, m_i is the number of valid trials for that participant, and $\underline{m}$ is the mean number of trials per participant. The lower CIs were compared to zero at the start of the ERP trace working forward and to the DC level at the end of the trace working backwards; yielding a window of analysis between 56-256ms. This time window was used in the MUA analysis of the factor intercept and to seed our second ROI.

We next constructed ROIs using two methods. Our first ROI targeted the P1 excursion and was based *a-priori* on the literature concerning this ERP feature (Bruyns-Haylett et al., 2017; Di Russo et

[2] This weighting generates the Aggregated Grand Average of Trials (Brooks et al, 2017), upon which regions of interest can be selected without inflating type-I error rates in the presence of trial-count asymmetry.

al., 2002; Vogel & Luck, 2000; Zhang et al., 2013) resulting in an ROI volume centred on co-ordinates x=0mm, y=-84mm, t=101ms with dimensions length = 92mm, width = 42mm, time = 62ms (for explanation see supplementary material). Note also that Adjamian et al. (2004) located MEG sources in response to similar stimuli in the occipital pole.

Our second ROI targeted the ERP components subsequent to P1. The best locations and time period to capture such features are less well determined in the literature, so we took a different approach using an orthogonal contrast to determine an ROI (Brooks et al., 2017). The key property that underlies the orthogonal contrast approach is that the contrast used to identify the ROI does not bias the contrast of interest under the null hypothesis. That is, under the null, statistically speaking, there is no sense to which the contrast of interest is more, or indeed less, likely to hold at the ROI than anywhere else in the data volume. Perhaps, the simplest orthogonal contrast approach to ROI selection is to average all conditions together, generating what is called the aggregated average. This is orthogonal to a typical contrast of interest over the conditions. In our context, the mean/intercept is orthogonal to any of the factors. We used our analysis of the factor intercept in the MUA (see results) to produce an ROI mask for further analysis; section "Further Justification of Window Selection" in the supplementary material gives further justification for the validity of this approach. To this end, we applied a *t*-threshold of 5.55 (which corresponded to $p<.001$) to the intercept image to capture a coherent space-time mask for our second ROI. In practice, this ROI captures posterior electrodes in the period of the N1 excursion.

Our statistical tests are one-sample t-tests, used to demonstrate that individual regression coefficients (for our factors and intercept) are statistically different from zero. Analyses of the mean/intercepts were run two-tailed, but, then, analyses over factors were run one-tailed. This is because the direction of the effect that defined the ROI (based on prior precedent for P1 and

mean/intercept for N1) governed the direction of interest for each factor effect. For example, if medium were largest for the mean/intercept, a positive correlation with a factor is the only theoretically plausible finding. This is because higher on the factor corresponds to a greater deficit, and our central hypothesis is that medium will induce a more extreme response from more impaired participants.

We did not perform statistical inference on our time-frequency plots. This is because any such analysis would be confounded by double dipping (Kriegeskorte et al., 2009), since we are interested in time-frequency features (including ROIs) that correspond to significant effects observed in our time-domain (ERP) analyses. Accordingly, we view our time-frequency analyses as explanatory, but the statistical robustness of our finding's rests upon our ERP analyses. A general linear model (GLM) analysis was performed on the data where the PGI over ERPs was the dependent variable, while the independent variables were the normalised factor scores of the trait and state data responses (which act as regressors). This same general linear model was fit to the ERP data at each time-space point in the data volume, providing beta parameter values for all the regressors (the intercept and three factors) at each such point. Intuitively, each parameter value indicates the extent to which the evoked response at the corresponding time-space point correlates (across subjects) with the relevant regressor. In this way, a mass univariate analysis is able to identify time-space regions in the data volume, which vary in a fashion consistent with a factor or intercept. Additionally, due to the mean centering of regressors, the intercept parameter is the mean of the evoked response at that time-space point.

2.3.7 Data Visualisation

MUA treats each factor as a continuous variable and looks for significant relationships between space-time maps and each factor. This approach produces space-time significance maps for the factors of concern but is limited for visualising the underlying ERPs. It also emphasises those participants who

score at the extremes on each factor. We therefore placed our participants into two groups for each factor based on median splits of the factor scores. We then derived weighted ERPs for each (median split) group based on the absolute deviation of the factor scores from the median (a positive scalar) for each participant multiplied by the amplitude at each timepoint in the ERP matrix. In this way, we scaled the ERPs according to the corresponding factor loadings in order to provide a visualisation that was more representative of the parametric regressor inferences of the MUA (see supplementary material for unweighted ERPs). These groupings differed between the factors.

2.3.8 Time-frequency analysis

We followed up our main MUA analysis with a time-frequency analysis to better understand the origin of one of our effects. To avoid edge effects (caused by the wavelet being partially outside the segment being analysed) during wavelet fitting, we expanded our EEG analysis window to include the -500 to 0 ms period. For each participant, we then examined amplitude (ie. power) and inter-trial phase coherence for frequencies in the range 5-40 Hz using 5-cycle morlet wavelets at 1 Hz intervals. Inter-trial coherence is a measure of the consistency of phase across trials. If a component presents at a similar phase on all trials, it means that there is a little variation in the latency of this component across replication, ie., there is little temporal jitter.

The results were then cropped between -100 and 800 ms, baseline rescaled using a logR ratio function to the (-100 – 0 ms) baseline window and then averaged. We present the results between 5 and 11 Hz. A further analysis of the lower frequencies used a 3-cycle wavelet to improve temporal resolution.

2.4 Results

In summary, MUA was nearly significant for Onset 1 (Figure 2.2) and MUA revealed significant space-time peaks in the factor intercept for Onsets 2-8 (Figure 2.3) as well as a significant cluster for Onset 1 on the discomfort factor (Figure 2.4) and a significant peak for Onsets 2-8 on the

headache factor. No other significant peaks or clusters were found and there were no significant effects on the visual stress factor.

2.4.1 Intercept effects

Figure 2.2 shows the results of the MUA for the factor mean/intercept for Onset 1 data only. Both unthresholded-*t* (A) and thresholded-*t* (B) maps are shown, where the latter shows a nearly significant effect, p=.054 [two-tailed] (which corresponds to $t(30)$ =5.37, p=.027, one-tailed), family-wise error (FWE) corrected at the peak-level, at around 180ms and centred at Oz. Panel C shows standard grand averages (in this case unweighted) for thick, medium and thin at this electrode. Recalling that the MUA analysis was conducted on the PGI (not raw ERPs), the nearly significant excursion in this index occurred in the N1 period, where thick and thin exhibit a minimum whereas medium undergoes what appears to be an early P2 deflection.

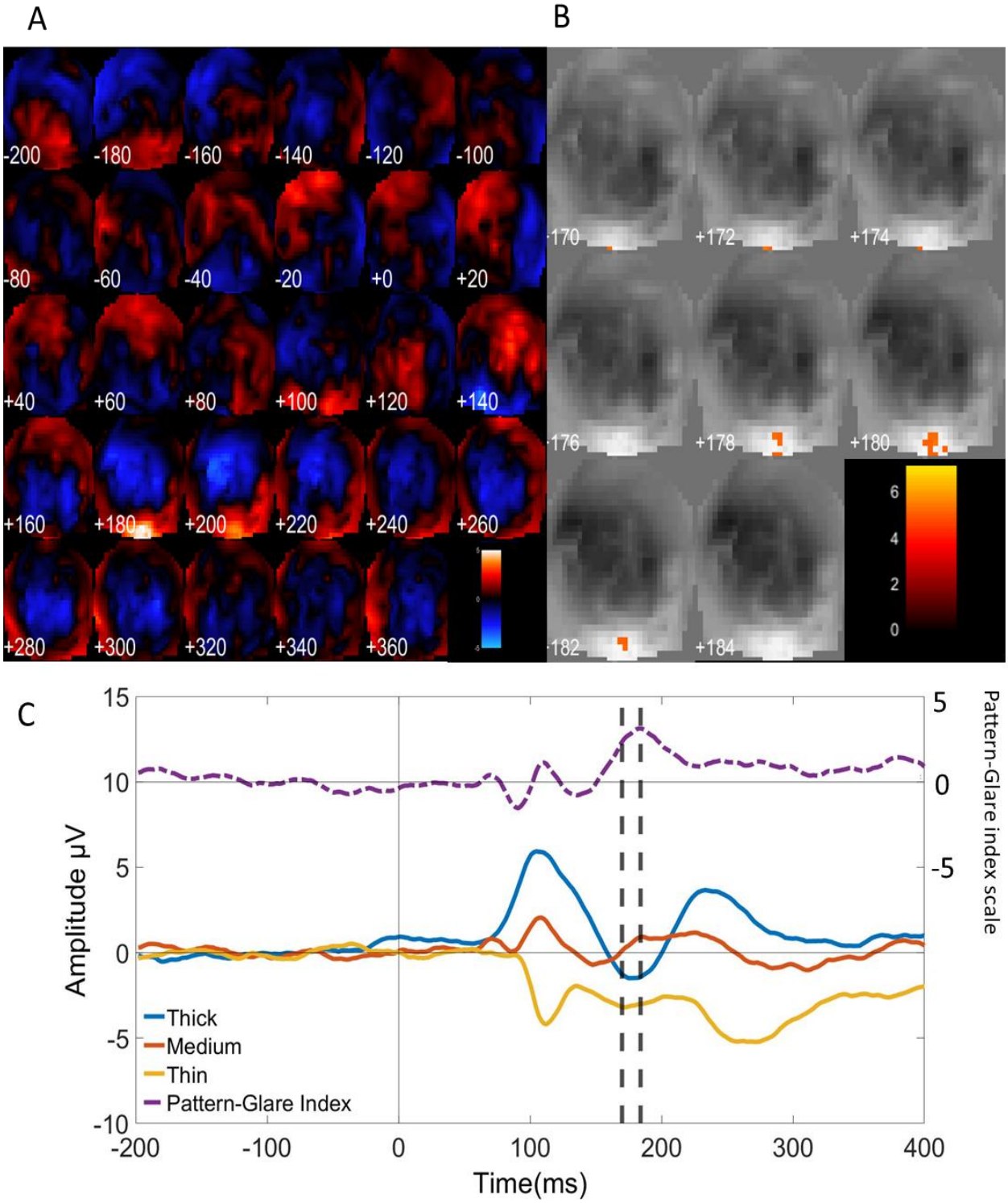
A
B
-200
-180
-160
-140
-120
-100
-80
-60
-40
-20
+0
+20
+40
+60
+80
+100
+120
+140
+160
+180
+200
+220
+240
+260
+280
+300
+320
+340
+360
170
+172
+174
176
+178
+180
182
+184
6
4
2
0
C
15
10
5
0
-5
-10
Amplitude μV
-200
-100
0
100
200
300
400
Time(ms)
Thick
Medium
Thin
Pattern-Glare Index
5
0
-5
Pattern-Glare index scale

Figure 2-2. Topographic maps with (one-tailed) t-values over pattern-glare index and ERPs for Mean/intercept Onset 1.

One-sample t-values are shown to enable the polarity of effects to be seen. A) Topographic maps that represent unthresholded t-values for Onset 1 from -200 to 380ms in 20ms intervals; scale is t-values from -5 to 5. B) Thresholded (FWE corrected at the peak-level) SPM maps from 170-184ms in 2ms intervals; the scale is t-values 0 to 7. C) ERPs representing Onset 1 for medium, thick, and thin at electrode Oz, which approaches significance two-tailed. The PGI was added to the plot with a +10 increase to amplitude. Vertical lines show start and end of significant effects. Positive is plotted up.

MUA intercept results for Onsets 2-8 showed a significant peak at 179ms at Oz $p<.001$[two-tailed] (which corresponds to t (30) =8.94, $p<.001$, one-tailed) FWE corrected at the peak-level (Figure 3). Interestingly, the ERP for Onsets 2-8 (Panel C) appears elevated relative to that for Onset 1 (Figure 2.2, Panel C), perhaps due to smaller N1 components. The late DC shift referred to above is also visible from around 350-400ms in the ERPs for thick and medium stimuli for Onsets 2-8.

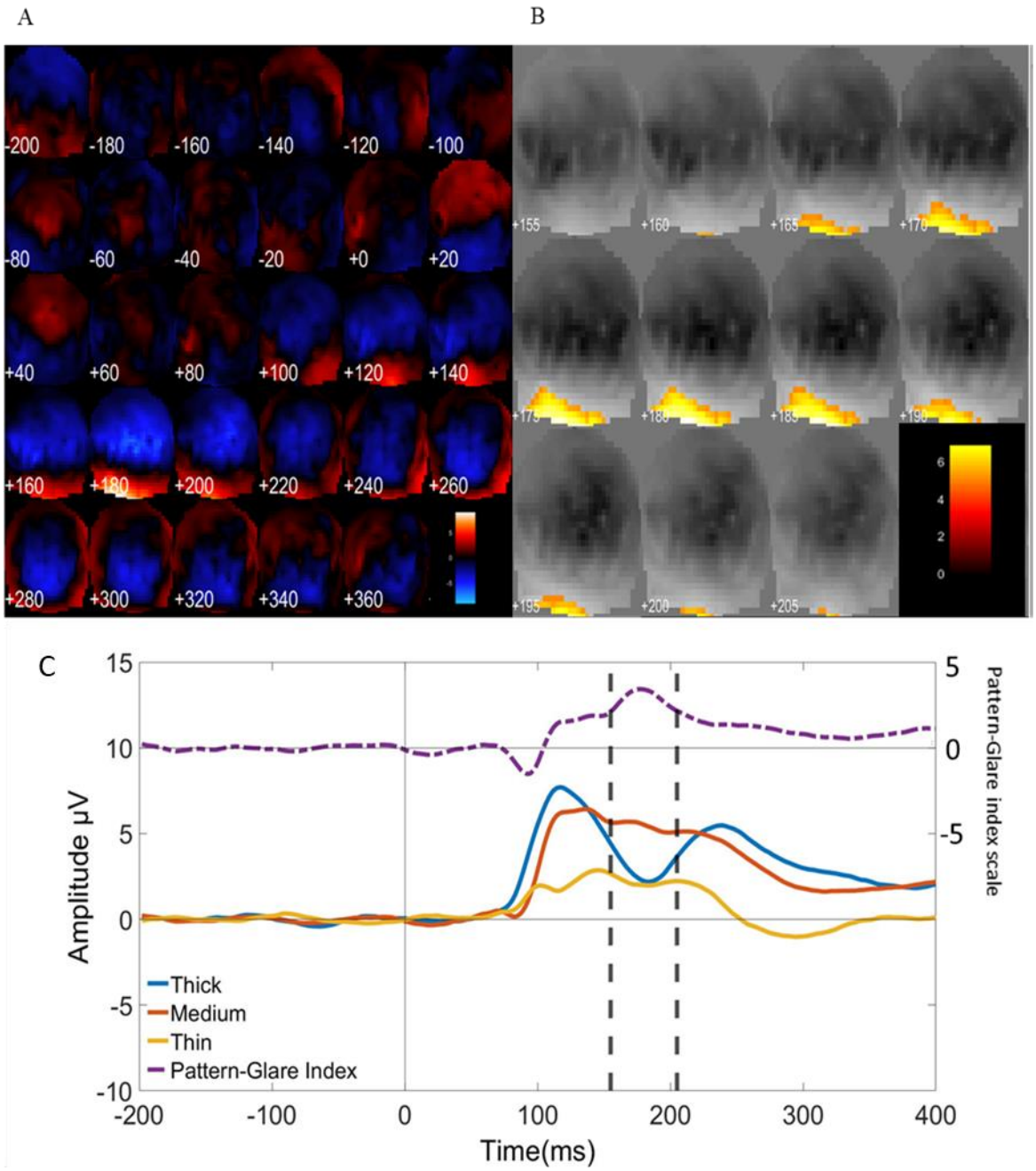
A
B
-200
-180
-160
-140
-120
-100
-80
-60
-40
-20
+0
+20
+40
+60
+80
+100
+120
+140
+160
+180
+200
+220
+240
+260
+280
+300
+320
+340
+360
+155
+160
+165
+170
+175
+180
+185
+190
+195
+200
+205
6
4
2
0
C
15
10
5
0
-5
-10
Amplitude µV
5
0
-5
Pattern-Glare index scale
Thick
Medium
Thin
Pattern-Glare Index
-200
-100
0
100
200
300
400
Time(ms)

Figure 2-3. Topographic maps with (one-tailed) t-values upon pattern-glare index and ERPs for mean/intercept, Onsets 2-8.

One-sample t-values are shown to enable the polarity of effects to be seen. A) Unthresholded topographic maps that represent t-values for Onsets 2-8 from -200 to 380ms in 20ms intervals; scale is t-values -9 to 9. B) Thresholded (FWE corrected at the peak-level) topographic maps; scale is t-values from 0 to 7. C) ERPs representing Onsets 2-8 for medium, thick, and thin at Oz electrode (the location of the significant cluster). The PGI was added to the plot with a +10 increase in amplitude. Vertical lines show the start and end of significant effects. Positive is plotted up.

2.4.2 Factor effects

Figure 2.4 shows the MUA results for Onset 1 on the discomfort factor based on the a-priori P1-ROI revealing two significant (FWE-peak corrected, with small volume correction) peaks at 97ms (Panel A) centred on electrodes A20 (Panel B; $t(30)=4.31$, $p=.027$, one-tailed) and A8 (Panel C; $t(30)=4.17$, $p=.036$, one-tailed). Comparing participants above and below the median value on the discomfort factor both electrodes show a marked P1 component for medium frequency stimuli that is present in the high-discomfort group but not those low on the factor. High discomfort is associated with a strong P1 peak for the first appearance (Onset 1) of medium stimuli.

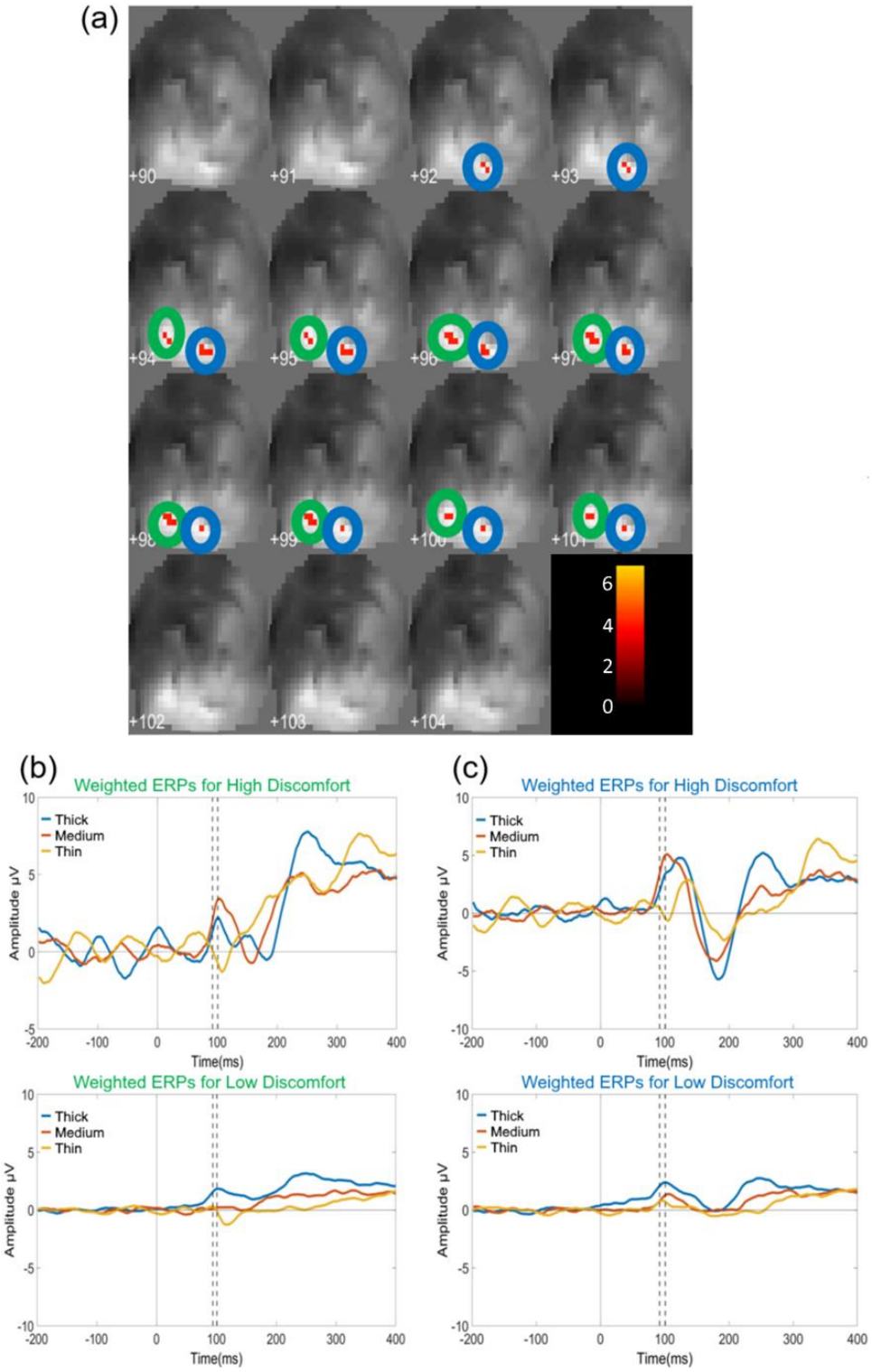
(a)
+90
+91
+92
+93
+94
+95
+96
+97
+98
+99
+100
+101
+102
+103
+104
6
4
2
0
(b)
Weighted ERPs for High Discomfort
Thick
Medium
Thin
Amplitude μV
Time(ms)
Weighted ERPs for Low Discomfort
(c)
Weighted ERPs for High Discomfort
Weighted ERPs for Low Discomfort

Figure 2-4. Topographic Maps with (one-sample, one-tailed) t-values on PGI using a ROI analysis and weighted ERPs at the significant electrodes for discomfort factor scores for Onset 1.

A) Thresholded (FWE corrected at the peak-level) topographic maps, using a ROI analysis derived a priori from the literature for 90-105ms, shown here in 1ms intervals. Scale represents t-values from 0 to 6. B & C) Weighted ERPs at the significant electrodes for the discomfort factor A20 (Green(B)) & A8 (Blue(C)) at the corresponding significant points in each cluster in Panel A. Vertical dashed lines show start and end of significant effects. Positive plotted up.

Figure 2.5 shows the MUA results for Onsets 2-8 on the headache factor based on the orthogonal contrast N1-ROI. We found a small but significant cluster (FWE peak-level corrected, with small volume correction; $t(30)=3.34$, $p=.047$, one-tailed) centred at electrode A29 (Figure 2.5) comprising 4 voxels but lasting over 22ms from 155-177ms with a peak at 173ms. ERPs (see Panel B) suggest that either the N1 deflection is missing for the medium stimulus in the high-headache group or that the P2 is accelerated and perhaps somewhat variable in latency in the high group. We explored these two possibilities further using a time-frequency analysis. ERPs were re-baselined over a 500ms period (to allow a broad wavelet) prior to stimulus onset and subjected to time-frequency analysis based on a wavelet size of 5 cycles to reveal changes in power and inter-trial phase coherence over time across a range of EEG frequency bands. As time-frequency analysis calculates average power and inter-trial phase coherence across trials and participants, an absence of N1 at the trial level would likely result in reduced theta band power for the high-group with medium stimuli. This is because theta is the dominant band for the P1-N1-P2 complex. In contrast, if the apparently weak N1 were due to variability in the timing of P2, we would expect power to be unaffected but inter-trial phase coherence to be weak in this time-period.

A

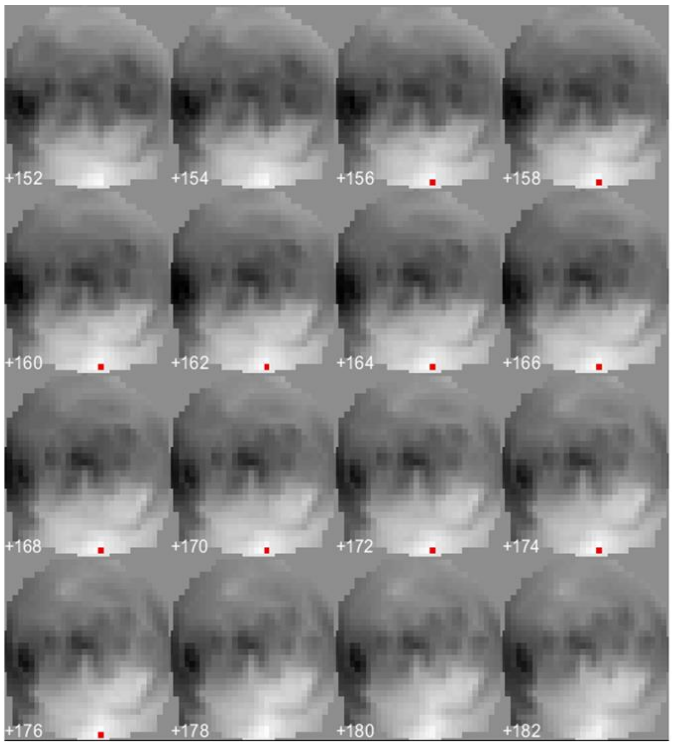
+152
+154
+156
+158
+160
+162
+164
+166
+168
+170
+172
+174
+176
+178
+180
+182

B

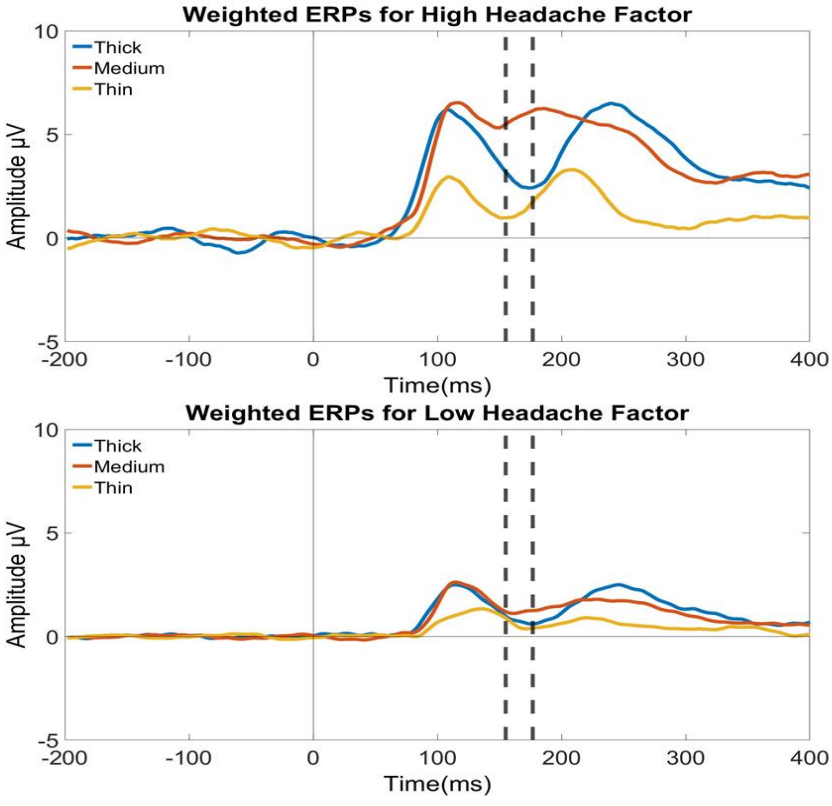
Weighted ERPs for High Headache Factor
Thick
Medium
Thin
Amplitude µV
Time(ms)
Weighted ERPs for Low Headache Factor
Thick
Medium
Thin
Amplitude µV
Time(ms)

Figure 2-5. Topographic maps of (one-sample, one-tailed) t-values and ERPs using an orthogonally derived mask from the mean/intercept of Onsets 2-8.
A) Thresholded (FWE corrected at the peak-level, small volume corrected) t-value maps for length and frequency of headaches from 152ms to 184ms in 2ms intervals; scale is t-values from 0 to 6. B) Weighted ERPs derived from a median split on headache parameters, which was at electrode A29 in the significant cluster.

Figure 2.6 shows time-frequency power plots for the high-headache group for the three stimuli. We have marked the ROI in the relevant power plots in Figure 2.6. Power is about as high for the medium stimulus in the theta band (around 7Hz) as for the thick stimulus. That is, the power plots for thick and medium stimuli are similar, despite the lack of visible N1 in the medium ERP. Figure 2.7 shows inter-trial phase coherence plots for the high (Figure 2.7 Panels A, B, C) and low (Figure 2.7 Panels D, E, F) groups for each type of stimulus. Phase coherence in the theta band in the relevant window is similar for the thick and medium stimuli in the low-headache group, but weaker for medium stimuli than thick in the high-headache group, suggesting that temporal jitter (Chennu et al., 2009) in the timing of the P2 is responsible for the altered ERPs. Jitter refers to variations of phase cycle in time, reflecting changes between trials in latency.

Another way of thinking about this would be that for those high on the Headache factor, in the relevant time window, the medium condition is exhibiting an induced response (i.e. high power, but less locking to the stimulus), while the thick condition is exhibiting a more typical evoked response (i.e. high power, with strong stimulus locking). The fact that there is low phase consistency across trials at the relevant time-frequency point for thin stimuli does not confound our argument. That could simply be explained by the lower power for thin, which would cause a

loss of inter-trial coherence because the noise in the data has a greater impact on the measurement of phase, when the signal has low amplitude (Chennu et al., 2009).

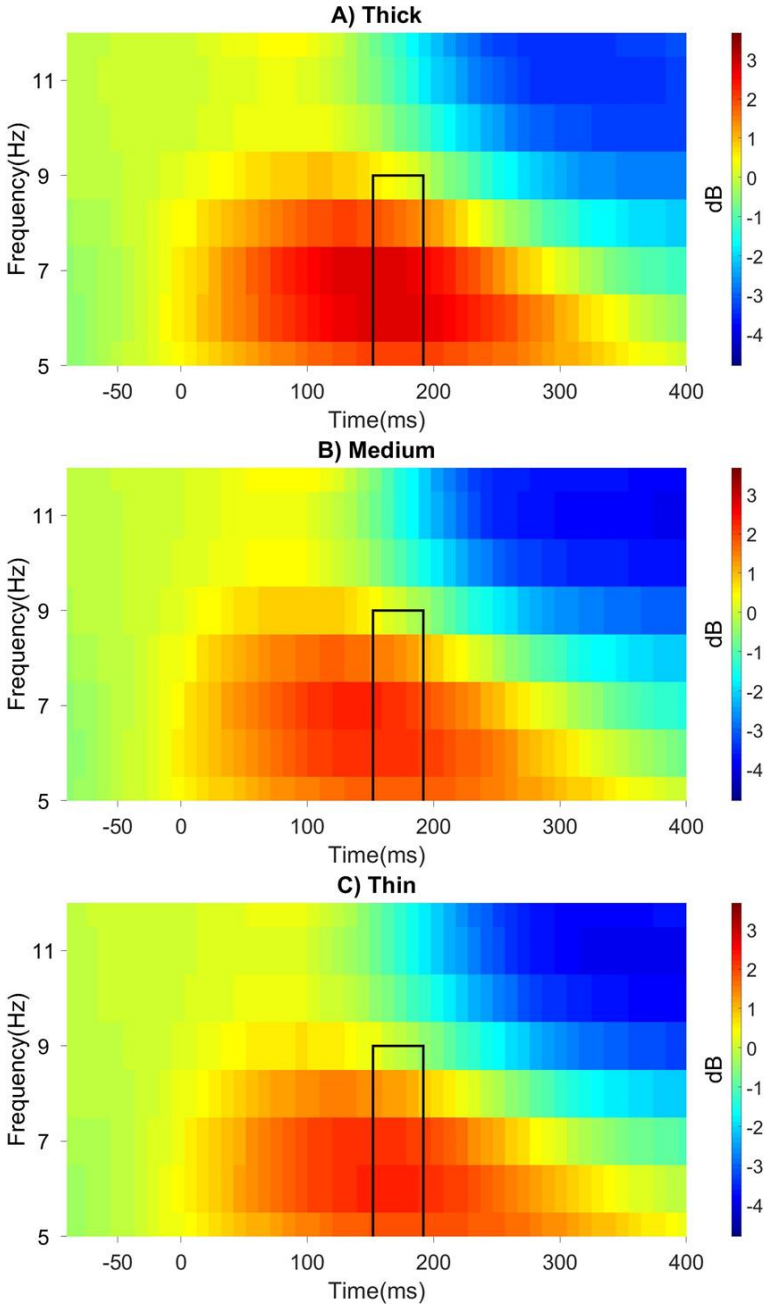

Figure 2-6 Time-frequency analysis for those high on the headache factor.

Power as a function of oscillation frequency and time is shown: A) Thick stimulus, B) Medium stimulus and C) Thin stimulus at electrode A29. Colours represent power in dB, which was calculated using a 5-cycle wavelet. Box shows window of interest based on significance window for headache factor from the time-domain.

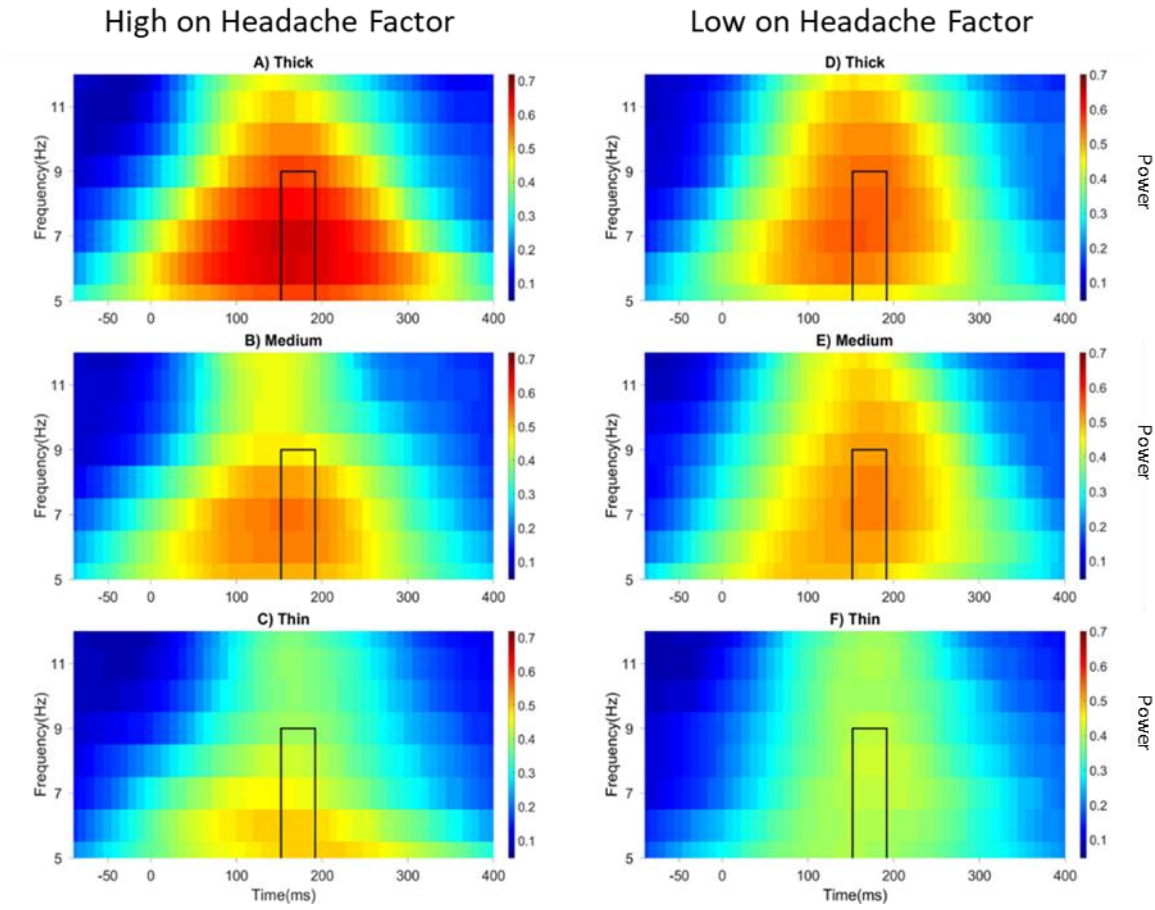

Figure 2-7. Time-frequency analysis for those high (left) and low (right) on the headache factor, showing inter-trial coherence as a function of oscillation frequency over time for Onsets 2-8: A, D) Thick stimulus, B, E) Medium stimulus, C, F) Thin stimulus at electrode A29. Colours represent inter-trial coherence, calculated using a 5-cycle wavelet. Box shows window of interest based on significance window for headache factor from the time-domain.

We decided that the initial analysis would be to see what difference we are observing in power between medium and thick, where thick is showing a strong oscillatory pattern. We noticed that the inter-trial coherence in thick was stronger than for medium in those high on headache Factor. We therefore constructed a confirmatory analysis in which we averaged before doing the power analysis, which gives us a better insight into what is going on at the ERP level.

To provide converging evidence for our jittered-P2 hypothesis for the high headache group's response to the medium stimulus, we conducted a power analysis on the grand averages. That is, we computed power after averaging rather than before. We would now expect to find a drop-in theta power for medium relative to thick at the relevant time period despite the absence of such a dip in the normal power-plot of Figure 2.6. Using a smaller 3-cycle wavelet (which improves temporal resolution but reduces frequency resolution) we indeed observe a loss in theta power at around 185ms as expected (see Figure 2.8).

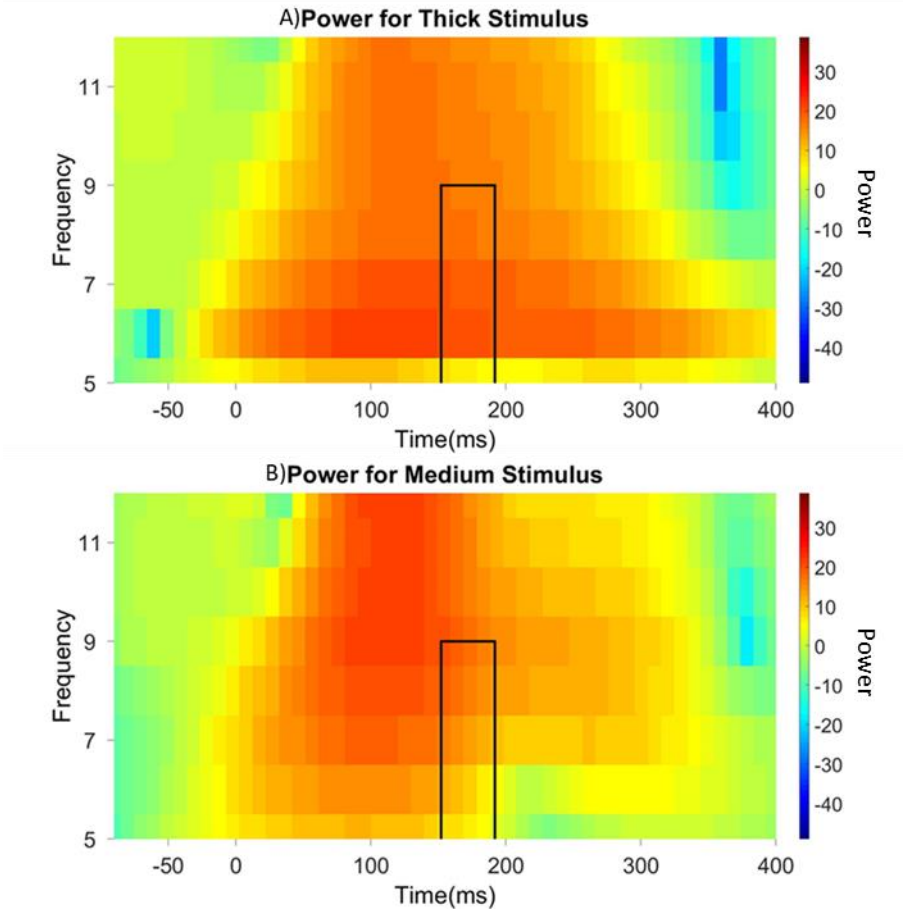

Figure 2-8. Time-Frequency plots for those high on the Headache factor on grand averages, A) Thick stimulus and B) Medium stimulus at electrode A29, analysed with 3 cycle wavelets. Box shows window of interest based on significance window for Headache factor from the time-domain.

2.5 Discussion

Migraine and tension headaches represent a major cause of disability and lost potential in the working age population. A better understanding of the neural factors that are associated with headaches may help to reduce their impact. Migraineurs are known to be sensitive to striped stimuli of a particular mid-range spatial frequency. In the present study, we considered evoked responses to such stimuli in the general population and related them to three factors: visual stress,

a tendency for headaches, and discomfort in response to aggravating stimuli. These factors were, by construction, uncorrelated. We found significant effects for the headache and discomfort factors operating at different times in terms of stimulus presentation and on different components in the ERP. Both these effects are new and would benefit from replication: while both are clearly significant (p=.027 and p=.036), even samples of size 34 (which is a good size for neuroimaging) are subject to substantial error (Lorca-Puls et al., 2018).

The state measure discomfort showed a significant effect only for the first presentation of the stimulus (Onset 1), suggesting that this factor may relate to the initial response to a new stimulus. The second factor combined headache frequency, intensity and duration and was associated with significant effects only for subsequent presentations of the stimulus (Onsets 2-8), suggesting that this factor relates to habituation. The separation between these effects across factor, time (from stimulus onset) and electrode sites suggests that they represent distinct physiological phenomena in the way the first stimulus presentation and the remaining onsets are processed. We will discuss these effects more fully below after discussing the stimulus driven effects that were not factor dependent.

2.5.1 Stimulus driven / factor intercept effects

Importantly, the mean/intercept effect for Onset 1 only approached significance (two-tailed, p=.054). Thus, at present, this effect needs to be treated with caution. This said, we have included the effect, since it somewhat mirrors what we see for Onsets 2-8, which is a more highly powered condition (as it involves many more trials), affording it some face validity. When looking at the mean intercept of both Onset 1 and Onset 2-8 trials, the most salient feature is that the window of time and position of the effect is similar for both subdivisions of trials, which suggests some sort of underlying connection. The P2 elicited by Onset 1 (see Figure 2.2) seems

to be accelerated in the medium condition relative to the thick/thin conditions, and visually there is attenuation of N1 in Onsets 2-8 for medium stripes relative to thick (see Figure 3), which could also relate to an accelerated P2. The similarity between this result for all participants and the N1-P2 effects found for the high-headache group on Onsets 2-8 only (see Figure 2.5 and later) is striking. This may suggest that the effect is driven by the medium stimulus regardless of participant characteristics but is accentuated in the high-headache group. The visual N1 is considered important in modulating spatial attention (Mangun, 1995; Hillyard et al., 1998) and discriminative processing (Ritter et al., 1979; Vogel & Luck, 2000; Hopf et al., 2002). However, one explanation to account for a reduction of the N1 attentional effect in sequences of bilateral stimuli (Heinz et al., 1990) is that physiological refractoriness due to the stimulus repetition might reduce the N1 amplitude (Luck et al., 1990). Additionally, N1 is affected by stimulus properties such as brightness of stimulus and intensity (Munte et al., 1995; Carrillo-De-La-Peña et al., 1999), although N1 amplitude is generally higher for stronger stimuli. We will return to this point when discussing the visually weak N1 component found for our high-headache group.

2.5.2 Discomfort

The discomfort factor reflects a state measure of how comfortable (low scores) or discomforting (high scores) participants found the medium stripes relative to the other stimuli during the course of the experiment. We found a stronger P1 for the high-discomfort group compared to low-discomfort in response to the medium striped stimuli (see Figure 2.4). Specifically, for the high-discomfort group, the medium stimuli elicited stronger P1 than the other stimuli. This was not so for the low-discomfort group. This supports our hypothesis that medium stripes would elicit significantly different early ERP components compared to thick and thin, but only in individuals showing evidence of visual sensitivity. Strong occipital P1 has been associated

with higher luminance suggesting that stronger stimuli may elicit a stronger P1 at posterior electrodes (Munte et al., 1995; Carrillo-De-La-Peña et al., 1999). In the context of our study, those with cortical hyperexcitability may respond more strongly to certain stimuli (particularly those that are aggravating) as if they were presented at higher strength. This group might also be more likely to find those stimuli discomforting. Thus, hyperexcitability alone could produce the enhanced P1 in the high-discomfort group. In addition, P1 is associated with spatial attention (Luck et al., 1994). In particular, P1 is reduced for unattended stimuli (Mangun & Hillyard, 1991; Van Voorhis & Hillyard, 1977; Munte et al., 1995). Therefore, in our experiment, the lack of P1 in the low discomfort group may also be because these participants were able to quickly shift attention away from this aggravating stimulus, thus avoiding discomfort. In contrast, the high-discomfort group may have been unable to withdraw attention from the medium stimulus.

Our P1 differences are specific to the first Onset; that is the initial presentation of each stimulus type in a series of repeated presentations. Noting that the P1 has been associated with surprise (Utama et al., 2009; Lassalle & Itier, 2013), it seems likely that even the high-discomfort group are able to ignore or attenuate the impact of the medium stimulus when they are expecting it to occur – in this group at least, habituation of P1 is effective.

2.5.3 Headache

The headache factor is a trait measure recording the participant's proneness to long, intense and frequent headaches. The high-headache group shows an abnormal N1 for the medium stimuli in Onsets 2-8. This may be due to an absent or attenuated N1 or an accelerated and temporally unreliable P2. Our time-frequency analyses suggest that the P2 account is more likely, but we cannot dismiss the N1 account entirely. Here, we briefly outline the implications of an attenuated N1 before discussing P2 more fully.

The low-headache group showed a strong N1 component for medium stimuli, but the high-headache group showed a slight opposite polarity deflection in the same period in weighted ERPs (see Figure 2.5B) and a reduced amplitude N1 in the unweighted ERPs (supplementary material). At first sight, this result appears opposite to that of Fong et al (2020) who found migraine sufferers to have more negative ERPs around 200ms (equivalent to our N1). However, they did not use repeated onsets and so could not have revealed our positive going effect for Onsets 2-8 (see supplementary material). Occipital N1 is also linked to stimulus intensity (Munte et al., 1995), with higher-amplitude and shorter latencies associated with stronger stimuli. The amplitude of the occipital N1 has also been linked to attention; with a stronger N1 at attended locations (Luck et al., 2000). Thus, assuming a link between cortical-hyperexcitability and headaches, neither a hyperexcitability account nor failure to withdraw attention would account for low N1 amplitudes in our high-headache group. However, in the auditory domain, reduced N1 amplitude has been associated with repetition suppression (Hsu et al., 2014). It is possible then that the high-headache group is successful in suppressing the repeated medium stimuli whereas the low-headache group do not feel the need to suppress this stimulus as, for them, it may be weaker in the first place. This would imply that the high-headache group habituates to the medium stimulus. There is conflicting evidence in the literature showing both that those with migraine fail to habituate to repeated stimulation of the same stimulus (Schoenen et al., 1995; Brighina et al., 2016) and conversely that habituation may be present in migraineurs (Omland et al., 2013;2016). However, this habituation account seems unlikely in the light of the time-frequency analysis described above and discussed next.

Our time-frequency analysis suggests that EEG power is relatively stable between the medium and thick stimuli in all frequency bands and in particular in the theta band over the

period of time for which ERPs for the two stimuli most differ in the high-headache group (see Figure 2.6). Reduced theta power, as might be associated with an absent N1, does not explain our data. However, inter-trial phase coherence is reduced for the high-headache group viewing medium stimuli during the critical period around 165ms after stimulus onset. This suggests that theta phase coherence (locking) may be weak in this group for this stimulus. Inter-trial theta phase coherence has been associated with the P2 component (Freunberger et al., 2007) and it is possible that variability in the timing of the P2 component, from trial-to-trial or between participants, spreads this component in time, masking the N1 in the ERP. We now further explore the role of the P2 component.

The P2 component has been associated with a number of top-down attentional tasks such as visual search (Luck & Hillyard, 1994). This association with top-down processing makes modulations of P2 an unlikely candidate in our study where the attentional load is minimal. However, we note that variations in P2 latency have been found across a range of conditions where neural inhibition is potentially compromised, including ADHD (Johnstone et al., 2009), schizophrenia (Shin et al., 2010) and ageing (Bourisly & Shuaib, 2018). Mostly, P2 onset is delayed in these conditions, which would not compromise the N1 region, but we note first that our high-headache group may not all have been migraineurs and second that migraine is not necessarily associated with poor inhibition but rather with an imbalance between excitation and inhibition. For example, Shepherd & Joly-Mascheroni (2017) reported stronger inhibitory illusions in those with migraine. It is possible therefore that our headache group exhibit unreliable P2 and poor inter-trial theta phase coherence around the P2 time period, with an advanced, rather than delayed, P2 on some trials. Importantly, theta-phase connectivity has been associated with increased frequency of epileptic attacks (Douw et al., 2010). Given our participants' high scores

on the headache factor, there may be overlap between some of these individuals and the migraine population. However, more work is required to pinpoint the cause of the absent N1 / unreliable P2 and relate it to inhibitory mechanisms.

In conclusion, we found two factors related to altered ERPs. Those scoring high on the discomfort factor exhibited an increased P1 component for the medium stimulus relative to both the other stimuli and the low-discomfort group. This state measure may relate to cortical hyper-excitability making the stimuli appear more potent or to an inability to disengage attention. Those scoring high on the headache factor showed a difference in the N1-P2 time window consistent with an early/jittered P2 masking N1. This could relate to poor inter-trial theta phase coherence and poorly regulated P2 timing but could also be evidence of successful suppression of repeated stimuli or habituation. The dissociation between these factors across time from stimulus onset, stimulus repeats, and electrode sites suggest that they relate to distant neural processes. Given previous results suggesting that differences in hyper-excitability and habituation in migraine are underpinned by different physiological phenomena, future studies are needed to see whether our results are transferable to clinically diagnosed migraineurs.

2.6 Acknowledgements

We want to thank Guillaume Flandin for their help with SPM use and expertise. They also assisted in refining analysis code. We would also like to thank Sara Assecondi for assistance with EEG pre-processing and Cathy Ghalib for help with data collection.

2.7 Funding

We were not funded for this research.

2.8 Competing interests

The authors report no competing interests.

2.9 Supplementary Material

2.9.1 Factor analysis

Factor analysis seeks to derive independent factors from a collection of variables. Thus, the correlations between our factors were zero. Rotation helps to clarify which variables load onto (belong to) each factor, as seen in the Rotated Component Matrix (Table 2-1) and helps with factor naming. Our factors scores were calculated in SPSS (IBM, NY) using the regression method in which all variables contribute to all factors according to the Component Score Coefficient Matrix (Table 2-2). For the headache and discomfort factors, the contribution from variables not obviously associated with these terms was minimal. The headache variables did contribute to the visual stress factor, but were pitted against each other such that intensity and frequency contributed positively onto this factor while duration contributed negatively. Since the headache variables correlate relatively strongly, the effect of these positive and negative weightings will be to cancel out the overall effect of headache on the VS factor. Although correlations between factors were zero by design, the correlation between discomfort ratings for the medium stimuli alone and headache frequency was 0.3 (p=.068) which, while not significant in our sample, is similar to previous measures.

Table 2-1. Rotated Component Matrix

Rotated Component Matrix

	Component		
	1	2	3
VSQ	0.636	0.035	0.062
CHi	0.845	0.212	-0.074

aura	0.789	0.122	0.292
H-duration	-0.470	0.764	0.040
H-intensity	0.366	0.716	-0.116
H-frequency	0.305	0.795	0.041
Discomfort	0.119	-0.028	0.977

Table 2-2. Component Score Coefficient Matrix

Component Score Coefficient Matrix			
	Component		
	1	2	3
VSQ	0.303	-0.055	-0.021
CHi	0.401	0.018	-0.172
aura	0.337	-0.012	0.187
H-duration	-0.332	0.51	0.135
H-intensity	0.108	0.372	-0.128
H-frequency	0.048	0.433	0.036
Discomfort	-0.065	0.013	0.934

2.9.2 Direct Comparison of Stimulus Responses

In EEG work, one often attempts to avoid differences in stimulus properties, particularly those that are low-level, such as spatial frequency. This is because one is typically seeking to identify differences in higher-level properties, such as, attentional state, affective salience or linguistic properties, and associated EEG features could be contaminated by differences in low-level features. However, this is not our situation, we are specifically seeking to observe differences in the brain's electrical response to changes in low-level stimulus features, i.e. spatial frequency.

Other researchers also looking at the brain's electrical response to aggravating stimuli, have sought to avoid making comparisons across stimuli with different spatial frequencies (Fong,

et al., 2020). A consequence of this choice is that effects of different spatial frequencies have to be judged informally, without a statistical test to quantify the confidence in an observed difference; effectively one is left considering *the difference of evidences* (e.g. comparing p-values), rather than assessing *the evidence for a difference*. There are, of course, many ways to investigate scientific questions, but, since the question of interest for us is how early brain responses change to stimuli that have different effective strengths for different groups, we have chosen to directly compare the EEG generated by stimuli of different spatial frequencies.

Additionally, our parametric regression onto the three factors we identified cannot be impacted by fixed baseline differences between gratings, such as, Thick generating an overall higher amplitude than Thin or Medium, since that difference would be consistent across participants. As a result, it would not create a differential pattern "down" the regressor, i.e. it could not generate a non-zero correlation between dependent variable and regressor. Thus, fixed baseline differences in brain responses to different gratings cannot impact our analysis of factors.

2.9.3 Further Justification of Window Selection

The second ROI that we analysed focussed on the time region of the N1 component, which follows the P1. As discussed in the "Mass Univariate Analysis" subsection of the "Methods" section, the spatial and temporal parameters of this component are less well defined in the literature. Consequently, we applied an orthogonal contrast approach to identify the ROI (Brooks et al., 2017). We used our analysis of the factor intercept in the MUA (see results) to produce an ROI mask for further analysis. This approach will not inflate the false-positive rate for the following reasons.

All our three factors are, by construction, orthogonal to the intercept. This can be seen from the fact that they are all de-meaned and consequently, their dot-product with the column

vector of all ones (i.e. the intercept regressor), which corresponds to taking the sum of the factor, equals zero. Additionally, the contrast vector for the one-sample t-test (the statistic of interest for us) for each regressor in our design (of which there are four: intercept and three factors) has a zero dot-product with any other. This is because each is a unit vector on one dimension, e.g. [0, 1, 0, 0]. Accordingly, the contrasts being performed are also orthogonal.

There are two further properties that support the parametric contrast orthogonality property, which is the gold-standard demonstration that the false positive rate is not inflated (Bowman, et al., 2020). The first of these is that there are no correlations running down the dependent variable, which holds because every participant is an independent sample. To clarify, in some neuroimaging analyses, the dependent variable contains a correlational structure. For example, in fMRI, first-level inference at each voxel is performed down the time-series of the entire experiment, which becomes the dependent variable and since this is a time-series, there are correlations down it. This raises further non-orthogonality concerns, but is not the situation we have to deal with. Regarding the last property, which considers trial count asymmetry across conditions, (Brooks et al., 2017) showed that such asymmetries have a negligible effect unless they are great. For example, Figure 3, Panel C of (Brooks et al., 2017) considers a t-test on an N170 component overlaid with noise at the human frequency spectrum. The N170 has a similar timeframe to that which we are considering in this paper. Essentially, there is very little evidence of an inflation of false positive rate when one condition has twice as many trials as the other, and indeed little until there is an 8 times asymmetry.

Since our main inference is parametric regression, the point of interest for us is whether differences in trial counts between participants could bias the mean/intercept ROI selection. Importantly, in our data, there is trial-count variability between participants, but that variability is

not great. For example, the mean trial-count is 350.4, while the standard deviation is 42.3. This standard deviation is very small relative to the mean, with a ratio of 0.12 (42.3/350.4). Additionally, the mean count is 1.412 times the lowest trial count and the highest trial count is 1.23 times the mean count. These levels of trial-count asymmetries between participants are very unlikely to bias ROI selection on the mean/intercept.

Note, at an earlier stage in our processing pipeline, there was more trial-count variability. That is, before we removed crown electrodes, see subsection "ERP pre-processing", trial-count asymmetry was a greater issue. This is because presence of the noisy crown electrodes, lead to a higher rate of trial rejection due to artefacts. Indeed, this is why we performed a *weighted* average when calculating the overall window of analysis in time by identifying the portion of the grand average ERP waveform that deviated from baseline; see "Mass Univariate Analysis" subsection of the "Methods" section.

2.9.4 Justification of Prior Precedent for P1 Window

We consulted the literature when choosing our P1 window for the ROI analysis. The P1 is described as having an onset in the interval 80-100ms over the posterior visual cortex (Figure 3.9; Luck et al., 1998), with a peak between 100-130 ms (Luck, 2014). It was also described as having a peak in the interval 90-110ms (Slotnick et al., 1999). Finally, Mangun (1995) described the P1 component as a positive going component that typically begins around 70–90ms with a peak around 80-130ms, with maximum amplitude over the peristriate cortex (Mangun et al., 1993).

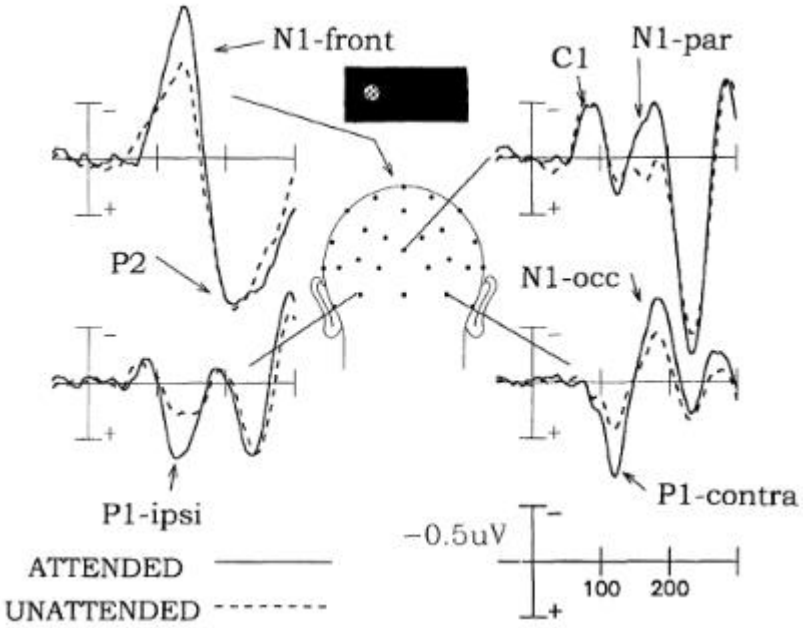

Figure 2-9. ERP electrode locations where the different visual components were analysed by Luck et al., 1998.

The P1-contra and P1-ipsi components are associated with electrodes O1 and O2 on the 10/20 cap, which are associated with electrodes B6,7 & A9,10 on our montage. Negative is plotted up. Image taken from Luck et al. (1998).

The electrode caps where the P1 was analysed used a 10/20 system (Figure 3.10; Kungl et al., 2017). We needed to convert this to our 128-electrode channel biosemi cap (see Methods section). The electrodes analysed were O1-Oz-O2 on the 10/20 cap, which are associated with electrodes B6,7 & A9,10 on our current set B6= [34, -94.625], B7= [34, -73.125], A9=[-38.25, -89.25], A10=[-38,25, -94.625]mm. Oz lies in the rectangle created by these electrodes; that is Oz=[-4.25, -94.625] mm, because we removed electrodes, the locations skewed somewhat. So, we decided to place a box centred at the midpoint of these electrodes: -2.125mm, -83.875mm. For the box to just reach those electrodes on the SPM maximum intensity projection (MIP), it

would be 72.25mm x 21.5mm. If these electrodes are the ones we are interested in, then we needed to make the box a bit bigger, so that it encompasses rather than just reaches them. Based on electrode spacing, we added an extra 20mm on each dimension, with 10mm at each end. This gave us a size of 92mm x 42mm.

For the time domain, we wanted to have a window big enough to include the entire P1 effect. We decided to use a window as close to 70-130ms as possible. We did this in order to encompass the time window precedents from all the literature (both onset and peak), which were described above. The dimensions of the ROI box go in both directions from the box location (which acts as the midpoint of the box). We had chosen to centre our time window at 100ms, choosing 61ms as the length of the time window (30.5ms in both directions). However, because the closest time point SPM could give us was 101ms, we had to adjust the window to fit the region of analysis. We ended up adjusting the time window to 62ms, which would fully cover the 70-132ms needed to investigate the P1.

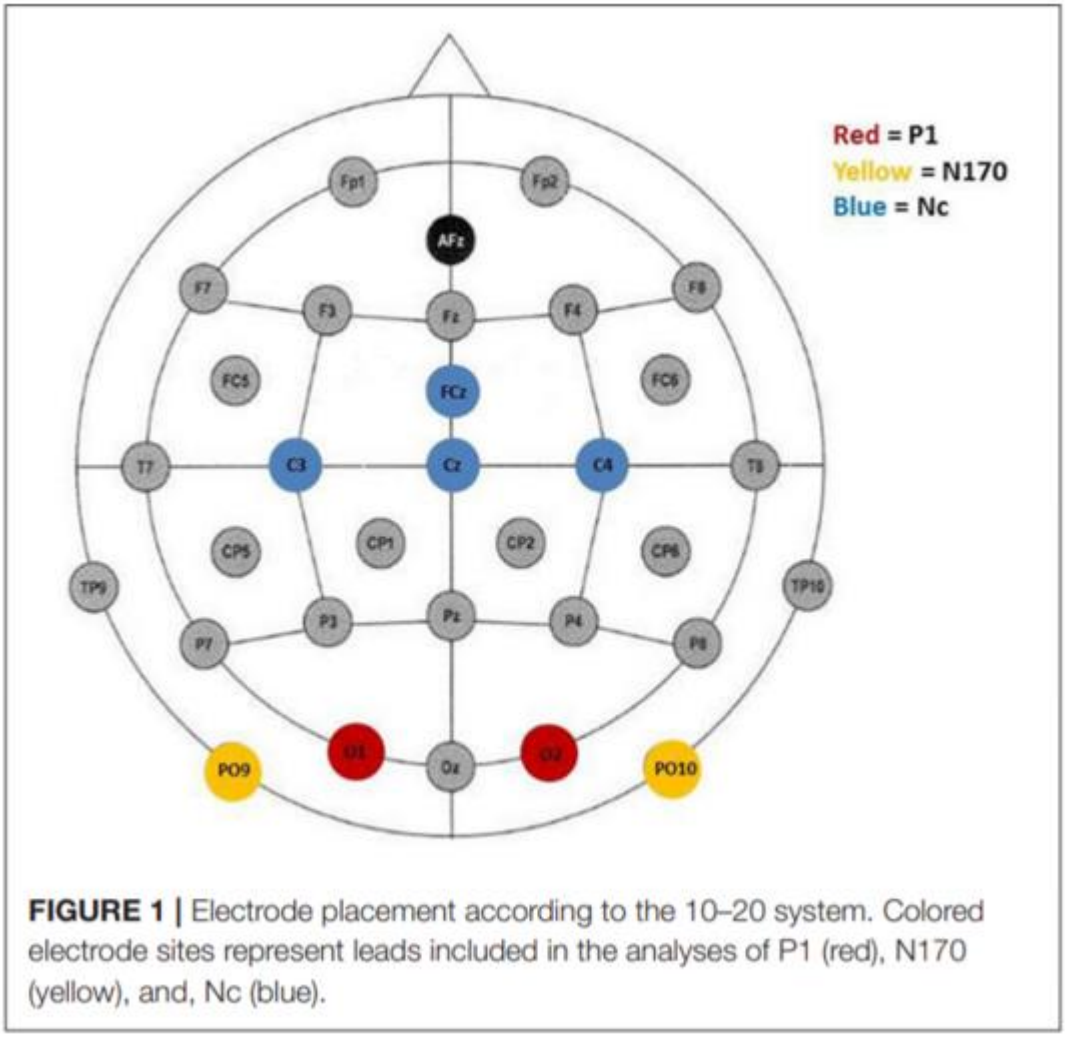

FIGURE 1 | Electrode placement according to the 10–20 system. Colored electrode sites represent leads included in the analyses of P1 (red), N170 (yellow), and, Nc (blue).

Figure 2-10. 10/20 Cap and electrode placements for components of interest.

The diagram colour codes the areas on the 10/20 cap used for detection of specific components.

Taken from Kungl et al. 2017.

2.9.5 Unweighted Grand Averages

In the "Factor effects" subsection of the "Results" section, we displayed the discomfort-and headache factor ERPs scaled by factor weights to better visualise the parametric regressor inferences in the MUA. Figure 2.11, provides the median split ERPs on factors (discomfort and headache), unweighted by the factor scores for significant electrodes (A8, A20, and A28).

Discomfort

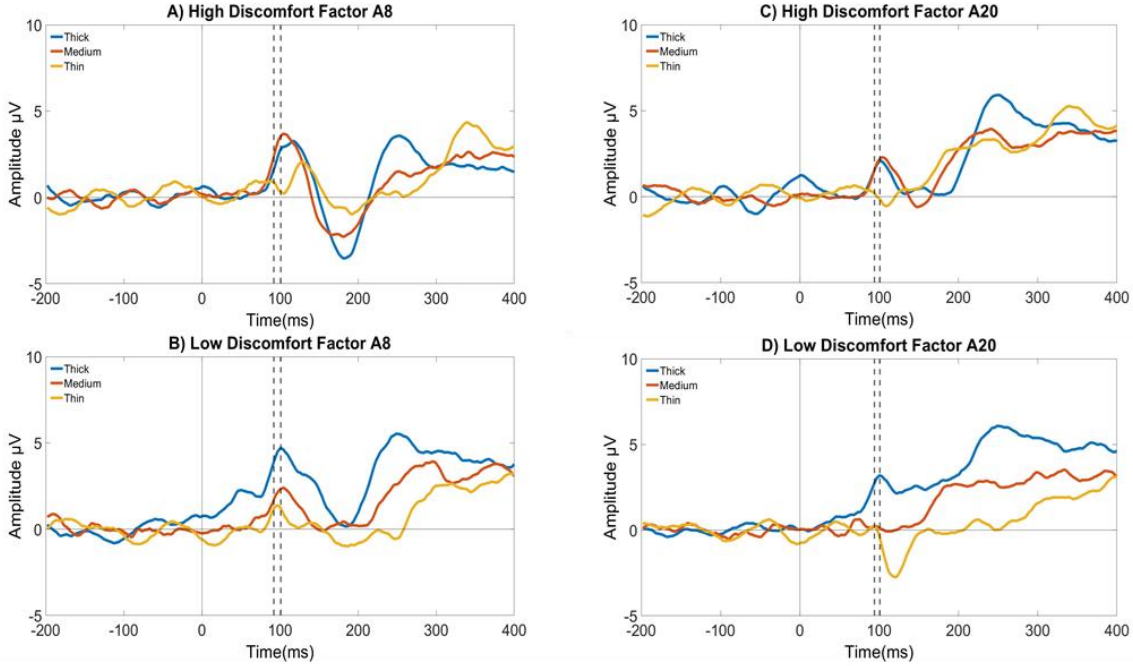

E) Headache

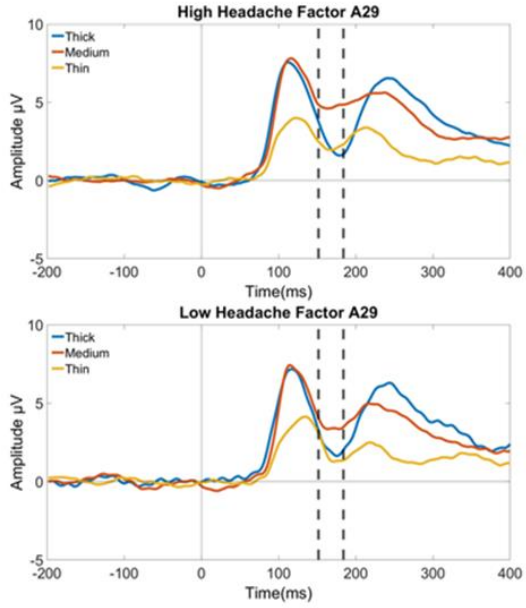

Figure 2-11 Unweighted median splits for ERPs from statistically significant electrodes for factor's discomfort (A8 & A20, Onset 1) and headache (A29, Onsets 2-8).
A, C) high discomfort B, D) low discomfort ERPs. E) high and low median splits for headache factor (electrode A29). Positive plotted up. Lines indicate start and end of statistically significant time window (See our analysis section for specific time windows).

2.9.6 Comparisons with Fong et al. (2020)

Fong et al. (2020) used a very similar paradigm to ours, presenting the three pattern glare stimuli, at spatial frequencies very close to our thick, medium and thin, to those with self-reported migraine. However, their stimulus timings were different from ours with a key difference being that they only presented single onsets in each trial, whereas we repeated our stimuli several times per trial.

In comparing our results, we first note a difference in nomenclature. Fong et al. (2020) observe a negative going deflection just prior to 100ms in response to high frequency stimuli and report this as N1 with the subsequent positive deflection termed P2 and a second negative deflection N2 at around 200ms. They then carry this labelling through to the ERP for the low frequency stimulus, which starts with a positive deflection around 100ms, which they label P2. P1 is absent in all ERPs, with N1 also absent in the ERP for low frequency gratings. However, a number of researchers (Alonso et al, 2015; Earls et al, 2016; Hogendoorn et al, 2015; Luck, 2005; Mangun, 1995; Woodman, 2010) have found a positive going occipital peak at around 100ms, which is called variously the P1 or P100 followed by a negative deflection between 150-200ms post stimulus, which is typically called the N1 component; see, for example, Figure 2.9. Our ERP for thick stimuli follows this typical P1-N1 pattern, as indeed does Fong et al's trace for their low-frequency stimulus. We thus prefer to label the positive peak at 100ms as P1 and the

subsequent deflections as N1 and P2 respectively. We note however that, in common with Fong et al. our thin (high frequency) stimulus tended to produce a negative deflection at 100ms as can be seen in the yellow trace of our Figure 2.2. Thus, our results have some superficial similarities to those of Fong et al. with a transposition of nomenclature. For the avoidance of doubt, we will refer to stimulus features in terms of milliseconds post stimulus in the comparisons below.

Owing to our initial data-driven ROI, we do not consider ERP components outside the 56-256ms window. We will therefore not comment on the reduced late negativity found by Fong et al (2020). at around 400ms, although we do note that those high on our headache factor have more positive EPRs between 300-400ms than those low on the same factor. Fong et al. also found significant between-group differences between migraineurs and controls at around 200ms, with the patient group having more negative ERPs for high-frequency stimuli in this region. This was to some extent also visible, but not significant, in the traces for medium frequency stimuli. At first sight, this result is at odds with our finding of more positive traces at 200ms for those high on our headache factor than those low on the same factor (see our Figure 2.5); this resulted in a significant relationship between the PGI and headache. However, we found this only for Onsets 2-8 and since Fong et al. did not use repeated stimulus presentations, our result could represent a habituation effect that they were unable to detect due to differences in methodology. Further, although we found no significant results in this region, an examination of our ERPs for the first onset of our medium stimuli, shows a greater negativity for those high on the headache factor at around 150ms not unlike that found by Fong et al., See Figure 3.12. We conclude that the apparent difference between the studies to a certain extent rests on stimulus presentation methods and our use of repeated onsets to address habituation effects.

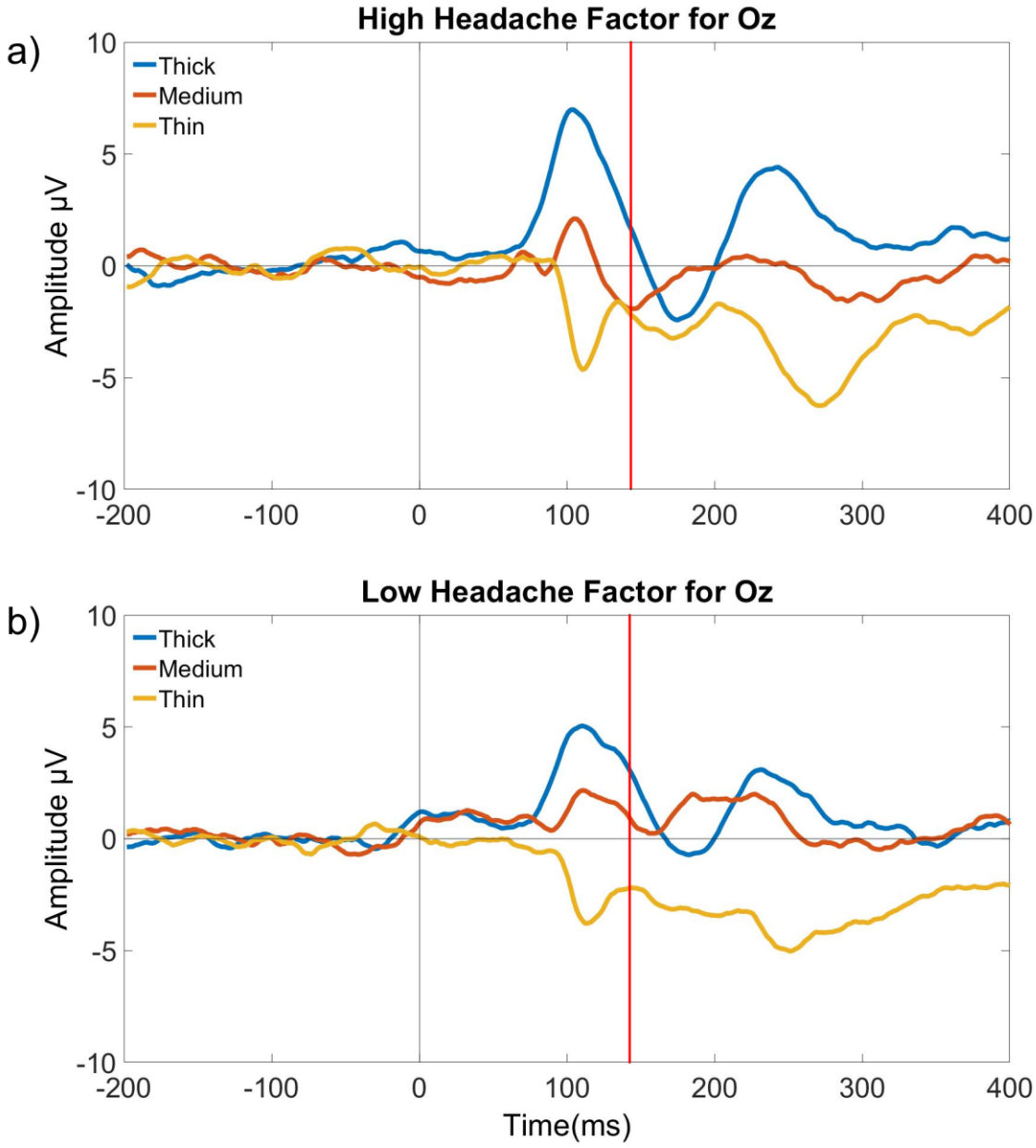

Figure 2-12. Unweighted ERPs derived from a median split on headache parameters at Oz (electrode A23) for the first onset of each stimulus.

a) ERPs for those high on the headache factor, b) low. Positive is up. Vertical red lines show effect of interest.

Fong et al. (2020) also posit that those with migraine and those controls with strong pattern glare have a “phantom” positive deflection at 200ms for the medium stimulus. We notice a similar effect; our medium stimuli tend to produce greater positivity at 200ms, which we describe as an early or jittered P2, but could be related to the proposed phantom P200 component.

Additionally, studies of visual stress and pattern glare typically associated both symptoms and increased neural activity with gratings at 3 c/deg: less so at higher frequencies. Indeed, PG symptoms at 11-13 c/deg are often used as a control for symptoms at 3 c/deg (Evans & Stevenson, 2008). Therefore, our findings of significant results on our PGI – which treats responses to the high-frequency grating as a control for medium – may be a better correlate of symptoms than responses to high-frequency gratings alone, upon which Fong et al focus their findings.

2.10 References

Adjamian, P., Holliday, I. E., Barnes, G. R., Hillebrand, A., Hadjipapas, A., & Singh, K. D. (2004). Induced visual illusions and gamma oscillations in human primary visual cortex. *European Journal of Neuroscience*, *20*(2), 587-592.

Afra, J., Cecchini, A. P., De Pasqua, V., Albert, A., & Schoenen, J. (1998). Visual evoked potentials during long periods of pattern-reversal stimulation in migraine. *Brain: A Journal of Neurology*, *121*(2), 233-241.

Aguila, M. E. R., Lagopoulos, J., Leaver, A. M., Rebbeck, T., Hübscher, M., Brennan, P. C., & Refshauge, K. M. (2015). Elevated levels of GABA+ in migraine detected using 1H-MRS. *NMR in Biomedicine*, *28*(7), 890-897.

Aguila, M. E. R., Rebbeck, T., Leaver, A. M., Lagopoulos, J., Brennan, P. C., Hübscher, M., & Refshauge, K. M. (2016). The association between clinical characteristics of migraine and brain GABA levels: an exploratory study. *The Journal of Pain*, *17*(10), 1058-1067.

Allen, M. (Ed.). (2017). *The SAGE encyclopedia of communication research methods*. Sage Publications.

Alonso, J. F., Romero, S., Ballester, M. R., Antonijoan, R. M., & Mañanas, M. A. (2015). Stress assessment based on EEG univariate features and functional connectivity measures. *Physiological measurement*, *36*(7), 1351.

Ambrosini, A., & Schoenen, J. (2006). Electrophysiological response patterns of primary sensory cortices in migraine. *The Journal of Headache and Pain*, *7*(6), 377-388.

Beasley, I. G., & Davies, L. N. (2012). Susceptibility to pattern glare following stroke. *Journal of Neurology*, *259*(9), 1832-1839.

Bigal, M. E., Hetherington, H., Pan, J., Tsang, A., Grosberg, B., Avdievich, N., ... & Lipton, R. B. (2008). Occipital levels of GABA are related to severe headaches in migraine. *Neurology*, *70*(22), 2078-2080.

Brainard, D. H. (1997). The psychophysics toolbox. *Spatial vision*, *10*(4), 433-436.

Braithwaite, J. J., Broglia, E., Bagshaw, A. P., & Wilkins, A. J. (2013). Evidence for elevated cortical hyperexcitability and its association with out-of-body experiences in the nonclinical population: new findings from a pattern-glare task. *Cortex*, *49*(3), 793-805.

Braithwaite, J.J., Marchant, R., Takahashi, C., Dewe, H., Watson, D (2015) The cortical hyperexcitability index (CHi): a new measure for quantifying correlates of visually driven cortical hyperexcitability. *Cognitive Neuropsychiatry*, *20* (4), 330-348.

Brighina, F., Palermo, A., & Fierro, B. (2009). Cortical inhibition and habituation to evoked potentials: relevance for pathophysiology of migraine. *The Journal of Headache and Pain*, *10*(2), 77.

Brighina, F., Cosentino, G., & Fierro, B. (2016). Habituation or lack of habituation: What is really lacking in migraine? *Clinical Neurophysiology*, 18-20.

Brinciotti, M., Guidetti, V., Matricardi, M., & Cortesi, F. (1986). Responsiveness of the visual system in childhood migraine studied by means of VEPs. *Cephalalgia*, *6*(3), 183-185.

Brooks, J. L., Zoumpoulaki, A., & Bowman, H. (2017). Data-driven region-of-interest selection without inflating Type I error rate. *Psychophysiology*, *54*(1), 100-113.

Bruyns-Haylett, M., Luo, J., Kennerley, A. J., Harris, S., Boorman, L., Milne, E., ... & Berwick, J. (2017). The neurogenesis of P1 and N1: a concurrent EEG/LFP study. *Neuroimage*, *146*, 575-588.

Bruyns-Haylett, M., Luo, J., Kennerley, A. J., Harris, S., Boorman, L., Milne, E., ... & Berwick, J. (2017). The neurogenesis of P1 and N1: a concurrent EEG/LFP study. *Neuroimage*, *146*, 575-588.

Bourisly, A.K., & Shuaib, A. (2018) Neurophysiologoical effects of ageing: A P200 ERP study, *Translational Neuroscience*, 9, 61-66.

Buzzi, M. G. (2001). Trigeminal pain pathway: Peripheral and central activation as experimental models of migraine. *Functional Neurology*, *16*(4; SUPP), 77-82.

Bowman, H., Brooks, J. L., Hajilou, O., Zoumpoulaki, A., & Litvak, V. (2020). Breaking the circularity in circular analyses: Simulations and formal treatment of the flattened average approach. *PLOS Computational Biology*, *16*(11), e1008286.

Carrillo-De-La-Peña, M., Holguín, S. R., Corral, M., & Cadaveira, F. (1999). The effects of stimulus intensity and age on visual-evoked potentials (VEPs) in normal children. *Psychophysiology*, *36*(6), 693-698.

Chennu, S., Craston, P., Wyble, B., & Bowman, H. (2009). Attention increases the temporal precision of conscious perception: verifying the neural-ST2 model. *PLoS Computational Biology, 5*(11), e1000576

Chennu, S., Noreika, V., Gueorguiev, D., Blenkmann, A., Kochen, S., Ibanez, A., …Bekinschtein, T..A. (2013).. Expectations and attention in hierarchical auditory prediction. *Journal of Neuroscience, 33*(27).

Clarke, C. E., MacMillan, L., Sondhi, S., & Wells, N. E. (1996). Economic and social impact of migraine. *Qjm*, *89*(1), 77-84.

Conlon, E. G., Lovegrove, W. J., Chekaluk, E., & Pattison, P. E. (1999). Measuring visual discomfort. *Visual Cognition*, *6*(6), 637-663.

Connolly, J. F., Gawel, M., & Rose, F. C. (1982). Migraine patients exhibit abnormalities in the visual evoked potential. *Journal of Neurology, Neurosurgery & Psychiatry*, *45*(5), 464-467.

Coppola, G., Pierelli, F., & Schoenen, J. (2009). Habituation and migraine. *Neurobiology of Learning and Memory*, *92*(2), 249-259.

Datta, R., Aguirre, G. K., Hu, S., Detre, J. A., & Cucchiara, B. (2013). Interictal cortical hyperresponsiveness in migraine is directly related to the presence of aura. *Cephalalgia*, *33*(6), 365-374.

Di Russo, F., Martínez, A., Sereno, M. I., Pitzalis, S., & Hillyard, S. A. (2002). Cortical sources of the early components of the visual evoked potential. *Human Brain Mapping*, *15*(2), 95-111.

Douw, L., van Dellen, E., de Groot, M., Heimans, J. J., Klein, M., Stam, C. J., & Reijneveld, J. C. (2010). Epilepsy is related to theta band brain connectivity and network topology in brain tumor patients. *BMC Neuroscience*, *11*(1), 103.

Denuelle, M., Fabre, N., Payoux, P., Chollet, F., & Geraud, G. (2008). Posterior cerebral hypoperfusion in migraine without aura. *Cephalalgia*, *28*(8), 856-862.

Earls, H. A., Curran, T., & Mittal, V. (2016). Deficits in early stages of face processing in schizophrenia: a systematic review of the P100 component. *Schizophrenia bulletin*, *42*(2), 519-527.

Enna, S. J., & McCarson, K. E. (2006). The role of GABA in the mediation and perception of pain. *Advances in Pharmacology*, *54*, 1-27.

Evans, B. J. W., & Stevenson, S. J. (2008). The Pattern Glare Test: a review and determination of normative values. *Ophthalmic and Physiological Optics*, *28*(4), 295-309.

Fong, C. Y., Law, W. H. C., Braithwaite, J., & Mazaheri, A. (2020). Differences in early and late pattern-onset visual-evoked potentials between self-reported migraineurs and controls. NeuroImage: *Clinical*, *25*, 102122.

Freunberger, R., Klimesch, W., Doppelmayr, M., & Höller, Y. (2007). Visual P2 component is related to theta phase-locking. *Neuroscience Letters*, *426*(3), 181-186.

Friedman, D. I., & De Ver Dye, T. (2009). Migraine and the environment. *Headache: The Journal of Head and Face Pain*, *49*(6), 941-952.

Gruber, T., & Müller, M. M. (2004). Oscillatory brain activity dissociates between associative stimulus content in a repetition priming task in the human EEG. *Cerebral Cortex*, *15*(1), 109-116.

Haigh, S. M., Cooper, N. R., & Wilkins, A. J. (2015). Cortical excitability and the shape of the haemodynamic response. *Neuroimage*, *111*, 379-384.

Harle, D. E., Shepherd, A. J., & Evans, B. J. (2006). Visual stimuli are common triggers of migraine and are associated with pattern glare. *Headache: The Journal of Head and Face Pain*, *46*(9), 1431-1440.

Head, M. L., Holman, L., Lanfear, R., Kahn, A. T., & Jennions, M. D. (2015). The extent and consequences of p-hacking in science. *PLoS Biology*, *13*(3), e1002106.

Heinze, H. J., Luck, S. J., Mangun, G. R., & Hillyard, S. A. (1990). Visual event-related potentials index focused attention within bilateral stimulus arrays. I. Evidence for early selection. *Electroencephalography and Clinical Neurophysiology*, *75*(6), 511-527.

Hogendoorn, H., Kammers, M., Haggard, P., & Verstraten, F. (2015). Self-touch modulates the somatosensory evoked P100. *Experimental brain research*, *233*(10), 2845-2858.

Hopf, J. M., Vogel, E., Woodman, G., Heinze, H. J., & Luck, S. J. (2002). Localizing visual discrimination processes in time and space. *Journal of neurophysiology*, *88*(4), 2088-2095.

Hougaard, A., Amin, F. M., Hoffmann, M. B., Rostrup, E., Larsson, H. B., Asghar, M. S., ... & Ashina, M. (2014). Interhemispheric differences of fMRI responses to visual stimuli in patients with side-fixed migraine aura. *Human Brain Mapping*, *35*(6), 2714-2723.

Hsu, Y-F., Hämäläinen, J.A., Waszak, F. (2014) Repetition suppression comprises both attention-independent and attention-dependent processes, Neuroimage, 98, 168-175.

Huang, J., Cooper, T. G., Satana, B., Kaufman, D. I., & Cao, Y. (2003). Visual distortion provoked by a stimulus in migraine associated with hyperneuronal activity. *Headache: The Journal of Head and Face Pain*, *43*(6), 664-671.

Huang, J., Zong, X., Wilkins, A., Jenkins, B., Bozoki, A., & Cao, Y. (2011). fMRI evidence that precision ophthalmic tints reduce cortical hyperactivation in migraine. *Cephalalgia*, *31*(8), 925-936.

Johnstone, S, J., Barry R.J., Markovska V., Dimoska, A., Clarke, A.R (2004) Response inhibition and interference control in children with AD/HD: A visual ERP investigation. *International Journal of Psychophysiology*, 72, 145-153.

Kientz, M. A., & Dunn, W. (1997). A comparison of the performance of children with and without autism on the Sensory Profile. *American Journal of Occupational Therapy*, *51*(7), 530-537.

Kleiner, M., Brainard, D., & Pelli, D. (2007). What's new in Psychtoolbox-3?.

Kungl, M. T., Bovenschen, I., & Spangler, G. (2017). Early Adverse Caregiving Experiences and Preschoolers' Current Attachment Affect Brain Responses during Facial Familiarity Processing: An ERP Study. *Frontiers in Psychology*, *8*, 2047.

Kriegeskorte, N., Simmons, W. K., Bellgowan, P. S., & Baker, C. I. (2009). Circular analysis in systems neuroscience: the dangers of double dipping. *Nature Neuroscience*, *12*(5), 535.

Lassalle, A., & Itier, R. J. (2013). Fearful, surprised, happy, and angry facial expressions modulate gaze-oriented attention: Behavioural and ERP evidence. *Social Neuroscience*, *8*(6), 583-600.

Lehtonen, J. B. (1974). Visual evoked cortical potentials for single flashes and flickering light in migraine. *Headache: The Journal of Head and Face Pain*, *14*(1), 1-12.

Litvak, V., Mattout, J., Kiebel, S., Phillips, C., Henson, R., Kilner, J., ... & Friston, K. (2011). EEG and MEG data analysis in SPM8. *Computational intelligence and neuroscience, 2011*.

Lorca-Puls, D. L., Gajardo-Vidal, A., White, J., Seghier, M. L., Leff, A. P., Green, D. W., ... & Price, C. J. (2018). The impact of sample size on the reproducibility of voxel-based lesion-deficit mappings. Neuropsychologia, 115, 101-111.

Luck, S. J., Heinze, H. J., Mangun, G. R., & Hillyard, S. A. (1990). Visual event-related potentials index focused attention within bilateral stimulus arrays. II. Functional dissociation of P1 and N1 components. *Electroencephalography and Clinical Neurophysiology*, *75*(6), 528-542.

Luck, S. J., & Hillyard, S. A. (1994). Electrophysiological correlates of feature analysis during visual search. Psychophysiology, 31, 291–308.

Luck, S. J. (2005). Ten simple rules for designing ERP experiments. *Event-related potentials: A methods handbook*, *262083337*.

Luck, S. J. (2014). *An Introduction to the Event-related Potential Technique*. MIT press.

Luck, S. J., Woodman, G. E., and Vogel, E. K. (2000). Event-related potential studies of attention. *Trends in Cognitive Sciences, 4,* 432-440.

MacLean, C., Appenzeller, O., Cordaro, J. T., & Rhodes, J. (1975). Flash evoked potentials in migraine. *Headache: The Journal of Head and Face Pain*, *14*(4), 193-198.

Mangun, G. R., Hillyard, S. A., & Luck, S. J. (1993). Electrocortical substrates of visual selective attention. In D. Meyer & S. Kornblum (Eds.), Attention and Performance XIV (pp. 219-243). Cambridge, Massachusetts: MIT Press.

Mangun, G. R. (1995). Neural mechanisms of visual selective attention. *Psychophysiology*, *32*(1), 4-18.

Marks, D. A., & Ehrenberg, B. L. (1993). Migraine-related seizures in adults with epilepsy, with EEG correlation. *Neurology*, *43*(12), 2476-2476.

Munte, T.F., Heinze, H.J., & Mangun, G.R. (1995) Luminance and spatial attention effects on early visual processing. *Cognitive Brain Research*, 2, 189-205

Olofsson, J. K., & Polich, J. (2007). Affective visual event-related potentials: arousal, repetition, and time-on-task. *Biological Psychology*, *75*(1), 101-108.

Olman, C. A., Ugurbil, K., Schrater, P., & Kersten, D. (2004). BOLD fMRI and psychophysical measurements of contrast response to broadband images. *Vision Research*, *44*(7), 669-683.

Omland, P. M., Nilsen, K. B., Uglem, M., Gravdahl, G., Linde, M., Hagen, K., & Sand, T. (2013). Visual evoked potentials in interictal migraine: no confirmation of abnormal habituation. *Headache: The Journal of Head and Face Pain*, *53*(7), 1071-1086.

Omland, P. M., Uglem, M., Hagen, K., Linde, M., Tronvik, E., & Sand, T. (2016). Visual evoked potentials in migraine: Is the “neurophysiological hallmark” concept still valid? *Clinical Neurophysiology*, *127*(1), 810-816.

Pietrobon, D. (2005). Migraine: new molecular mechanisms. *The Neuroscientist*, *11*(4), 373-386.

Pelli, D. G. (1997). The VideoToolbox software for visual psychophysics: Transforming numbers into movies. *Spatial vision*, *10*(4), 437-442.

Richey, E. T., Kooi, K. A., & Waggoner, R. W. (1966). Visually evoked responses in migraine. *Electroencephalography and Clinical Neurophysiology*, *21*(1), 23-27.

Saksida, A., Iannuzzi, S., Bogliotti, C., Chaix, Y., Démonet, J. F., Bricout, L., ... & George, F. (2016). Phonological skills, visual attention span, and visual stress in developmental dyslexia. *Developmental Psychology*, *52*(10), 1503.

Schoenen, J., Wang, W., Albert, A., & Delwaide, P. J. (1995). Potentiation instead of habituation characterizes visual evoked potentials in migraine patients between attacks. *European Journal of Neurology*, *2*(2), 115-122.

Schwedt, T. J., Chiang, C. C., Chong, C. D., & Dodick, D. W. (2015). Functional MRI of migraine. *The Lancet Neurology*, *14*(1), 81-91.

Shahaf, G. (2016). Migraine as dysfunctional drive reduction: Insight from electrophysiology. *Medical Hypotheses*, *91*, 62-66.

Shapiro, R. E., & Goadsby, P. J. (2007). The long drought: the dearth of public funding for headache research.

Shepherd, A. J., & Joly-Mascheroni, R. M. (2017). Visual motion processing in migraine: enhanced motion after-effects are related to display contrast, visual symptoms, visual triggers and attack frequency. *Cephalalgia*, *37*(4), 315-326.

Shirazibeheshti, A., Cooke, J., Chennu, S., Adapa, R., Menon, D. K., Hojjatoleslami, S. A., ... & Bowman, H. (2018). Placing meta-stable states of consciousness within the predictive

coding hierarchy: The deceleration of the accelerated prediction error. *Consciousness and Cognition, 63,* 123-142.

Shin, Y-W., Krishnan, G., Hetrick, W.P., Brenner, C.A., Shekhar, A., Malloy, F.W., O'Donnell, B.F. (2010) Increased temporal variability of auditory event-related potentials in schizophrenia and Schizotypal Personality Disorder. *Schizophrenia Research,* 124, 110-118.

Slotnick, S. D., Klein, S. A., Carney, T., Sutter, E., & Dastmalchi, S. (1999). Using multi-stimulus VEP source localization to obtain a retinotopic map of human primary visual cortex. *Clinical neurophysiology*, *110*(10), 1793-1800.

Spierings, E. L., Ranke, A. H., & Honkoop, P. C. (2001). Precipitating and aggravating factors of migraine versus tension-type headache. *Headache: The Journal of Head and Face Pain*, *41*(6), 554-558.

Steiner, T. J., Scher, A. I., Stewart, W. F., Kolodner, K., Liberman, J., & Lipton, R. B. (2003). The prevalence and disability burden of adult migraine in England and their relationships to age, gender and ethnicity. *Cephalalgia*, *23*(7), 519-527.

Steiner, T. J., Stovner, L. J., & Birbeck, G. L. (2013). Migraine: the seventh disabler. *Headache: The Journal of Head and Face Pain*, *53*(2), 227-229.

Tanner, D., Morgan-Short, K., & Luck, S. J. (2015). How inappropriate high-pass filters can produce artifactual effects and incorrect conclusions in ERP studies of language and cognition. *Psychophysiology*, *52*(8), 997-1009.

Utama, N. P., Takemoto, A., Koike, Y., & Nakamura, K. (2009). Phased processing of facial emotion: an ERP study. *Neuroscience Research*, *64*(1), 30-40.

Van Gelder, N. M. (1987). Calcium mobility and glutamic acid release associated with EEG abnormalities, migraine, and epilepsy. In *Migraine and Epilepsy* (pp. 367-378). Butterworths, Boston.

Van Voorhis, S., & Hillyard, S. A. (1977). Visual evoked potentials and selective attention to points in space. *Perception & psychophysics*, *22*(1), 54-62.

Vazquez, A. L., & Noll, D. C. (1998). Nonlinear aspects of the BOLD response in functional MRI. *Neuroimage*, *7*(2), 108-118.

Vecchia, D., & Pietrobon, D. (2012). Migraine: a disorder of brain excitatory–inhibitory balance? *Trends in Neurosciences*, *35*(8), 507-520

Vogel, E. K., & Luck, S. J. (2000). The visual N1 component as an index of a discrimination process. *Psychophysiology*, *37*(2), 190-203.

Wang, W., Wang, G. P., Ding, X. L., & Wang, Y. H. (1999). Personality and response to repeated visual stimulation in migraine and tension-type headaches. *Cephalalgia*, *19*(8), 718-724.

Welch, K. M. (2005). Brain hyperexcitability: the basis for antiepileptic drugs in migraine prevention. *Headache: The Journal of Head and Face Pain*, *45*, S25-S32.

World Health Organization. (2016). Headache Disorders. Fact Sheet No 277 (2007).

Woodman, G. F. (2010). A brief introduction to the use of event-related potentials in studies of perception and attention. *Attention, Perception, & Psychophysics*, *72*(8), 2031-2046.

Wilkins, A., Nimmo-Smith, I. A. N., Tait, A., McManus, C., Sala, S. D., Tilley, A., ... & Scott, S. (1984). A neurological basis for visual discomfort. *Brain*, *107*(4), 989-1017.

Wilkins, A. (1986). Intermittent illumination from visual display units and fluorescent lighting affects movements of the eyes across text. *Human Factors*, *28*(1), 75-81.

Wilkins, A. J. (1995). *Visual stress* (No. 24). Oxford University Press.

Wilkins, A. J. (2003). Reading through colour. *How Coloured Filters Can Reduce*

Wilkins, A. J., Darby, C. E., & Binnie, C. D. (1979). Neurophysiological aspects of pattern-sensitive epilepsy. *Brain*, *102*(1), 1-25.

Wilkins, A., -Smith, I. A. N., Tait, A., McManus, C., Sala, S. D., Tilley, A., ... & Scott, S. (1984). A neurological basis for visual discomfort. *Brain*, *107*(4), 989-1017.

Wilkins, A. J., Nimmo-Smith, I., Slater, A. I., & Bedocs, L. (1989). Fluorescent lighting, headaches and eyestrain. *Lighting Research & Technology*, *21*(1), 11-18.

Wilkins, A. J., & Evans, B. J. W. (2001). Pattern glare test instructions. London, UK: IOO Sales Ltd.

Wright, B. N., Wilkins, A. J., & Zoukos, Y. (2007). Spectral filters can improve reading and visual search in patients with multiple sclerosis. *Journal of Neurology*, *254*(12), 1729-1735.

Zhang, G. L., Cong, L. J., Song, Y., & Yu, C. (2013). ERP P1-N1 changes associated with Vernier perceptual learning and its location specificity and transfer. *Journal of Vision*, *13*(4), 19-19.

CHAPTER 3: PATTERN-GLARE DRIVEN BY BROADBAND GAMMA IS MODULATED BY DISCOMFORT RATINGS

Austyn J. Tempesta[1], Claire E. Miller[1], Andrew J. Schofield[3,1], & Howard Bowman[1,2]

3.1 Introduction

Visual stress (VS) is a form of abnormal response when the visual cortex is exposed to certain types of striped patterns falling in the medium spatial frequency (3 cycles per degree) range (Mears, 1980; Irlen, 1983; Wilkins, 1995). These abnormal responses are characterised by illusions of colour, shape, and motion. In some cases, people experience migraines and more severely epileptic attacks (Wilkins et al., 1979,1980). Using magnetoencephalography (MEG), Adjamian et al. (2004) have provided evidence that gamma oscillations underlie hyperexcitability in area V1, peaking for gratings at three cycles per degree. They hypothesize that such visual stress is caused by the visual cortex's hyperexcitability, which induces spreading activity among neurons usually associated with sensory input, thus producing hallucinations. The somatic effect sometimes found in visual stress may be due to activity spreading outside of the visual cortex.

In some cases, these effects may not be appropriately regulated by GABAergic inhibitory mechanisms. Visual symptoms might thus be the precursor to a photo-paroxysmal response. This, if not sufficiently controlled by inhibitory mechanisms, may lead to epileptic seizures and migraines. The stimuli that are most likely to induce such anomalies, typically 3 cycles per degree (c/deg) high-contrast stripes, are precisely those most likely to cause attacks of migraine and epilepsy in those with a visual trigger (Wilkins, 1986, 1995; Wilkins et al., 1979, 1980). Most importantly, a minority report seeing such visual distortions when viewing printed text (Meares-Irlen syndrome or VS; Mears, 1980). While such distortions could be due to poor ocular

accommodation and binocular convergence, they are found even when such abnormalities are excluded (Evans et al., 1995).

Migraine and headache disorders account for the 3rd highest cause of disability worldwide (Steiner et al., 2013; Steiner et al., 2015; Strovner et al., 2007). Globally, the percentage of the adult population with an active headache disorder is 46% for headache in general, 11% for migraine, 42% for tension-type headache, and 3% for chronic daily headache (Stovner et al., 2018). Missed work from migraines is estimated to cause £250 million in lost revenue in the UK each year (Clarke et al., 1996). Migraine is also the least funded of all neurological illnesses globally (House of Commons, 2014; Shapiro & Goadsby, 2007).

The pattern glare (PG, Figure 3.1) test was published in 2001 by Wilkins and Evans (2001) as a way for physicians to examine if a patient had some proclivity to experiencing VS. Wilkins and Evans designed this test as a standard way for researchers to analyse VS. The test is intended to induce visual stress in susceptible patients; patterns are also presented horizontally to appear like text and at different spatial frequencies (SF) (.37, 3, and 12) (Evans & Stevenson, 2008).

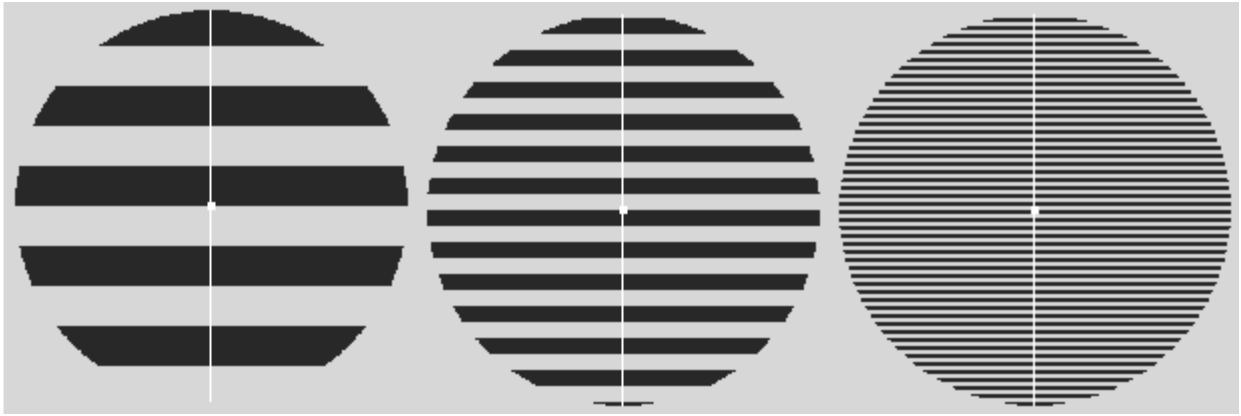

Figure 3-1.Pattern-glare Stimuli.

Left to right, thick (.37 c/deg), medium (3 c/deg), and thin (12 c/deg) gratings with a central fixation and vertical dividing line. The images shown here are representative of the stimuli but have been rendered to aid visibility in print.

As mentioned previously, there has been important prior work, using MEG, showing increased gamma power for pattern glare (Adjamian et al., 2004). We seek to build from this previous work. Because MEG is expensive, Adjamian et al. (2004) were only able to run analysis on a small sample n=7. Importantly, Adjamian et al. did not present stimuli in such a manner that they could isolate habituation effects. We respond to this by repeating the same stimulus in trains of onsets. Finally, they tested each grating from .5 c/deg to 6 c/deg in .5 cycle-steps presented over 2-3 days. Thus, they did not test a 12cpd spatial frequency, which, has been argued to be, a control for optical factors, versus neurological controls (Conlon et al., 2001). Pattern 1 (thick) is intended to be a control for low SF and is not supposed to trigger distortions in most participants. However, it is useful in detecting 'which patients who may be highly suggestible and may respond yes to any question about visual perception distortions' (Evans & Stevenson, 2008). Pattern 2 (medium) is the only clinically relevant stimulus, falling between SF's 1-4. It is this stimulus that is known to elicit migraines and epileptic seizures (Braithwaite et al., 2013; Wilkins, 2016). Pattern 3 (thin) is also a control as it is argued to have poor convergence, reflecting a large contribution from optical as opposed to neurological factors (Conlon et al., 2001).

Alpha desynchronisation has been shown to be particularly important when the brain is representing stimuli and encoding them into memories or retrieving them from memories (Parish et al., 2018), with alpha power decreasing during semantic encoding and retrieval (Klimesch et al., 1996, 1997). However, this oscillation may reflect the brain representing any sort of stimulus

and not be specific to pattern glare. Some models have shown that alpha amplitude modulations regulate the inhibitory level of the cortex (Klimesch et al., 2007; Jensen & Mazaheri, 2010), with synchronisation reflecting habituation and desynchronisation representing active information processing (Hanslmayr, 2012). Thus an absence of alpha synchronisation could represent a lack of inhibition as the brain continues to process a stimulus that might otherwise be attenuated.

This paper builds from the Adjamian et al. (2004) findings and from the previous work on oscillations. Specifically, our hypotheses are: first, that there will be a deeper alpha desynchronisation for pattern glare. Second, there will be greater gamma power for pattern glare, which relates to a failure to habituate. Third, these EEG effects on pattern glare will be modulated by state and trait measures of sensitivity to headache, discomfort, and visual hallucinations. We investigated these hypotheses through a PG task where we recorded EEG data in response to the PG stimuli (Figure 3.1) over several hours, which we analysed in the frequency domain, using mass univariate analysis (MUA). Participants were asked to fill in a series of questionnaires, which we then ran factor analysis on revealing 3 factors, that we interpret as visual stress, headache proneness, and discomfort. Because we used EEG, we have a sample of 34, which is likely to give us considerably increased confidence in the robustness of our findings (Lorca-Puls et al., 2018).

3.1.1 State-Dependent Measures

The PGT is an easy to use clinical tool but, like some of the physiological measures, it may be state-dependent – varying with migraine phase (Wilkins et al., 1984). State physiological measures are useful for judging if an individual is suffering from visual hypersensitivity at a particular moment in time but maybe inadequate measures of their general tendency to suffer hyper-sensitivity. Hypersensitivity results in distortions of the visual image, which can be disruptive for everyday tasks such as reading and can cause discomfort in everyday

environments. Based on these and other symptoms, Conlon and colleagues developed a 23 item questionnaire (Visual Discomfort Scale - VDS; Conlon et al., 1999) for which scores correlate positively with headache severity and visual distortions when viewing square-wave gratings (similar to the pattern-glare (PG) stimuli) and letter stimuli; and negatively with reading speed and performance on the digit symbol sub-test from the revised Wechsler Intelligence Scale for Children (WISC-R). In an attempt to address cortical hyper-excitability more broadly, if still indirectly, Braithwaite et al. (2015) developed the Cortical Hyper-Excitability index (CHi), a 27-item questionnaire in which symptoms are rated for both intensity and frequency of occurrence; although these scores can be merged. Both the VDS and CHi can be regarded as trait measures of cortical hyper-excitability in that they measure the proneness of the participant to episodes of hyper-excitability based on their previous experience.

Cortical hyper-excitability is not limited to those who experience migraine. Stimuli that are disruptive for migraine sufferers are also triggers for those with photosensitive epilepsy (Adjamian et al., 2004; Wilkins et al., 1984). Further, visual hypersensitivity as observed with the PGT or similar metrics is co-morbid with a range of conditions including multiple sclerosis (Wright et al., 2007), stroke (Beasley & Davies, 2012), autism (Irlen, 1997; Kientz & Dunn, 1997), and dyslexia (Irlen, 1991); however, some do not find a connection to dyslexia (Saksida et al., 2016). In many of these conditions, visual distortions in-text inhibit reading but can be alleviated using coloured filters.

Some individuals have disrupted reading and high scores on measures of visual discomfort, hyper-excitability and PGT but few other symptoms. Wilkins and colleagues describe such individuals as suffering from visual stress and posit that this condition is separate from but co-morbid with other conditions – especially where there is no apparent brain injury (Wilkins, 2003). This overlap of symptoms may increase the generality of findings from the migraine

literature; however, it does also suggest that when comparing patient and control groups to assess cortical hyperexcitability, some members of the control group may have some degree of latent hyper-excitability. This possibility can be countered by recording several measures of hyper-excitability as possible covariates for analysis rather than relying on whether or not the participant is in the control or experimental group as the sole predictor of atypical neural activity.

In this study, participants were not selected based on their migraine or headache status. Instead, EEG results were correlated with scores on a range of headache and hyper-excitation measures within a single group drawn from the general population. We measured EEG responses to visual stimuli based on those used in the PGT in a novel paradigm where stimuli were repeated (flicked on and off) at a low temporal frequency allowing the recording of steady-state EEG, while also allowing us to consider habituation effects. Thus, we compared stimuli known to be aggravating in migraine with those that are less aggravating, in a paradigm that allows the separation of initial and habituated responses.

3.2 Materials and Methods

3.2.1 Participants

Forty undergraduate and postgraduate participants, recruited at the University of Birmingham, gave their informed consent and were compensated with £24 for participating. Participants with a history of psychiatric, psychological, and neurological conditions, or a history of unconsciousness, convulsions or epilepsy were excluded from the study. One participant chose to leave the experiment; one was removed due to an equipment malfunction, one due to an artefact that could not be removed and three were removed during data pre-processing due to a lack of usable trials (fewer than 20% per condition). There were thus 34 usable datasets (male=13, female=21, mean age= 22.5y, range=18-32y, standard deviation=2.86). This study was

approved by The Science Technology Engineering and Maths Ethics Committee at the University of Birmingham in adherence with The Declaration of Helsinki.

3.2.2 Stimuli and Equipment

We used stimuli similar to those used in the PGT (Wilkins, 2001). Stimuli comprised horizontal square-wave gratings (contrast = 75%) at 3 different spatial frequencies (.37, 3, and 12 c/deg: described as thick, medium, and thin, respectively, see Figure 3.1) displayed in a circular window with diameter (15.2 deg). These stimuli were created in MATLAB using the Psychophysics Toolbox (Brainard, 1997; Pelli, 1997; Kleiner et al., 2007) and displayed on a Samsung 932BF LCD monitor (Samsung Electronics, Suwon, South Korea) (Figure 3.1.).

Questionnaires were used to assess participants headache history (Headache and General Health Questionnaire, HGHQ) and tendency to suffer visual stress (Cortical Hyper-Excitability index (Chi), Braithwaite et al., 2015; Visual Discomfort Scale (VDS), Conlon et al., 1999). EEG recordings were made using a 128-channel BioSemi (University of Amsterdam) EEG system in a dark, quiet room.

3.2.3 Procedure

After the EEG electrodes had been applied, participants began the experiment with a 5-minute resting period. They then were presented with three blocks, each containing six trials for each of the three stimuli. Thus, each participant observed 18 trials per stimulus type. Each trial contained between seven and nine onsets of the same stimulus, in each of which the stimulus stayed on for three-seconds followed by a variable interval of 1 – 1.4 seconds. After each trial, the participant was asked to rate how discomforting they found each stimulus on a 5-point scale (1 = comfortable, 5 = highly discomforting) and to indicate how many onsets they saw. This additional task was designed to ensure attention to the stimuli. At the end of each block, participants were shown the three stimuli in turn and asked to rate the extent to which they had

experienced a range of possible pattern glare symptoms (Wilkins & Nimmo-Smith, 1984). After each block and at the end of the experiment, participants had a further resting period of 5 minutes, during which they were requested to close their eyes and relax. Stimulus order and number of onsets per trial were counterbalanced (subjecting them to variation, increasing interval validity) (Allen, 2017).

3.2.4 Discomfort ratings and questionnaires

Working with the 39 participants who completed the study, we computed mean discomfort ratings for each participant and stimulus type across the three blocks. Discomfort ratings tend to co-vary across the stimulus types, so we computed a discomfort index for each participant by dividing discomfort ratings for the medium stimulus by the mean of the thick and thin ratings. High scores on this index identify those participants who find the medium stimulus relatively discomforting compared to the two control stimuli. Overall scores for the CHi and VDS were computed according to the instructions for those tools. Finally, data for headache frequency, intensity and duration and the experience of sensory aura were extracted from the headache and general health questionnaire. These seven measures were then entered into a factor analysis, which identified 3 factors based on a Scree plot analysis. Following a Varimax rotation, the three factors were identified as visual stress (a combination of the CHi, VDS and aura), headache (frequency, intensity and duration) and discomfort (discomfort index). This factor structure is not surprising given the nature of the variables included, but the analysis also served to provide uncorrelated factors to aid the subsequent mass univariate analysis (MUA). It also provided factor scores with which individuals can be compared.

3.2.5 EEG pre-processing

We decimated the EEG data from a sampling rate of 2048Hz to 512Hz using the BioSemi toolbox. EEGs were then band-pass filtered using a second-order Butterworth filter with a

passband of 0.1 to 80 Hz (½ power -3dB, fall-off at 12 dB per octave; for prior precedent for this choice, see Luck, 2014; Tanner, Morgan-Short, & Luck, 2015). For each participant, we performed a time-frequency analysis using a morlet wavelet (a wavelet composed of a complex exponential [carrier]F multiplied by a Gaussian window [envelope], used for time-frequency analysis of non-stationary time series data) with 5-cycles in the frequency range 5-80 Hz, with steps of 1 Hz between each wavelet frequency, and a notch-filter at 50hz. The baseline was initially 500ms long for the wavelet estimation, but after estimation, we cropped the epoch from -100ms pre-stimulus to 800ms post-stimulus, then the conditions were averaged, and baseline (-100ms to zero ms) was rescaled using a logR function in SPM.

3.2.6 Frequency band Selection

We divided the frequency domain into separate bands on onsets 1-8, with stimulus condition (thin, medium and thick) collapsed. The frequencies from Onset 1 and Onset 2-8 were averaged with the spm averaging tool, with weighting by replications (trial counts). Then the windows were selected based on visual inspection of the time-frequency plot at Oz (see Figure 3.2). This does not inflate the false positive rate, because the inspection of the frequency bands was on the aggregated average of the stimulus (i.e., average of activation in response to all three stimulus types) and all onsets, making the frequency selection image blind to stimulus conditions and also to differences between onsets. As a result, the selection of a frequency band is not differentially influenced by a particular stimulus or onset; ensuring that the selection of the frequency bands is not biased. (For justification of this line of reasoning (see Brooks et al, 2017; Bowman et al, 2020)). For each selected frequency band, we collapsed across power values, to generate a single time-series. Frequency bands were as follows:

Alpha: 8-13hz

Beta: 20-35hz

Low Gamma: 30-45hz

Mid Gamma: 45-60hz

High gamma: 60-80hz

We were very explicitly seeking to place windows that isolated the key spectral power features in Figure 3.2, with some windows selected to be narrow to ensure we isolate the "sweet spot" of the feature, see for example our choice regarding alpha. Additionally, we selected overlapping windows for beta and low gamma, in order to include a late (between 700ms and 800ms) power increase in the beta frequency. Thus, we are making a priori decisions concerning our key contrast, which is on the Pattern Glare Index, about placing frequency bands, which necessarily means that we will not place optimally for effects in the data. This is the standard trade-off between type-I and type-II error rates (Bowman et al., 2020).

Eye-blink artefacts were removed using independent component analysis (ICA), with ICA components associated with eye blinks removed and the dataset reconstructed. The crown electrodes were removed to further reduce the presence of muscle and eye-movement artefacts (Chennu et al., 2013), in line with previous work (Shirazibeheshti et al., 2018), who argue that this additional noise may confound MUA (electrodes removed = A11, A12, A13, A14, A24, A25, A26, A27, B8, B9) and the data referenced to the new electrode set. Data for individual onsets were then deleted if any channel exceeded a +/-100 μV threshold, thus removing large artefacts such as movement. The data for each participant were split into 27 bins, one for each stimulus type (thick, medium or thin) and Onset number (1 to 9). Finally, we discarded data from Onset 9 - the number of onsets varied between 7 and 9 on each trial, so the occurrence of the 9th onset was rare, making these data unreliable. Tallying across onset number, three participants who did not

have at least 20% of usable stimulus repeats per stimulus type were removed (decided a priori, based on Luck, 2014). In addition, one participant was removed because an artefact could not be removed, and a further participant was removed because they had EEGs that were flat (i.e. equipment malfunction). For interpolation, approximate values between electrodes of the biosemi and the internal spm grid were calculated when the electrode locations from EEGLAB were combined with the SPM software. This enabled the interrogation of positions on the scalp beyond the electrode locations. In order to compare the stimulus onset with habituation-effects, we divided the repeated onsets into two groups. The initial onsets were analysed separately from Onsets 2-8; the latter being combined. We drew a logical distinction between the first stimulus onset in each trial (where the observer was unaware of the stimuli to be presented) and the remaining onsets (where the participant was able to anticipate the stimulus) and thus analysed Onset 1 separately from Onsets 2-8; the latter being combined so as to aggregate over the maximum number of onsets.

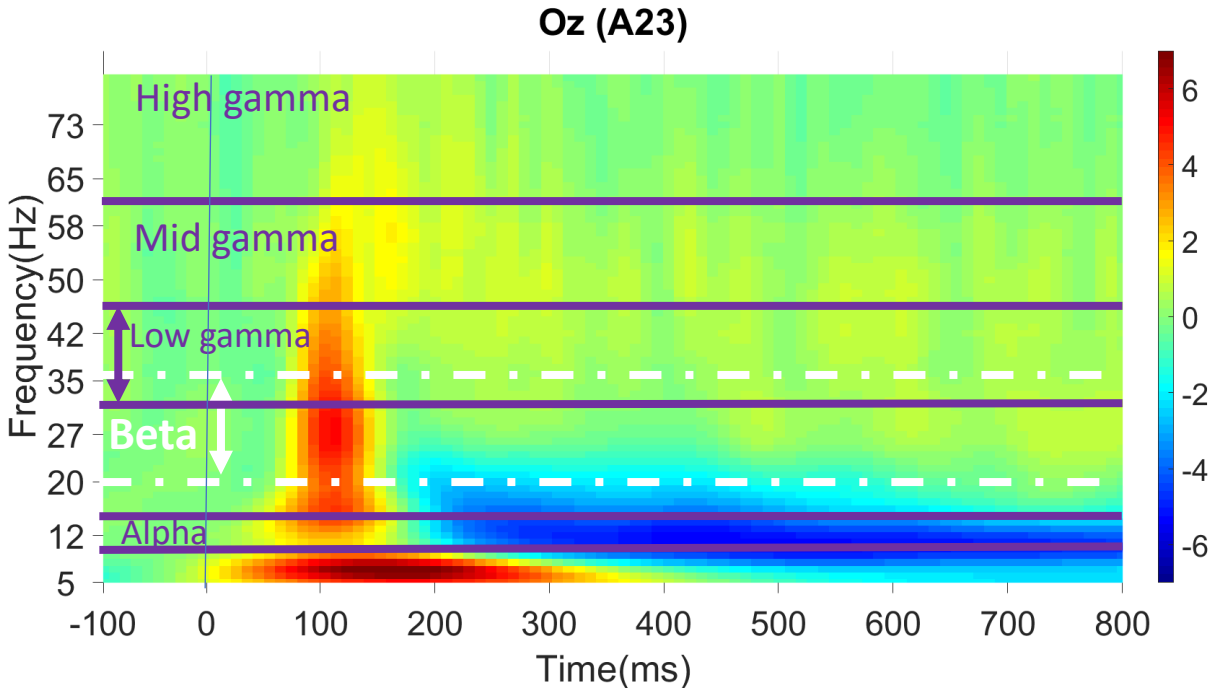

Figure 3-2. Time-Frequency plots of Weighted Average of Onsets 1:8 Aggregated Across all Stimuli (Thick, Medium and Thin) at Electrode Oz.

Bottom to top: frequency bands used for analysis, chosen from electrode Oz: Alpha: 8-13hz, Beta: 20-35hz, Low Gamma: 30-45hz, Medium Gamma: 45-60hz, High gamma: 60-80hz. Colour Scale is -7 to 7dB power. Frequency scale is 5 to 80hz. The frequency ranges were selected through visual inspection; the selection of windows was based on where a strong effect in power could be seen visually (i.e. where there is a marked difference in colour from green in the figure). However, since stimulus conditions (thick, medium and thin) are aggregated across in this plot, this selection is orthogonal to our pattern-glare contrasts that are our central finding, as well as contrasts between Onsets. Note, this selection of frequency ranges was done in order to isolate salient features in this map, consequently some frequencies were narrow, not all frequencies were included, and some ranges overlap. Necessarily, these windows may not be placed appropriately for some pattern-glare effects that may be present, but this is the standard trade-off between type I and type II error rates for a priori selection of features.

3.2.7 Mass Univariate Analysis

A mass univariate analysis (MUA) is the analysis of a large number of simultaneously measured dependent variables (e.g. voxels or samples) via the performance of the same univariate hypothesis tests (e.g., t-tests) across all of those dependent variables. This method allows for powerful error corrections for multiple comparisons.

An MUA was conducted in SPM-12 (Wellcome Trust Centre for Neuroimaging, London, England) on three-dimensional images (two of space, one of time) derived from the ERP data. Images were created using the data for each stimulus type (thick, medium, and thin). Images are

the file type used in the SPM data matrices in order to perform analysis of models or statistical tests. Statistical analyses of M/EEG data in SPM use the same mechanisms as all other data types (PET, fMRI, and structural MRI in voxel-based morphometry ((VBM)).

This simply requires transforming data from SPM M/EEG format to image files (see NIfTI format, http://nifti.nimh.nih.gov/nifti-1/). The result of statistical inference is a summary statistic image, an image representing the data feature summarising treatment effects that one wants to make an inference about. More formally, when this summary statistic is itself a maximum likelihood estimate based on within-subject data, the analysis is called a summary-statistic procedure for random-effects models (Litvak et al., 2011).

In the context of this paper, we will be regressing the dependent variable (the EEG data) onto parametric regressors (the factors). Consequently, our summary statistic images reflect the extent to which the dependent variable correlates with the factor, as reflected in beta coefficients and one-sample t-tests exhibiting a difference from zero.

A contrast image was created based on what we call the pattern glare index (PGI). This index enables us to focus our analysis on regions of the data volume where the clinically relevant, medium stimulus exhibits an extreme response relative to the thick and thin stimuli. Which is the response to EEG of the particular stimulus.

PGI = (medium image – average (thick image, thin image)).

Then, we used the factor scores derived from the factor analysis as parametric regressors in the MUA, excluding factor scores from the five participants whose EEG data failed our screening tests. A general linear model (GLM) analysis was performed on the data where the PGI over ERPs was the dependent variable, while the independent variables were the normalised

factor scores of the trait and state data responses (which act as regressors). This same general linear model was fit to the ERP data at each time-space point in the data volume, providing beta parameter values for all the regressors (the intercept and three factors) at each such point. Intuitively, each parameter value indicates the extent to which the evoked response at the corresponding time-space point correlates (across subjects) with the relevant regressor. In this way, a mass univariate analysis is able to identify time-space regions in the data volume, which vary in a fashion consistent with a factor or intercept. Additionally, due to the mean centring of regressors, the intercept parameter is the mean of the evoked response at that time-space point.

Mean/intercept. We first tested the mean/ intercepts over the whole volume in all five frequency bands, both positive-going and negative-going. We used a one-tailed, 1-sample t-test: We checked for a significant peak (FWE .05, peak-level) or cluster (unc .001, 0.05 FWE corrected) levels in both +1 and -1 directions on the mean/intercept of aggregated (thin+medium+thick) and then on mean/intercept of PGI. Most of our visualisation use thresholded and unthresholded t-maps for both aggregated and PGI. We also show PGI and factor score effects in the form of time-series.

3.2.8 Orthogonal Contrast Methods for Selecting Exploratory Factor Effects

As previously discussed, our factor analysis identified three orthogonal factors: 1) visual stress (a combination of the CHi, VDS and aura measures), 2) headache (frequency, intensity and duration) and 3) discomfort (discomfort index). The electrophysiological effects that we observe on these three factors are generally lower amplitude than those arising from mean/intercept contrasts. This becomes a particular issue, since in order to reliably perform FWE correction in SPM with random field theory (RFT), which is 'a body of mathematics defining theoretical results for smooth statistical maps' which is used to FWE (i.e. multiple comparisons) correct in neuroimaging research (Brett, et al., 2003). Only voxels that, in a first level test (i.e. just on that

voxel), cross this threshold, can contribute to clusters. Such a threshold is likely to be conservative for EEG/ MEG data, where effects tend to be broad in extent, i.e. comprising a large proportion of the volume, but low in amplitude.

As a result, we have applied two orthogonal contrast approaches (Brooks et al., 2017; Bowman et al., 2020) to identify effects on these factors. The orthogonality here is based upon the observation that, by construction, each of our factors is orthogonal to the mean/intercept, and indeed, factors are orthogonal to each other, i.e. dot-products of the corresponding pairs of regressors are zero.

Thus, the methods we apply are statistically robust and do not inflate false positive rates: see Brooks et al., 2017 for simulations and Bowman et al., 2020 for further simulations and a mathematical proof that confirm that type I errors are not inflated. Nonetheless, since several contrasts have had to be performed in the procedures we now outline, we consider these findings on factors as exploratory, and requiring of replication before they can be conferred the mark of reliability.

The orthogonal contrast procedure that we perform proceeds as follows:

1) We are specifically interested in effects on factors inside the significant clusters that we observe on the mean/intercept of the PGI. We are seeking to link these PGI effects to participants' state and trait characteristics, as encoded in the factors. Consequently, it is natural to employ an ROI approach, in which ROIs are selected from the PGI mean/intercept effects, and we look for effects on factors in these ROIs. This is the strategy we employ.
2) Cluster inference in ROI: our first strategy is to perform cluster-inference on factors within each ROI that is extracted from the mean/intercept. This approach does not substantially increase statistical power if the mean/intercept of PGI cluster, and thus the resulting ROI is very large. This is simply because the statistical power of FWE correction goes down with the size of the

volume over which it is performed. Many of the ROIs that we take forward from the mean/intercept of PGI are indeed very large. Consequently, although there are strong effects on factors within these PGI ROIs, they in all but one case, do not both cross the 0.001 threshold and survive FWE correction in the associated ROI.

3) Uncorrected at peak in ROI: our second strategy is to focus on peaks in the PGI mean/intercept clusters, i.e. take one-point ROIs forward from the PGI mean/intercept. Since peaks are single points in the volume, there is no need to FWE correct with them. Accordingly, an effect on a factor that is significant uncorrected at a peak in a PGI mean/intercept cluster is reliable as long as the PGI mean/intercept, and corresponding factor are orthogonal, which, as we have discussed, they are by construction.

These two orthogonal contrast approaches are interestingly sensitive in different ways. The cluster inference in ROI approach will detect effects that are high amplitude (since the 0.001 threshold is applied), but are not necessary throughout a very large proportion of the ROI. In contrast, the Uncorrected at peak in ROI approach will be sensitive to lower amplitude effects (since only an uncorrected 0.05 threshold needs to be crossed). However, for these effects to happen to fall at peaks of a mean/intercept of PGI cluster (which only reflect a small overall part of the mean/intercept cluster), they will typically need to be broadly distributed throughout the cluster/ROI. In this sense, the Uncorrected at peak in ROI approach is likely to do better for low amplitude, but broad in ROI, effects, which we have argued is the way that signal often manifests in EEG, and indeed, we do find this second approach more sensitive than the cluster inference in ROI approach.

3.3 Results

For this experiment, we performed several analysis steps (see materials and methods for full explanation). For this section, we will first discuss the aggregated effects, then PGI

mean/intercept effects, and finally, PGI effects on factors. For a breakdown of statistics, each analysis step has associated tables for statistics (either table 3.1, 3.2, or 3.3). In summary, we have significant results on the aggregated (table 3.1), the PGI index (table 3.2), and on the factors (table 3.3).

3.3.1 Aggregated mean/intercept contrasts

Figure 3.3 shows the results of the aggregated mean/intercept contrasts, topographic maps, the rows from top to bottom indicate if the topographic maps are either thresholded or unthresholded. Onset 1 or Onset 2:8 is indicated on the right. The columns indicate what frequency band is being shown. Within the unthresholded topographic maps, we have indicated effects of interest, early positive transients or sustained synchronisations (see key for full breakdown), with, for example, alpha showing a large desynchronisation on Onset 1 and 2:8. In contrast, we see a synchronisation in the other frequency bands. We can also see that beta and low gamma are showing strong posterior peaks.

Note, the early positive transient bleeds into the baselining window for alpha Onset 2:8, see feature highlighted with dotted rectangles in unthresholded maps. This is just because of the smoothing effect of the wavelet, when frequencies are low. A consequence of this is that the thresholded maps for alpha, specifically alpha 2:8, cut off a period where there is a significant effect, i.e. before 50ms.

There is no consistent scale across thresholded maps, in order to avoid colour saturating in some maps. The white vertical line indicates onset of the stimulus.

As a summary of Figure 3.3, we can identify four main features in this power analysis of aggregated, which, as just discussed, can be divided into early positive transients and sustained

responses. The four features are highlighted with white framing in panels where they are particularly evident (see Figure 3.3 and Legend).

Early Positive Transients

1) *Posterior to anterior, constant amplitude*: this transient bleeds from over occipital along midline to over frontal, with *similar* amplitude throughout (e.g. alpha 2-8, dotted framing).

2) *Clear posterior peak*: this has a higher peak over occipital (e.g. beta and low gamma for onsets 1 and 2-8, dashed framing).

Sustained Responses

1) *Desynchronisation*: this starts after the positive transient and can be quite broadly distributed across the scalp (e.g. alpha 2-8, long dash, dot framing).

2) *Synchronisation*: this starts after the positive transient or after the desynchronisation has subsided and tends to be relatively local to occipital regions (e.g. mid-gamma 2-8, unbroken framing).

The resolution of uncertainty associated with onset 1 (before which the stimulus to be presented is not known) seems only to increase the strength of a single feature, which is the sustained desynchronisation. For example, the response to onset 1 compared to for onsets 2-8, seems to be somewhat more occipitally focused for alpha and beta and also continues into higher frequencies: low, mid and high gamma.

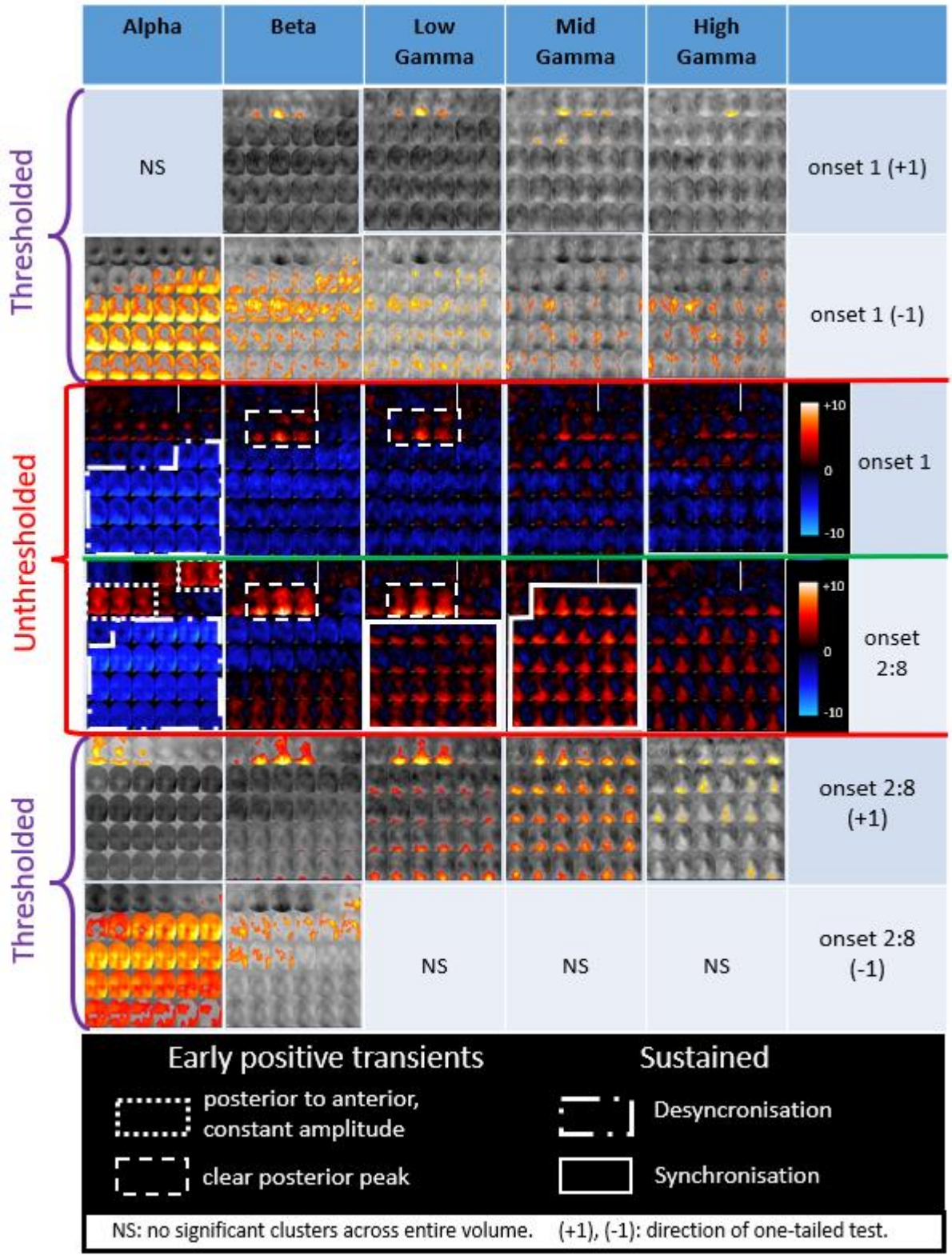
Alpha
Beta
Low Gamma
Mid Gamma
High Gamma
Thresholded
Unthresholded
Thresholded
NS
onset 1 (+1)
onset 1 (-1)
onset 1
onset 2:8
onset 2:8 (+1)
onset 2:8 (-1)
NS
NS
NS
+10
0
-10
Early positive transients
posterior to anterior, constant amplitude
clear posterior peak
Sustained
Desyncronisation
Synchronisation
NS: no significant clusters across entire volume.
(+1), (-1): direction of one-tailed test.

Figure 3-3. Time-frequency effects on the mean/intercept of aggregated (Thin+Medium+Thick): frequency bands are presented in five columns (from left to right: alpha, beta, low gamma, mid gamma and high gamma); first two rows present thresholded maps for onset 1, next two rows present unthresholded maps (onset 1 and then onset 2:8), last two rows present thresholded maps for onsets 2:8. Thresholded maps show one-tailed t-tests, with direction indicated by bracketed terms (e.g. "(+1)" is right-tailed). Each panel of the plot shows scalp maps through time, laid out from top left to bottom right in the panel. Unthresholded maps (blue, black and red) show scalp maps from -100ms to 775ms in steps of 25ms, with 0ms, indicated with a white vertical line. Thresholded maps (yellow, orange, grey) show scalp maps from 50 to 775ms in steps of 25ms. Key findings are most evident in unthresholded maps (middle two rows). Raw one-sample t-values are presented for difference to zero, with red positive-going and blue negative-going. Four features are highlighted with white framing in panels where they are particularly evident (see legend and main text). Thresholded maps result from whole-volume cluster-level familywise error correction (first level, cluster-forming, threshold set at 0.001; second-level FWE correction at 0.05), see table 3.1 for full presentation of these statistics. There is no consistent scale across thresholded maps, in order to avoid colour saturating in some maps. Note, the early positive transient bleeds into the baselining window for alpha onset 2:8, see feature highlighted with dotted rectangles in unthresholded maps. This is just because of the smoothing effect of the wavelet, when frequencies are low. A consequence of this is that the thresholded maps for alpha, specifically alpha 2:8, cut off a period where there is a significant effect, i.e. before 50ms.

Table 4.1 shows the results breakdown of the associated statistics of the effects from Figure 3.3. Each cluster is given with its Xmm, Ymm, Zms location and time with both *T* and *P* values. From left to right, the columns indicate the frequency of interest and the rows indicate Onset 1 or 2:8. NS means that there was no statistical effect found. Loc is the location of the

cluster; LC means largest cluster, SLC, second-largest cluster and NLC means the next largest cluster.

Alpha	Beta	Low Gamma	Mid Gamma	High Gamma	
NS	LC: *t*(30)=7.98 *P*<.001 Loc:13, -79, 105 K:654	LC: *t*(30)=7.78,*P*<.001 Loc: 4,-89, 96 K:661	LC: *t*(30)=6.51, *P*<.001 Loc: 4, -84, 105 K:549 SLC: *t*(30)=4.42,*P*<.001 Loc: -13, -73, 252 K:260	LC: *t*(30)=6.03, *P*<.001 Loc: 9, -89, 125 K:257	onset 1 (+1)
LC: *t*(30)=7.67, *P*<.001 Loc: 13, -79, 477 K:34316	LC: *t*(30)=7.29, *P*<.001 Loc: -9, 2, 379 K:15731	LC: *t*(30)=6.27,*P*<.001 Loc: -51, -36, 311 K:2909 SLC: *t*(30)=5.54, *P*<.001 Loc: 9,-30,730 K:1786 NLC:t(30)=5.39, *P*<.001, Loc: 0, --25, 516, K:315 NLC:*t*(30)=5.25, *P*<.001,Loc: 60,-68,721 K:379 NLC:*t*(30)=4.84, *P*=.004, Loc: 58,-14, 574, k:203	LC: *t*(30)=7.67,*P*<.001 Loc: -60, 8, 398 K:628 SLC:*t(*30)=6.31,*P*<.001 Loc: -51,-25,662 K:843 NLC:*t*(30)=5.73, *P*<.001 Loc: 21, -14, 389 K:558 NLS:*t*(30)=5.48, P=.005, -55, 34, 701 K: 141 NLS:*t*(30)=5.23, *P*<.001, Loc: -47, -30, 740 K:247 NLS:*t*(30)=4.73, *P*<.001, Loc: 60, -9, 730 K:219	LC: *t*(30)=7.97,P<.001 Loc: 47, -19, 379 K:2379 SLC:t(30)=6.74 Loc: -55,-19 652 K:1491 NLC: *t*(30)=6.66, *P*<.001 Loc: -38, 13, 369 K:1140	onset 1 (-1)
LC: *t*(30)=6.50, *P*<.001 Loc: 30, -89, 18 K:3727	LC: *t*(30)=10.86, *P*<.001 Loc: 0, -62, 105 K:2909 SLC: t(30)=5.11, *P*=.001 Loc:-4, -95, 799 K:468	LC: *t*(30)=9.98, *P*<.001 Loc: -26, -84, 115 K: 2512 SLC- t(30)=8.84, *P*<.001 Loc:0, -89, 799 K:4255	LC: *t*(30)=8.84, *P*<.001 Loc: 9, -73, 86 K:9929	LC: *t*(30)=5.75, *P*<.001 Loc: 4,-79, 86 K:663 SLC: t(30)=4.92, *P*<.001 Loc: -9, -52, 252 K:445 NLC: t(30)=4.82, *P*<.001 Loc: -4, -68, 359 K:748 NLC: t(30)=4.54, P<.001 Loc:4, -19, 760 K:307	onset 2:8 (+1)

LC: ***t*(30)=9.55,** ***P*<.001** **Loc:64,** **-41, 281** **K:44785**	LC: *t*(30)=7.36, *P*<.001 Loc:43, -36, 184 K:5735	NS	NS	NS	onset 2:8 (-1)

NS: no significant clusters across entire volume. (+1), (-1): direction of one-tailed test. LC=largest cluster

SLC: second largest cluster NLC: next largest cluster K: Cluster Size Loc: location of cluster, location is Xmm,Ymm, Zms p-values are familywise error corrected at the cluster-level t-values

Table 3-1. ***Aggregated, mean/intercept contrasts****.*

Raw one-sample t-values (uncorrected at peak of cluster) are presented for difference to zero (direction indicated by bracketed terms (e.g. "(+1)" is right-tailed)) and associated p-values (FWE-corrected at 0.05 at the cluster-level, cluster-forming threshold 0.001). Location of cluster is listed in Xmm, Ymm, Zms format. The columns from left to right are alpha, beta, low gamma, mid gamma, and high gamma. The rows from top to bottom are (onset 1 and then onset 2:8). NS means not significant, Loc is the location of cluster, LC is the largest cluster, SLC is the second largest cluster, and NLC is the next largest cluster. K is the size of the cluster in voxels.

3.3.2 PGI mean/intercept contrasts

Figure 3.4 shows the results of the PGI mean/intercept contrasts, topographic maps, the rows from top to bottom indicate if the topographic maps are either thresholded or unthresholded. Onset 1 or onset 2:8 is indicated on the right. The columns indicate what frequency band is being shown. Within the unthresholded topographic maps, we have indicated effects of interest, which were discussed previously, either early positive transients or sustained synchronisations (see key for full breakdown), with white framing. The w, x, y, v, and z letters on the topographic maps indicate their relation to Figure 3.6. Precisely, each letter corresponds to a different effect indicated by a vertical line in the Figure 3.6 graph. The reader can then refer back to Figure 3.4 to

see that indicated effect in the context of the broader findings. Notice, that in Onset 2:8 Unthresholded we see the large, sustained synchronisation in time, which extends from beta to mid gamma frequencies, with some even coming out on high gamma. There is no consistent scale across thresholded maps, in order to avoid colour saturating in some maps. The white vertical line indicates the onset of the stimulus.

With the framing interpretation we just presented and the resulting four phenomena we identified for aggregated, we can see the following in the pattern-glare plots with key features again presented with white framing (see Figure 3.4 and Legend). We begin with the early positive transients

1) *Posterior to anterior, constant amplitude*: there is little evidence of modulation of this by medium grating.
2) *Clear positive peak*: there are only a few frequencies at which we see modulation of this feature. All of these are restricted to Onset 2:8. The feature is somewhat present for mid gamma, and particularly for high gamma (see dashed framing). There may be small effects in beta 2-8 and low gamma 2-8, but these are not obviously separate features form the sustained synchronisation (see below).

Points 1) and 2) here suggest that early positive transients are not markedly increased in amplitude by medium grating, apart from for mid and high frequencies for Onset 2-8. Now focussing on the two sustained effects identified in the aggregated analysis, we can see the following in Figure 3.4.

1) *Negative-Going effect* (see also Figure 3.5): There is no evidence in figure 3.4 of a sustained negative-going effect for any frequency for either Onset 1 or 2:8. In particular, this feature is not present for alpha, where it was strong for the aggregated contrast. The time series in Figure 3.5 show a representation of the alpha effects, showing particularly,

that medium is not influencing the desynchronisation more than thick and thin, i.e. medium, thick and thin exhibit similar desynchronisations. Thus there is no clear evidence that pattern-glare induces a deeper desynchronisation in alpha.

2) *Positive-Going effect* (See also Figure 3.6): as previously discussed, there is robust evidence that pattern glare can enhance the sustained positive-going effects, especially where it is most marked in aggregated: mid and low gamma for 2-8. There is evidence such an enhancement can also be seen in beta 2-8, but this may be explainable by the beta frequency partially overlapping with low gamma 2-8; note for aggregated, beta 2-8 exhibited a sustained desynchronisation followed by a synchronisation for aggregated.

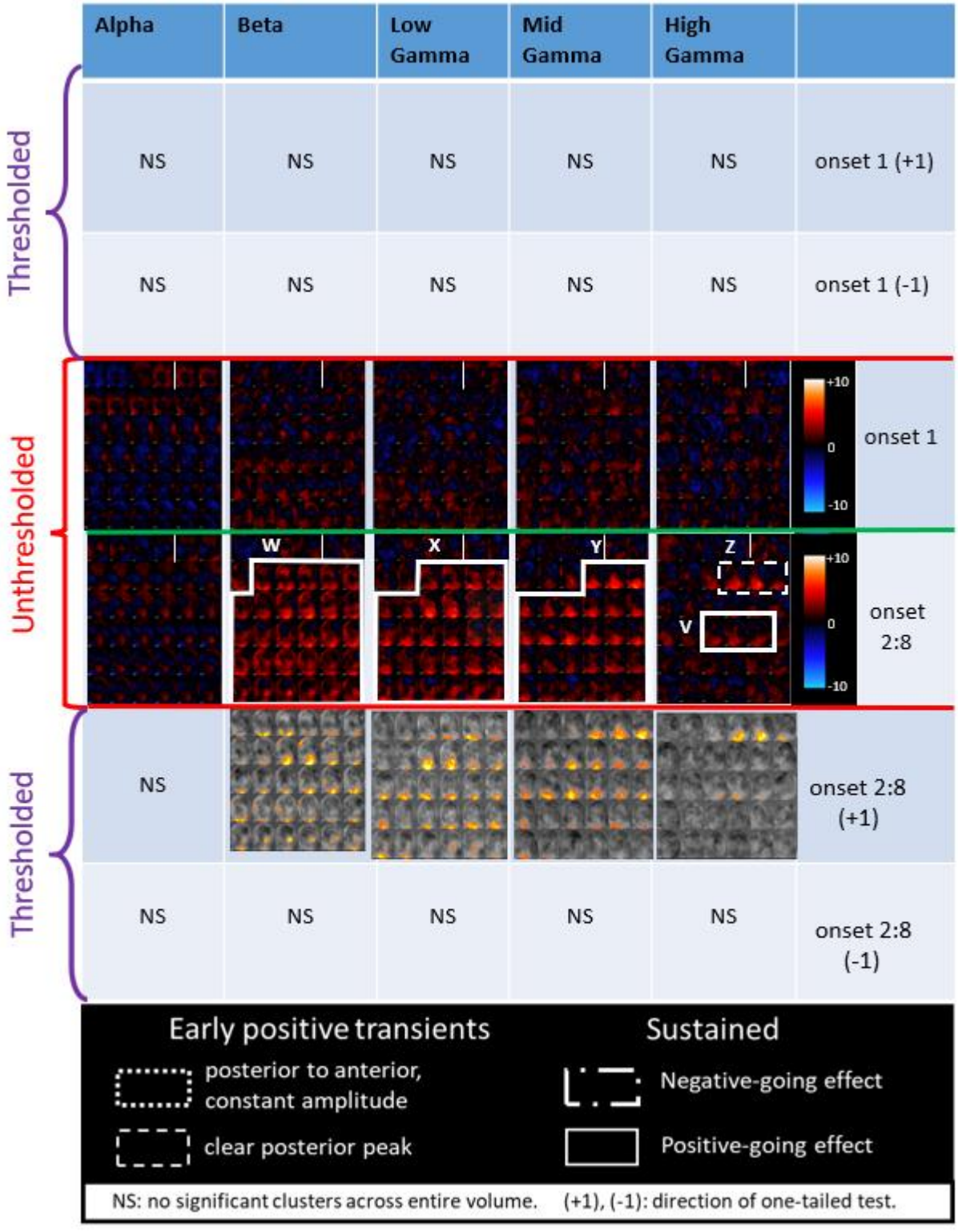
Alpha
Beta
Low Gamma
Mid Gamma
High Gamma
Thresholded
NS
NS
NS
NS
NS
onset 1 (+1)
NS
NS
NS
NS
NS
onset 1 (-1)
Unthresholded
+10
0
-10
onset 1
W
X
Y
Z
V
+10
0
-10
onset 2:8
Thresholded
NS
onset 2:8 (+1)
NS
NS
NS
NS
NS
onset 2:8 (-1)
Early positive transients
posterior to anterior, constant amplitude
clear posterior peak
Sustained
Negative-going effect
Positive-going effect
NS: no significant clusters across entire volume.
(+1), (-1): direction of one-tailed test.

Figure 3-4. Time-frequency effects on the mean/intercept of PGI (PGI=medium-mean (thick, thick)):

Frequency bands are presented in five columns (from left to right: alpha, beta, low gamma, mid gamma and high gamma); first two rows present thresholded maps for onset 1, next two rows present unthresholded maps (onset 1 and then onset 2:8), last two rows present thresholded maps for onsets 2:8. Thresholded maps show one-tailed t-tests, with direction indicated by bracketed terms (e.g. "(+1)" is right-tailed). Each panel of the plot shows scalp maps through time, laid out from top left to bottom right in the panel. Unthresholded maps (blue, black and red) show scalp maps from -100ms to 775ms in steps of 25ms, with 0ms, indicated with a white vertical line. Thresholded maps (yellow, orange, grey) show scalp maps from 50 to 775ms in steps of 25ms. Key findings are most evident in unthresholded maps (middle two rows). Raw one-sample t-values are presented for difference to zero, with red positive-going and blue negative-going. Key features are again presented with white framing (see legend and main text). Thresholded maps show result from whole-volume cluster-level familywise error correction (first level, cluster-forming, threshold set at 0.001; second-level correction at 0.05); see Table 3.2 for full presentation of these statistics. There is no consistent scale across thresholded maps, in order to avoid colour saturating in some maps.

Table 3.2 shows the results breakdown of the associated statistics of the effects from Figure 3.4. Each cluster is given with its Xmm, Ymm, Zms location and time with both *T* and *P* values. The frequency and number order of cluster is given in bold, e.g. B1 is the largest cluster form beta. From left to right, the columns, indicate the frequency of interest and the rows indicate whether it is onset 1 or 2:8. NS means that there was no statistical effect found.

Alpha	Beta	Low Gamma	Mid Gamma	High Gamma	
NS	NS	NS	NS	NS	onset 1 (+1)
NS	NS	NS	NS	NS	onset 1 (-1)
NS	NS	NS	NS	NS	onset 2:8 (-1)
NS	**B1**: LC-*t*(30)=7.01, *P*<.001 Loc: 9, -84, 271 K=2943 **B2:** SLC: *t*(30)=6.34,*P*<.001 Loc: 17, -30, 691 K=350 **B3:** NLC:*t*(30)=5.04 *P*=.002 Loc: -43, -14, 545 **B4:** NLC: *t*(30)=4.99, *P*=.016 Loc:4, -84, 779 K=171 **B5:** NLC:*t*(30)=4.97, *P*=.041 Loc: -43, 40, 271	**LG1**: LC-*t*(30)=7.19, *P*<.001 Loc: 17,-41, 262 K=3969 **LG2**: SLC: *t*(30)=5.30, *P*=.020 Loc: 4, -84, 770 K=118 **LG3**: NLC:*t*(30)=4.84, *P*=.001 Loc: 17, -9, 730 K=207	**MG1**: LC-*t*(30)=7.56, *P*<.001 Loc: -9, -89, 408 K=3724 **MG2**: SLC:*t*(30)=4.64, *P*<.001 Loc: -17, -79, 652 K=375	**HG1**: LC-*t*(30)=6.72, *P*<.001 Loc:17, -68, 145 K=731 **HG2**: SLC:*t*(30)=4.63, *P*=.002 Loc: -13, -89, 408 K=144	onset 2:8 (+1)

Table 3-2. Pattern-Glare Index, mean/intercept statistics.

One-sample t-values (uncorrected) at peak of cluster are presented for difference to zero (direction indicated by bracketed terms (e.g. "(+1)" is right-tailed)) and associated p-values (FWE-corrected at cluster-level, with alpha level 0.05 and cluster-forming at 0.001). Location of cluster is listed in format Xmm, Ymm, Zms and cluster size if taken forward for factor analysis (i.e.., it is posterior in location). The columns from left to right are alpha, beta, low gamma, mid gamma, and high gamma. The rows from top to bottom are (onset 1 and then onset 2:8). NS means not significant, Loc is the location of cluster, LC is the largest cluster, SLC is the second largest cluster, and NLC is the next largest cluster.

As previously discussed, Figure 3.5 shows time-series illustrating that sustained alpha desynchronisation is not driven by medium, i.e. medium, thick and thin exhibit similar desynchronisations.

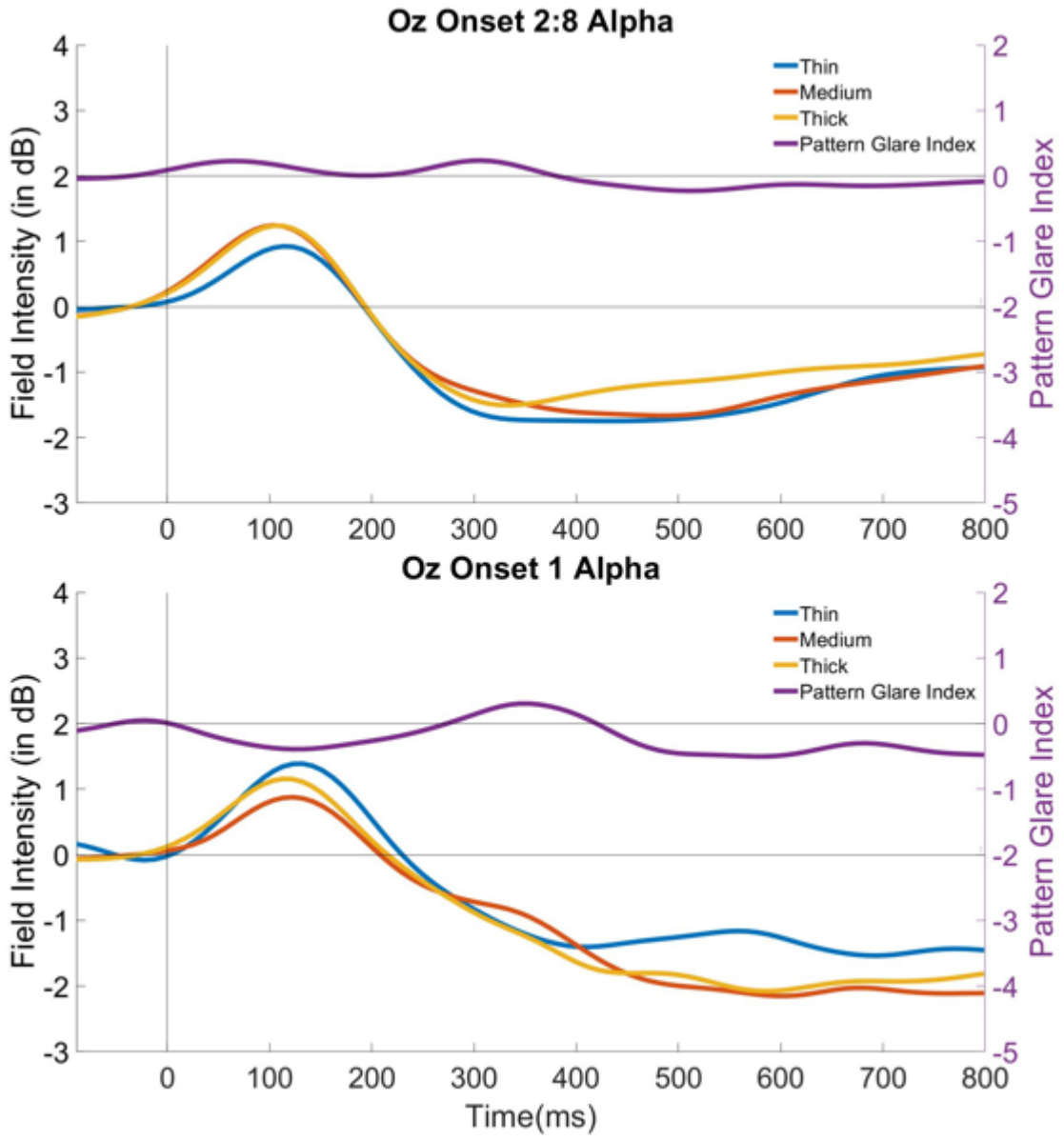

Figure 3-5. Sustained alpha desynchronisation is not driven by medium.
Time series of power summed across Alpha frequency for Onset 2:8 and Onset 1, showing medium, thick, and thin at electrode Oz (A23), along with the pattern glare index. The time series here show a representation of the Alpha effects, specifically, that medium is not influencing the desynchronisation more than thick and thin. This figure shows that medium, thick and thin exhibit similar desynchronisations.

Figure 3.6 shows graphs to illustrate that sustained synchronisation is driven by medium in the (A) beta, (B) low gamma, (C) mid gamma, and (D) high gamma bands for the mean/intercept of the PGI. These panels plot posterior electrodes: A30, A16, and A31. A red arrow indicates the relevant electrode in the glass-map on the upper left-hand side of each plot, v, w, x, y, and z indicate effects that the reader can link back to Figure 3.4, in order to see the effect in the broader context. We can observe that, beta, low gamma, and mid gamma, show large, sustained synchronisations in time driven by medium, with the same effect present, but more intermittent in high gamma.

As previously alluded to, it is striking that for the PGI mean/intercept; the earlier positive transient only seems to yield a clearly distinct effect from the sustained positivity for the higher frequencies (high and mid gamma). Figure 3.6 shows this, where, for thin and thick, the early positive transient subsides to nothing from low to mid to high gamma, while remaining present for medium (see z in panel D and the same feature in panel C).

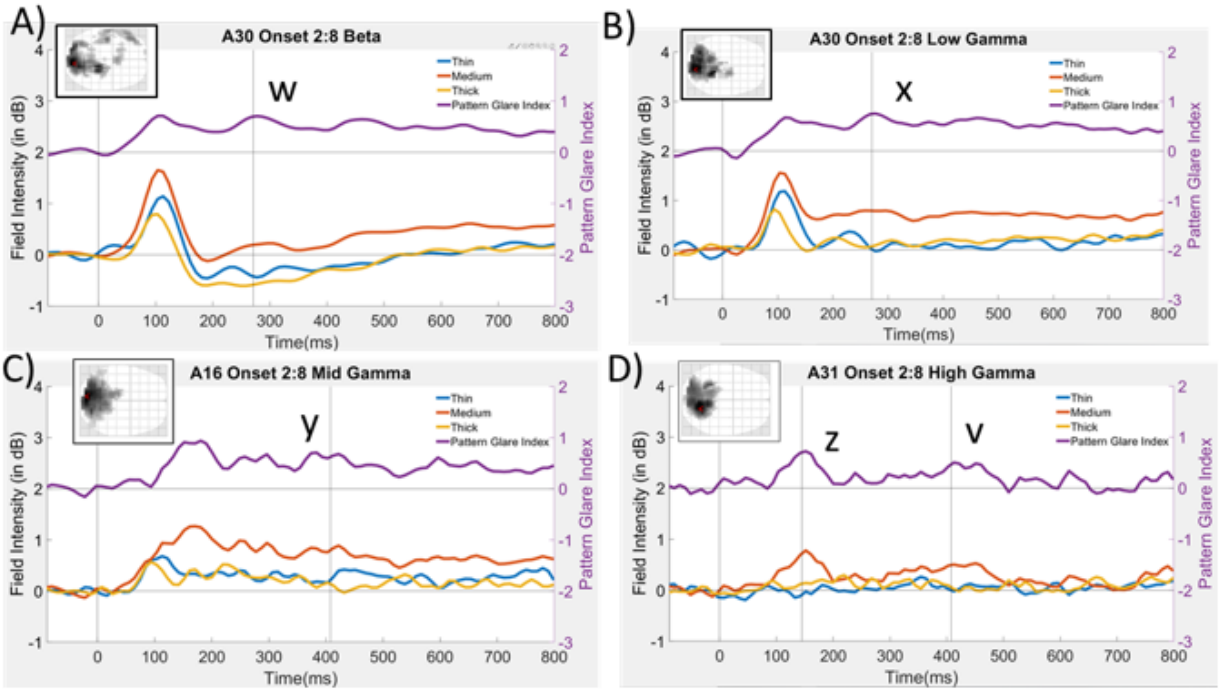

Figure 3-6. time-series of (A) beta, (B) low, (C) mid, and (D) high gamma frequencies, onsets 2:8, at different posterior electrodes, showing synchronisation (both sustained and early positive transient) for medium grating:

Time series of power summed across each frequency band, showing medium, thick, and thin at electrodes A30, A16, A31 (see red arrow in inset scalp map). Plots correspond to different effects in Figure 3.4: (A) beta to effect w; (B) low gamma to x; (C) mid gamma to y; and (D) high gamma to v and z. These effects can also be seen in the PGI time-series in these plots, see right-side y-axes. The scalp maps here show an spm glass scalp, in which all significant effects through time are collapsed onto a two-dimensional representation. It shows that the electrode being plotted (red arrow) is at a position where there is considerable significance through time. Positive is plotted up on time-series.

3.3.3 Factor Effects

Figure 3.7 shows the results of regressing the PGI onto the three-factor effects, with factor scores presented in three columns (from left to right: F1 (headache) +1, F2 (VSQ) +1, F3 (Discomfort) +1); the rows represent topographic maps for the different averaged frequencies (from top to bottom: beta, low gamma, mid gamma, and high gamma). These maps are unthresholded, allowing the full quantitative pattern of the data to be observable. The white outlines indicate the areas where the effects of interest for us arise a, b, c, d, e, and f. These letters also appear in the figures of the time-series for factors, which follow, enabling effects in topographic maps and time-series to be linked.

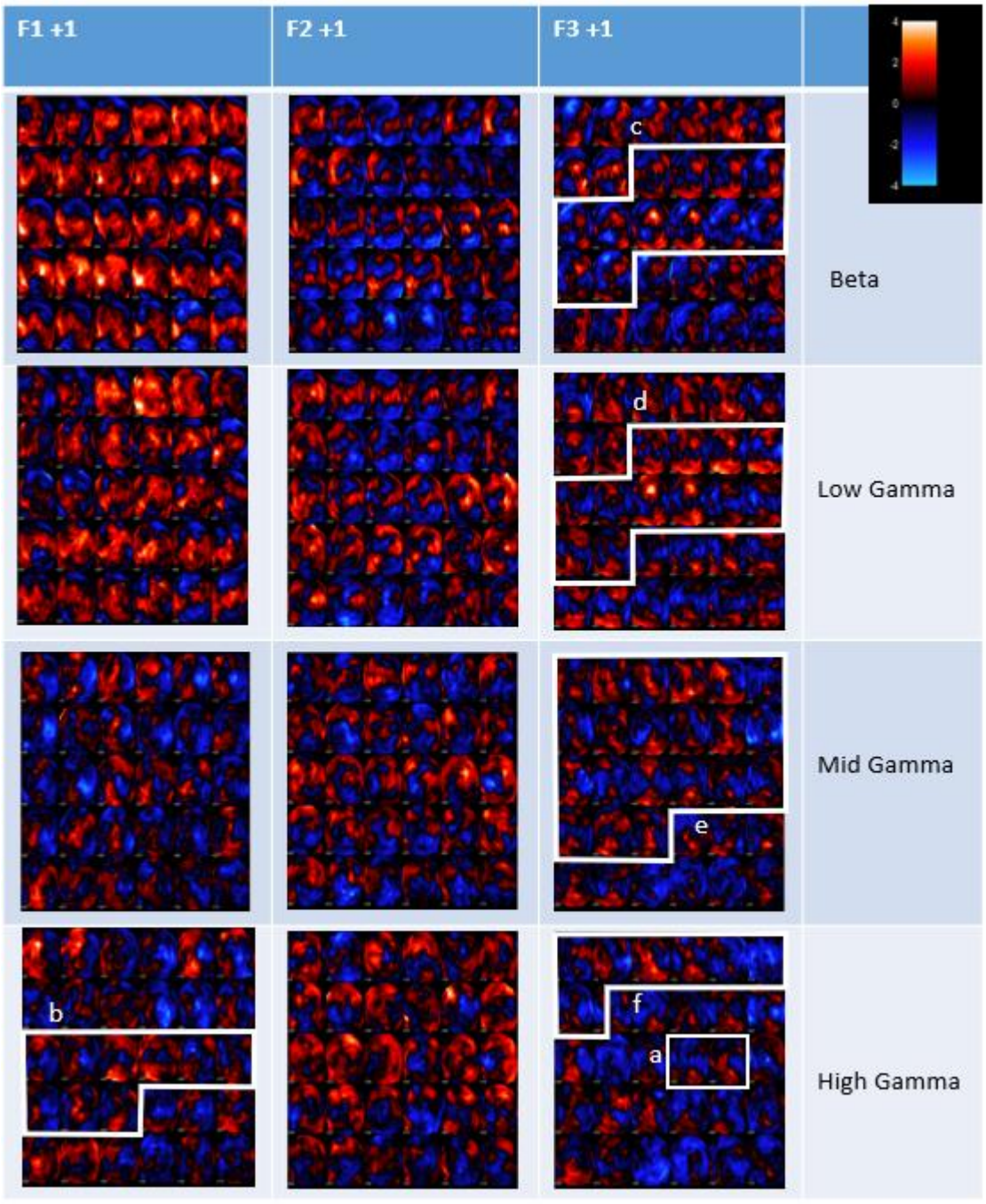
F1 +1
F2 +1
F3 +1
c
Beta
d
Low Gamma
e
Mid Gamma
b
f
a
High Gamma

Figure 3-7. Onset 2:8 results of regressing PGI onto factor scores.
Factors are presented in three columns (from left to right: F1+1(VSQ, Chi, Aura, positive-going effect), F2 +1(Length, Intensity, Duration of headache, positive-going effect), F3 +1 (Discomfort, positive-going effect)); the rows represent topographic maps for the different averaged frequencies (from top to bottom: beta, low gamma, mid gamma, and high gamma). Each panel of the plot shows scalp maps through time, laid out from top left to bottom right in the panel. Scalp maps are from 50ms to 775ms in steps of 25ms. Scale is from -4 to 4.
The maps in Figure 3.7 are unthresholded, not enabling us to make statistical inferences. As previously discussed, in this respect, we are specifically interested in the effects on factors that enable us to explain the PGI mean/intercept effects identified in the previous section. Accordingly, as discussed in the methods, we employ a procedure that looks explicitly for significant effects in ROIs selected from the clusters observed in Figure 3.7.

Two methods of analysis were conducted on the results of regressing PGI onto factors (see Figure 3.7). These two methods are as follows:

1. *Orthogonal cluster inference in the region of interest (ROI).*

An ROI was produced using the clusters of interest from the PGI mean/intercept contrast. This is used because it is orthogonal to the factors by design. This procedure identified one peak for high gamma for factor 3 at 438ms ($t(30)=3.51$ (uncorrected at peak of cluster), $p=.038$ (FWE-corrected at cluster-level)); see Figure 3.8.

2. *Uncorrected analysis at peak of region of interest*.

Eleven of the peaks that were identified in significant cluster ROIs from the PGI mean/intercept yielded significant effects (uncorrected) on positive-going factors (see Figure 3.7). Of these, seven were on F3 (+1); three F1 (+1); and one F2 (+1) (see Table 3 for full statistical

breakdown). We applied the following criteria to determine the effects at peaks to focus on particularly: - *posterior*: effects should be approaching Oz, since we have the greatest prior precedent for such effects (Adjamian et al., 2004); *contiguous to substantial cluster*: effect being observed at a single point is not isolated, i.e. it is contiguous to a substantial cluster, particularly that is extended in time. Effects that did not satisfy these criteria can be found in the Appendix. Table 3 shows the results breakdown of the associated statistics of the factor effects from Figure 3.7. Each peak is given within the mean/intercept cluster/ ROI that it sits in, stated in the format Xmm, Ymm, Zms (two spatial locations and one of time), with associated *t*-values. The mean/intercept cluster/ROI, if it was posterior near occipital lobe, is given, with the frequency band and order in cluster size given in bold, e.g. B1 is the largest cluster from beta. From left to right, the first column indicates the mean/intercept cluster/ROI; the second the regressor of interest (either mean/intercept, factor 1,2 or 3), the following columns indicate peaks of the frequency-band cluster/ROI being examined. From top to bottom, the rows indicate what cluster of what frequency band is indicated, e.g. B1, is the largest cluster in the beta frequency. NS means that there was no statistical effect found.

T-values	Parametric-Regressor (All on onset 2:8, positive-going effects)	Peak 1	Peak 2	Peak 3
B1	**Mean/intercept**	**9,-84, 271**	**9,-84,428**	**13,-84, 438**
	F1	NS	NS	NS
	F2	NS	NS	NS
	F3	***1.86***	NS	NS
B2	**Mean/intercept**	**17,-30, 691**	**26,-30, 701**	**30,-25,740**
	F1	NS	***2.02***	NS
	F2	NS	NS	NS
	F3	NS	NS	NS
B3	**Mean/intercept**	**4,-84,779**	**-13,-84,779**	**No 3rd major peak**
	F1	NS	NS	
	F2	NS	NS	
	F3	NS	NS	
LG1	**Mean/intercept**	**17, -41, 262**	**9, -84, 271**	**-9,-73,252**
	F1	NS	NS	***2.15***
	F2	NS	NS	NS
	F3	NS	***2.704***	NS
LG2	**Mean/intercept**	**17, -9, 730**	**21,-9,643**	**13,-46,740**
	F1	NS	NS	NS
	F2	NS	***3.81***	NS
	F3	NS	NS	NS
LG3	**Mean/intercept**	**4,-84,770**	**13,-89,760**	**-9,-73,799**
	F1	NS	NS	NS
	F2	NS	NS	NS
	F3	NS	NS	NS
MG1	**Mean/intercept**	**-9, -89, 408**	**0, -89, 145-A23**	**-9, -89, 135**
	F1	NS	NS	NS
	F2	NS	NS	NS
	F3	***2.58***	***1.85***	***2.5***
MG2	**Mean/intercept**	**-17, -79, 652**	**-9,-89,564**	**13, -79,564**
	F1	NS	NS	NS
	F2	NS	NS	NS
	F3	NS	NS	NS
HG1	**Mean/intercept**	**17, -68, 145**	**9, -68,145**	**9,-52,145-A32**
	F1	NS	NS	NS
	F2	NS	NS	NS
	F3	NS	NS	***2.02***

Table Continued

HG2	**Mean/intercept** **F1** **F2** **F3**	**-13,-89, 408,** ***3.12*** NS NS	**17,-57,438-A32** NS NS ***3.09***	**-17,-79,438** NS NS NS

Table 3-3. ***Factor effects at peaks from Pattern-Glare Index mean/intercept effects.*** *(Uncorrected) one-sample t-values are presented for difference to zero (right-tailed) and associated locations. Location of cluster is listed as Xmm, Ymm, Zms. The columns from left to right are, first, identifier of mean/intercept cluster/ ROI, second a description of the regressor (mean/intercept, F1, F2, or F3), then the remaining columns are peaks within that ROI. The rows from top to bottom are the clusters/ROI in order of size denoted by the first letter/s of the name of the frequency band, i.e., HG= High Gamma. NS means not significant.*

To interpret the peaks and clusters we obtain, we perform median splits on the corresponding factor, and present the corresponding (thin, medium and thick) time-series for high and low groups. We also present PGI time-series for high and low, as well as the difference of PGI. The difference of PGI is an indicative visualisation of an effect on a factor. However, it is no more than indicative. That is, it will frequently be the case that when there is a large positive PGI effect on a factor, those in a high median split group will have bigger PGI than those in a low median split group. However, this is not always going to be the case, since a median split goes not take into account the factor loadings for different participants, i.e. it effectively assumes that all loadings in the high group are +1 and all loadings on the low group are -1. Consistent with this, we, in some cases, see differences of PGI near zero at the position of a significant PGI effect on a factor.

We start by considering the single effect that was significant under our first statistical inference approach (*Orthogonal cluster inference in the region of interest (ROI)*) Figure 3.8

shows thresholded and unthresholderd topographic maps, and time series at electrode A32, for factor 3 high gamma (HG) on onsets 2:8. As just stated, this effect was significant according to the orthogonal cluster inference at the region of interest (ROI) method,for HG at 438ms ($t(30)=3.51$, $p=.038$). The left topographic maps are thresholded. The right is the unthresholded map. The white box indicates the significant electrode and associated cluster of effect. High [A] and Low [B] on median split of Factor 3 (discomfort) are presented, showing in both cases, Thin, Medium and Thick, and PGI. PGI for High and Low median splits, along with difference of High and Low PGIs are also presented [C]. The 'a' on the graph can be used to refer back to Figure 3.7 to compare effects in the broader context. Both topographic maps are from 430 to 450ms in 2ms steps. The vertical line on all 3 time series at 438ms shows the peak of significance. As we can see, this effect is limited in time, and positioned somewhat anterior to Oz.

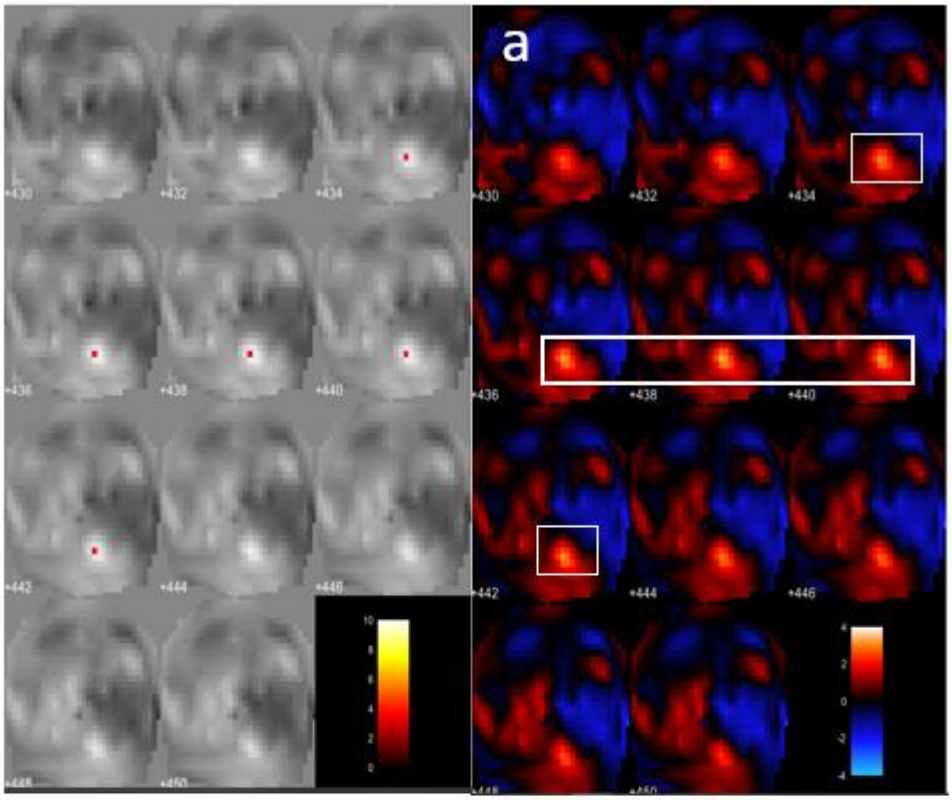
a
+430
+432
+434
+436
+438
+440
+442
+444
+446

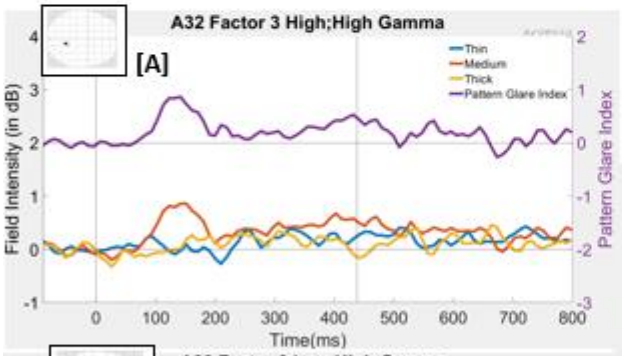
A32 Factor 3 High;High Gamma
[A]
Thin
Medium
Thick
Pattern Glare Index
Field Intensity (in dB)
Pattern Glare Index
Time(ms)

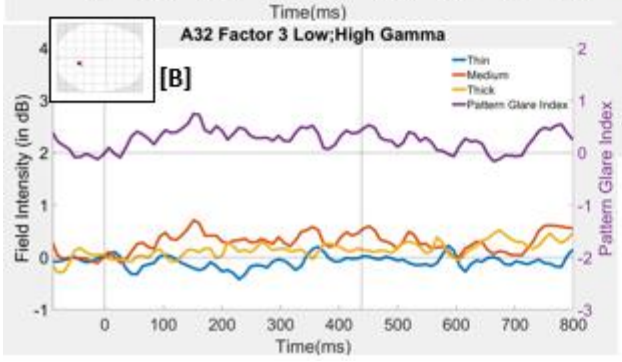
A32 Factor 3 Low;High Gamma
[B]
Thin
Medium
Thick
Pattern Glare Index
Field Intensity (in dB)
Pattern Glare Index
Time(ms)

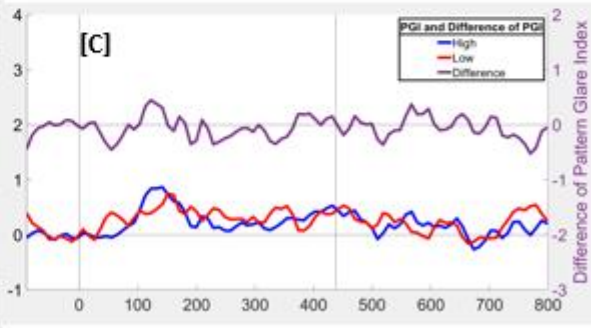
[C]
PGI and Difference of PGI
High
Low
Difference
Difference of Pattern Glare Index

Figure 3-8. thresholded and unthresholded topographic maps, and time-series at electrode A32 illustrating effect on factor 3 positive going within ROI from PGI mean/intercept, High Gamma frequency, Onset 2:8:

Peak in PGI mean/intercept cluster is at 13mm, -57mm, 438ms, see vertical line, here placed on the closest electrode. The vertical line is the same in the difference of PGI time-series as well. Topographic maps (upper half of figure) are from 430 to 450ms, in 2ms steps. Left side maps are thresholded, and have a scale of 0 to 10. Right side maps are unthresholded, and have a scale from -4 to 4. The "a" links to the effect in Figure 3.7. White boxes indicate the cluster where the effect sits. Stimulus time series are of power summed across High Gamma frequency. [A] High and [B] Low on median split of factor 3, showing in both cases, Thin, Medium and Thick, and PGI. [C] PGI for High and Low median splits, along with difference of High and Low PGIs. The scalp maps on panels [A] and [B] show an SPM glass scalp, in which all significant effects through time are collapsed onto a two-dimensional representation. It shows the electrode being plotted as the red arrow. Positive is plotted up on time-series.

We now move to effects that are significant with our second ROI approach (*uncorrected analysis at the peak of ROI*). Figure 3.9 shows the high gamma effect for factor 1 at Oz using this uncorrected analysis at the peak of ROI approach on onsets 2:8. The topographic maps shown are unthresholded from 350 to 550ms in 25ms steps. The peak of PGI mean/intercept cluster is at -13mm, -89mm, 408ms. The white box indicates the significant electrode and associated cluster of effect. High [A] and Low [B] on median split of factor 1 are presented, showing in both cases, Thin, Medium and Thick, and PGI. Panel [C] presents PGI for High and Low median splits, along with difference of High and Low PGIs. The 'b' on the scalp maps can be used to refer back to Figure 3.7 to compare effects in the broader context. High gamma was significant $t(30)=3.12$, $p<.05$, (for full statistical breakdown see, table 3, refer to HG2, row). This F1 effect is positioned

close to Oz, where we have a strong prior precedent, and is placed within a clear cluster on the difference of PGIs (see panel C).

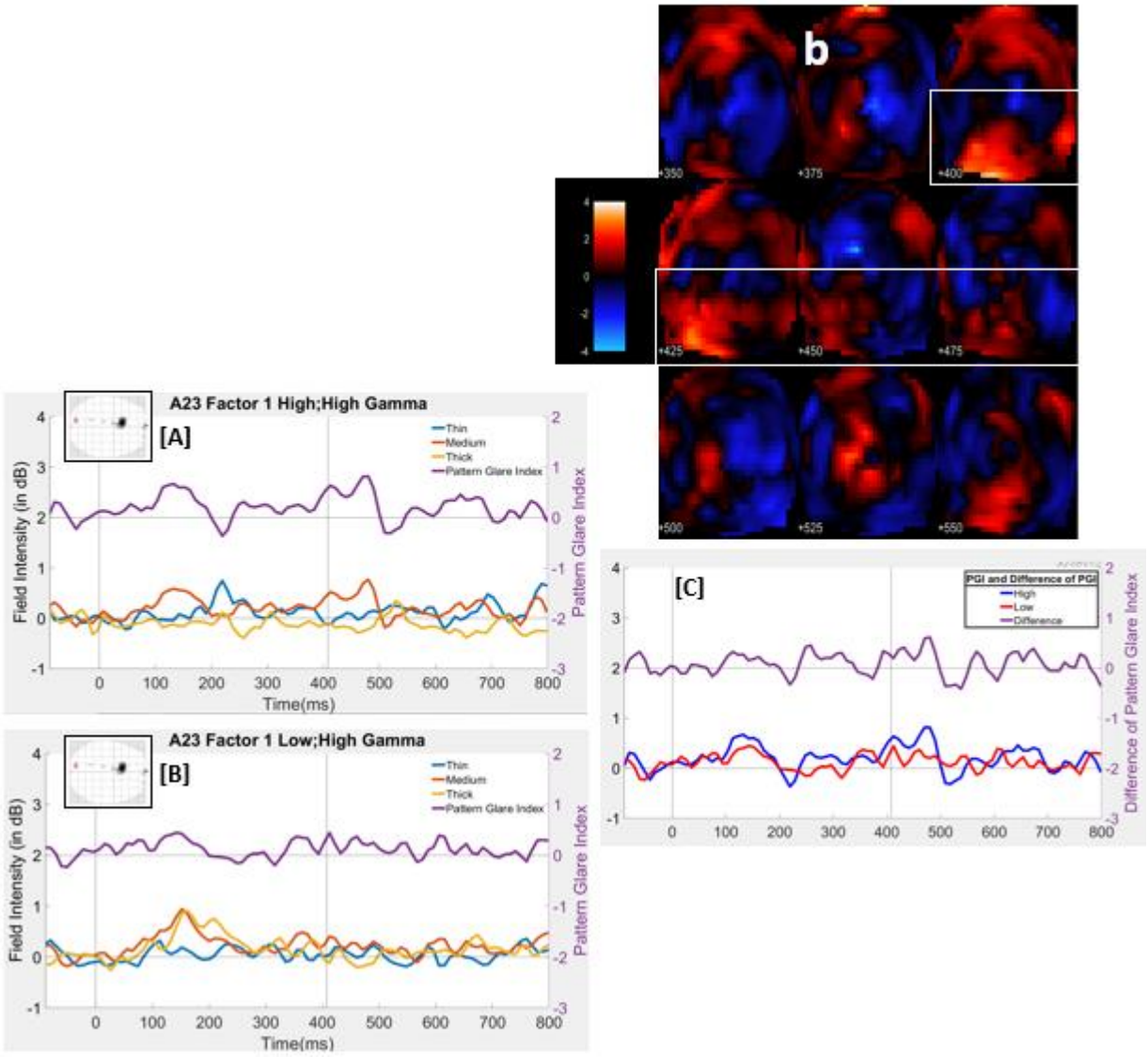

Figure 3-9. Topographic maps and time-series at electrode A23 (Oz), illustrating the effect on factor 1 positive-going, High Gamma frequency, Onset 2:8:

Peak of PGI mean/intercept cluster is at -13mm, -89mm, 408ms, see vertical line, here placed on the closest electrode. The topographic maps are unthresholded and from 350 to 550ms, in 25ms steps, the scale is from -4 to 4. The "b" links to effect in Figure 3.7. The white boxes indicate the cluster where the effect sits. Stimulus time series are of power summed across High Gamma frequency. [A] High and [B] Low on median split of factor 1, showing in both cases, Thin, Medium and Thick, and PGI. [C] PGI for High and Low median splits, along with difference of High and Low PGIs. The SPM glass scalps shown on [A] and [B] depict all significant effects through time collapsed onto a two-dimensional representation. It shows the electrode being plotted as the red arrow. Note, Oz is off the midline in this depiction, since crown electrodes were removed. Positive is plotted up on time-series.

Figure 3.10 shows the effect for Beta on factor 3 at electrode A30 using the uncorrected analysis at the peak of ROI approach on onsets 2:8. The topographic maps shown are unthresholded from 250 to 525ms in 25ms steps. The peak from the PGI mean/intercept cluster is at 9mm, -84mm, 271ms. The white boxes indicate the region and associated cluster that contains the significant (uncorrected) peak on the factor. High [A] and Low [B] on the median split of factor 3 are presented, showing in both cases, Thin, Medium and Thick, and PGI. PGI for High and Low median splits [C] is also shown, along with difference of High and Low PGIs. The 'c' on the graph can be used to refer back to Figure 3.7 to compare effects in the broader context. Beta was significant uncorrected $t(30)=1.86$, $p<.05$, (for full statistical breakdown see, table 3 and refer to B1, F3 row). This effect is clearly posterior, where we have our strongest prior precedents, and sits at the start of an extended cluster through time of a strong difference between High and Low on PGI; see panel [C].

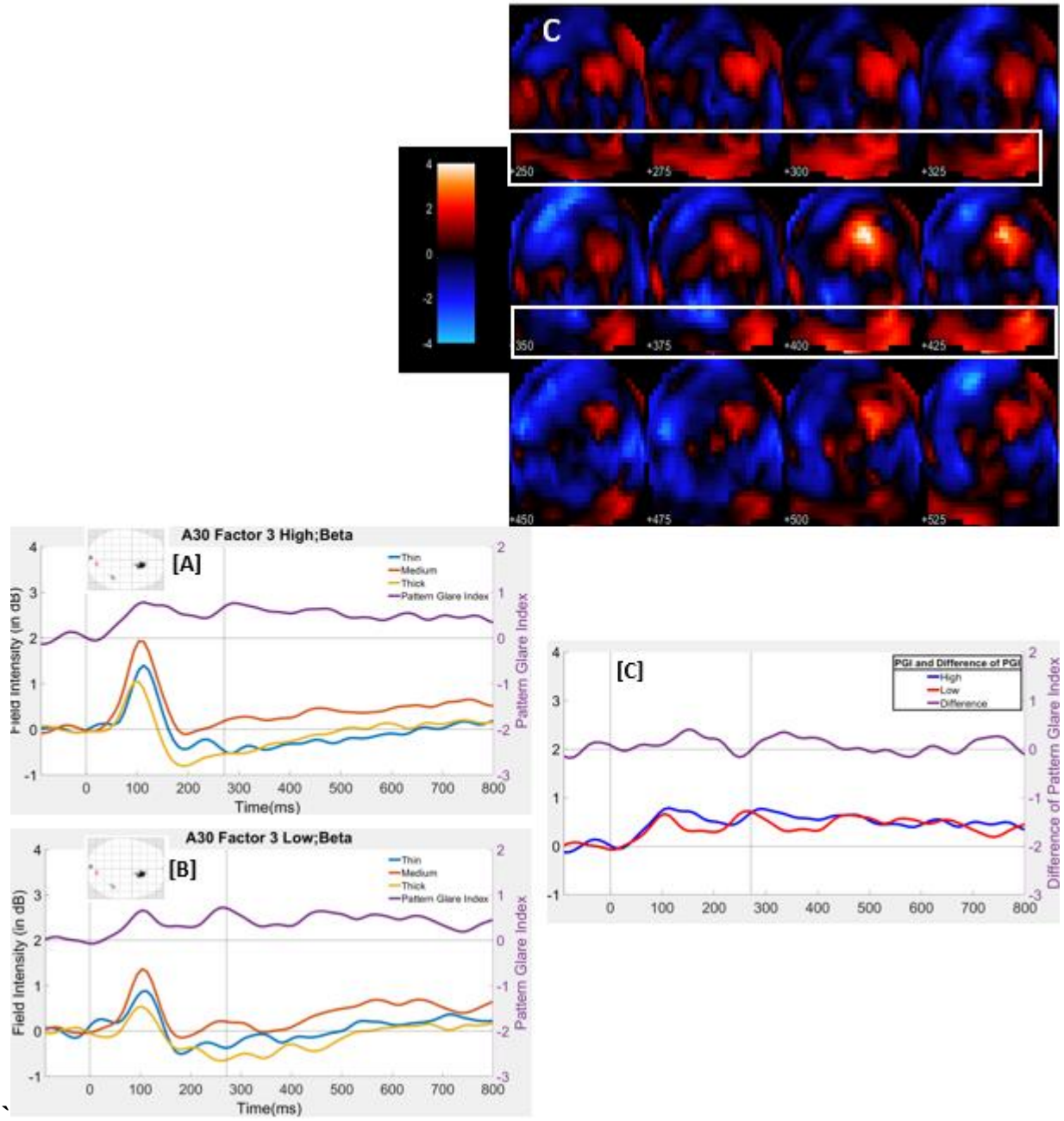
C
4
2
0
-2
-4
+250
+275
+300
+325
350
+375
+400
+425
+450
+475
+500
+525
A30 Factor 3 High;Beta
[A]
Thin
Medium
Thick
Pattern Glare Index
Field Intensity (in dB)
Pattern Glare Index
Time(ms)
A30 Factor 3 Low;Beta
[B]
Field Intensity (in dB)
[C]
PGI and Difference of PGI
High
Low
Difference
Difference of Pattern Glare Index

Figure 3-10. Topographic maps and time-series at electrode A30, illustrating effect on factor 3 positive-going, Beta frequency, Onset 2:8:

Peak of PGI mean/intercept cluster is at 9mm, -84mm, 271ms, see vertical line, here placed on closest electrode. The topographic maps are unthresholded from 250 to 525ms, in 25ms steps, the scale is from -4 to 4. The "c" links to effect in Figure 3.7. Stimulus time series are of power summed across Beta frequency. [A] High and [B] Low on median split of factor 3, showing in both cases, Thin, Medium and Thick, and PGI. [C] PGI for High and Low median splits, along with difference of High and Low PGIs. The white boxes indicate the cluster where the effect (uncorrected at peak on factor) sits. The SPM glass scalps shown on [A] and [B] depict all significant effects through time collapsed onto a two-dimensional representation. It shows the electrode being plotted as the red arrow. Positive is plotted up on time-series.

Figure 3.11 shows the effect for low gamma on factor 3 at electrode A30 using the uncorrected analysis at the peak of ROI approach on onsets 2:8. The topographic maps shown are unthresholded from 250 to 525ms in 25ms steps. The peak of the PGI mean/intercept cluster/ROI is at 9,-84, 271ms. The white boxes indicate the region and cluster that contains our significant (uncorrected) peak on the factor. High [A] and Low [B] on the median split of factor 3, showing in both cases, Thin, Medium and Thick, and PGI. PGI [C] for High and Low median splits, along with difference of High and Low PGIs. The 'd' on the graph can be used to refer back to Figure 3.7 to compare effects in the broader context. Low gamma was significant (uncorrected) $t(30)=2.704$, $p<.05$ (for full statistical breakdown see, table 3, with this effect on LG1, F3 row). Similarly to what we observed for Beta (do note that Beta and Low Gamma frequencies overlap), the significant peak on this factor is positioned at the start of an extended cluster where PGI is bigger for High than for Low. Additionally, the effect is posterior on the scalp, where we have our strongest prior precedents.

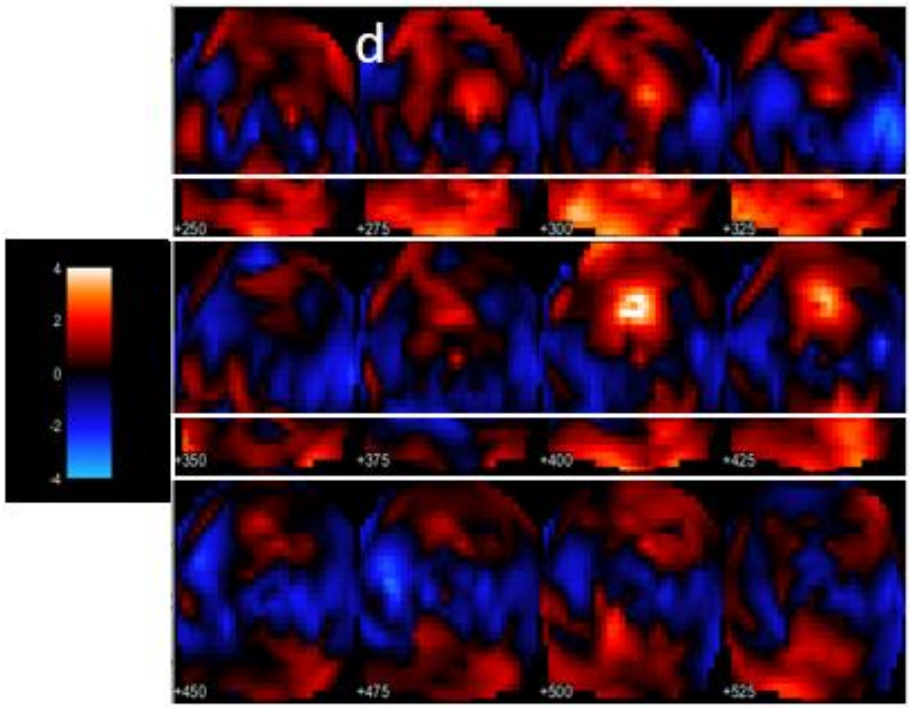
d
+250
+275
+300
+325
+350
+375
+400
+425
+450
+475
+500
+525

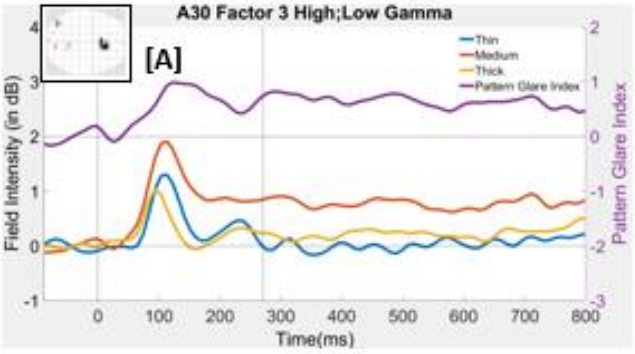
A30 Factor 3 High;Low Gamma
[A]
Thin
Medium
Thick
Pattern Glare Index
Field Intensity (in dB)
Pattern Glare Index
Time(ms)

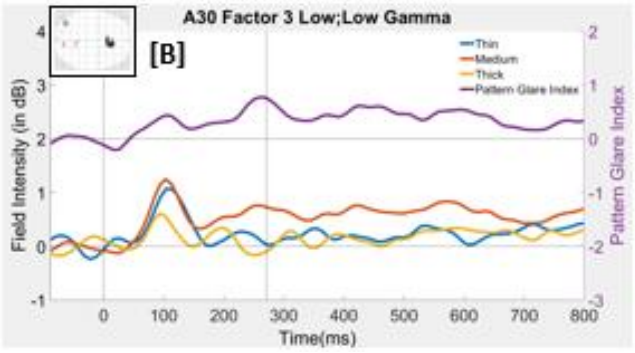
A30 Factor 3 Low;Low Gamma
[B]
Thin
Medium
Thick
Pattern Glare Index
Field Intensity (in dB)
Pattern Glare Index
Time(ms)

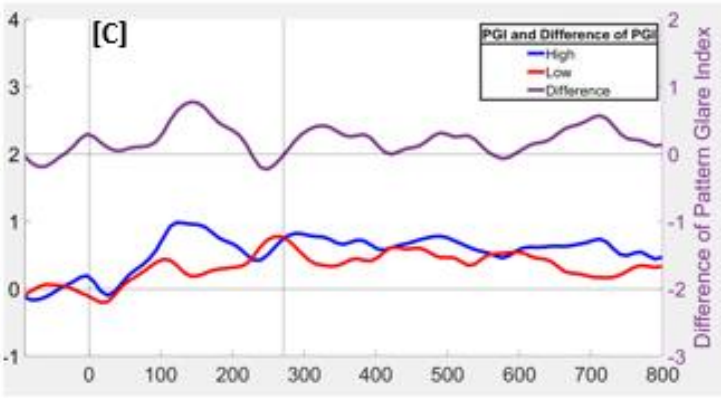
[C]
PGI and Difference of PGI
High
Low
Difference
Difference of Pattern Glare Index

Figure 3-11. topographic maps and time-series at electrode A30, illustrating the effect on factor 3 positive-going, Low Gamma frequency, Onset 2:8:

Peak of PGI mean/intercept cluster is at 9mm, -84mm, 271ms, see vertical line, here placed on the closest electrode. The topographic maps are unthresholded maps from 250 to 525ms, in 25ms steps, the scale is from -4 to 4. The "d" links to effect in Figure 3.7. Stimulus time series are of power summed across low gamma frequency. [A] High and [B] Low on median split of factor 3, showing in both cases, Thin, Medium and Thick, and PGI. [C] PGI for High and Low median splits, along with difference of High and Low PGIs. The white boxes indicate the region/cluster in which the (uncorrected) peak effect on the factor sits. The SPM glass scalps shown on [A] and [B] depict all significant effects through time collapsed onto a two-dimensional representation. It shows the electrode being plotted as the red arrow. Positive is plotted up on time-series.

Figure 3.12 shows the three significant effects for mid gamma for factor 3 at electrode a23 (Oz) using the uncorrected analysis at the peak of ROI approach on onsets 2:8. The topographic maps shown are unthresholded from 50 to 425ms in 25ms steps. High [A] and Low [B] on median split of factor 3 are presented, showing in both cases, Thin, Medium and Thick, and PGI. PGI [C] for High and Low median splits are shown, along with difference of High and Low PGIs. The 'e' on the graph can be used to refer back to Figure 3.7 to compare effects in the broader context. Peaks of PGI mean/intercept clusters where we observe an (uncorrected) effect on the mid gamma frequency are at -9mm,-89mm, 408ms $t(30)=2.58$, $p<.05$; 0mm,-89mm, 145ms $t(30)=1.85$, $p<.05$; & -9mm,-89mm, 135ms $t(30)=2.5$, $p<.05$ (for full statistical breakdown see, table 3, with this effect on MG1, F3 row). The white boxes indicate the region and clusters that contain the significant (uncorrected) peaks on the factor. Notably, we have solid prior precedents for observing effects at Oz, particularly in the early window around 100ms (Adjamian et al., 2004; Tempesta et al., in submission, chapter 3), which is exactly what we are observing here in

our earlier effects (around 150ms) These early uncorrected peaks are also placed within an extended cluster in which High PGI is bigger than Low, see panel [C].

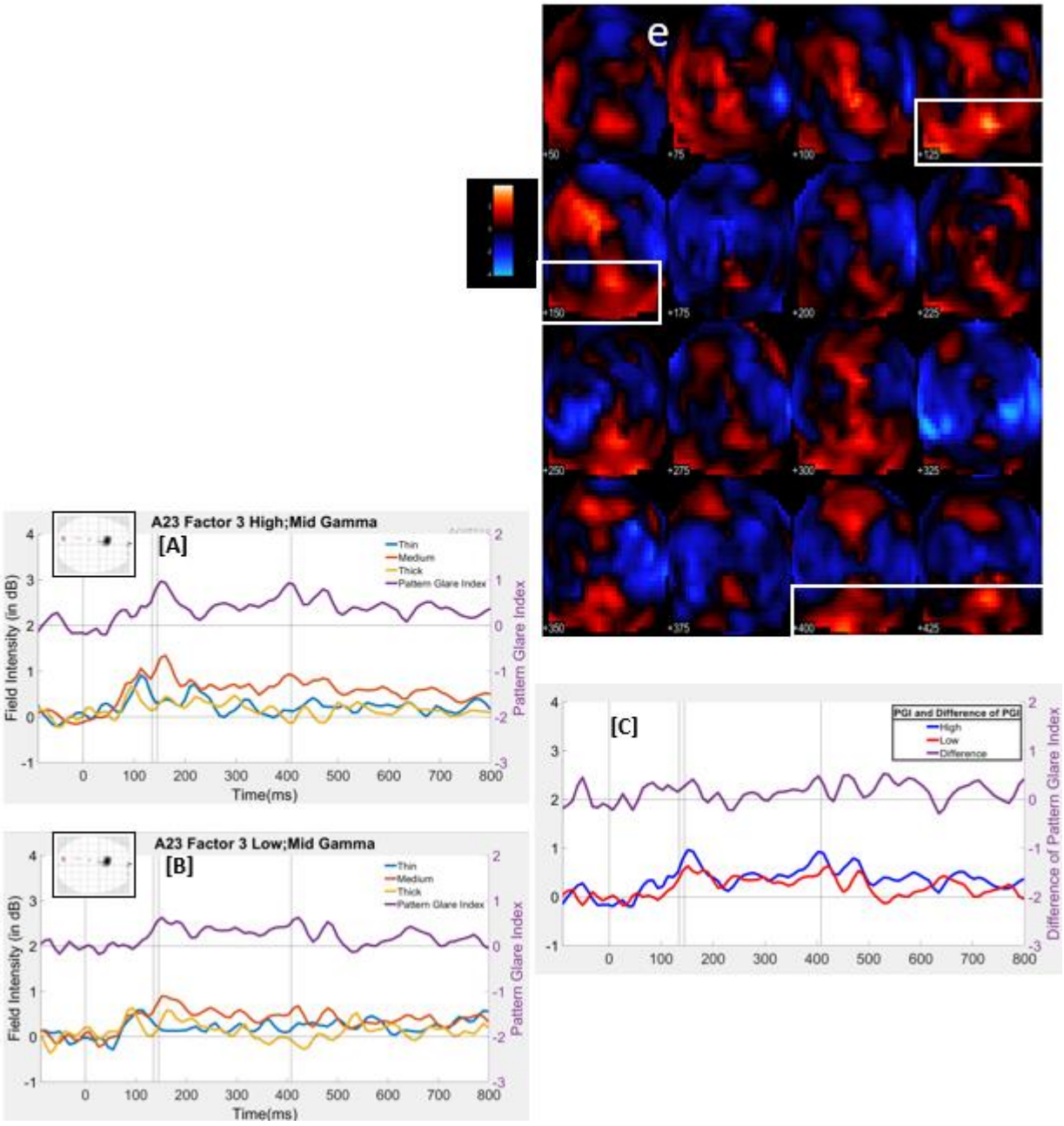

Figure 3-12: topographic maps and time-series at electrode A23 (Oz), illustrating the effect on factor 3 positive-going, Mid Gamma frequency, Onset 2:8:

Peaks of PGI mean/intercept clusters, where uncorrected factor effects arise, are at, -9mm,-89mm, 408ms, 0mm,-89mm, 145ms, & -9mm,-89mm, 135ms, see vertical lines, here placed on the closest electrode. The topographic maps are unthresholded from 50 to 425ms, in 25ms steps, the scale is from -4 to 4. The "e" links to effect in Figure 3.7. The white boxes indicate the regions/clusters that contain the significant (uncorrected) peaks on the factor. Stimulus time series are of power summed across Mid Gamma frequency. [A] High and [B] Low on median split of factor 3, showing in both cases, Thin, Medium and Thick, and PGI. [C] PGI for High and Low median splits, along with difference of High and Low PGIs. The SPM glass scalps shown on [A] and [B] depict all significant effects through time collapsed onto a two-dimensional representation. It shows the electrode being plotted as the red arrow. Note, Oz is off the midline in this depiction, since crown electrodes were removed. Positive is plotted up on time-series.

Figure 3.13 shows the three significant effects for high gamma for factor 3 at electrode A32 using the uncorrected analysis at the peak of ROI approach on onsets 2:8. The topographic maps shown are unthresholded from 50 to 200ms in 10ms steps. High [A] and Low [B] on median split of factor 3 are depicted, showing in both cases, Thin, Medium and Thick, and PGI. PGI [C] for High and Low median splits are shown, along with difference of High and Low PGIs. The 'f' on the graph can be used to refer back to Figure 3.7 to compare effects in the broader context. Peak of PGI mean/intercept cluster, where uncorrected effect on factor occurs on mid gamma frequency is at 9mm, -52mm,145ms $t(30)=3.09$, $p<.05$ (for full statistical breakdown see, table 3, with this effect on row HG2, F3). The white boxes indicate the region/cluster in which the (uncorrected) peak effect on the factor occurs. This peak sits in a time-extended cluster that sits somewhat anterior of Oz.

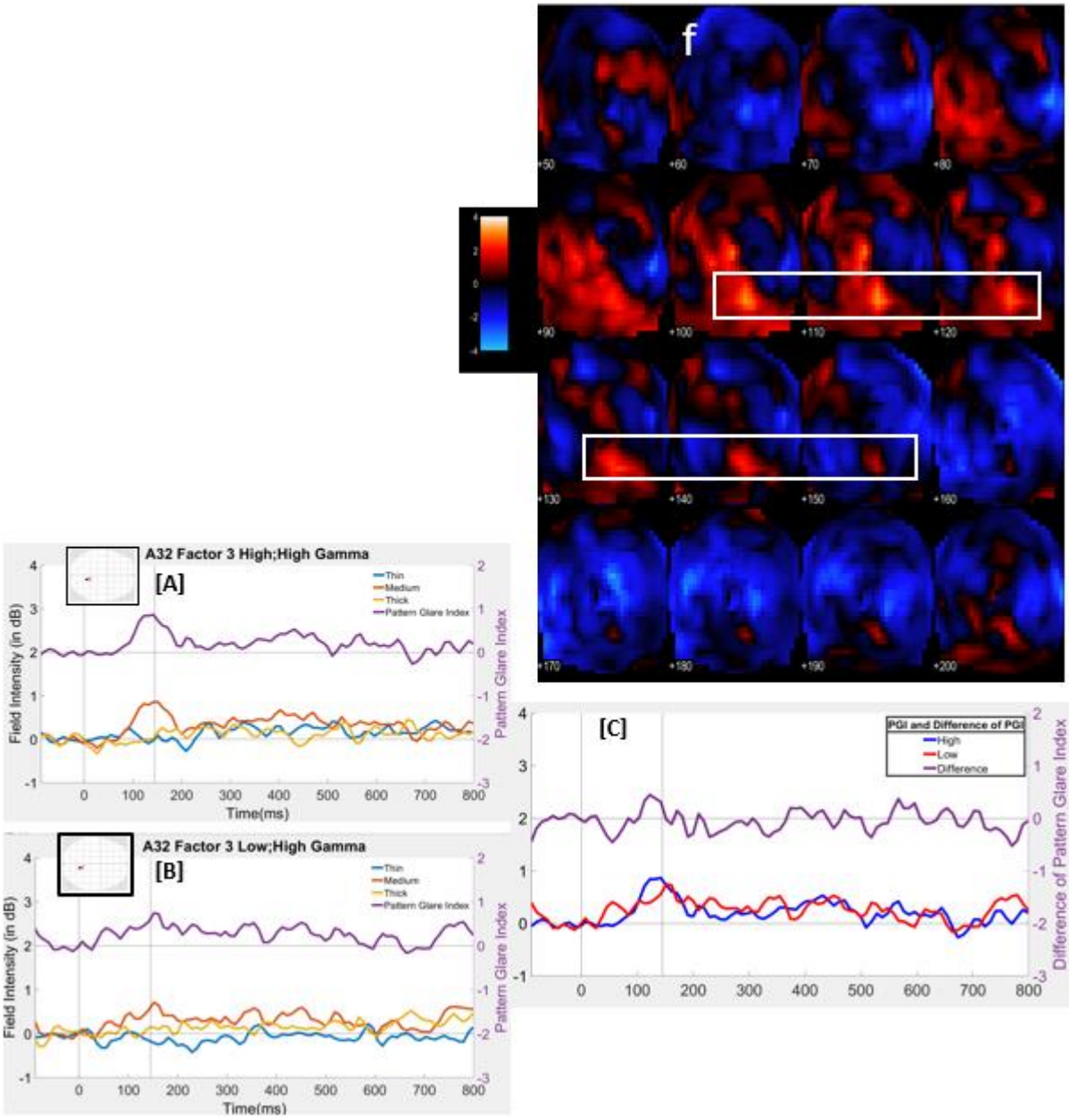
f
+50
+60
+70
+80
+90
+100
+110
+120
+130
+140
+150
+160
+170
+180
+190
+200
A32 Factor 3 High;High Gamma
[A]
Thin
Medium
Thick
Pattern Glare Index
Field Intensity (in dB)
Pattern Glare Index
Time(ms)
A32 Factor 3 Low;High Gamma
[B]
[C]
PGI and Difference of PGI
High
Low
Difference
Difference of Pattern Glare Index

Figure 3-13: Topographic maps and time-series at electrode A32, illustrating the effect on factor 3 positive-going, High Gamma frequency, Onset 2:8:

Peak of PGI mean/intercept cluster, where uncorrected factor effect arises is at 9mm, -52mm, 145ms, see vertical line, here placed on the closest electrode. The topographic maps are unthresholded from 50 to 200ms, in 10ms steps, the scale is from -4 to 4. The "f" links to effect in Figure 3.7. The white boxes indicate the region/cluster that contains the significant (uncorrected) peak on the factor. Stimulus time series are of power summed across High Gamma frequency. [A] High and [B] Low on median split of factor 3, showing in both cases, Thin, Medium and Thick, and PGI. [C] PGI for High and Low median splits, along with difference of High and Low PGIs. The SPM glass scalp shown on [A] and [B] depict all significant effects through time collapsed onto a two-dimensional representation. It shows the electrode being plotted as the red arrow. Positive is plotted up on time-series

3.4 Discussion

Understanding the underlying neurological factors that affect visually induced migraines is essential. It is a significant cause of disability and causes issues at work. In this analysis, we looked at the frequency domain, within the general population, we looked at the responses to aggregated and PGI and related them to three factors: visual stress, a tendency for headaches, and discomfort. Our 3 hypotheses were that firstly there will be a deeper alpha desynchronisation for PG. Secondly there will be greater gamma power for PG, which relates to a failure to habituate and finally, these EEG effects on pattern glare will be modulated by state and trait measures of sensitivity to headache, discomfort, visual hallucinations. The increased alpha desynchronisation for PG hypothesis was not confirmed: medium was not observably different to thick and thin in how it affected synchronisation in the alpha frequency band (Figure 3.5). However, for the PGI analysis on the mean/intercept, there was greater gamma power for PGI (Figure 3.6, Panels C and

D); we will discuss this further by looking at the factor effects on the PGI. Finally, we did have a significant finding for many of the factors on state and trait measures (Figure 3.7).

3.4.1 Aggregated mean/intercept contrasts

We described in the results section that there were four main features in the power analysis, which we divided between early positive transients and sustained responses (Figure 3.3). For the early positive transient, we saw a clear posterior peak for beta and low gamma for onset 1 and onset 2:8 (dashed framing), which means that this is probably not being affected by lack of habituation, but reflects information processing (Hanslmayr, 2012). However, alpha onset 2:8 showed an early anterior to posterior synchronisation (dotted framing), which does not occur in onset 1. Additionally, while this early anterior to posterior effect in alpha 2:8 has some overlap with the effect in beta and low gamma; there is a clear posterior peak for beta and low gamma localised to Oz. Note that Adjamian and colleagues (2004) only directly investigated a localised gamma effect for V1.Then, almost directly after the Onset 2:8 anterior to posterior effect, we observe a large sustained desynchronisation (dotted-dash framing) for both onset 1 and 2:8 for alpha.

Additionally, in low gamma and mid gamma frequencies, we observe a sustained synchronisation effect happening only for Onsets 2:8 (Unbroken framing). This sustained synchronisation is continuously present as we progress through the time series of the topographic maps across all gamma frequencies, except high gamma. This may be related to a high stimulus driver.

3.4.2 Pattern-Glare Index mean/intercept contrasts

The PGI mean/intercept effects follow along the same lines of aggregated mean/intercept, i.e., early positive transients and sustained synchronisations (see Figure 3.4). As we can observe, beta showed a sustained synchronisation effect that continued in time and through low and mid

gamma in onset 2:8 (see solid framing). The effects underlying the PGI mean/intercept findings presented in Figure 3.4 are presented in Figure 3.6, showing time series at different posterior electrodes one for each relevant frequency. Observe that in panel A) for beta, all three stimuli display an early positive transient, and then medium continues on into a d/c shift. We also observed this continuation in panel B) and panel C), albeit with the early positive transient progressively diminishing. Finally, in panel D) we observe that the early positive transient is wholly gone for thick and thin, but the medium still shows such a transient. Thus, when for high gamma there is not just a quantitative change between medium, thin and thick, there is a qualitative (all-or-none) change; i.e. the feature is completely absent for thin and thick. One possible explanation for this is a failure to habituate, i.e., the synchrony is continuing because the stimulus cannot be habituated to, a phenomenon that might be expected to connect with our discomfort factor (Schoenen et al., 1995; Afra et al., 1998; Wang, Wang, et al., 1999).

It is also interesting to note that our finding of high gamma in onset 2-8, and not onset 1, does stand against some operationalisations of predictive coding (Den Ouden et al., 2012). Onset 1 should be the condition that generates a prediction error, since stimuli are equiprobable (Hawkins, 2004; Friston, 2005; Bar, 2009), and some have argued that prediction errors should manifest in increased gamma (Todorovic et al., 2011), since they would be registered in superficial layers of the cortical column. We saw precisely the opposite of this in high gamma for 2-8. This suggested that a lack of habituation is a more probable interpretation of this feature in our data.

It is striking that we observed such a substantial effect on the sustained positivity for the pattern-glare index for onset 2:8, but there is nothing significant for onset 1; see Figure 3.4. One might argue that this is due to onset 1 having less statistical power than onset 2:8, since it involves fewer trials per participant. We cannot rule out this possibility completely, but it is

notable that we do observe large effects for onset 1 for the aggregated analysis (see Figure 3.3). We also observe effects on onset 1 in the time-domain (Tempesta et al., 2021; also Chapter 2). Thus, it seems that there is sufficient statistical power to observe robust effects for onset 1.

However, for high gamma, the D/C shift that continues beyond the time window is gone. Additionally, the early positive transient in high gamma has an increased latency in time, peaking at 150ms. This is slightly after the rising arm of the event-related P1, the feature that is likely to coincide with the early positive transient seen in panels A) and B), which peaks around 100ms. Accordingly, this high and mid gamma transient peaking at 150ms might be considered a distinct feature. Additionally, interestingly, it peaks at about the point that our missing N1 in the time-domain starts (Tempesta et al., 2021; also Chapter 2).

A possible physiological explanation for what we observe would be that there are two sorts of cell-assemblies (Hebb, 1949) in relevant visual areas. One sort is "somewhat" densely interconnected and thus oscillate at beta, low gamma and to some extent mid gamma, and the other sort is more densely interconnected, generating shorter cycle times, that oscillate at mid and high gamma. This second set activate slightly later following a stimulus onset. Thick, medium and thin all drive the "somewhat" densely interconnected assemblies, but only medium drives the most densely interconnected assemblies.

3.4.3 Factors Effects

As we can recall from the results section, there were two methods used to analyse the factors in our data set - orthogonal cluster inference in an ROI from mean/intercept of PGI and uncorrected analysis at a peak of interest from the mean/intercept of PGI clusters. Figure 3.7 shows the major significant effects of factors. Notably, we observed most of our effects on the discomfort factor, the factor that is dominated by a state, rather than a trait, response. As a result, in line with other studies (Csikszentmihalyi & Larson, 1987; Finnigan & Vazire, 2018), one might believe that

discomfort is a more reliable measure than the trait measures, which require subjective reflection on past experiences

Consequently, it is reassuring, and perhaps also not surprising, that the most apparent correlations we observed with brain response are from the discomfort factor. The orthogonal cluster inference in an ROI approach identified a small cluster for discomfort for high gamma within a region of interest (see Figure 3.8), which means that participants who scored high on discomfort for high gamma felt uncomfortable during the study.

Eleven peaks came out on the uncorrected analysis at peaks of the ROIs; 7 were on the discomfort factor, three were on the VSQ, Chi and Aura factor, and one was related to the length and frequency of headaches factor. Figure 3.9 shows topographic maps for electrode A23 (Oz) for the VSQ, Chi, and Aura factor for high gamma; participants who scored high on this factor responded high on these trait measures. Importantly, these effects were observed at a posterior site, for which we have the strongest prior precedent (Adjamian et al., 2004). Figure 3.10, discomfort for beta, showed the start of a sustained cluster, which means that those who score high on discomfort have increased beta for PGI. In Figures 3.11, 3.12 and 3.13, we showed similar effects for low gamma, mid gamma and high gamma on the discomfort factor. This means that those who have higher discomfort are experiencing more higher PGI in these frequency bands. It is important to note that mid gamma for Oz, for which we have the strongest prior precedents (Adjamian et al., 2004; Tempesta et al., 2021; also Chapter 2), shows three significant peaks for discomfort, suggesting that for mid gamma there is a particularly high effect on pattern glare for those high on the discomfort factor.

3.4.4 Limitations

Our study is not without its caveats. Critically, although the PG test uses 12 c/deg, there are some questions over this stimulus, partly because the 12cpd pattern is not always well reproduced (see discussion in Wilkins et al., 2016). We see glare-induced gamma primarily for onset 2:8, but not onset 1. The fact this is only in 2:8, may suggest that it is an electrophysiological correlate of the brain's inability to habituate to PG, although one would like an analysis that would show that later onsets, e.g. 5:8, have similar, or even, increased levels of gamma power to early ones, e.g. 2:4. Given the differences in the explanations of gamma synchrony as either a cognitive example of habituation or failure of habituating, more studies are needed to see which of these results might be transferable to a patient population.

3.4.5 Conclusion

We observed a substantial effect on the sustained positivity for the PGI for onset 2:8 on gamma band. Notably, we observed most of our effects on the discomfort factor, the factor that is dominated by a state, rather than a trait, response. As a result, one might believe that discomfort is a more reliable measure than the trait measures, which require subjective reflection on past experiences. Finally, eleven peaks came out on the uncorrected analysis at peaks of the ROIs; 7 were on the discomfort factor, three were on the VSQ, Chi and Aura factor, and one was related to the length and frequency of headaches factor in posterior on the scale.

3.5 Acknowledgements

We want to thank Guillaume Flandin for their help with SPM use and expertise. Vladimir Litvak was also extremely helpful for understanding some technicalities of SPM. They also assisted in refining analysis code. We would also like to thank Sara Assecondi for assistance with EEG pre-processing and Cathy Ghalib for help with data collection.

3.6 Funding

We were not funded for this research.

3.7 Competing interests

The authors report no competing interests.

3.8 Supplementary Material

3.8.1 Factor analysis

Factor analysis seeks to derive independent factors from a collection of variables. Thus, the correlations between our factors were zero. Rotation helps to clarify which variables load onto (belong to) each factor, as seen in the Rotated Component Matrix (Table 3-4) and helps with factor naming. Our factors scores were calculated in SPSS (IBM, NY) using the regression method in which all variables contribute to all factors according to the Component Score Coefficient Matrix (Table 3-5). For the headache and discomfort factors, the contribution from variables not obviously associated with these terms was minimal. The headache variables did contribute to the visual stress factor, but were pitted against each other such that intensity and frequency contributed positively onto this factor while duration contributed negatively. Since the headache variables correlate relatively strongly, the effect of these positive and negative weightings will be to cancel out the overall effect of headache on the VS factor. Although correlations between factors were zero by design, the correlation between discomfort ratings for the medium stimuli alone and headache frequency was 0.3 (p=.068) which, while not significant in our sample, is similar to previous measures.

Table 3-4. Rotated Component Matrix

Rotated Component Matrix

	Component		
	1	2	3
VSQ	0.636	0.035	0.062
CHi	0.845	0.212	-0.074
aura	0.789	0.122	0.292
H-duration	-0.470	0.764	0.040
H-intensity	0.366	0.716	-0.116
H-frequency	0.305	0.795	0.041
Discomfort	0.119	-0.028	0.977

Table 3-5. Component Score Coefficient Matrix

Component Score Coefficient Matrix

	Component		
	1	2	3
VSQ	0.303	-0.055	-0.021
CHi	0.401	0.018	-0.172
aura	0.337	-0.012	0.187
H-duration	-0.332	0.51	0.135
H-intensity	0.108	0.372	-0.128
H-frequency	0.048	0.433	0.036
Discomfort	-0.065	0.013	0.934

3.8.2 Direct Comparison of Stimulus Responses

In EEG work, one often attempts to avoid differences in stimulus properties, particularly those that are low-level, such as spatial frequency. This is because one is typically seeking to identify differences in higher-level cognitive functions, such as, attentional state, affective salience or linguistic properties, and associated EEG features could be contaminated by

differences in low-level features. However, this is not our situation: we are specifically seeking to observe differences in the brain's electrical response to changes in *low-level* stimulus features, i.e. spatial frequency.

Other researchers also looking at the brain's electrical response to aggravating stimuli have sought to avoid making comparisons across stimuli with different spatial frequencies (Fong et al., 2020). A consequence of this choice is that effects of different spatial frequencies have to be judged informally, without a statistical test to quantify the confidence in an observed difference; virtually one is left considering *the difference of evidences* (e.g. comparing p-values), rather than assessing *the evidence for a difference*. There are, of course, many ways to investigate scientific questions, but, since the question of interest for us is how early brain responses change to stimuli that have different effective strengths for different groups, we have chosen to directly compare the EEG generated by stimuli of different spatial frequencies. Additionally, our parametric regression onto the three factors we identified cannot be impacted by fixed baseline differences between gratings, such as, Thick generating an overall higher amplitude than Thin or Medium, since that difference would be consistent across participants. As a result, it could not generate a non-zero correlation between the dependent variable and regressor, i.e. it would impact the intercept term of the regression, but not the slope, which gives the beta we are interested in. Thus, fixed baseline differences in brain responses to different gratings cannot impact our analysis of factors.

3.8.3 Difference of Evidences

The previous section justifies our use of the pattern-glare index to quantify evidence for a difference between the three types of stimuli. There is, though, one caveat to our capacity to quantify evidence for a difference.

If we were to look for statistical differences between conditions in a fully principled way, we should not only compare Onset 1 to Onset 2 to 8, but we should also compare what we see for different frequency bands. That is, one could, for say PGI mean/intercept, run a 2 (Onset_1 vs Onset 2_8) by 5 (alpha, beta, low gamma, mid gamma, high gamma) ANOVA.

Such a 2 by 5 ANOVA is going to suffer from gross non-sphericity, since, for example, what one sees for low gamma and mid gamma are going to be highly correlated, but what one sees for alpha and high gamma are going to be much less correlated. One could attempt a Greenhouse-Geisser correction, but it would be challenging.

Because it is so difficult to perform such inference uncontaminated by loss of sphericity, we decided to rely on comparing evidences. This does, at least, enable us to be informed by the amount of across subject variability. However, since the final comparison is only informal, we will only consider effects that are strong as anything other than exploratory.

3.8.4 Further Factor Effects

A number of the effects on factors that arose through our "Uncorrected analysis at peak of region of interest" approach are placed here in the appendix. As discussed in the main-body of this paper, we applied the following criteria to determine the effects at peaks to keep in the main-body:

1. posterior: effects should be approaching Oz, since we have the greatest prior precedent for such effects (Adjamian, 2004);
2. continuous to substantial cluster: an effect being observed at a single point is not isolated, i.e. it is continuous to a substantial cluster, particularly that is extended in time.

Effects that did not satisfy these criteria are placed here.

On each Figure below, we discuss why this electrode was not included in the main body, i.e. which of the two criteria above it failed to meet, and show the peak of significance with a vertical

line. Visualisations of the median splits, and the difference of high-low with [A] representing the high group, [B] representing the low group and [C] the difference between high and low are given below.

Figure 3.14 was not considered in our main body because the electrode was relatively anterior, e.g. it is closer to Cz than to Oz, meaning we had less a priori precedent to study it. The Figure shows electrode B18 for factor 1 on the Beta frequency.

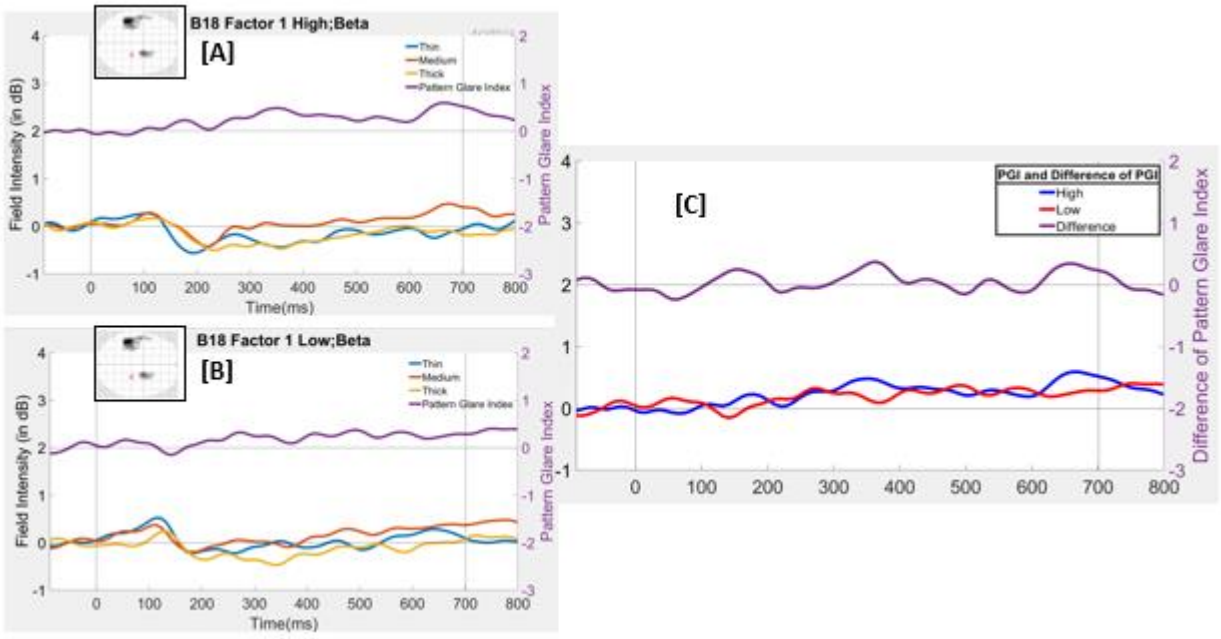

Figure 3-14. Time-series at electrode B18, illustrating effect on factor 1 positive going, Beta frequency, Onset 2:8:

Peak of PGI mean/intercept cluster is at 26mm, -30mm, 701ms, see vertical line, here placed on closest electrode. [A] High and [B] Low on median split of factor 1, showing in both cases, Thin, Medium and Thick, and PGI. Stimulus time series are of power summed across Beta frequency. [C] PGI for High and Low median splits, along with difference of High and Low PGIs. The SPM glass scalps depict all significant effects through time collapsed onto a two-dimensional representation. It shows the electrode being plotted as the red arrow. Positive is plotted up.

Figure 3.15 was not considered in the main body, because it is a relatively isolated effect in time and not continuous with a clear cluster; see panel C, purple line. The Figure shows A21, for factor 1 Low gamma.

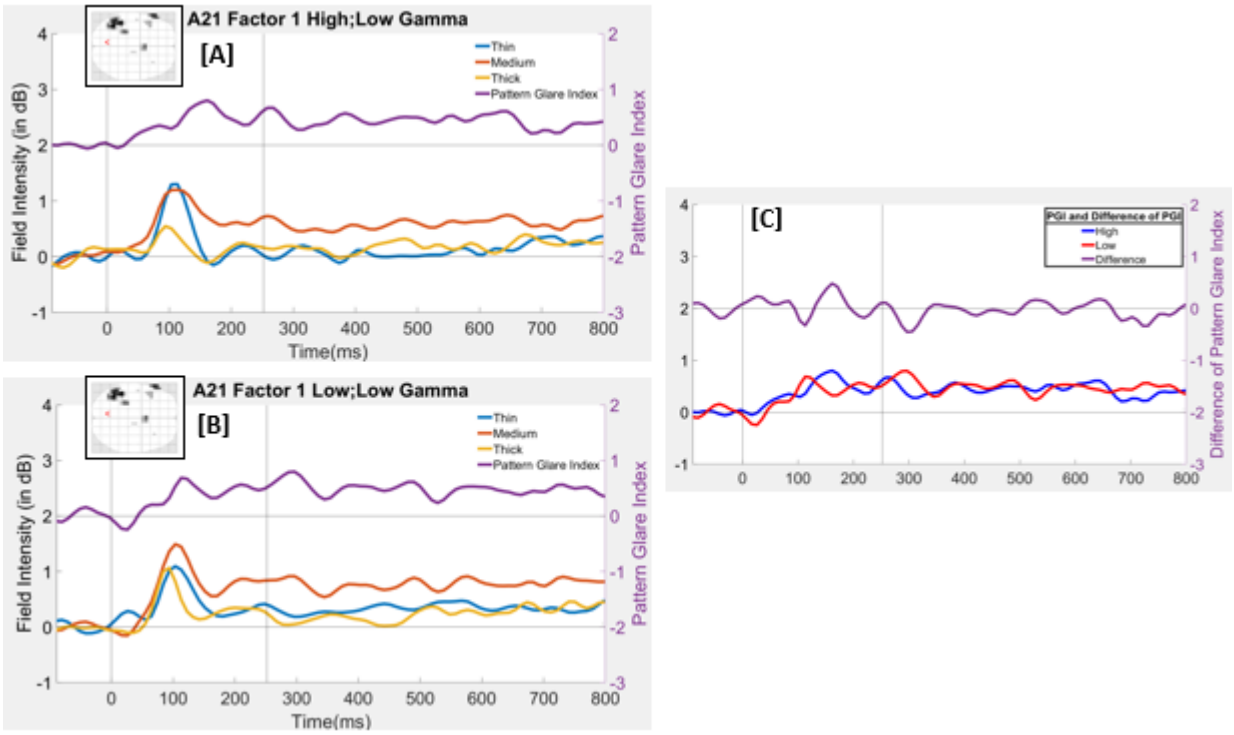

Figure 3-15. Time-series at electrode A21, illustrating the effect on factor 1 positive-going, Low Gamma frequency, Onset 2:8:

Peak of PGI mean/intercept cluster is at -9mm, -73mm, 252ms, see vertical line, here placed on the closest electrode. [A] High and [B] Low on median split of factor 1, showing in both cases, Thin, Medium and Thick, and PGI. Stimulus time series are of power summed across Low Gamma frequency. [C] PGI for High and Low median splits, along with difference of High and Low PGIs. The SPM glass scalps depict all significant effects through time collapsed onto a two-dimensional representation. It shows the electrode being plotted as the red arrow. Positive is plotted up.

Figure 3.16 was not considered in the main-body because it is located anterior relative to Oz; in fact it is very close to Cz. The Figure shows B32, which is significant for low gamma for factor 2.

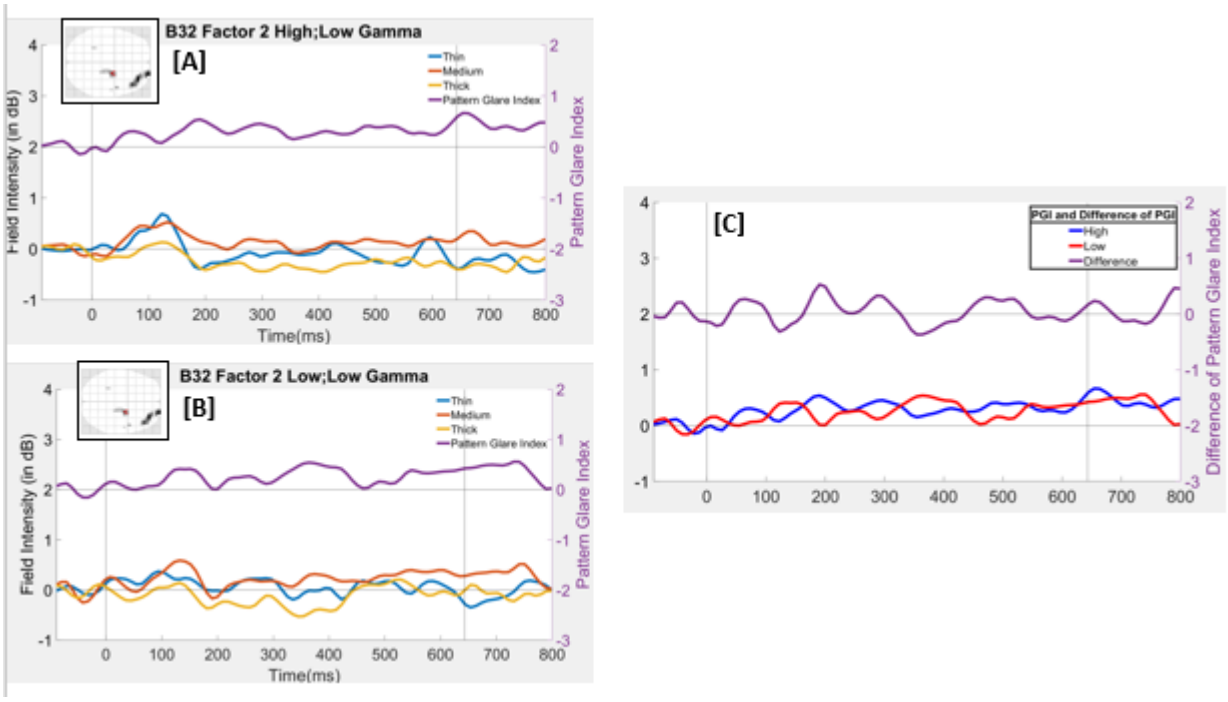

Figure 3-16. Time-series at electrode B32, illustrating the effect on factor 2 positive-going, Low Gamma frequency, Onset 2:8:

Peak of PGI mean/intercept cluster is at 21mm, -9mm, 643ms, see vertical line, here placed on the closest electrode. [A] High and [B] Low on median split of factor 2, showing in both cases, Thin, Medium and Thick, and PGI. Stimulus time series are of power summed across Low Gamma frequency. [C] PGI for High and Low median splits, along with difference of High and Low PGIs. The SPM glass scalps show all significant effects through time collapsed onto a two-dimensional representation. It shows the electrode being plotted as the red arrow in the MIP. Positive is plotted up.

Figure 3.17 shows A32 for high gamma on Factor 3. It was not used because it does now have a clear cluster in time associated with it.

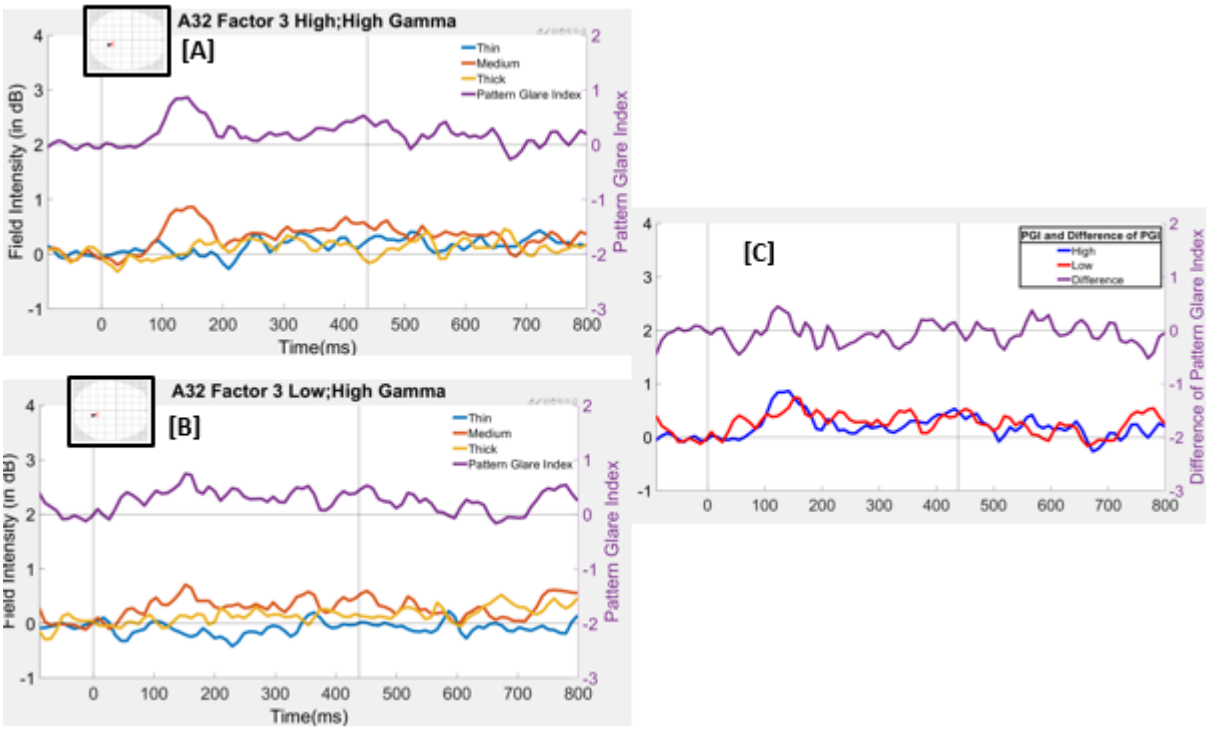

Figure 3-17: time-series at electrode A32, illustrating the effect on factor 3 positive-going, High Gamma frequency, Onset 2:8:

Peak of PGI mean/intercept cluster is at 17mm, -57mm, 438ms, see vertical line, here placed on the closest electrode. [A] High and [B] Low on median split of factor 3, showing in both cases, Thin, Medium and Thick, and PGI. Stimulus time series are of power summed across High Gamma frequency. [C] PGI for High and Low median splits, along with difference of High and Low PGIs. The glass scalps show all significant effects through time collapsed onto a two-dimensional representation. It shows the electrode being plotted as the red arrow. Positive is plotted up.

3.9 References

Adjamian, P., Holliday, I. E., Barnes, G. R., Hillebrand, A., Hadjipapas, A., & Singh, K. D. (2004). Induced visual illusions and gamma oscillations in human primary visual cortex. *European Journal of Neuroscience*, *20*(2), 587-592.

Ambrosini, A., & Schoenen, J. (2006). Electrophysiological response patterns of primary sensory cortices in migraine. *The Journal of Headache and Pain*, *7*(6), 377-388.

Afra, J., Cecchini, A. P., De Pasqua, V., Albert, A., & Schoenen, J. (1998). Visual evoked potentials during long periods of pattern-reversal stimulation in migraine. *Brain: A Journal of Neurology*, *121*(2), 233-241.

Allen, M. (Ed.). (2017). *The SAGE encyclopedia of communication research methods*. Sage Publications.

Bar, M. (2009). Predictions: a universal principle in the operation of the human brain.

Brainard, D. H. (1997). The psychophysics toolbox. *Spatial vision*, *10*(4), 433-436.

Braithwaite, J. J., Broglia, E., Bagshaw, A. P., & Wilkins, A. J. (2013). Evidence for elevated cortical hyperexcitability and its association with out-of-body experiences in the nonclinical population: new findings from a pattern-glare task. *Cortex*, *49*(3), 793-805.

Braithwaite, J.J., Marchant, R., Takahashi, C., Dewe, H., Watson, D (2015) The cortical hyperexcitability index (CHi): a new measure for quantifying correlates of visually driven cortical hyperexcitability. *Cognitive Neuropsychiatry*, *20* (4), 330-348.

Brett, M., Penny, W., & Kiebel, S. (2003). Introduction to random field theory. *Human brain function*, *2*, 867-879.

Beasley, I. G., & Davies, L. N. (2012). Susceptibility to pattern glare following stroke. *Journal of Neurology*, *259*(9), 1832-1839.

Brooks, J. L., Zoumpoulaki, A., & Bowman, H. (2017). Data-driven region-of-interest selection without inflating Type I error rate. Psychophysiology, 54(1), 100-113.

Bowman, H., Brooks, J. L., Hajilou, O., Zoumpoulaki, A., & Litvak, V. (2020). Breaking the Circularity in Circular Analyses: Simulations and Formal Treatment of the Flattened Average Approach. PLoS Computational Biology.

Brunet, N. M., Bosman, C. A., Vinck, M., Roberts, M., Oostenveld, R., Desimone, R., ... & Fries, P. (2014). Stimulus repetition modulates gamma-band synchronization in primate visual cortex. *Proceedings of the National Academy of Sciences*, *111*(9), 3626-3631.

Clarke, C. E., MacMillan, L., Sondhi, S., & Wells, N. E. (1996). Economic and social impact of migraine. *Qjm*, *89*(1), 77-84.

Conlon, E. (2000, July). Visual perceptual problems in reading: Their relationship to reading disability and neural processing. In 6th Irlen International Conference, Australia.

Conlon, E. G., Lovegrove, W. J., Chekaluk, E., & Pattison, P. E. (1999). Measuring visual discomfort. *Visual Cognition*, *6*(6), 637-663.

Conlon, E., Lovegrove, W., Barker, S. *and* Chekaluk, E. *(*2001*)* Visual discomfort: the influence of spatial frequency. Perception 30, 571–581.

Csikszentmihalyi, M., & Larson, R. (1987). Validity and reliability of the experience-sampling method. *Journal of Nervous and Mental Disease,* 175, 526–536. https://doi.org/10.1097/00005053-198709000-00004

Den Ouden, H. E., Kok, P., & De Lange, F. P. (2012). How prediction errors shape perception, attention, and motivation. *Frontiers in psychology*, *3*, 548.

Eklund, A., Nichols, T. E., & Knutsson, H. (2016). Cluster failure: Why fMRI inferences for spatial extent have inflated false-positive rates. Proceedings of the national academy of sciences, 113(28), 7900-7905.

Evans, B. J., Busby, A., Jeanes, R., & Wilkins, A. J. (1995). Optometric correlates of Meares–Irlen syndrome: a matched group study. *Ophthalmic and Physiological Optics*, *15*(5), 481-487.

Evans, B. J. W., & Stevenson, S. J. (2008). The Pattern Glare Test: a review and determination of normative values. *Ophthalmic and Physiological Optics*, *28*(4), 295-309.

Finnigan, K. M., & Vazire, S. (2018). The incremental validity of average state self-reports over global self-reports of personality. *Journal of Personality and Social Psychology*, 115, 321–337. https://doi.org/10.1037/pspp0000136.

Flandin, G., & Friston, K. J. (2019). Analysis of family-wise error rates in statistical parametric mapping using random field theory. Human brain mapping, 40(7), 2052-2054.

Friston, K. (2005). A theory of cortical responses. *Philosophical transactions of the Royal Society B: Biological sciences*, *360*(1456), 815-836.

Good, P. A., Taylor, R. H., & Mortimer, M. J. (1991). The use of tinted glasses in childhood migraine. *Headache: The Journal of Head and Face Pain*, *31*(8), 533-536.

Hanslmayr, S., Staudigl, T., & Fellner, M. C. (2012). Oscillatory power decreases and long-term memory: the information via desynchronization hypothesis. *Frontiers in human neuroscience*, *6*, 74.

Hawkins, J., & Blakeslee, S. (2004). *On intelligence*. Macmillan.

Hebb, D. O. (1949). *The organization of behavior: a neuropsychological theory*. J. Wiley; Chapman & Hall.

House of Commons, (2014). Headache Services in England. All-Party Parliamentary Group on Primary Headache Disorders.

Irlen, H. (1983, August). Successful treatment of learning disabilities. In *91st annual Convention of the American Psychological Association, Anaheim, CA, USA*.

Irlen, H. (1991). Reading by the colours. *New York: Avery*.

Irlen, H. (1994). Scotopic sensitivity/Irlen syndrome: Hypothesis and explanation of the syndrome. *Journal of Behavioral Optometry*, *5*(62), 65-66.

Irlen, H. (1997). Reading problems and Irlen coloured lenses. *Dyslexia review*, *8*, 4-7.

Jensen, O., & Mazaheri, A. (2010). Shaping functional architecture by oscillatory alpha activity: gating by inhibition. *Frontiers in human neuroscience*, *4*, 186.

Kleiner, M., Brainard, D., & Pelli, D. (2007). What's new in Psychtoolbox-3?.

Klimesch, W., Schimke, H., Doppelmayr, M., Ripper, B., Schwaiger, J., and Pfurtscheller, G. (1996). Event-related desynchronization (ERD) and the Dm effect: does alpha desynchronization during encoding predict later recall performance? Int. J. Psychop

Klimesch, W., Doppelmayr, M., Schimke, H., and Ripper, B. (1997). Theta synchronization and alpha desynchronization in a memory task. *Psychophysiology* 34, 169–176.

Klimesch, W., Sauseng, P., and Hanslmayr, S. (2007). EEG alpha oscillations: the inhibition-timing hypothesis. *Brain Res. Rev.* 53, 63–88.

Kientz, M. A., & Dunn, W. (1997). A comparison of the performance of children with and without autism on the Sensory Profile. *American Journal of Occupational Therapy*, *51*(7), 530-537.

Lorca-Puls, D. L., Gajardo-Vidal, A., White, J., Seghier, M. L., Leff, A. P., Green, D. W., ... & Price, C. J. (2018). The impact of sample size on the reproducibility of voxel-based lesion-deficit mappings. *Neuropsychologia*, *115*, 101-111.

Luck, S. J. (2014). *An Introduction to the Event-related Potential Technique*. MIT press.

Mears, O. (1980). Figure/background brightness/contrast and reading disability. *Visible Language*, *15*, 13-29.

Parish, G., Hanslmayr, S., & Bowman, H. (2018). The sync/desync model: How a synchronized hippocampus and a desynchronized neocortex code memories. *Journal of Neuroscience*, *38*(14), 3428-3440.

Pelli, D. G. (1997). The VideoToolbox software for visual psychophysics: Transforming numbers into movies. *Spatial vision*, *10*(4), 437-442.

Saksida, A., Iannuzzi, S., Bogliotti, C., Chaix, Y., Démonet, J. F., Bricout, L., ... & George, F. (2016). Phonological skills, visual attention span, and visual stress in developmental dyslexia. *Developmental Psychology*, *52*(10), 1503.

Salinias, E., & Sejnowski, T. J. (2001). Gain modulation in the central nervous system: Where behavior. *Neurophysiology, and Computation Meet, Neuroscientist*, *7*, 430-440.

Schoenen, J., Wang, W., Albert, A., & Delwaide, P. J. (1995). Potentiation instead of habituation characterizes visual evoked potentials in migraine patients between attacks. *European Journal of Neurology*, *2*(2), 115-122.

Steiner, T. J., Stovner, L. J., & Birbeck, G. L. (2013). Migraine: the seventh disabler. *Headache: The Journal of Head and Face Pain*, *53*(2), 227-229.

Steiner, T. J., Birbeck, G. L., Jensen, R. H., Katsarava, Z., Stovner, L. J., & Martelletti, P. (2015). Headache disorders are third cause of disability worldwide.

Stovner, L. J., Hagen, K., Jensen, R., Katsarava, Z., Lipton, R. B., Scher, A. I., ... & Zwart, J. A. (2007). The global burden of headache: a documentation of headache prevalence and disability worldwide. *Cephalalgia*, *27*(3), 193-210.

Stovner, L. J., Nichols, E., Steiner, T. J., Abd-Allah, F., Abdelalim, A., Al-Raddadi, R. M., ... & Edessa, D. (2018). Global, regional, and national burden of migraine and tension-type headache, 1990–2016: a systematic analysis for the Global Burden of Disease Study 2016. *The Lancet Neurology*, *17*(11), 954-976.

Shapiro, R. E., & Goadsby, P. J. (2007). The long drought: the dearth of public funding for headache research.

Shirazibeheshti, A., Cooke, J., Chennu, S., Adapa, R., Menon, D. K., Hojjatoleslami, S. A., ... & Bowman, H. (2018). Placing meta-stable states of consciousness within the predictive coding hierarchy: The deceleration of the accelerated prediction error. *Consciousness and Cognition*, *63*, 123-142.

Tanner, D., Morgan-Short, K., & Luck, S. J. (2015). How inappropriate high-pass filters can produce artifactual effects and incorrect conclusions in ERP studies of language and cognition. *Psychophysiology*, *52*(8), 997-1009.

Tempesta, A. J., Miller, C. E., Litvak, V., Bowman, H., & Schofield, A. J. (2021). The Missing N1 or Jittered P2: Electrophysiological Correlates of Pattern Glare in the Time and Frequency Domain. *European Journal of Neuroscience*.

Todorovic, A., van Ede, F., Maris, E., & de Lange, F. P. (2011). Prior expectation mediates neural adaptation to repeated sounds in the auditory cortex: an MEG study. *Journal of Neuroscience*, *31*(25), 9118-9123.

Wang, W., Wang, G. P., Ding, X. L., & Wang, Y. H. (1999). Personality and response to repeated visual stimulation in migraine and tension-type headaches. *Cephalalgia*, *19*(8), 718-724.

Wilkins, A., Nimmo-Smith, I. A. N., Tait, A., McMANUS, C., SALA, S. D., Tilley, A., ... & Scott, S. (1984). A neurological basis for visual discomfort. *Brain*, *107*(4), 989-1017.

Wilkins, A. (1986). Intermittent illumination from visual display units and fluorescent lighting affects movements of the eyes across text. *Human Factors*, *28*(1), 75-81.

Wilkins, A. J. (1995). *Visual stress* (No. 24). Oxford University Press.

Wilkins, A. J. (2003). Reading through colour. *How Coloured filters Can Reduce*.

Wilkins, A. (2016). A physiological basis for visual discomfort: Application in lighting design. *Lighting Research and Technology*.doi:10.1177/1477153515612526.

Wilkins, A.J., Binnie, C.D. (1980) Visually induced seizures *Prog. Neurobiol., 15*, 85-117.

Wilkins, A. J., Darby, C. E., & Binnie, C. D. (1979). Neurophysiological aspects of pattern-sensitive epilepsy. *Brain*, *102*(1), 1-25.

Wilkins, A. J., & Evans, B. J. W. (2001). Pattern glare test instructions. London, UK: IOO Sales Ltd.

Wilkins, A., Allen, P. M., Monger, L. J., & Gilchrist, J. M. (2016). Visual stress and dyslexia for the practicing optometrist. *Optometry in Practice*, *17*(2).

Wright, B. N., Wilkins, A. J., & Zoukos, Y. (2007). Spectral filters can improve reading and visual search in patients with multiple sclerosis. *Journal of Neurology*, *254*(12), 1729-1735.

CHAPTER 4: PATTERN-GLARE IMPACTS THETA AND GAMMA FREQUENCIES DURING THE D/C SHIFT

Austyn J. Tempesta[1], Claire E. Miller[1], Andrew J. Schofield[3,1], & Howard Bowman[1,2]

4.1 Introduction

Within the natural environment, human vision is constantly responding to many different types of stimuli such as colours, shapes and patterns. However, some of these patterns are aggravating to some people's brains. Of specific interest to this experiment is visual stress (VS), an aberrant response in the visual cortex in the brain that arises when exposed to different types of striped patterns (Mears, 1980; Irlen, 1983; Wilkins, 1995). The symptoms of visual stress arising from pattern-glare (PG) include eye strain, illusions of colour, shape, motion, and in severe cases, epilepsy and migraines (Wilkins et al. 1979, 1980), however, these might not be occurring because of the same condition. Specifically, migraines and headaches are essential to understand as they are the third-highest cause of disability worldwide (Steiner et al., 2013; Steiner et al., 2015; Strovner et al., 2007). 'Globally, the percentage of the adult population with an active disorder of this nature is 46% for headache in general, 11% for migraine, 42% for tension-type headache and 3% for chronic daily headache' (Stovner et al., 2007). Missed work from migraines is estimated to cost £250 million in lost revenue in the UK each year (Clarke et al., 1996). Migraine is also the least funded of all neurological illnesses globally (House of Commons, 2014; Shapiro & Goadsby, 2007).

Adjamian et al. (2004) hypothesised that such visual stress is caused by the visual cortex's hyperexcitability, which induces spreading activity among neurons usually associated with sensory input, thus producing hallucinations. They used magnetoencephalography (MEG) to

study this and found that gamma oscillations underlie hyperexcitability in visual area V1, which peaked for stimuli that was 3 cycles per degree (c/deg). In some cases, these effects may not be appropriately regulated by GABAergic inhibitory mechanisms. Visual symptoms might thus be the precursor to a photo-paroxysmal response. This, if not sufficiently controlled by inhibitory mechanisms, may lead to epileptic seizures and migraines. The stimuli that are most likely to induce such anomalies, typically 3 c/deg high-contrast stripes, are precisely those most likely to cause attacks of migraine and epilepsy in those with a visual trigger (Wilkins, 1986, 1995; Wilkins et al., 1979, 1980). Most importantly, a minority of people report seeing such visual distortions when viewing printed text (Meares-Irlen syndrome or VS; Mears, 1980). While such distortions could be due to poor ocular accommodation and binocular convergence, they are found even when such abnormalities are excluded (Evans et al., 1995).

The PG test (Figure 4.1) was published by Wilkins and Evans (2001). They designed this test as a standard way for researchers to analyse VS. The test is intended to induce visual stress in susceptible patients; patterns are presented horizontally to appear like text and at different spatial frequencies (SF) (.5, 3, and 12) (Evans & Stevenson, 2008).

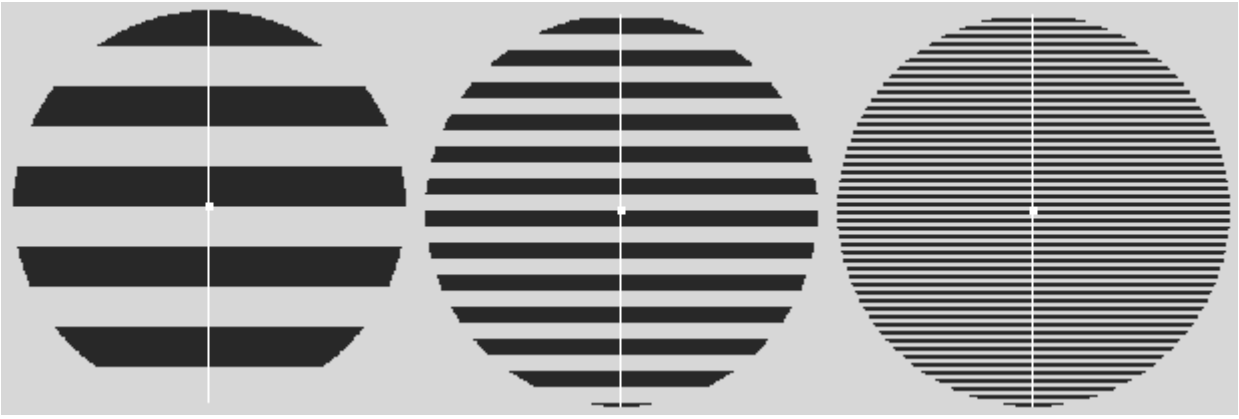

Figure 4-1. Pattern-glare Stimuli:
Left to right, thick (.37 c/deg), medium (3 c/deg) and thin (12 c/deg) gratings with a central fixation and vertical dividing line. The images shown here are representative of the stimuli but have been rendered to aid visibility in print.

As mentioned previously, there has been crucial prior work, using MEG, showing increased gamma power for PG (Adjamian et al., 2004). Importantly, Adjamian et al. did not present stimuli in such a manner that they could isolate habituation effects. They tested each grating from .5 c/deg to 6 c/deg in .5 cycle-steps presented over 2-3 days. Thus, they did not test a 12cpd spatial frequency (SF), which has been argued to be a control for optical factors (Conlon et al., 2001). Pattern 1 (Thick) is intended to be a control for low SF and is not intended to trigger distortions in most participants. However, it is useful in detecting 'which patients who may be highly suggestible and may respond yes to any question about visual perception distortions' (Evans & Stevenson, 2008). Pattern 2 (medium) is the only clinically relevant stimulus, falling between SF's 1-4. It is stimuli in this range that is known to elicit migraines and epileptic seizures (Braithwaite et al., 2013; Wilkins, 2016). Thus, in this study, we respond to the work of Adjamian et al. (2004) by repeating the same stimulus in trains of onsets in order to isolate habituation effects.

Alpha desynchronisation has been shown to be particularly important when the brain is representing stimuli and encoding them into memories or retrieving them from memories (Parish et al., 2018), with alpha power decreasing during semantic encoding and retrieval (Klimesch et al., 1996, 1997). However, this oscillation may reflect the brain representing any sort of stimulus and not be specific to pattern glare.

Some models have shown that alpha amplitude modulations regulate the inhibitory level of the cortex (Klimesch et al., 2007; Jensen & Mazaheri, 2010), with synchronisation reflecting habituation and desynchronisation representing active information processing (Hanslmayr, 2012).

We investigated these hypotheses through a PG task where we recorded EEG data in response to the PG test (PGT, Figure 4.1) over several hours, which we analysed in the frequency domain, using mass univariate analysis (MUA). Because we used EEG (which is relatively cheap), we have collected a reasonably large sample of 35, which is likely to give us increased confidence in the robustness of our findings (Lorca-Puls et al., 2018). In our previous study, we found that we had effects from low beta to high gamma that continued onto the d/c shift period (a sustained period with baseline shifted from zero, the start of which can be seen after 300ms in figure 3.3(C) of Tempesta et al, in submission, Chapter 3), so we wanted to explore that time period.

Hypersensitivity results in distortions of the visual image, which can be disruptive for everyday tasks such as reading, and can cause discomfort in everyday environments. Cortical hyper-excitability is not limited to those who experience migraine. Stimuli that are disruptive for migraine sufferers are also triggers for those with photosensitive epilepsy (Adjamian et al., 2004; Wilkins et al., 1984). Further, visual hypersensitivity as observed with the PGT or similar metrics is co-morbid with a range of conditions including multiple sclerosis (Wright et al., 2007), stroke (Beasley & Davies, 2012), autism (Irlen, 1997; Kientz & Dunn, 1997), and dyslexia (Irlen, 1991), although a connection to dyslexia is disputed (Saksida et al., 2016). In many of these conditions, visual distortions in-text inhibit reading but can be alleviated using coloured filters.

In this study, participants were not selected based on their migraine or headache status. We measured EEG responses to visual stimuli based on those used in the PGT in a novel paradigm where stimuli were repeated (flicked on and off) at a low temporal frequency, allowing

the recording of steady-state EEG, while also allowing us to consider habituation effects. Thus, we compared stimuli known to be aggravating in migraine with those that are less aggravating, in a paradigm that allows the separation of initial and habituated responses.

This paper builds upon the findings of Adjamian et al. (2004) and upon our previous work on oscillations. Specifically, our hypotheses are:

1. High gamma power observed immediately after the onset transient in (Tempesta et al., in preparation, Chapter 3) will continue throughout the D/C shift period and will be driven by the medium stimulus. Explicitly we should expect to see desyncrony in the low frequency bands and synchrony in the high frequency bands.
2. There will be a broadband effect at stimulus offset, by analogy with the broadband effect we see at onset.
3. Medium frequency stimuli lead to greater activity in the brain. Processing of the early visual areas representing the three different spatial frequencies of these gratings will be visibly different from each other in either synchrony or desynchrony.
4. Delta and theta will show a desynchrony during the D/C shift period with aggregated EEG responses to the stimuli (medium+thick+thin), mimicking our earlier result for alpha in aggregate responses (Tempesta et al., in preparation, Chapter 3). This may be related to information processing. There may also be a difference between onset 1 and onset 2:8, as onset 1 may be due to a surprise or prediction effect, whilst onset 2:8 reflects a failure to habituate specifically for the medium grating.

4.2 Materials and Methods

4.2.1 Participants

Forty undergraduate and postgraduate participants, recruited at the University of Birmingham, gave their informed consent and were compensated with £24 for participating.

Participants with a history of psychiatric, psychological, and neurological conditions, or a history of unconsciousness, convulsions or epilepsy were excluded from the study. One participant chose to leave the experiment, and four were rejected during data pre-processing due to a lack of usable trials (fewer than 20% per condition). There were thus 35 usable datasets (male=14, female=21, mean age= 22.5y, range=18-32y, standard deviation=2.86). This study was approved by The Science Technology Engineering and Maths Ethics Committee at the University of Birmingham in adherence with The Declaration of Helsinki.

4.2.2 Stimuli and Equipment

We used stimuli similar to those used in the PGT (Wilkins, 2001). Stimuli comprised horizontal square-wave gratings (contrast = 75%) at 3 different spatial frequencies (.37, 3, and 12 c/deg: described as thick, medium, and thin, respectively, see Figure 4.1) displayed at 75% contrast in a circular window with diameter (15.2 deg) at a viewing distance of 86 cm. These stimuli were created in MATLAB using the Psychophysics Toolbox (Brainard, 1997; Pelli, 1997; Kleiner et al., 2007) and displayed on a Samsung 932BF LCD monitor (Samsung Electronics, Suwon, South Korea). EEG recordings were made using a 128-channel BioSemi (University of Amsterdam) EEG system in a dark, quiet room.

4.2.3 Procedure

After the EEG electrodes had been applied, participants began the experiment with a 5-minute resting period and then were presented with three blocks, each containing six trials for each of the three stimuli. Thus, each participant observed 18 trials per stimulus type. Each trial contained between seven and nine onsets of the same stimulus each lasting three seconds, followed by a variable interval of 1 – 1.4 seconds. After each trial, the participant was asked to rate how uncomfortable they found each stimulus on a 5-point scale (1 = comfortable, 5 =

extremely uncomfortable) and to indicate how many onsets they saw. This additional task was designed to ensure attention to the stimuli. At the end of each block, participants were shown the three stimuli in turn and asked to rate the extent to which they had experienced a range of possible pattern glare symptoms for each stimulus (Wilkins & Nimmo-Smith, 1984). After each block and at the end of the experiment, participants had a further resting period of 5 minutes, during which they were requested to close their eyes and relax. Stimulus order and number of onsets per trial were counterbalanced (subjecting them to variation, increasing interval validity) (Allen, 2017).

4.2.4 ERP pre-processing

We decimated the EEG data from a sampling rate of 2048Hz to 512Hz using the BioSemi toolbox. EEGs were then band-pass filtered using a second-order Butterworth filter with a pass band of 0.075 to 80 Hz (½ power -3dB, fall-off at 12 dB per octave; for prior precedent for this choice, see Luck, 2014; Tanner et al., 2015). We used a baseline of -500 for the EEG data that would be subjected to the frequency-domain analysis; this long baseline was required to encompass the full wavelet at low frequencies. For each participant, we performed a time-frequency analysis using a morlet wavelet with 5-cycles in the frequency range 3-80 Hz, with steps of 1 Hz between each wavelet frequency, and a notch-filter at 50hz. Additionally, we performed another time-frequency analysis using a 3-cycle wavelet from frequency ranges 1-10 Hz, with steps of 1Hz between each wavelet frequency. As stated previously, the baseline was initially 500ms long for the wavelet estimation. However, after estimation, we cropped the epoch from -100ms pre-stimulus to 3900ms post-stimulus, then the conditions were averaged, and the baseline (-100ms to zero ms) was rescaled using a logR function in SPM.

Eye-blink artefacts were removed using independent component analysis (ICA), with ICA components associated with eye blinks removed and the dataset reconstructed. The crown electrodes were removed to further reduce the presence of muscle and eye-movement artefacts (Chennu et al., 2013), in line with previous researchers (Shirazibeheshti et al., 2018) who argue that this additional noise may confound Mass-Univariate Analysis (MUA) (electrodes removed = A11, A12, A13, A14, A24, A25, A26, A27, B8, B9) and the data was referenced to the new electrode set. Data for individual onsets were then deleted if any channel exceeded a +/-100 µV threshold, thus removing large artefacts such as movement. The data for each participant were split into 27 bins, one for each stimulus type (thick, medium or thin) and onset number (1 to 9). Finally, we discarded data from Onset 9 - the number of onsets varied between 7 and 9 on each trial, so the occurrence of the 9^{th} Onset was rare, making these data unreliable. Tallying across onset number, four participants who did not have at least 20% of usable stimulus repeats per stimulus type were removed (decided a priori, based on Luck, 2014). For interpolation, approximate values between electrodes of the biosemi and the internal spm grid were calculated when the electrode locations from EEGLAB were combined with the SPM software. This enabled the interrogation of positions on the scalp beyond the electrode locations. In order to compare stimulus onset with habituation-effects, we divided the repeated onsets into two groups. The initial onsets were analysed separately from Onsets 2-8, the latter being combined. We drew a logical distinction between the first stimulus onset in each trial (where the observer was unaware of the stimuli to be presented) and the remaining onsets (where the participant was able to anticipate the stimulus) and thus analysed Onset 1 separately from Onsets 2-8; the latter being combined so as to aggregate over the maximum number of onsets.

4.2.5 Frequency band selection

We divided the frequency domain into separate bands on onsets 1-8. The frequencies from onset 1 and onset 2-8 were averaged with the spm averaging tool weighting by replications (trial counts). A 5-cycle wavelet was used for frequencies 4-80 Hz (Figure 4.2) as we did not have a long enough baseline to observe effects below 3 Hz due to edge artefacts swamping the segment. The windows were selected based upon visual inspection of the time-frequency plot at Oz (see Figure 4.2). For 1-10hz, we used a 3-cycle wavelet (Figure 4.3). This does not inflate the false positive rate, because the inspection of the frequency bands was on the aggregated average of the stimuli (i.e., average of activation in response to all three stimulus types) and onsets (1 to 8), making the frequency selection image blind to conditions. As a result, the selection of a frequency band is not differentially influenced by a particular stimulus, ensuring that the selection of the frequency bands is not biased (for justification of this line of reasoning see Brooks et al, (2017); Bowman et al, (2020)). For each selected frequency band, we collapsed across power values, to generate a single time-series. Frequency bands were as follows:

For 5-cycle wavelet:

Theta:4-10hz

Alpha: 9-13hz

Low Beta: 17-25hz

Low Gamma/High Beta: 25-45hz

Mid Gamma: 45-60hz

High Gamma: 60-80hz

For 3-Cycle wavelet:

Delta: 2-3hz

We were very explicitly seeking to place windows that isolated the key spectral power features in Figures 4.2 & 4.3, with some windows selected to be narrow to ensure that we select the "sweet spot" of the feature; see, for example, our choice regarding alpha. Additionally, we selected overlapping windows for alpha and theta. Thus, we are making a priori decisions concerning our key contrast, which is on the PGI, regarding the placing of frequency bands, which necessarily means that we will not place optimally for effects in the data. This is the standard trade-off between type-I and type-II error rates (Bowman et al., 2020).

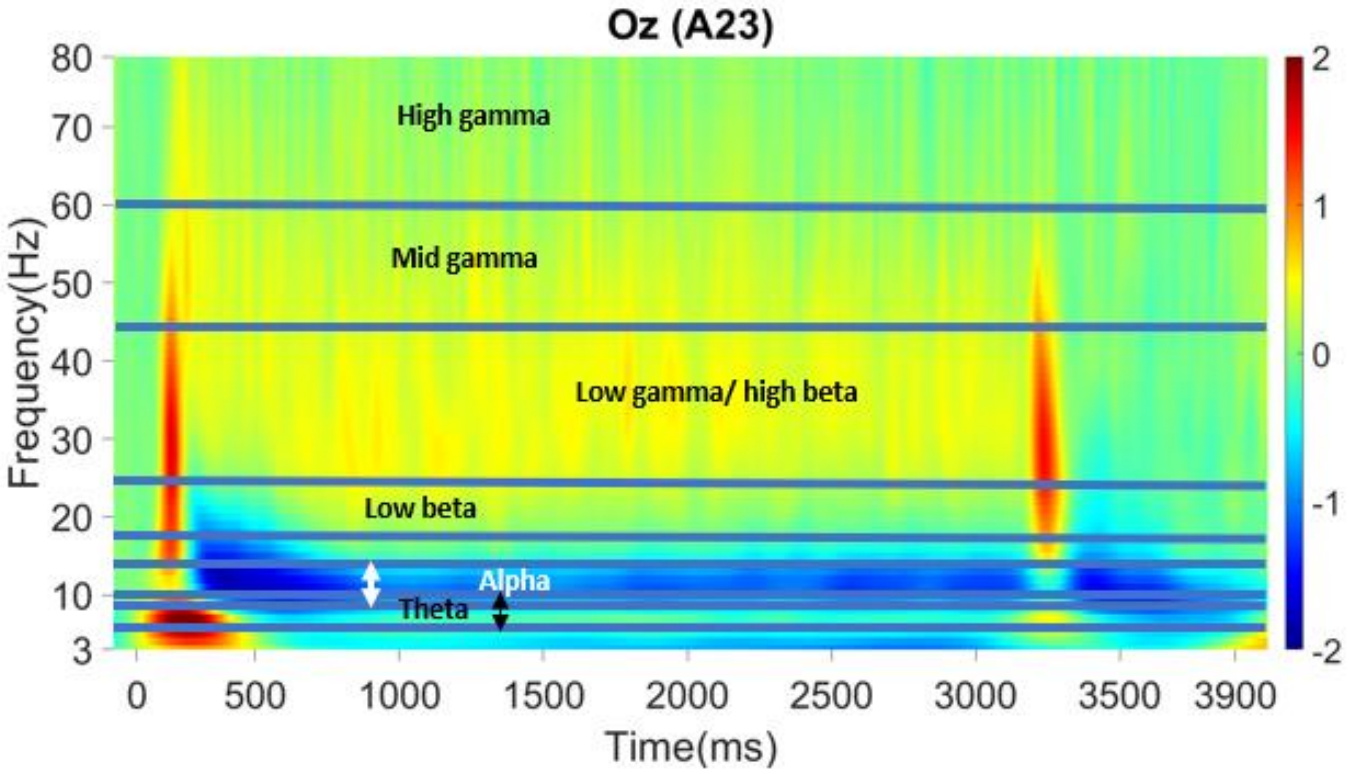

Figure 4-2. Time-Frequency plot of Weighted Average of Onsets 1:8 Aggregated Across all Stimuli (Thick, Medium and Thin) at Electrode Oz, excluding lowest frequencies.
Bottom to top: frequency bands used for analysis, chosen from electrode Oz: Theta:4-10hz, Alpha: 9-13hz, Low Beta: 17-25hz, Low Gamma/High Beta: 25-45hz, Mid Gamma: 45-60hz, High Gamma: 60-80hz. Colour Scale is -2 to 2dB power. Frequency scale is 3 to 80hz. The frequency ranges were selected through visual inspection - the selection of windows was based on where a strong effect in power could be seen visually. However, since stimulus conditions (Thick, Medium and Thin) are aggregated across in this plot, this selection is orthogonal to our pattern-glare contrasts that are our central finding. Note, this selection of frequency ranges was made in order to isolate salient features in this map; consequently some frequencies were narrow, some frequencies overlapped and not all frequencies were included. Necessarily, these windows may not be placed appropriately for some pattern-glare effects that may be present, but this is the standard trade-off between type I and type II error rates for a priori selection of

features.

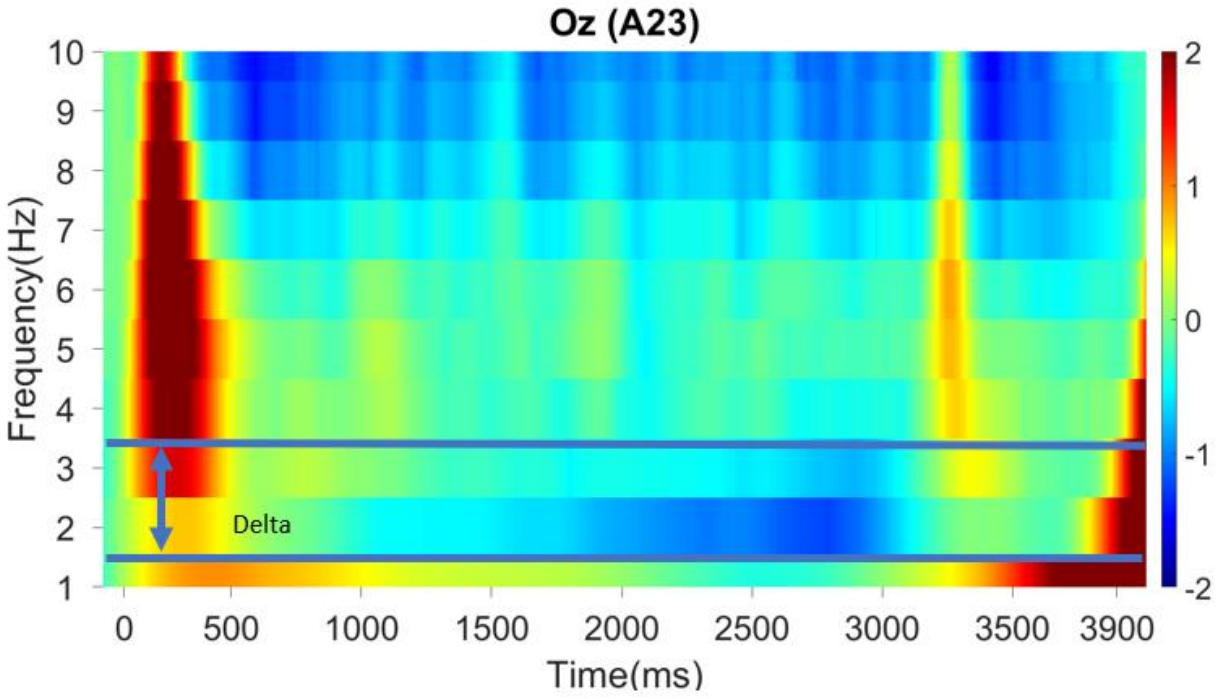

Figure 4-3 Time-Frequency plot of Weighted Average of Onsets 1:8 Aggregated Across all Stimuli (Thick, Medium and Thin) at Electrode Oz, for lowest frequencies.

Frequency band used for analysis chosen from electrode Oz: Delta:2-3hz. Colour Scale is -2 to 2dB power; frequencies are from 1 to 10hz. The frequency ranges were selected through visual inspection - the selection of windows was based on where a strong effect in power could be seen visually. However, since stimulus conditions (Thick, Medium and Thin) are aggregated across in this plot, this selection is orthogonal to our pattern-glare contrasts that are our central finding. Note, this selection of frequency ranges was made in order to isolate salient features in this map; consequently, the frequency band selected here is relatively narrow. Necessarily, these windows may not be placed appropriately for some pattern-glare effects that may be present, but this is the standard trade-off between type I and type II error rates for a priori selection of features.

4.2.6 Mass Univariate Analysis

A mass univariate analysis (MUA) is the analysis of a large number of simultaneously measured dependent variables (e.g. voxels or samples) via the performance of the same univariate hypothesis tests (e.g., t-tests) across all of those dependent variables. This method allows for powerful error corrections for multiple comparisons.

An MUA was conducted in SPM-12 (Wellcome Trust Centre for Neuroimaging, London, England) on three-dimensional images (two of space, one of time) derived from the data resulting from collapsing across each frequency band. Images were created using the data for each stimulus type (thick, medium, and thin). A contrast image was created based on what we call the pattern glare index (PGI). This index enables us to focus our analysis on regions of the data volume where the clinically relevant, medium stimulus exhibits an extreme response relative to the thick and thin stimuli.

PGI = (medium image – average (thick image, thin image)).

We then tested the mean intercept over the whole volume in all seven frequency bands, both positive-going and negative-going. We did this first for aggregated (thick, thin and medium collapsed) and then for PGI. We used a one-tailed, 1-sample t-test: We checked for a significant peak (FWE .05, peak-level) or cluster levels (unc .001, 0.05 FWE corrected) in both +1 and -1 directions on aggregated and PGI on mean/intercept. A general linear model (GLM) analysis was performed on the data where the PGI over ERPs was the dependent variable, while the independent variables were the normalised factor scores of the trait and state data responses (which act as regressors). This same general linear model was fit to the ERP data at each time-space point in the data volume, providing beta parameter values for all the regressors (the intercept and three factors) at each such point. Intuitively, each parameter value indicates the

extent to which the evoked response at the corresponding time-space point correlates (across subjects) with the relevant regressor. In this way, a mass univariate analysis is able to identify time-space regions in the data volume, which vary in a fashion consistent with a factor or intercept. Additionally, due to the mean centring of regressors, the intercept parameter is the mean of the evoked response at that time-space point.

4.3 Results

We performed several analysis steps (see materials and methods for full explanation). In this section, the aggregated effects are discussed, followed by the PGI mean/intercept effects. The frequencies of interest were split into low and high. (To visualise the effects, see Figures 4.4, 4.5, 4.6 and 4.8, for both aggregated and PGI analyses.) A breakdown of statistics for each analysis step can be found in associated tables (see tables 4.1, 4.2, 4.3 and 4.4).

Our results are summarized by four main features, which can, for example, be seen in the unthresholded maps in figures 4.4 and 4.5, and which we now describe briefly before considering each in more detail:

Early Positive Transients:

1. *Posterior to anterior, constant amplitude*: this transient bleeds from over occipital along the midline to over frontal, with *similar* amplitude throughout (e.g. theta, delta and alpha 1 and 2:8, dotted framing).
2. *Clear posterior peak*: this has a higher peak over occipital (and is not present in aggregate low frequencies; but can be seen for higher frequencies, e.g. Low Gamma/ High Beta and Mid Gamma).

Sustained Responses:

3. *Desynchronisation*: this starts after the positive transient and can be quite broadly distributed across the scalp (e.g. theta, delta and alpha 1 & 2:8, long dash, dot framing).

4. *Synchronisation*: this starts after the positive transient has subsided and tends to be broadly distributed over the scalp, with strong areas in occipital (e.g. delta 2-8, unbroken framing).

4.3.1 Aggregated mean/intercept contrasts for low frequencies

Figure 4.4 shows the results of the aggregated mean/intercept contrasts as topographic maps. The rows from top to bottom display thresholded and unthresholded topographic maps for the low frequencies. Onset 1 or Onset 2:8 is indicated on the right. The columns indicate the frequency bands. Within the unthresholded topographic maps, we have indicated effects of interest, early positive transients or sustained synchronisations (see key for full breakdown), with, for example, delta showing a posterior to anterior early positive transient, followed by a large desychronisation on onset 1; for onset 2:8 we see a synchronisation. In contrast, we see a sustained desynchronisation in the other frequency bands on both onset 1 and onset 2:8. There is no consistent scale across thresholded maps, in order to avoid colour saturating in some maps.

In summary, in Figure 4.4, we can identify three of the four main features in this power analysis on aggregated, which, as mentioned, can be divided into early positive transients and sustained responses. These features are highlighted with white framing in panels where they are particularly evident (see Figure 4.4 and Legend). Not all effects mentioned in the key are present in every graphic.

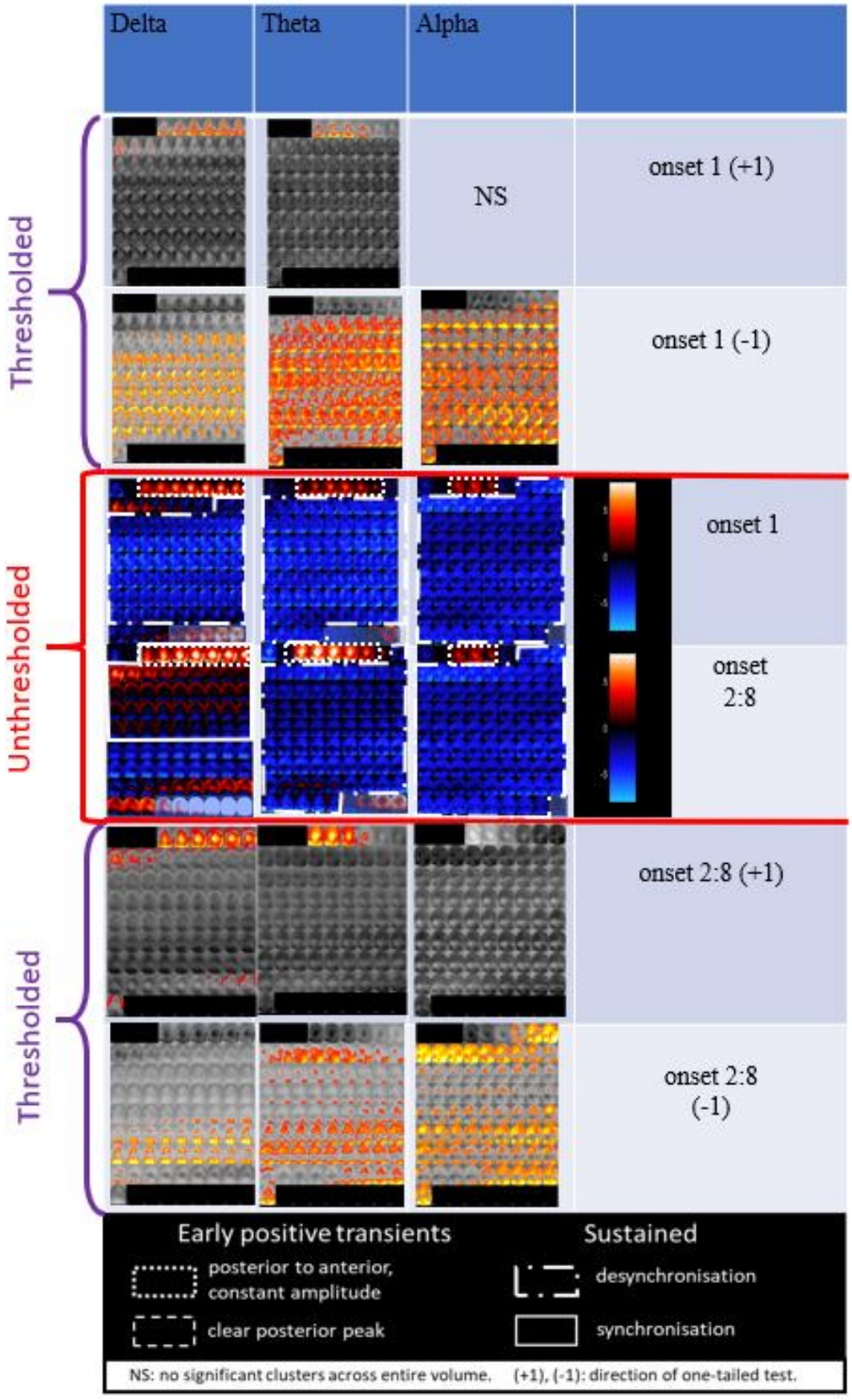
Delta
Theta
Alpha
Thresholded
NS
onset 1 (+1)
onset 1 (-1)
Unthresholded
onset 1
onset 2:8
Thresholded
onset 2:8 (+1)
onset 2:8 (-1)
Early positive transients
posterior to anterior, constant amplitude
clear posterior peak
Sustained
desynchronisation
synchronisation
NS: no significant clusters across entire volume.
(+1), (-1): direction of one-tailed test.

Figure 4-4. Time-frequency effects on the mean of aggregated (Thin+Medium+Thick) for low frequencies:

Frequency bands are presented in three columns (from left to right: Delta, Theta, and Alpha); first two rows present thresholded maps for onset 1, next two rows present unthresholded maps (onset 1 and then onset 2:8), last two rows present thresholded maps for onsets 2:8. Thresholded maps show one-sample one-tailed t-tests, with direction indicated by bracketed terms (e.g. "(+1)" is right-tailed). Each panel of plot shows scalp maps through time, laid out from top left to bottom right in the panel. Unthresholded maps (blue, black and red) show scalp maps from -100ms to 3900ms in steps of 50ms. There is a 50% opacity filter to show the area of the edge effect. Thresholded maps (yellow, orange, grey) show scalp maps from -100 to 3900ms in steps of 50ms. Note, that the analysis window was only 50-3500ms, so for Thresholded maps the non-analysed region is black. For thresholded maps, Alpha +1 was presented FWE-corrected at the peak-level; all others are corrected at the cluster-level. The scale of the unthresholded maps is -8 to 8. Key findings are most evident in unthresholded maps (middle two rows). Raw one-sample t-values are presented for difference to zero, with red positive-going and blue negative-going. Key features are presented with white framing (see legend and main text).

Table 4.1 shows the results breakdown of the associated statistics of the effects from Figure 4.4. Each cluster is given with its Xmm, Ymm, Zms location and time with both *T* and *P* values. Alpha onset 2:8 (+1(right-tailed)) is corrected at the peak-level. From left to right, the columns indicate the frequency of interest, and the rows indicate Onset 1 or 2:8. NS means that there was no statistical effect found. Loc is the location of the cluster.

Delta	Theta	Alpha	Aggregate Low Frequencies
t(34)=8.17, *p*<.001, Loc:43, 79, 105ms	*t*(34)=8.87, *p*=.001, Loc:-34,-84, 135ms *t*(34)=6.19, *p*=.012, Loc:-13,-14, 125ms	NS	onset 1 (+1)
t(34)=7.07, *p*<.001, Loc:-42, 34, 1854ms	*t*(34)=9.03, *p*<.001, Loc:38,-79, 2977ms	*t*(34)=8.13, *p*<.001, -Loc:38, 8 3455ms	onset 1 (-1)
t(34)=11.82, *p*<.001, 4 -95, 86ms *t*(34)=5.82, *p*=.028, Loc:64, 29, 3504ms *t*(34)=4.38, *p*=.033,Loc: -47, 34, 3504ms	*t*(34)=10.80, *p*<.001, Loc:0,-14, 47ms	peak-*t*(34)=4.97, *p*=.046, Loc:-4,-36,47ms	onset 2:8 (+1)
t(34)=7.67, *p*<.001, loc:-26, -62, 2430ms *t*(34)=6.59, *p*<.001, Loc:0, 24, 2811ms	*t*(34)=8.51, *p*<.001, Loc:34,-89, 3504ms	*t*(34)=6.89, *p*<.001, Loc:47, -46, 330ms	onset 2:8 (-1)

NS: no significant clusters across entire volume, Loc: location of cluster, location is Xmm,Ymm, Zms

Table 4-1. Aggregated, mean/intercept contrasts, statistics at low frequencies.

Raw one-sample t-values are presented for difference to zero at the peak of a cluster (direction indicated by bracketed terms (e.g. "(+1)" is right-tailed)) and associated p-values, which are, in all but one case, for encompassing cluster, FWE-corrected at the cluster level. In contrast, alpha onset 2:8 (+1) is corrected at the peak-level. Location of peak of cluster is listed in Xmm, Ymm, Zms format. The columns from left to right are delta, theta, and alpha. The rows from top to bottom are (onset 1 and then onset 2:8). NS means not significant, Loc is the location of cluster.

4.3.2 Aggregated mean/intercept contrasts for high frequencies

Figure 4.5 shows the results of the aggregated mean/intercept contrasts of the high frequencies, topographic maps. The rows from top to bottom display thresholded and unthresholded topographic maps for the low frequencies. Onset 1 or Onset 2:8 is indicated on the right. The columns indicate the frequency band. Within the unthresholded topographic maps, we have indicated effects of interest, early positive transients or sustained synchronisations (see key for full breakdown), with, for example, low gamma/high beta 2:8 showing an early posterior to anterior positive-transient followed by a large synchronisation across the scalp.

4.3.3 Early Positive Transients and Sustained Responses

With the framing interpretation presented above and the resulting four phenomena we identified for aggregated low frequencies, we can see the following in the aggregated plots, with key features again presented with white framing (see Figure 5.5 and legend). We begin with the early positive transients:

1. *Posterior to anterior, constant amplitude*: There is an effect that bleeds from occipital across the cortex within frequencies low beta and low gamma/high beta onset 2:8.
2. *Clear posterior peak*: Onset 1 low gamma/high beta and onset 2:8 mid gamma show a clear posterior effect that is localised to occipital lobe. Note that in low frequencies, there was no localised posterior peak, the early positive transients were only observable broadly across the scalp.

For the sustained response effects, we can observe the following:

1. *Sustained Desychronisation*: In stark contrast to low frequencies where most frequencies both onset 1 & 2:8 showed large desyncs, only onset 1 shows the strong desynchronisation.

2. *Sustained synchronisation*: There is an early positive transient followed by a strong sustained synchronisation for two frequencies: low gamma/high beta and mid gamma for onset 2:8. There is evidence of a similar response for high gamma onset 2:8, but it is much briefer than for the other gamma frequencies.

Generally, there is a sense to which all frequencies for onset 1 and onset 2:8 exhibit a similar pattern – brief positivity followed by extended negativity – apart from low beta and gamma frequencies for onset 2:8, which show strong sustained synchronisations. It is also notable that these sustained synchronisations are strongly stimulus-bound, in the sense that they finish sharply at stimulus offset; see unbroken framing.

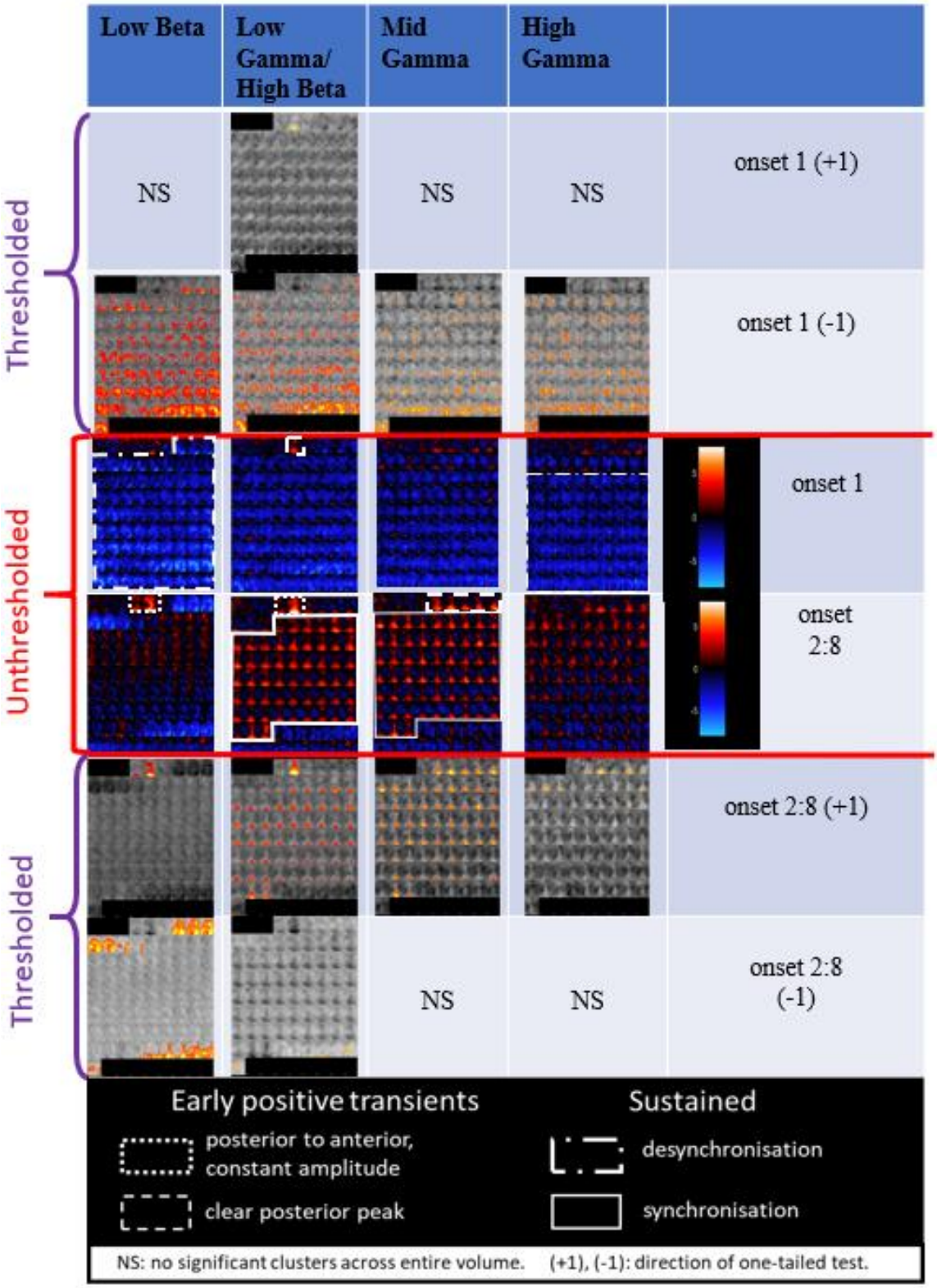
Low Beta
Low Gamma/ High Beta
Mid Gamma
High Gamma
Thresholded
Unthresholded
Thresholded
NS
NS
NS
onset 1 (+1)
onset 1 (-1)
onset 1
onset 2:8
onset 2:8 (+1)
NS
NS
onset 2:8 (-1)
Early positive transients
posterior to anterior, constant amplitude
clear posterior peak
Sustained
desynchronisation
synchronisation
NS: no significant clusters across entire volume.
(+1), (-1): direction of one-tailed test.

Figure 4-5. Time-frequency effects on the mean of aggregated (Thin+Medium+Thick) for high frequencies:

Frequency bands are presented in four columns (from left to right: Low Beta, Low gamma/High Beta, Mid Gamma, High Gamma); first two rows present thresholded maps for onset 1, next two rows present unthresholded maps (onset 1 and then onset 2:8), last two rows present thresholded maps for onsets 2:8. Thresholded maps show one-tailed one-sample t-tests, with direction indicated by bracketed terms (e.g. "(+1)" is right-tailed). Each panel of plot shows scalp maps through time, laid out from top left to bottom right in the panel. Unthresholded maps (blue, black and red) show scalp maps from -100ms to 3900ms in steps of 50ms. The scale of the unthresholded maps is -8 to 8. Thresholded maps (yellow, orange, grey) show scalp maps from -100 to 3900ms in steps of 50ms. Note that the analysis window was only 50-3500ms, so for thresholded maps the non-analysed region is black.

Key findings are most evident in unthresholded maps (middle two rows). Raw one-sample t-values are presented for difference to zero, with red positive-going and blue negative-going. Key features are again presented with white framing (see legend and main text). There are no substantial qualitative differences between onset 1 and onset 2:8 for aggregated low frequencies, as in the earlier (see Figure 5.4), but there are substantial differences, especially in the DC shift period, for the higher frequencies being seen in this figure.

Table 5.2 shows the results breakdown of the associated statistics of the effects from Figure 5.5. Each cluster is given with its Xmm, Ymm, Zms location and time with both *T* and *P* values. From left to right, the columns indicate the frequency of interest and the rows indicate whether it is onset 1 or onset 2:8. NS means that there was no statistical effect found.

Low Beta	Low Gamma/ High Beta	Mid Gamma	High Gamma	
NS	$t(34)=5.96$, $p=.001$, Loc:0,-89, 96ms	NS	NS	onset 1 (+1)
$t(34)=10.87$, $p<.001$, loc:26, -36, 3455ms	$t(34)=8.39$, $p<.001$, Loc:-38,-39,3299ms, $t(34)=7.92$, $p<.001$, Loc:30,-41,1414ms $t(34)=6.33$, $p<.001$, Loc:13,-30,2117ms	$t(34)=6.89$, $p<.001$, Loc:17, -3, 3367 $t(34)=6.22$, $p=.001$, Loc:34,-30,1053ms $t(34)=5.81$, $p<.001$, Loc:34,-25, 1873ms	$t(34)=7.28$, $p<.001$, Loc:17,-9, 1736ms $t(34)=6.84$, $p<.001$, Loc:-51,-14, 3318 $t(34)=6.45$,$p<.001$, Loc:-64,-3369ms	onset 1 (-1)
$t(34)=12.95$, $p<.001$, Loc:4, -84, 86ms	$t(34)=9.86$,$p<.001$,-17,-84, 105ms $t(34)=7.81$,$p<.001$, Loc:9, -84, 3113ms	$t(34)=7.89$, $p<.001$, 13,-4,3094ms $t(34)=7.78$,$p<.001$, 4,-73,1141ms, $t(34)=6.14$,$p<.001$ -13,-73,2791ms	$t(34)=6.32$,$p=.006$, Loc:4,-46,1141ms $t(34)=5.54$,$p<.001$, Loc:0,-62,164ms $t(34)=5.51$,$p<.001$, Loc:4,-68,379ms	onset 2:8 (+1)
$t(34)=7.94$, $p<.001$, Loc:51,-68, 3318ms $t(34)=7.27$,$p<.001$, Loc:34,-52, 203ms	$t(34)=6.15$,$p<.001$, Loc:21, 13, 3455ms $t(34)=5.02$,$p<.001$, Loc:47-73,3309ms	NS	NS	onset 2:8 (-1)

NS: no significant clusters across entire volume, Loc: location of cluster, location is Xmm,Ymm, Zms

Table 4-2. Aggregated, mean/intercept contrasts statistics for high frequencies.

Raw one-sample t-values are presented for difference to zero at the peak of a cluster (direction indicated by bracketed terms (e.g. "(+1)" is right-tailed)) and associated p-values, which are for encompassing cluster, FWE-corrected at the cluster level. Location of peak cluster is listed in Xmm, Ymm, Zms format. The columns from left to right are low beta, low gamma/high beta, mid gamma, high gamma. The rows from top to bottom are (onset 1 and then onset 2:8). NS means not significant; Loc is the location of the cluster.

4.3.4 PGI mean/intercept contrasts for low frequencies

Figure 4.6 shows the results of the PGI mean/intercept contrasts for the low frequencies, topographic maps. The rows from top to bottom indicate if the topographic maps are thresholded or unthresholded. Onset 1 or onset 2:8 is indicated on the right. The columns indicate what frequency band is being shown. Within the unthresholded topographic maps, we have indicated effects of interest, which were discussed previously, either early positive transients or sustained positive and negative-going effects (see key for full breakdown), with white framing. For this figure, the peak of the contrast theta 2:8 +1 is significant at the peak level (this is circled in black). The x and y letters on the topographic maps indicate their relation to Figure 4.7. Precisely, each letter corresponds to a different effect indicated by a vertical line in the Figure 4.7 graph. The reader can then refer back to Figure 4.6 to see that indicated effect in the context of the broader findings.

With the framing interpretation we just presented above, there is one difference between PGI and aggregated contrasts. In the PGI contrasts, because PGI is a measure of the difference of medium to the mean of thick and thin, it is not truly a measure of synchronicity but of a positive or negative going effect. Thus, we use the terms positive going and negative going effect here.

We can see the following in the pattern-glare plots with key features again presented with white framing (see Figure 4.6 and legend). We again begin with the early positive transients:

1. *Posterior to anterior, constant amplitude*: This effect is not present for PGI in the low-frequency band.
2. *Clear posterior peak*: There is a clear posterior peak for theta (see x). This is interesting because Adjamian and colleagues (2004), did not see this effect in their data.

For sustained responses, we can observe the following:

1. *Positive going effect*: For theta, a sustained positive-going effect can be observed after the early positive transient. However, due to the way in which we overlapped the frequency bands of theta and alpha, this effect may continue into alpha but with insufficient statistical power to show significance in the alpha band. In order to visualise this effect, we have plotted both theta and alpha at electrode C2 (see Figure 4.7). Notwithstanding the edge effect, it appears that the PGI effect continues beyond the offset transient for these frequencies. This is not the case for the higher frequencies, where the PGI effect seems to be obliterated by the offset transient. Additionally, this sustained positivity is maximal near Cz, so substantially anterior to the sustained PGI effects we will observe for higher frequencies.
2. *Negative going effect*: We do not observe any statistically significant negative-going effects for low frequencies on the PGI.

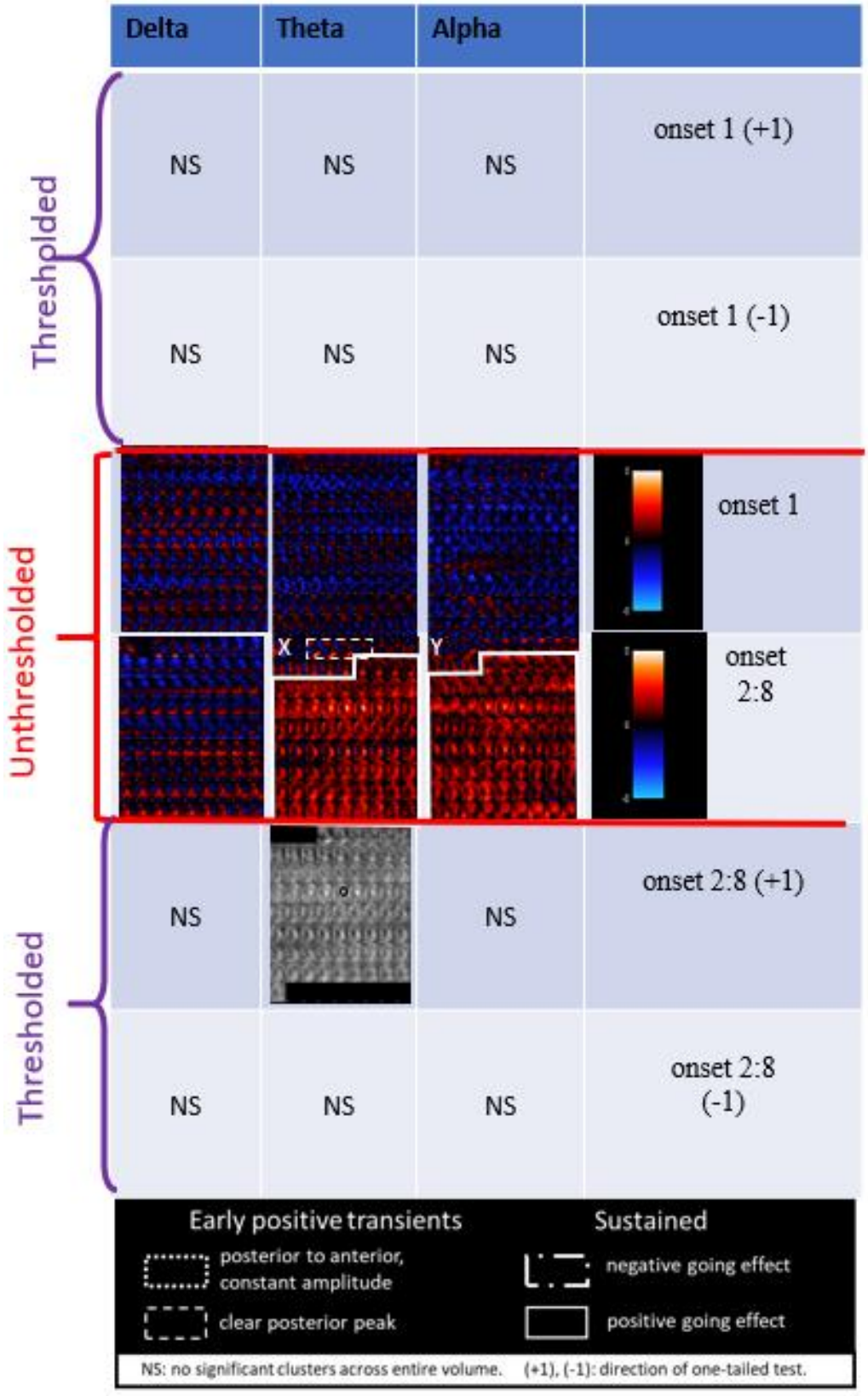
Delta
Theta
Alpha
Thresholded
NS
NS
NS
onset 1 (+1)
NS
NS
NS
onset 1 (-1)
Unthresholded
onset 1
X
Y
onset 2:8
Thresholded
NS
NS
onset 2:8 (+1)
NS
NS
NS
onset 2:8 (-1)
Early positive transients
posterior to anterior, constant amplitude
clear posterior peak
Sustained
negative going effect
positive going effect
NS: no significant clusters across entire volume.
(+1), (-1): direction of one-tailed test.

Figure 4-6. Time-frequency effects on the mean of PGI index for low frequencies: Frequency bands are presented in three columns (from left to right: Delta, Theta, and Alpha); the first two rows present thresholded maps for onset 1; the next two rows present unthresholded maps (onset 1 and then onset 2:8); the last two rows present thresholded maps for onset 2:8. Thresholded maps show one-sample one-tailed t-tests, with direction indicated by bracketed terms (e.g. "(+1)" is right-tailed). Each panel of plot shows scalp maps through time, laid out from top left to bottom right in the panel. Unthresholded maps (blue, black and red) show scalp maps from -100ms to 3900ms in steps of 50ms. The scale of the unthresholded maps is -5 to 5. Thresholded maps (yellow, orange, grey) show scalp maps from -100 to 3900ms in steps of 50ms. Note that the analysis window was only 50-3500 ms, so for thresholded maps, the non-analysed region is black.

Key findings are most evident in unthresholded maps (middle two rows). Raw one-sample t-values are presented for difference to zero, with red positive-going and blue negative-going. Key features are again presented with white framing (see legend and main text).

Table 4.3 gives a breakdown of results in statistical form, in relation to the effects shown in Figure 4.6. The peak is given with its Xmm, Ymm, Zms location and time with both *T* and *P* values. From left to right, the columns indicate the frequency of interest and the rows indicate whether it is onset 1 or onset 2:8. NS means that there was no statistical effect found.

Delta	Theta	Alpha	
NS	NS	NS	onset 1 (+1)
NS	NS	NS	onset 1 (-1)
NS	Peak: *t*(34) =5.23, *p*=.025, Loc:17,-3, 1463ms	NS	onset 2:8 (+1)
NS	NS	NS	onset 2:8 (-1)

NS: no significant clusters across entire volume, Loc: location of cluster, location is Xmm,Ymm, Zms

Table 4-3. PGI, mean/intercept contrasts statistics for low frequencies.
Raw one-sample t-values are presented for difference to zero (direction indicated by bracketed terms (e.g. "(+1)" is right-tailed)) and associated p-values, FWE-corrected at the peak level. Location of peak is listed in Xmm, Ymm, Zms format. The columns from left to right are delta, theta, and alpha. The rows from top to bottom are (onset 1 and then onset 2:8). NS means not significant; Loc is the location of the cluster.

Figure 4.7 shows the effect for theta and alpha on low frequencies at electrode C2. The peak from the PGI mean/intercept is at 17mm, -3mm, 1463ms. The 'x' on theta and the 'y' on alpha on the graph can be used to refer back to figure 4.6 to compare effects in the broader context. Theta was significant FWE-corrected at the peak-level, with p=.025, and uncorrected $t(34)$=5.23 at the peak (for full statistical breakdown see, table 4.3).

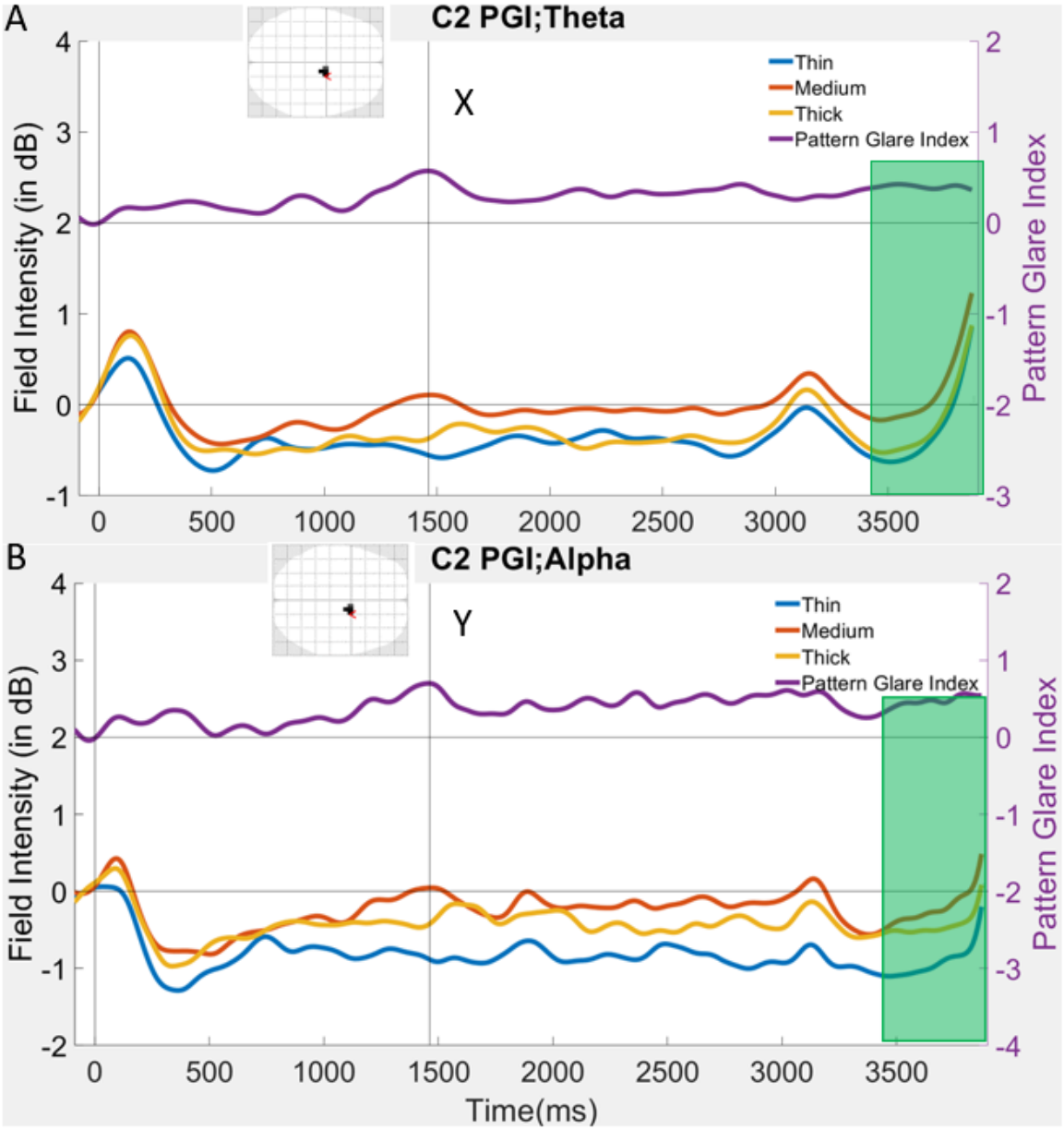
A
C2 PGI;Theta
X
Thin
Medium
Thick
Pattern Glare Index
Field Intensity (in dB)
Pattern Glare Index
B
C2 PGI;Alpha
Y
Thin
Medium
Thick
Pattern Glare Index
Field Intensity (in dB)
Pattern Glare Index
Time(ms)

Figure 4-7: time-series of (A) theta and (B) alpha, frequencies, onsets 2:8, at the same posterior electrode, showing positive effect (both sustained and early positive transient) for medium, thick and thin gratings:

Time series of power summed across each frequency band, at electrode C2 (see red arrow in inset scalp map). Plots correspond to different effects in Figure 4.8: (A) theta to effect x; (B) alpha to y. These effects can also be seen in the PGI time-series in these plots, see right-side y-axis. The scalp maps here show spm glass scalps, in which all significant effects at this peak are collapsed onto a two-dimensional representation. It shows that the electrode being plotted (red arrow) is at a position where there is considerable significance through time. Positive is plotted up on time-series. The green 50% opacity filter is to show where there is an edge effect present.

4.3.5 PGI mean/intercept contrasts for high frequencies

Figure 4.8 shows the results of the PGI mean/intercept contrasts for the high frequencies, presented as topographic maps. The rows from top to bottom indicate if the topographic maps are either thresholded or unthresholded. Onset 1 or onset 2:8 is indicated on the right. The columns indicate what frequency band is being shown. Within the unthresholded topographic maps, we have indicated effects of interest, which were discussed previously, either early positive transients or sustained positive and negative-going effects (see key for full breakdown), with white framing. The w, x, y and z letters on the topographic maps indicate their relation to Figure 4.9. Specifically, each letter corresponds to a different effect indicated by a vertical line in the Figure 4.9 graph. The reader can then refer back to Figure 4.8 to see that indicated effect in the context of the broader findings. With the framing interpretation we presented in PGI mean/intercept low frequencies, we can see the following in the pattern-glare plots with key features again presented with white framing (see Figure 4.8 and legend). We again begin with the early positive transients:

1. *Posterior to anterior, constant amplitude*: For onset 2:8 there is a posterior to anterior, constant amplitude for low gamma/high beta. This is not present for any other high frequencies
2. *Clear posterior peak*: Interestingly, there is a clear posterior peak for both onset 1 and onset 2:8 for mid gamma.

For sustained responses, we can observe the following:

1. Negative going effect: There are no negative-going effects occurring for onset 1 or onset 2:8. However, there is a specific significance FWE-(familywise error corrected at peak-level) $t(34)=6.65$, $p=.010$, at 3104ms for low gamma/ high beta for onset 1. Shown with a blue circle.
2. Positive going effect: for onsets 2:8 PGI, we see an early positive transient followed by a sustained positive-going effect for low gamma/high beta and mid gamma.

Whilst we see sustained synchronisations for Onset 2:8 for both low and high frequencies, the synchronisation is maximal more anteriorly (close to Cz) for low frequencies, but more posteriorly for high frequencies.

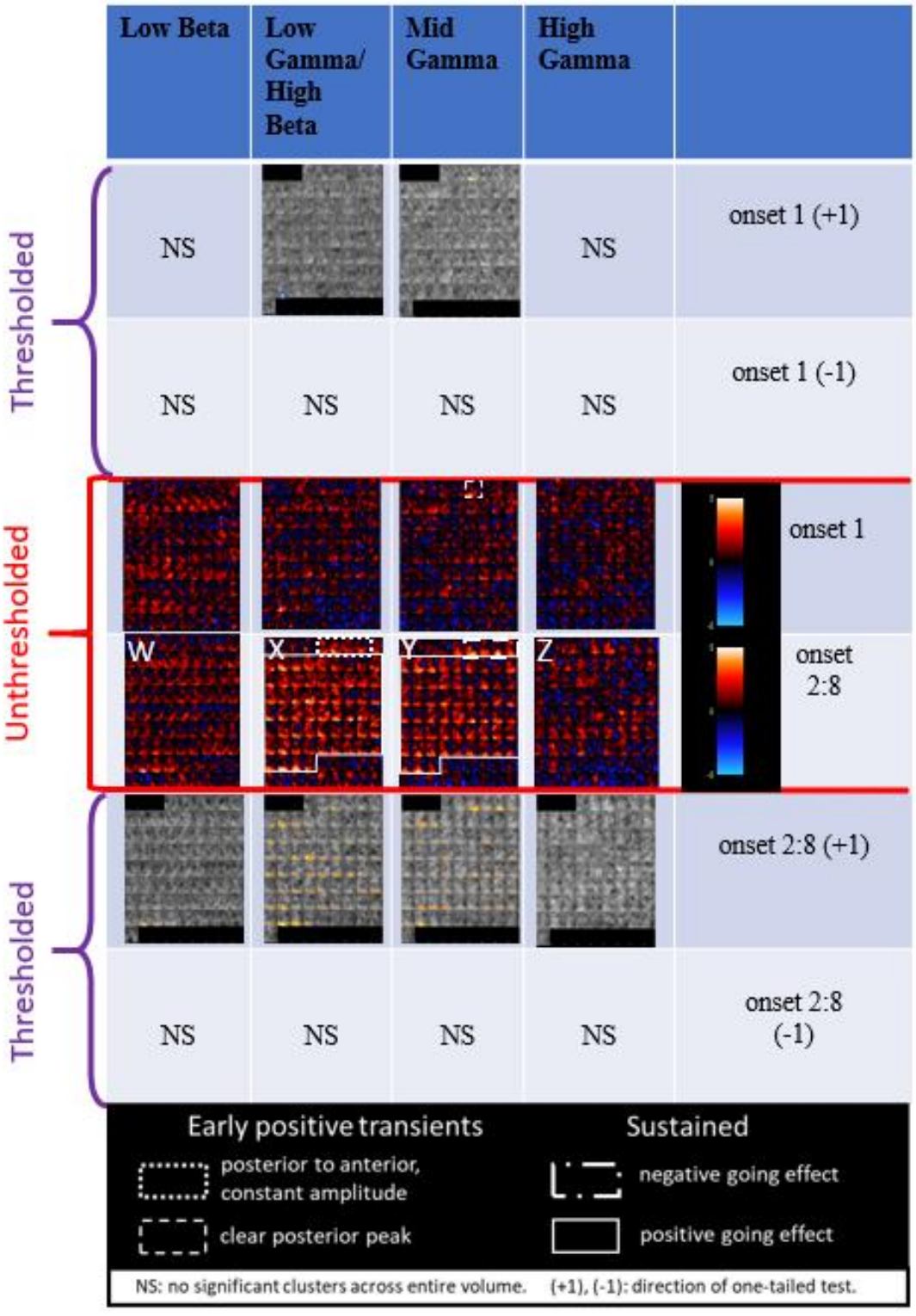
Low Beta
Low Gamma/ High Beta
Mid Gamma
High Gamma
Thresholded
Unthresholded
Thresholded
NS
NS
NS
NS
NS
NS
NS
NS
onset 1 (+1)
onset 1 (-1)
onset 1
onset 2:8
onset 2:8 (+1)
onset 2:8 (-1)
W
X
Y
Z
Early positive transients
posterior to anterior, constant amplitude
clear posterior peak
Sustained
negative going effect
positive going effect
NS: no significant clusters across entire volume.
(+1), (-1): direction of one-tailed test.

Figure 4-8. Time-frequency effects on the mean of PGI, for high frequencies: Frequency bands are presented in four columns (from left to right: low beta, low gamma/high beta, mid gamma, high gamma); first two rows present thresholded maps for onset 1, next two rows present unthresholded maps (onset 1 and then onset 2:8), last two rows present thresholded maps for onsets 2:8. Thresholded maps show one-sample one-tailed t-tests, with direction indicated by bracketed terms (e.g. "(+1)" is right-tailed). Each panel of plot shows scalp maps through time, laid out from top left to bottom right in the panel. Unthresholded maps (blue, black and red) show scalp maps from -100ms to 3900ms in steps of 50ms. The scale of the unthresholded maps is -5 to 5. Thresholded maps (yellow, orange, grey) show scalp maps from -100 to 3900ms in steps of 50ms. Note that the analysis window was only 50-3500ms, so for Thresholded maps, the non-analysed region is black. Low gamma/high beta +1 for onset 1 comes out at the peak level only, circled in blue (see thresholded map). Key findings are most evident in unthresholded maps (middle two rows). Raw one-sample t-values are presented for difference to zero, with red positive-going and blue negative-going, again presented with white framing (see legend and main text).

Table 4.4 shows the results breakdown of the associated statistics of the effects from Figure 4.8. Each cluster is given with its Xmm, Ymm, Zms location and time with both *T* and *P* values. For contrasts that had more than three significant clusters, we have given only the three most significant clusters. Note that for Onset 1 low gamma/high beta, this was significant family-wise error correct at the peak level $t(34)=6.65$ (uncorrected $p=.010$) not cluster. From left to right, the columns, indicate the frequency of interest and the rows indicate whether it is onset 1 or 2:8. NS means that there was no statistical effect found.

Low Beta	Low Gamma/ High Beta	Mid Gamma	High Gamma	
NS	Peak: $t(34)=6.65$, $p=.010$, Loc: -17,-84, 3104ms	$t(34)=5.48$, $p=.009$, Loc:-13,-79, 145ms	NS	onset 1 (+1)
NS	NS	NS	NS	onset 1 (-1)
$t(34)=6.16$,$p=.001$, Loc: 0,-84,3113ms	$t(34)=6.55$, $p<.001$, Loc: -38, -62, 1414ms $t(34)=6.37$,$p<.001$, Loc: 13,-89,2000 $t(34)=6.24$,$p<.001$, Loc: -26,-79, 3094ms	$t(34)=6.41$, $p<.001$, Loc: 4,-84,330ms $t(34)=6.22$,$p<.001$, Loc: 13,-84, 1961ms $t(34)=6.15$,$p<.001$, Loc:-4,-79, 3104ms	$t(34)=5.28$,$p=.004$, Loc: 17,-46,428ms $t(34)=4.97$, $p<.001$ loc: 13,-73, 125ms $t(34)=4.64$,$p=.021$, loc: -21,-89, 2713ms	onset 2:8 (+1)
NS	NS	NS	NS	onset 2:8 (-1)

NS: no significant clusters across entire volume, Loc: location of cluster, location is Xmm,Ymm, Zms

Table 4-4. PGI mean/intercept contrasts, statistics for high frequencies.

Raw one-sample t-values are presented for the difference to zero at the peak of a cluster (direction indicated by bracketed terms (e.g. "(+1)" is right-tailed)) and associated p-values, which are, in all but one case, for the encompassing cluster, FWE-corrected at the cluster level. In contrast, low gamma/ high beta Onset 1 (+1) is corrected at the peak-level. Location of peak of cluster is listed in Xmm, Ymm, Zms format. The columns from left to right are low beta, low gamma/high beta, mid gamma, and high gamma. The rows from top to bottom are (onset 1 and then onset 2:8). NS means not significant; Loc is the location of the cluster.

Figure 4.9 shows the effect for low beta, low gamma/high beta, mid gamma and high gamma on high frequencies at electrodes A22, D30, A29, and B3. Plots correspond to different effects in Figure 4.8: (A) low beta to effect w; (B) low gamma/high beta to x; (C) mid gamma to y; and (D) high gamma to z. There is an enhancement of medium relative to thick and thin in all figures but visually looks biggest at low beta. This enhancement seems to be quashed by stimulus offset, suggesting that the pattern-glare gamma is strongly driven by stimulus presence. This enhancement continues through the gamma frequencies. Additionally, there is a very large difference between medium and thick and thin at the offset transient for low beta (see w). This is true, as the effect moves to higher gamma frequencies until High Gamma where the effect disappears.

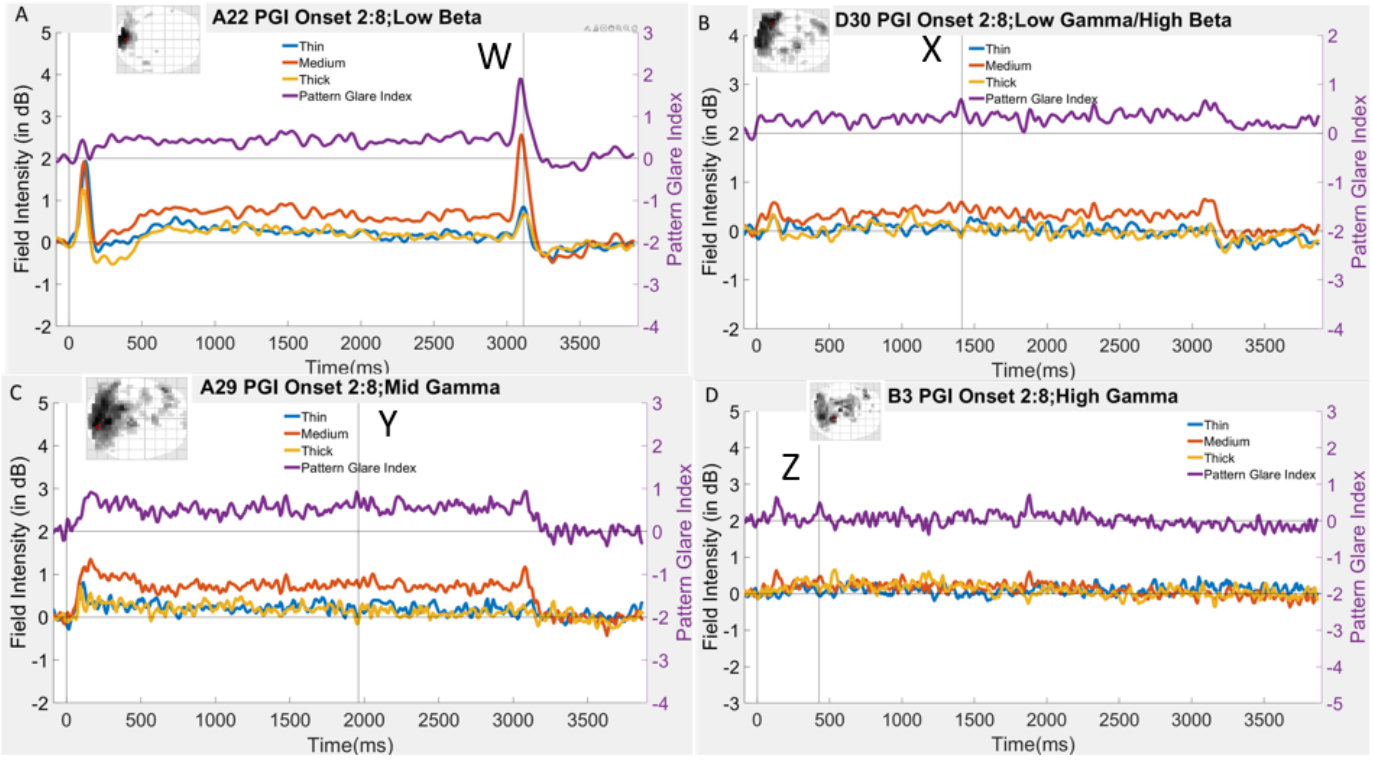

Figure 4-9. time-series of (A) low beta, (B) low gamma/high beta, (C) mid and (D) high gamma frequencies, onsets 2:8, at different posterior electrodes, showing increased positivity (both sustained and early positive transient) for medium grating:

Time series of power summed across each frequency band, at electrodes A22, D30, A29, and B3 (see red arrow in inset scalp map) is shown. Plots correspond to different effects in Figure 4.8: (A) low beta to effect w; (B) low gamma/high beta to x; (C) mid gamma to y; and (D) high gamma to z. These effects can also be seen in the PGI time-series in these plots, see right-side y-axes. Large peaks are indicated with a vertical line. The scalp maps here show an spm glass scalp, in which all significant effects through time are collapsed onto a two-dimensional representation. It shows that the electrode being plotted (red arrow) is at a position where there is considerable significance through time. Positive is plotted up on time-series. This figure only presents time-series at a single electrode, a number of the effects we are looking at here have multiple peaks within the significant clusters.

4.4 Discussion

In this analysis, we wanted to understand the underlying neurological factors related to visually induced migraines. Specifically, our focus was on what was happening in posterior areas of the brain during the D/C shift period. Our hypotheses were:

1. High gamma power observed immediately after the onset transient in (Tempesta et al., in preparation, Chapter 4) will continue throughout the D/C shift period and will be driven by the medium stimulus. Explicitly we should expect to see desyncrony in the low frequency bands and synchrony in the high frequency bands.
2. There will be a broadband effect at stimulus offset, by analogy with the broadband effect we see at onset.

3. Medium frequency stimuli lead to greater activity in the brain. Processing of the early visual areas representing the three different spatial frequencies of these gratings will be visibly different from each other in either synchrony or desynchrony.
4. Delta and theta will show a desynchrony during the D/C shift period with aggregated EEG responses to the stimuli (medium+thick+thin), mimicking our earlier result for alpha in aggregate responses (Tempesta et al., in preparation, Chapter 4). This may be related to information processing. There may also be a difference between onset 1 and onset 2:8, as onset 1 may be due to a surprise or prediction effect, whilst onset 2:8 reflects a failure to habituate specifically for the medium grating.

We found evidence for the first part of hypothesis one (seen in Figure 4.9, for PGI, panel B and C). Note that this effect is also present in low beta but at some time points with higher power for medium (panel A) compared to panels (B and C). We did observe an increased positive-going gamma effect in low gamma/high beta and mid gamma (see table 4.4 for full statistical breakdown); however, this effect seems diminished, if not absent, in high gamma (panel D). In the topographic maps of Figure 4.8 (with the correspond time-series in Figure 4.9), we can only say that the PGI effect in onset 2:8 is positive-going; however, when we look at Figure 4.9, we see that medium is positive relative to zero for low beta, low gamma/high beta and mid gamma. Therefore, there is a synchrony happening for onset 2:8 medium. This is supported by the findings of Adjamian et al., (2004), who observed high power for mid/low gamma continuing up to four seconds after stimulus presentation for a similar grating to our medium. This may reflect a failure to habituate, which may be affecting the processing of the stimulus as it is very aggravating for the participant making it more challenging to habituate. Neurophysiological data has suggested that a lack of habituation during stimulus repetition is a genetically determined property of the migraine brain (Coppola et al., 2013).

For the second part of the first hypothesis, which is observing a change in synchrony across frequencies from a desyncronisation to synchronisation, we do not observe a change in synchrony in aggregate onset 1 or 2:8, contrary to the second part of the first hypothesis. Note, there is a change in synchrony from desynchrony to synchrony from theta and alpha to higher frequencies. However, because delta is synchronous for an initial period following the early transient in Onset 2:8, we have taken a strict stance on this hypothesis. Also, for PGI, we do not observe a negative-going to positive-going effect across frequencies for onsets 1 or 2:8.

The results show that for Figure 4.9 (panel A), there is a large offset transient for low beta (see W), which is statistically significant. Since this feature is also present at low gamma/high beta and mid gamma, the feature is broadband, this confirms our second hypothesis. Note that the offset transient effect diminishes from low gamma/high beta to mid gamma (although this is partially due to the electrodes chosen in Figure 4.9 – see also Figure 4.8 offset features in X and Y frames), and is ultimately lost in high gamma. Gamma oscillations may reflect stimulus prevalence or may facilitate conscious perception (Gray et al., 1989) and perception of pain (Gross et al., 2007). A further possible physiological explanation (as stated previously in Tempesta et al., in preparation, Chapter 4) for what we observe in the D/C shift would be that there are two sorts of cell-assemblies (Hebb, 1949) in relevant visual areas. One sort are 'somewhat' densely interconnected and thus oscillate at low beta; the other sort is more densely interconnected, generating shorter cycle times, that oscillate at low gamma/high beta, mid and high gamma. Thick, medium and thin all drive the 'somewhat' densely interconnected assemblies, but only medium drives the most densely interconnected assemblies (Tempesta et al., in preparation, Chapter 4).

Note that, as previously stated, aggregate is the EEG responses to each of the stimuli added together (medium+thin+thick), and PGI is a measurement of the difference in responses to

medium compared to the average of think and thin.. Therefore, comparing PGI to aggregate is analogous to comparing the effect of the medium stimuli to general activity trends across the scalp. With reference to the third hypothesis, there is a noticeable difference in statistical significance on the high frequencies for aggregated versus PGI. Notably, in the D/C shift period, aggregate shows more significant effects across onset 1 and 2:8, contrasting with PGIs effects, which are limited to peak effects in low gamma/high beta for onset 1 and onset 2:8 positive-going at the cluster-level. For low frequencies, again aggregate has more significant effects across onset 1 and 2:8. However, our central finding is that theta was statistically significant for onset 2:8 positive-going` at peak level (see Figure 4.6, circled in black). This is a robust finding coming out whole-volume (in what is a large volume), which has not previously been reported. Our theta effect is relatively anterior in space; this may reflect a mechanism of cognitive control, as some research has observed that theta frequency is associated with interference control (Cavanagh & Frank, 2014; Cooper et al., 2015). Anterior theta may be regulating posterior gamma effects across the scalp; however, we have not done any connectivity analyses (such as cross-frequency coupling) in order to be able to confirm this hypothesis.

With regard to hypothesis 4 (see Figures 4.6 and 4.7), the effect of theta may be bleeding into alpha. For Figure 4.7, the vertical line labelled X indicates significance in theta; Y is in the same position as X, which is a peak for alpha that does not quite reach significance. However, theta and alpha's frequency windows do overlap; therefore, alpha may not reach significance because the window to alpha is limited. Nevertheless, the effect still looks present there, albeit to a weaker extent. Previous research posits that alpha-band synchrony has been observed to facilitate information integration across anatomically segregated regions (Sadeghiani et al., 2019), however, linking our findings to this interpretation is difficult because EEG only records from the scalp, and we have not projected into source space. However, alpha synchrony affects

top-down processing, which is illustrated by the strength of the alpha band frequency in the frontal-parietal network and is evidenced in patients with lesions to the dorsolateral prefrontal cortex, who showed reduced cognitive flexibility (Sadeghiani et al., 2019). Thus, overall, these synchrony effects in theta and alpha may suggest the action of more executive brain functions in controlling the hyper-excitation being observed more posteriorially, but, again, confirmation of this hypothesis awaits work on connectivity in this data set.

As for the early positive transients for the low frequencies, we can observe posterior to anterior effects on delta, theta, and alpha, for onsets 1 and 2:8 for aggregate (Figure 4.4). However, for the PGI index (Figure 4.6), we only observe a posterior peak of theta for onset 2:8. This may mean that medium is driving posterior effects early on for onset 2:8.

There are several limitations to the analysis. Identifying habituation by comparing effects on onset 1 to onset 2:8 is not definitive; in particular, onset 1 has less statistical power than onset 2:8, since it involves fewer trials per participant. Thus, it could be the case that we observe PGI effects in onset 2:8, but not onset 1, simply because onset 1 has less statistical power. We cannot rule out this possibility altogether, but it is notable that we do observe here and in previous work (Tempesta et al., in preparation, Chapter 3, Figure 3.3) large effects for onset 1 for the aggregated analysis. We also observe effects on onset 1 in the time-domain (Tempesta et al., 2021, Chapter 2). Thus, it seems that there is sufficient statistical power to observe robust effects for onset 1, if they are present.

As mentioned in previous work (Tempesta et al., in preparation, Chapter 3), although the PG test uses 12 c/deg, some say this is not a good control and that the 12cpd pattern is not always well reproduced (see discussion in Wilkins et al., 2016). An additional limitation is that, as previously discussed, for PGI, we have not linked the anterior theta effect we observe with the posterior gamma effect. For example, we have not performed a cross-frequency coupling

analysis, so we do not know how they relate. This leaves the possibility that they are causally unrelated phenomena.

4.5 Conclusions

The work presented here revealed a theta effect, which has not previously been reported. There is evidence that the theta band is responding differently for medium stimulus as opposed to thin and thick during the D/C shift period and may be modulating low gamma/high beta and mid gamma frequencies, although connectivity work is required to confirm this. Overall, the work in this paper goes some way to understanding the underlying neurological processes relating to the response of the posterior areas of the brain to PG stimuli. However, more research is needed to confirm this line of thought. In future work, we would like to include participants who have a diagnosis of migraine. The findings reported here are limited to healthy populations, and additional work is needed. Finally, we believe that having participants maintain a headache diary would help with understanding when a migraine attack is happening or if it already happened. We could then record EEG before and after an attack to see if the frequencies differ.

4.6 Acknowledgements

We want to thank Guillaume Flandin for his help with SPM use and expertise. Vladimir Litvak was also extremely helpful for understanding some technicalities of SPM. They also assisted in refining analysis code. We would also like to thank Sara Assecondi for assistance with EEG pre-processing and Cathy Ghalib for help with data collection.

4.7 Funding

We were not funded for this research.

4.8 Competing interests

The authors report no competing interests.

4.9 References

Adjamian, P., Holliday, I. E., Barnes, G. R., Hillebrand, A., Hadjipapas, A., & Singh, K. D. (2004). Induced visual illusions and gamma oscillations in human primary visual cortex. *European Journal of Neuroscience*, *20*(2), 587-592.

Allen, M. (Ed.). (2017). *The SAGE encyclopedia of communication research methods*. Sage Publications.

Beasley, I. G., & Davies, L. N. (2012). Susceptibility to pattern glare following stroke. *Journal of Neurology*, *259*(9), 1832-1839.

Bowman, H., Brooks, J. L., Hajilou, O., Zoumpoulaki, A., & Litvak, V. (2020). Breaking the circularity in circular analyses: Simulations and formal treatment of the flattened average approach. *PLOS Computational Biology*, *16*(11), e1008286.

Brainard, D. H. (1997). The psychophysics toolbox. *Spatial vision*, *10*(4), 433-436.

Brooks, J. L., Zoumpoulaki, A., & Bowman, H. (2017). Data-driven region-of-interest selection without inflating Type I error rate. *Psychophysiology*, *54*(1), 100-113.

Cavanagh, J. F., & Frank, M. J. (2014). Frontal theta as a mechanism for cognitive control. *Trends in cognitive sciences*, *18*(8), 414-421.

Chennu, S., Noreika, V., Gueorguiev, D., Blenkmann, A., Kochen, S., Ibanez, A., …Bekinschtein, T..A. (2013).. Expectations and attention in hierarchical auditory prediction. *Journal of Neuroscience*, *33*(27).

Clarke, C. E., MacMillan, L., Sondhi, S., & Wells, N. E. (1996). Economic and social impact of migraine. *Qjm*, *89*(1), 77-84.

Conlon, E., Lovegrove, W., Barker, S. *and* Chekaluk, E. *(*2001*)* Visual discomfort: the influence of spatial frequency. Perception 30, 571–581.

Cooper, P. S., Wong, A. S., Fulham, W. R., Thienel, R., Mansfield, E., Michie, P. T., & Karayanidis, F. (2015). Theta frontoparietal connectivity associated with proactive and reactive cognitive control processes. *Neuroimage*, *108*, 354-363.

Coppola, G., Di Lorenzo, C., Schoenen, J., & Pierelli, F. (2013). Habituation and sensitization in primary headaches. *The journal of headache and pain*, *14*(1), 65.

Evans, B. J. W., & Stevenson, S. J. (2008). The Pattern Glare Test: a review and determination of normative values. *Ophthalmic and Physiological Optics*, *28*(4), 295-309.

Good, P. A., Taylor, R. H., & Mortimer, M. J. (1991). The use of tinted glasses in childhood migraine. *Headache: The Journal of Head and Face Pain*, *31*(8), 533-536.

Gray, C. M., König, P., Engel, A. K., & Singer, W. (1989). Oscillatory responses in cat visual cortex exhibit inter-columnar synchronization which reflects global stimulus properties. *Nature*, *338*(6213), 334-337.

Gross, J., Schnitzler, A., Timmermann, L., & Ploner, M. (2007). Gamma oscillations in human primary somatosensory cortex reflect pain perception. *PLoS Biol*, *5*(5), e133.

Hanslmayr, S., Staudigl, T., & Fellner, M. C. (2012). Oscillatory power decreases and long-term memory: the information via desynchronization hypothesis. *Frontiers in human neuroscience*, *6*, 74.

Hebb, D. O. (1949). *The organization of behavior: a neuropsychological theory*. J. Wiley; Chapman & Hall.

House of Commons, (2014). Headache Services in England. All-Party Parliamentary Group on Primary Headache Disorders.

Irlen, H. (1983, August). Successful treatment of learning disabilities. In *91st annual Convention of the American Psychological Association, Anaheim, CA, USA*.

Irlen, H. (1991). Reading by the colours. *New York: Avery*.

Irlen, H. (1997). Reading problems and Irlen coloured lenses. *Dyslexia review*, *8*, 4-7.

Jensen, O., & Mazaheri, A. (2010). Shaping functional architecture by oscillatory alpha activity: gating by inhibition. *Frontiers in human neuroscience*, *4*,

Kleiner, M., Brainard, D., & Pelli, D. (2007). What's new in Psychtoolbox-3?.

Klimesch, W., Schimke, H., Doppelmayr, M., Ripper, B., Schwaiger, J., and Pfurtscheller, G. (1996). Event-related desynchronization (ERD) and the Dm effect: does alpha desynchronization during encoding predict later recall performance? Int. J. Psychop

Klimesch, W., Doppelmayr, M., Schimke, H., and Ripper, B. (1997). Theta synchronization and alpha desynchronization in a memory task. *Psychophysiology* 34, 169–176.

Klimesch, W., Sauseng, P., and Hanslmayr, S. (2007). EEG alpha oscillations: the inhibition-timing hypothesis. *Brain Res. Rev.* 53, 63–88.

Kientz, M. A., & Dunn, W. (1997). A comparison of the performance of children with and without autism on the Sensory Profile. *American Journal of Occupational Therapy*, *51*(7), 530-537.

Lorca-Puls, D. L., Gajardo-Vidal, A., White, J., Seghier, M. L., Leff, A. P., Green, D. W., ... & Price, C. J. (2018). The impact of sample size on the reproducibility of voxel-based lesion-deficit mappings. *Neuropsychologia*, *115*, 101-111.

Luck, S. J. (2014). *An Introduction to the Event-related Potential Technique*. MIT press.

Mears, O. (1980). Figure/background brightness/contrast and reading disability. *Visible Language*, *15*, 13-29.

Parish, G., Hanslmayr, S., & Bowman, H. (2018). The sync/desync model: How a synchronized hippocampus and a desynchronized neocortex code memories. *Journal of Neuroscience*, *38*(14), 3428-3440.

Pelli, D. G. (1997). The VideoToolbox software for visual psychophysics: Transforming numbers into movies. *Spatial vision*, *10*(4), 437-442.

Sadaghiani, S., Dombert, P. L., Løvstad, M., Funderud, I., Meling, T. R., Endestad, T., ... & D'Esposito, M. (2019). Lesions to the Fronto-Parietal Network Impact Alpha-Band Phase Synchrony and Cognitive Control. *Cerebral Cortex*, *29*(10), 4143-4153.

Saksida, A., Iannuzzi, S., Bogliotti, C., Chaix, Y., Démonet, J. F., Bricout, L., ... & George, F. (2016). Phonological skills, visual attention span, and visual stress in developmental dyslexia. *Developmental Psychology*, *52*(10), 1503.

Shapiro, R. E., & Goadsby, P. J. (2007). The long drought: the dearth of public funding for headache research.

Shirazibeheshti, A., Cooke, J., Chennu, S., Adapa, R., Menon, D. K., Hojjatoleslami, S. A., ... & Bowman, H. (2018). Placing meta-stable states of consciousness within the predictive coding hierarchy: The deceleration of the accelerated prediction error. *Consciousness and Cognition*, *63*, 123-142.

Steiner, T. J., Stovner, L. J., & Birbeck, G. L. (2013). Migraine: the seventh disabler. *Headache: The Journal of Head and Face Pain*, *53*(2), 227-229.

Steiner, T. J., Birbeck, G. L., Jensen, R. H., Katsarava, Z., Stovner, L. J., & Martelletti, P. (2015). Headache disorders are third cause of disability worldwide.

Stovner, L. J., Hagen, K., Jensen, R., Katsarava, Z., Lipton, R. B., Scher, A. I., ... & Zwart, J. A. (2007). The global burden of headache: a documentation of headache prevalence and disability worldwide. *Cephalalgia*, *27*(3), 193-210.

Stovner, L. J., Nichols, E., Steiner, T. J., Abd-Allah, F., Abdelalim, A., Al-Raddadi, R. M., ... & Edessa, D. (2018). Global, regional, and national burden of migraine and tension-type

headache, 1990–2016: a systematic analysis for the Global Burden of Disease Study 2016. *The Lancet Neurology*, *17*(11), 954-976.

In Preparation: Tempesta, A. J., Miller, C. E., Schofield, A. J. & Bowman, H., (2020). Pattern-glare driven broadband gamma is modulated by discomfort ratings. Chapter 3.

Tempesta, A. J., Miller, C. E., Litvak, V., Bowman, H., & Schofield, A. J. (2021). The Missing N1 or Jittered P2: Electrophysiological Correlates of Pattern-Glare in the Time and Frequency Domain. *European Journal of Neuroscience*.

Wilkins, A. J. (1995). *Visual stress* (No. 24). Oxford University Press.

Wilkins, A.J., Binnie, C.D. (1980) Visually induced seizures *Prog. Neurobiol., 15,* 85-117.

Wilkins, A. J., Darby, C. E., & Binnie, C. D. (1979). Neurophysiological aspects of pattern-sensitive epilepsy. *Brain*, *102*(1), 1-25.

Wilkins, A., Nimmo-Smith, I. A. N., Tait, A., McMANUS, C., SALA, S. D., Tilley, A., ... & Scott, S. (1984). A neurological basis for visual discomfort. *Brain*, *107*(4), 989-1017.

Wilkins, A. (1986). Intermittent illumination from visual display units and fluorescent lighting affects movements of the eyes across text. *Human Factors*, *28*(1), 75-81.

Wilkins, A. J. (1995). *Visual stress* (No. 24). Oxford University Press

Wilkins, A. (2016). A physiological basis for visual discomfort: Application in lighting design. *Lighting Research and Technology*.doi:10.1177/1477153515612526.

Wilkins, A. J., & Evans, B. J. W. (2001). Pattern glare test instructions. London, UK: IOO Sales Ltd.

Wright, B. N., Wilkins, A. J., & Zoukos, Y. (2007). Spectral filters can improve reading and visual search in patients with multiple sclerosis. *Journal of Neurology*, *254*(12), 1729-1735.

CHAPTER 5: DISCUSSION

The overarching theme of this PhD thesis is how pattern glare stimuli give rise to symptoms of VS and associated electrophysiological correlates in the occipital lobe, and how the symptoms are associated with headaches. Headaches are the second most prevalent disease worldwide (James et al., 2018) and cost the US $17 billion a year (Goldberg, 2005). In Europe, an estimated 27 billion euros per year is lost due to loss of productivity caused by headaches (Olesen et al., 2010; Stovner et al., 2008). This is indeed a vital pathology both economically and in terms of world prevalence. Understanding how this disease arises in the brain can inform the treatment of this neuropsychological phenomenon. The investigated results and findings of this study were reviewed in each of the chapters. Specifically, Chapter 2 explored evoked responses in the time domain. In Chapters 3 and 4, this thesis investigated evoked/induced responses in the frequency domain. This chapter will explore the findings in the broader context of the literature and where this thesis lies in the greater visual-neuroscientific field.

5.1.1 Analysis One

In analysis one, we analysed event-related potentials (ERPs) in response to PGT gratings, using mass univariate analysis, a major effect for onset 1 in the time domain (Figure 2.2), showed a peak in the PGI (mean/intercept analysis) between 170-184 on the posterior part of the scalp. For onset 2:8 mean/intercept (Figure 2.3), medium showed an extreme response at 179 ms, which was posterior on the scalp. Thus, we obtained a more extreme response for medium on the posterior of the scalp relatively late in the segment analysed for both onset 1 and onsets 2:8.

Considering the three previously specified factors in the normal population: headache proneness, visual stress and discomfort, we found significant relationships between ERP features and the headache and discomfort factors. Participants with high discomfort ratings had larger P1

components for medium stimuli suggesting cortical hyperexcitability. The participants with high headache ratings showed abnormal N1-P2 components for medium stripes relative to the other stimuli, indicating an effect of habituation (this is explored further below in the 'Factor Effects' section).

There is also evidence of a P2 latency and jitter effect. The P2 elicited by onset 1 (see Figure 2.2) may be accelerated in the medium condition relative to the thick and thin conditions; visually, there is attenuation of N1 for onsets 2:8 for medium stripes relative to thick (Figure 2.3). This attenuation is particularly strong for those high on the headache factor (see Figure 2.5).

This attenuated N1 may be related to an accelerated P2 (all these findings are explored more deeply in Chapter 2). Combining such acceleration with high temporal jitter (i.e. variability in latency across trials) could generate the observed attenuation of N1. We return to this point shortly.

5.1.2 Analysis Two

In analysis two, we focused on the frequency-domain; we looked at the responses to aggregated (average of thick, thin and medium) and PGI and related them to our three factors: visual stress, a tendency for headaches, and discomfort. We found four key phenomena: two in the early positive transient period and two sustained responses. This is explored in Chapter 3. We also found that for PGI, there was a synchronisation for beta, which continued in time and through low and mid gamma frequencies on onset 2:8, but not onset 1. For factor effects, we found a small significant cluster for participants who scored higher on discomfort, having higher power for high gamma. Additionally, 11 peaks were identified as significant in a cluster analysis of different ROIs from the PGI contrast. Seven of these were related to the discomfort scale.

5.1.3 Analysis Three

In analysis three, we again explored the frequency-domain, but this time, we looked at the responses to aggregated and PGI during the D/C shift period, a sustained period of baseline shift. We found a PG induced theta effect that had not previously been reported in the literature on the medium stimulus, which may reflect a mechanism of cognitive control. Additionally, we observed a large positive-going extreme response for medium relative to zero, in low gamma/high beta and mid gamma. We also found a large offset transient effect for low beta, with this effect quashed in high gamma frequency. This is explored further in Chapter 4.

5.2 Connection with Cell Assemblies

There is a strong positive-going effect for PGI for onset 2:8 (see Figure 3.4). If we look at the time series for beta, low gamma, mid gamma and high gamma (Figure 3.6), we observe that at the statistically significant points (marked with vertical lines), the medium is more extreme from zero, relative to thick and thin. Additionally, there is a sustained synchronisation effect for almost the entire time series in medium, albeit not in high gamma, which exhibits two separate clusters. Clearly, the medium is driving a broadband effect in beta and gamma.

A possible physiological explanation for these observations is that two sorts of cell assemblies (Hebb, 1949) are being driven by the medium stimulus (see discussions in Chapters 3 and Chapter 4). One sort is "somewhat" interconnected and thus oscillates at beta, low gamma and to some extent mid gamma, and the other sort is more densely interconnected, generating shorter cycle times that oscillate at mid and high gamma.

It is also possible that the strong positive-going effect of PGI on beta, low gamma, mid gamma and high gamma for onset 2:8 represents a failure to habituate for the medium grating – i.e., the stimulus cannot be habituated to (Schoenen et al., 1995; Afra et al., 1998; Wang et al.,

1999), especially since the phenomena is present for onsets 2:8, but, within the statistical power we have available, was absent for onset 1.

5.3 Theta Effect in Migraine

Chapter 4 primarily builds upon the results from Chapter 3 by looking at both low frequencies and high frequencies in a more extended time window. Theta shows an early posterior peak and a sustained positive-going effect for PGI (Figure 4.6). There is a significant peak in the D/C shift period (close to 1500ms after stimulus onset), which is an essential finding for this thesis, as this phenomenon has never previously been reported. While acknowledging the uncertainties associated with relating patterns on the scalp to brain areas, if we consider that the statistically significant peak for theta may be detected above the scalp's somatosensory area, a reasonable line of argument arises around pain. Recent research posits that migraine is associated with aberrant connections from the somatosensory cortex to the frontal lobe, indicating that migraineurs have hyperactive cortical networks (Ren et al., 2019). Recent literature in mice (Iwamoto et al., 2021) has shown a coupling of theta and gamma oscillations that is increased during nociceptive phases in the somatosensory cortex, which represented the ongoing status of pain perception. (Nociceptive phases are the central nervous system [CNS] and peripheral nervous system [PNS] processing phases of noxious stimuli, which causes the brain to perceive the sensation of pain.) This may mean that our activity being observed in theta band may be due to perception by the participants during our experiment that could be the precursors of pain perception. In addition, since we observe this effect for the PG index, this perception would be stronger for the (aggravating) medium stimulus.

An additional line of reasoning is that if we think about theta as reflecting a mechanism for cognitive control, previous research has shown that theta is associated with interference control (Cavanah & Frank, 2014; Cooper et al., 2015). This effect seems to have continued into alpha (Figure 4.7 shows that alpha is having a similar impact to theta); however, potentially because of

how we selected frequency bands, we do not have sufficient statistical power to detect effects in relatively narrow, and therefore noisy, frequency bands. Additionally, some models have shown that alpha amplitude modulations regulate the inhibitory level of the cortex (Klimesch et al., 2007; Jensen & Mazaheri, 2010), with synchronisation reflecting habituation and desynchronisation representing active information processing (Hanslmayr, 2012).

Despite the fact that this alpha effect only exhibited a trend towards significance, it may have implications for cognitive phenomena because alpha has been associated with facilitating information integration, and alpha synchrony has been related to top-down processing in the frontoparietal network, strengthening our previous statements that increased theta may reflect cognitive control (Sadeghiani et al., 2019). In particular, it is quite plausible that (more anterior) cognitive control areas of the brain could be attempting to inhibit hyper excitation responses in posterior areas. Furthermore, this inhibition might be specific for the medium stimulus, as suggested by our effect being seen as a positive PGI effect.

Interestingly, we do observe effects in the theta frequency both in our first (Chapter 2) and third (Chapter 4) analyses. It should be noted that the first analysis was a theta effect that came out on a factor, and in the third analysis, the theta effect was on the mean/intercept. The former of these effectively reflects the early evoked response, which exhibits a theta frequency; the latter arises in the DC shift period and may not even correspond to an evoked response. Accordingly, it is unclear at this stage whether or not these two effects are related.

5.4 Factor effects

In Chapter 2, we found significant effects for the headache and discomfort factors, operating at different presentations in terms of the repetition of stimuli and on various components of the ERP. These are new findings. The discomfort factor, which has a strong state contribution, showed a significant effect only for onset 1 (Figure 2.4). This may suggest a stimulus-driven or

surprise effect. Further, a second-factor effect emerged for headache frequency, intensity and duration (a trait factor), which was only significant for onsets 2:8 (Figure 2.5), suggesting a relationship with habituation.

As stated previously, the discomfort factor largely reflects how comfortable people found the medium stripes relative to the other stimuli. We found a stronger P1 for medium for the high-discomfort group compared to low-discomfort. Those with cortical hyperexcitability may respond more strongly to certain stimuli that are aggravating; this alone could have an effect on P1, as the P1 is reduced for unattended stimuli (Mangun & Hillyard, 1991; Voorhis & Hillyard, 1977; Munte et al., 1995). The relative lack of a P1 in the low discomfort group may be because these participants are able to quickly shift attention away from this aggravating stimulus, thus avoiding discomfort. In contrast, the high-discomfort group may have been unable to withdraw attention from the medium stimulus. The P1 is associated with surprise (Utama et al., 2009; Lassalle & Itier, 2013), and we see these effects of P1 only on the first onset where all the three stimuli are equally likely and therefore potentially surprising.

For the headache factor the high-headache group showed an abnormal N1 for the medium stimuli on Onsets 2:8. This may be related to an absent or attenuated N1 or, as just discussed, an accelerated and temporally unreliable P2 (for a deeper explanation, refer to Chapter 2). The components in this P1-N1-P2 ERP complex can be seen to be at a theta frequency. Notably, there was a drop in inter-trial phase coherence in this theta frequency band at around 165ms for the high headache group viewing the medium stimulus - which was less evident for the low headache group (see Figure 2.7). The inter-trial theta phase coherence has been associated with the P2 component (Freunberger et al., 2007), which has also been associated with a number of top-down attentional tasks, such as visual search (Luck & Hillyard, 1994). We posit that the effects seen in this N1-P2 time window could relate to poor inter-trial theta phase coherence, suggesting a temporally poorly

regulated P2, i.e., increased variability in latency at the single-trial level. Additionally, since this is observed in onsets 2:8, this could also be evidence of unsuccessful suppression of repeating stimuli, i.e., poor habituation.

In Chapter 3, which moved beyond the theta frequency band response set-up by the ERP transients, 11 peaks came out on the uncorrected analysis at peaks of the ROIs; 7 were on the discomfort factor, three were on the VSQ, Chi and Aura factor, and one was related to the length and frequency of headaches factor. Participants who scored high on these factors responded high on these state and trait measures. Importantly, these effects were observed at a posterior site, for which we have a strong prior precedent (Adjamian et al., 2004). Figure 3.10 (discomfort factor for beta) showed the start of a sustained cluster, which means that those who score high on discomfort have increased PGI in the beta band. In Figures 3.11, 3.12 and 3.13, we showed similar effects for low gamma, mid gamma and high gamma on the discomfort factor. This suggests that those who have higher discomfort are experiencing substantially higher PGI across these frequency bands. It is important to note that mid gamma for Oz, for which we have the most substantial prior precedents (Adjamian et al., 2004; Chapter 2), shows three significant peaks for discomfort, suggesting that for mid gamma there is a particularly high effect on pattern glare for those high on the discomfort factor.

5.5 Frequency Domain Response Differences between Onset 1 and Onset 2:8

The aggregate response in the low-frequency bands mostly did not confirm our overarching hypothesis concerning differences between Onset 1 and 2:8. In Chapter 4, we found few significant differences between Onset 1 and Onset 2:8 for aggregated responses in terms of synchronisation in the theta and alpha bands; however, there are some differences between onsets in delta. For onset 1, there is a desychronisation which is broadly distributed across the scalp and,

although only a trend, there is a sychronisation which is broadly distributed over the scalp for onset 2:8 for the first half of the time segment (Figure 4.4).

For the high frequencies (Figure 4.5), we can observe desynchronisations (power reductions relative to baseline) for onset 1 across all high frequencies; however, there are synchronisations from low gamma/high beta to high gamma for onset 2:8, confirming our hypothesis. For the PGI in the low-frequency bands (Figure 4.6), we can observe that our hypothesis is confirmed - only theta and alpha show a positive-going effect in onset 2:8. Further, for high frequencies (Figure 4.8), we again confirm our hypothesis of a difference between onset 1 and onset 2:8, since only for onset 2:8 do low gamma/high beta and mid gamma, show a strong sustained positive-going effect.

Prediction Error and Gamma: It is also interesting to note that our finding of high gamma in onset 2-8, and not onset 1, does stand against some operationalisations of predictive coding (Den Ouden et al., 2012). Onset 1 should be the condition that generates a prediction error, since stimuli are equiprobable (Hawkins, 2004; Friston, 2005; Bar, 2009), and some have argued that prediction errors should manifest in increased gamma (Todorovic et al., 2011), since they would be registered in superficial layers of the cortical column. We saw precisely the opposite of this in high gamma for 2-8. This suggested that a lack of habituation is a more probable interpretation of this feature in our data.

Gamma and perception: a further possibility is that the increased gamma we observed for the medium stimulus could be directly related to the experience associated with this stimulus. Gamma oscillations may reflect stimulus prevalence or may facilitate conscious perception (Gray et al., 1989) and perception of pain (Gross et al., 2007).

5.6 Alpha Suppression and Cortical Hyperactivity

Singh et al. (2003) was one of the first to find that areas of the cortex that showed an increase in fMRI signal, also showed event-related desynchronization in the alpha band (which is a measure of alpha suppression). Mayhew et al. (2013) found that the fluctuations in the alpha response could explain some of the variance in the BOLD response. Furthermore, visual stimuli that were presented during the trough of the alpha wave produced a larger BOLD response compared to stimuli presented during the peak of the alpha wave, suggesting that the alpha response is closely related to cortical excitability (Scheeringa et al., 2011).

Previously, alpha suppression was localised to the visual cortex consistent with cortical hyperexcitation (Haigh, et al., 2018). Haigh and colleagues (2018) posit that greater cortical excitation (as indicated by greater alpha suppression), in response to chromaticity differences in chromaticity pairs (i.e. pairs of colours presented as pattern-glare stimuli), may indicate why certain pairs give more visual discomfort. However, as seen in our data (see, Figure 3.5), the frequency analysis did not show an alpha suppression for medium only. It showed an alpha suppression for all stimulus types. This may be because in this study, chromaticity differences were not utilised. An alternative explanation may be that although one of our hypotheses from analysis 2 did predict a deeper activation for PG, this may indicate that something other than cortical hyperexcitability is influencing the medium striped patterns. It may be the case that by virtue of our population being non-clinical, we do not see this deeper desychronisation as strongly in medium for alpha. However, neurobiological evidence supports a theory of hyperexcitability in VS, in a clinical population. This evidence is explored in more detail in the following sections.

5.7 Support for Hyperexcitability and Energy Impairment from the Neurobiology Research in Migraine

There is evidence from recent neurobiological research that there is a brain energy deficit between migraine attacks that results from increased energy demands from hyperactivity in the brain, which leads the brain to trigger acute migraine attacks (Borkum, 2021). Magnetic Resonance Spectroscopy (MRS) has shown that between and during attacks, lower phosphocreatine-to-creatine ratio and increased concentration of adenosine diphosphate (ADP) cause a brain energy deficit (Reyngoudt et al., 2012; Younis et al., 2017). There is also some evidence that reduced energy available from adenosine triphosphate (ATP) hydrolysis in the occipital lobe correlates with severity of migraine type (Lodi et al., 2001) and attack frequency (Reyngoudt et al., 2012). This may explain why we observed a deficit in habituation for onsets 2:8 for participants that scored high on headache duration and intensity factor; that is, a brain energy deficit prevents normal habituation.

However, it is not clear in the literature whether high-energy phosphate levels result from the dysfunction in the production of energy in the system or the increased demand of energy from hyperactive neurons. Still, it seems to be the case that both occur in the clinical migraine population.

5.7.1 Increased Energy Demands in Migraines

This thesis and other research support the theory of cortical hyperexcitation in the occipital lobe in migraine (Coppola et al., 2007). Indeed, failure to habituate in ERPs from our PG stimulus (see Chapter 2, Tempesta et al., 2021) and literature showing a habituation deficit in the P300 (Evers et al., 1999) supports this theory. This suggests that the cortical response to sensory and attention demands in migraine are heightened relative to normal participants, requiring higher energy usage (Ambrosini et al., 2011; Evers et al., 1999; Gauntenbein et al.,

2013). Other research in fMRI measuring cerebral blood flow indicates increased metabolic rate in response to the PG stimuli at 3 (c/deg) (Huang et al., 2003). This increased energy demand can have an effect on the brain's ability to inhibit this ongoing excitatory response.

5.7.2 Decreased Energy Production in Migraine

Migraine is 3-4 times more prevalent in people with mitochondrial disorders (Tiehius et al., 2020). This is regardless of the type of mitochondrial disorder (Kraya et al., 2018; Vollono et al., 2017), meaning that energy generation, more generally, is the problem underlying acute migraine attacks. Studies of PET and fMRI show that repeated migraine attacks modified metabolism in regions of the brain involved in sensory and pain processing (see Russo et al., 2017 for review). These studies also support the theory that ATP depletion existed in migraine patients with aura due to deficient mitochondrial metabolism (Sarchielli et al., 2005). Figure 5.1 shows the relationship between repeated migraine attacks and mitochondrial functioning, compromising the cell’s ability to create ATP (Fila et al., 2019).

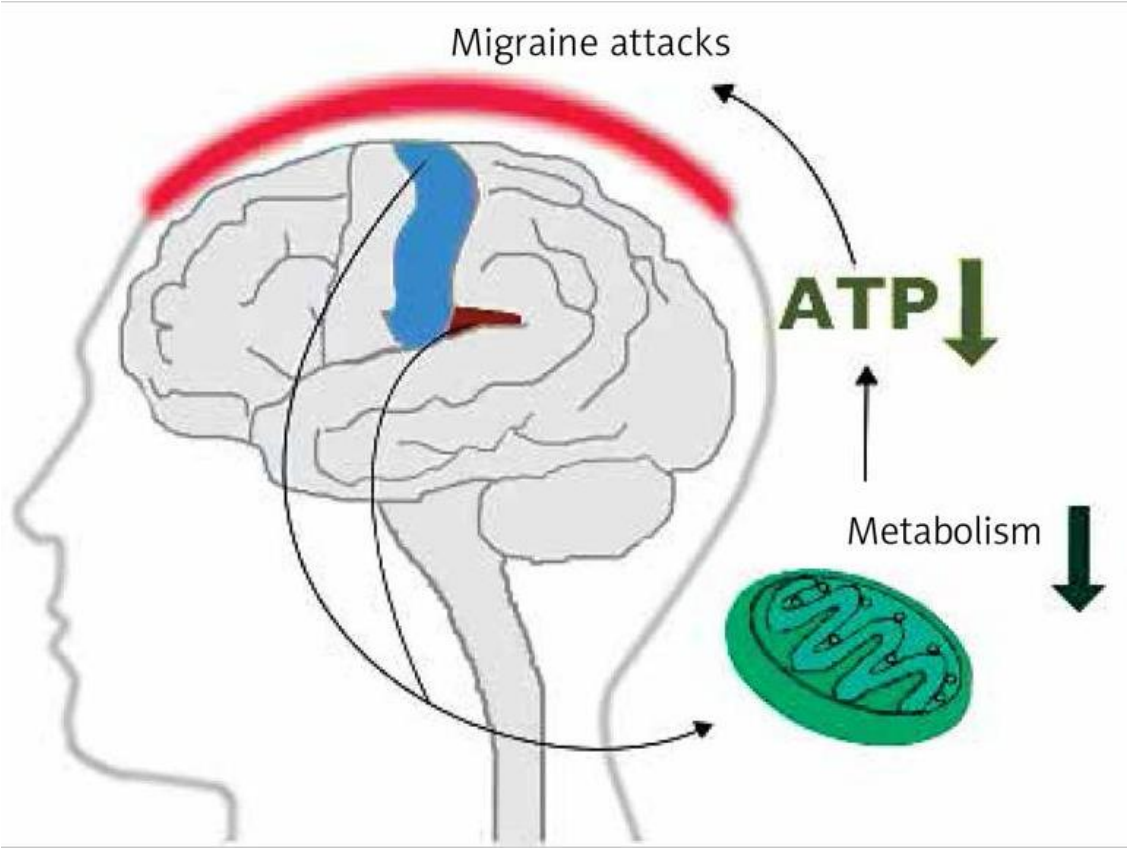

Figure 5-1. Migraine attacks and their effect on mitochondrial functioning and ATP generation. Repeated migraine attacks cause a modification of metabolic functioning in the primary somatosensory (blue) and secondary (brown) somatosensory cortices. This results in impaired mitochondrial functioning, affecting the ability to produce ATP (taken from Fila et al., 2019).

It seems plausible that the biological explanation instead of the electrophysiological explanation better explains the underlying causes of VS at the cellular level. Until now, we have discussed and analysed how PG gives rise to VS as a response to specific medium stimuli (3 c/deg), as a conceptual understanding at the electrophysiological level. We reported on EEG in the time and frequency domains and have shown how cortical hyperexcitability, the aspect of prediction (surprise), and oscillatory responses from the occipital lobe are responding at an

aggregate level to the PG stimulus. However, a system of energy demands at the cellular and metabolic level underpins the electrophysiological migraine response in the brain. It seems that there is a dysfunction in energy generation and/or an increased energy demand that underlies the entire process that is ultimately manifesting in migraine and, more severely in some people, epilepsy. We return to this concept in detail shortly.

5.7.3 Oxidation Stress in Migraine

It is the case that, due to technical limitations, reduced nicotinamide adenine dinucleotide (NADH) cannot be studied directly. Nevertheless, this can be inferred through in-vivo studies of (Cortical Spreading Depression) CSD, which physiologically underpins migraine. The threshold for CSD is lowered by migraine triggers and increased by migraine medications (Harriot et al., 2019). Additionally, because CSD activates the trigeminovascular system, it is used as a model for studying migraines (Harriot et al., 2019). Some studies have also shown that CSD is a substrate of visual aura (Leao, 1944; Smith et al., 2006). In CSD phases, increased energy demands can be observed due to the stripping of oxygen in the system (Takano et al., 2007). This energy-deficiency between migraine attacks or inadequate energy production may cause oxidation stress and trigger a migraine attack. Oxidant-sensing switches in the body trigger this homeostatic response. This occurs when brain energy is insufficient and leads to oxidative stress (an imbalance between free radicals and antioxidants in the body), leading to cell and tissue damage (Borkum, 2021). It follows then that the brain may use migraines as a defensive mechanism as it enforces rest and withdrawal from a sensory environment and reduces processing demands (Montagna et al., 2010), reducing the likelihood of cell and tissue damage. Borkum (2021) states that energy deficiency is caused by increased energy demand. Even so, not everyone withdraws from sensory and information processing demands. A hyperexcitable brain

or mitochondrial impairment will ultimately lead to oxidative stress. It is a typical feature in cellular metabolism. While Borkum (2021) describes a hyperexcitable brain, our investigation was limited to the excitability and habituation of the occipital lobe, albeit we did report on the theta effect (which is not an occipital effect).

5.7.4 Could Energy Deficiency Demands Explain our Findings?

Throughout the previous three sections, we have discussed two systems that could underlie the electrophysiological migraine results of our analysis (see Figure 5.2, System A and System B). It seems plausible that the sort of excitation we observe in the gamma band for onsets 2:8 could initiate a cascade of metabolic processes that lead to migraine, as described in System A. It could be the case that the PG stimulus is eliciting a hyperexcitation in the gamma band. When a neuron is hyperexcitable, the threshold to fire is lower than normal, so the cell fires more easily. This increases metabolic demand in the occipital lobe, which results in an energy deficiency. This in turn, causes oxidative stress, which can lead to acute migraine attacks as a defensive mechanism. This would arise from the brain attempting to reduce incoming stimuli to prevent cell and tissue damage.

We do not have direct evidence for System B in our research results. However, if it were present, it would reverse the direction of causation associated with System A; that is, metabolic changes would induce energy deficiencies, which would, in turn, induce electrophysiological changes. This said, the key finding of our work and Adjamian's work is an *increase* in gamma. It seems unlikely that a deficiency of energy could increase the firing of excitatory neurons. This leaves the possibility of the energy-deficiency specifically impacting, and reducing the firing of, inhibitory interneurons. This could induce reduced inhibitory action on excitatory neurons, leading to increased gamma power. However, this explanation relies upon the hypothesis that

energy-deficiencies only act on inhibitory interneurons and not on excitatory neurons, which may be considered implausible.

A further possibility could be that the energy deficiency reduces the firing of both excitatory and inhibitory neurons. However, self-sustaining dynamics counter the effects of the energy deficiency specifically in the excitatory units. This could lead to increased gamma, because the impact of reduced inhibition outweighs the effect of energy depletion on the excitatory units. However, these hypotheses remain highly speculative at the moment.

As shown in the red arrows in figure 3, there is of course the further possibility that *both* systems are functioning and interacting.

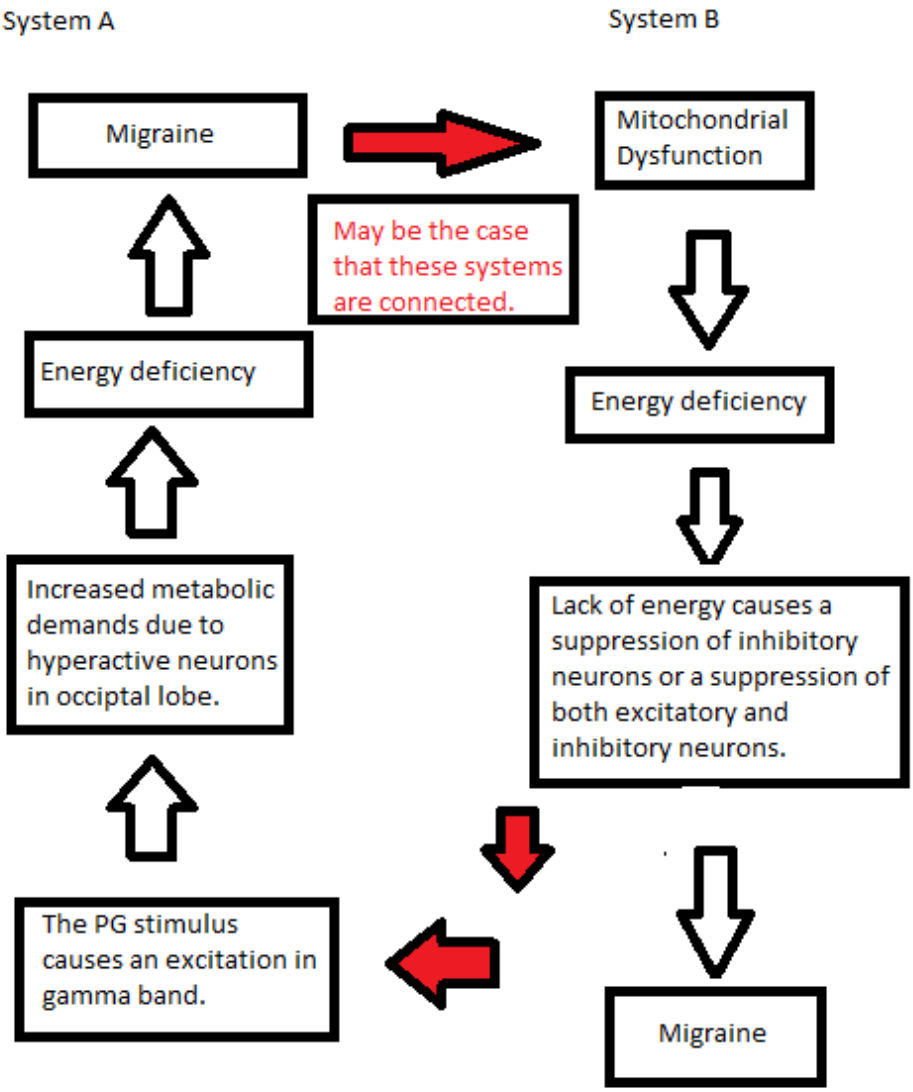

Figure 5-2. Hypothesis for Systems A and B.

The arrows show the relationship between the boxes indicated. This is a theory of what may explain our data and how it relates to the biological literature. The red-coloured arrows indicate where the connections would lie if system A and B are connected, and the no fill arrows specify system-specific influences.

5.8 Implications of This Research to Clinical Applications

Although the associated symptoms of VS do not exist in their severe manifestations in healthy controls, healthy participants still report perceptual illusions and distortions (Haung & Zhu, 2017;

Wilkins, 1995; Wilkins et al., 1984). The way in which these symptoms manifest is of interest. Often, when conducting research in specific populations, it is difficult to recruit at-risk populations, especially if they are clinical or vulnerable. Therefore, it is important to be absolutely certain about the specific focus of any investigation. Undertaking research on normal populations allows basic research to be done in order to help direct further research at the clinical/translational level. The results of the research reported in this thesis give clear indications regarding the focus required in a clinical population. Although the level of dysfunction in this normal population sample is insufficient to meet the criteria to label these participants migraineurs, the study does signpost specific aspects of the clinical brain that would be useful to investigate for comparison. For example, looking for the jittered P2 component in migraine patients may reveal a biomarker for migraine phenotype. This would be clinically useful and facilitate the development of better diagnostic tools.

5.9 Gamma Activity Mediating Perceptual Binding

Sensory systems are constantly given an influx of information that requires organization in a sensible way. During this process, the brain interprets sensory input as a neural representation of what we are seeing in the world in order for us to interact with it. Perceptual binding is the process of merging individual aspects of information into a perceptual representation (Livingstone & Hubel, 1988). One issue that arises in this literature is how these features are bound together (Treisman, 1996). It may be the case that gamma activity is mediating perceptual binding; some research in the past has supported this idea in the macaque visual cortex (Friedman-Hill et al., 1999; Maldando et al., 2000).

Based on what we observe in the gamma activity in our previous analysis Chapters 3 & 4 it may be the case that the participants are seeing the stationary stimulus as a moving stimulus. For example, the Enigma image (Figure 1.2) in Chapter one contains only static radial stripes and

purple disks but is widely reported to induce a sensation of motion within the rings in most people. It may be the case that the participant perceives the stimulus as moving; this may be caused by a dysfunction in gamma activity, which mediates the perceptual binding of the stimuli that is causing a misfiring of neurons in V1 to specifically clinically relevant patterns. Previous research, self-reports and our analysis of EEG and oscillatory responses indicate this may be occurring in the normal population. More research would be needed that explores the role of gamma in perceptual feature binding, in order to clarify this further.

Although not in gamma, a related finding in this thesis arises from the temporal jitter investigation of the theta feature in our time-frequency analysis, which we have argued corresponds to the P1-N1-P2 event related potential complex we observed in the time-domain. The increased temporal jitter (reduced inter-trial coherence, with little reduction in power) we observed for those high on the headache factor, may represent an electrophysiological correlate of the participant perceiving motion in the stimulus. That is, a perception of movement might vary the latency of the P2 component across trials. However, extrapolating this argument to perceptual binding would require us to also observe an effect on a factor of jitter in the gamma band. This awaits further analysis work.

5.10 Habituation of Evoked Potentials in Migraine

There are various neurophysiological studies that have explored migraine during and between attacks, revealing cortical hyperexcitability (see review by Schoenen, 1992). It is suggested that migraine causes insufficient habituation, affecting cortical information processing, which may affect the amplitude of average evoked potentials (Schoenen, 1996). Habituation has been seen to be a protective mechanism for protection against overstimulation and/or learning (Kandel, 1991). Although for a conclusive demonstration, we would need to see EEG responses change through onsets 2:8, our results in Chapter 2 may be argued to be suggestive of an

habituation effect. Specifically, we saw clear increases in the response in onsets 2:8 relative to onset 1, suggesting that there was a problem with habituation, which might be expected to reduce the EEG response across the 2:8 repetitions.

5.11 Other Variables

Although this thesis has acted to explore the role of PG stimuli, specifically, the clinically relevant, medium 3 c/deg stimulus and its effect on the occipital lobe, stimulus features other than pattern may affect the brain's response. For example, it has been observed that significant colour differences evoke greater visual discomfort and metabolic response; that greater alpha suppression occurs in response to the large colour difference; and finally, that these chrominance differences can drive hyperactivity in the cortex (Haigh et al., 2019). However, in our experiment, we used grey and black stimuli, so this does not affect our investigation.

Another variable that one might argue could explain the EEG effects we have observed is contrast sensitivity. Aldrich and colleagues (2019) showed that those with lateralized visual aura have heightened sensitivity in the visual field in which they see the aura. Additionally, Huang et al. (2003) linked reduced contrast sensitivity/discrimination to reduced BOLD response, which might suggest that increased contrast sensitivity could generate increased EEG responses. It may be the case that some of our participants who self-reported that they suffer from aura may have contrast sensitivity in the visual field that affected their EEG response to the stimuli; this would have affected the analysis. However, our key findings were on headache and discomfort, not on aura.

Additionally, it may be the case that the temporal jitter that we observed in Chapter 2 is due to nonuniformity in the hyperexcitability in the occipital lobe of different participants. Previous research has shown that hyperexcitability is unlikely to be uniform in patients with pattern-sensitive epilepsy (Wilkins et al., 1979). However, the inter-trial coherence measure, that

underlies out temporal jitter analysis, is looking at differences in phase coherence across trials. There is an averaging step across participants, but the basic measure is across trials. Consequently, across participant variation in hyperexcitability is not likely to confound our jitter findings.

5.11.1 The Appropriateness of Studying Gamma in EEG

It is essential to study scalp-EEG as it can contribute to the development of paradigms that allow neurophysiological function in humans to be investigated through a non-invasive measure. Additionally, being able to explore high frequencies enables more discriminating EEG measures to be identified. Several instances where EEG can be used are in etiological studies of patient cohorts, large-scale genetic studies, development, ageing, and understanding the neuropharmacological basis of high-frequency activity (Muthukumaraswamy, 2013). However, criticism has been levelled at the viability of the gamma frequencies (30-80hz), namely that the neural activity in gamma overlaps with the spectral bandwidth of muscle activity (20-300hz). Muscle activity may contaminate non-invasive high-frequency brain activity (Whitham et al., 2007).

However, we do not believe that our high-frequency findings were contaminated by muscle activity. We used many techniques during pre-processing to lower the number of artefacts in our data; specifically, we conducted an ICA in which eye-blink artefacts and other components that could be identified as muscle artefacts were removed. The EEG data were then recompiled. An additional method that was utilised was threshold rejection of -100 and +100μv, which is used to control for muscle artefacts. Finally, electromyographic activity demonstrates considerable spectral variability in terms of amplitude, peak frequency, and bandwidth, which is dependent on factors such as muscle strength, muscles used and sex (Kumar et al., 2003; Muthukumaraswamy, 2013). Such variability in activity will in theory be averaged out when computing the ERPs from

the EEG data because one tenet of ERP theory is that signal is consistent while noise is random, meaning that the noise should theoretically average out to zero. However, the number of participants needed to be sure that noise is sufficiently suppressed is not known for particular experimental paradigms and could be high. Fortunately though, there is a further and particularly strong reason for believing our effects are driven by signal: research by Adjamian et al. (2004) showed that gamma activity in the primary visual cortex is associated with the spatial frequency (SF) of the stimulus and visual discomfort. Critically, Adjamian et al. were using MEG, rather than EEG, which is typically argued to have a higher signal-to-noise ratio for high frequencies. Their findings were completely consistent with the gamma results that we observed. This is strong evidence that the gamma activity we are observing is signal and not noise.

5.11.2 Contrast Sensitivity Function (CSF) as a possible explanation?

The strong gamma activity seen in Adjamian et al's (2004) work may have indicated a relationship to the CSF, which also peaks at 3 (c/deg). However, this does not seem to be the case, and even if so, this alone would not rule out a link to VS. This can be observed in Figure 5.3.

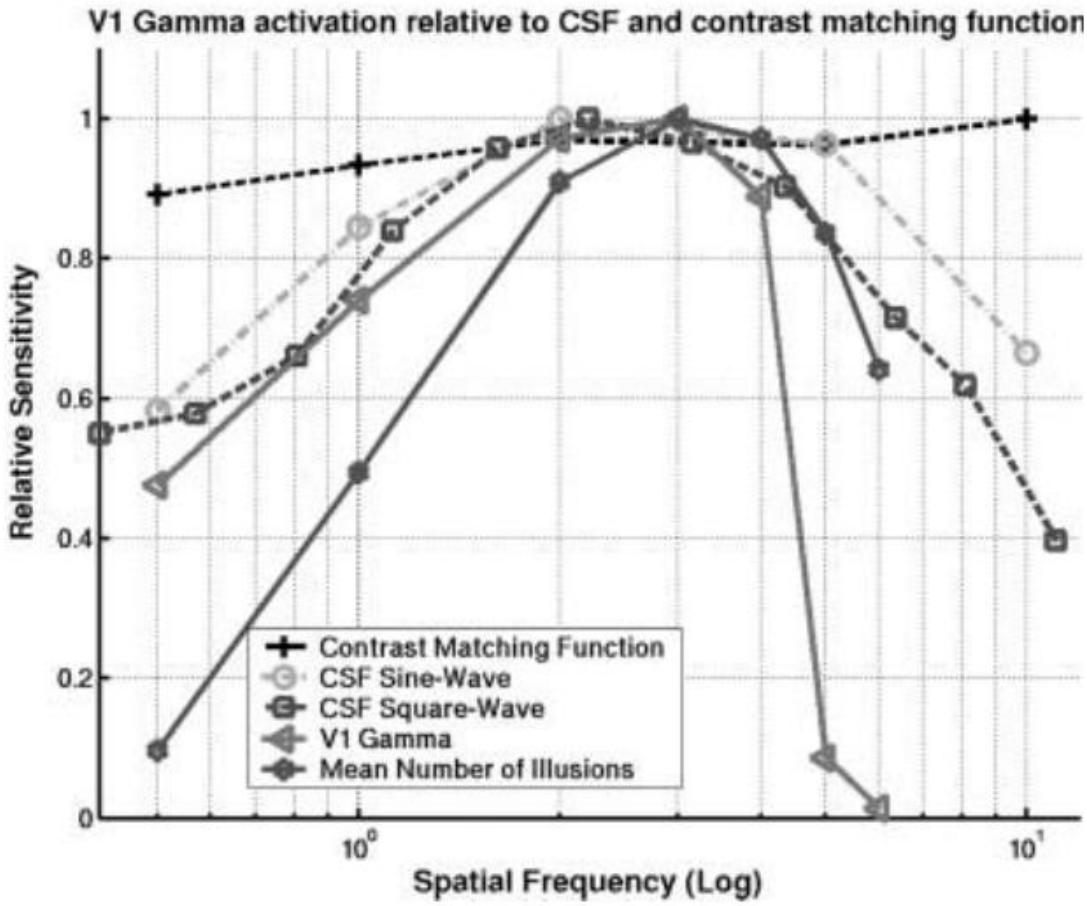

Figure 5-3.The CSF in relation to spatial frequency.

'Five sensitivity functions (normalized to maximum). CSF using square-wave gratings (Campbell & Robson, 1968). CSF using sine-wave gratings, and the contrast matching function (Georgeson & Sullivan 1975); V1 Gamma activity; and mean number of illusions and discomfort is also shown (Taken from Adjamian et al., 2004).'

The power of gamma falls of much more steeply with increased spatial frequency than does the CSF. Further Adjamian's stimulus (and indeed our own) had much higher contrast than the threshold level stimuli used to measure the CSF. Thus if the CSF were determining gamma oscillations, gamma power should remain high beyond 5c/deg whereas in fact is in near zero at this point. It seems unlikely then that the CSF is the main driver of our observed gamma effect

with the 3 (c/deg) stimuli in either Adjamian et al's (2004) work or our own. It seems likely that this effect is more driven by cortical hyperexcitability than any other explanation.

5.12 Limitations of Work

As we did not use clinical populations, we cannot generalize the findings in this thesis to a clinical group. As stated previously, we might also expect that we would find more significant effects in a clinical group compared to controls. Further experiments would therefore benefit from having access to a patient group.

An additional limitation is that, as previously discussed, for PGI (See Chapter 4), we have not linked the anterior theta effect we observe with the posterior gamma effect. For example, we have not performed a cross-frequency coupling analysis, so we do not know how or if they relate. This leaves the possibility that they are casually unrelated phenomena.

Identifying habituation by comparing effects on onset 1 to onset 2:8 is not definitive; in particular, onset 1 has less statistical power than onset 2:8, since it includes fewer trials per participant. Thus, it could be the case that we observe PGI effects in onset 2:8, but not onset 1, simply because onset 1 has less statistical power. We cannot rule out this possibility altogether, but it is notable that we do observe large effects for onset 1 for the aggregated analysis within the frequency domain (Chapters 3 and 4). We also observe effects on onset 1 in the time-domain (see Chapter 2). Thus, it seems that there is sufficient statistical power to observe robust effects for onset 1, if they are present.

EEG inherently has limitations, as they are recordings from the scalp impeded by bone, meaning that some of the signals are lost. It would be advantageous to do intracranial electrode recordings (iEEG) and analyse that data; however, this is difficult as the NHS ethics are quite complex, and iEEG is challenging to get approval for as it is typically performed during neurosurgery and in an at-risk population, such as patients with severe epilepsy.

5.13 Further Research

Further research could involve a more extended time baseline period. This would allow the researcher to use a longer wavelet and observe lower frequencies without the current edge effects and broaden our findings' scope into even lower frequencies. It might be informative also to break the data into onsets throughout the trial blocks. It would be good to know if the habituation effect we see in onset 2:8 is a build-up effect, i.e., increasing from onsets 2-3, 4-5, and 6-7, although this might require more trials to obtain reliable effects and this would make the experiment very long.

It would be interesting for participants to keep headache diaries. Asking participants to keep headache diaries in the days prior to data collection might improve the reliability of reporting and, in migraineurs, help to identify their migraine phase. It would be valuable to collect data from different populations (individuals with epilepsy, those with dyslexia and other reading difficulties, individuals with autism, and migraineurs), with different imaging modalities, possibly MEG, because it would give higher resolution in source space and might help to establish links and differences between conditions. An exploration of the role of gamma in mediating perceptual binding may be useful in order to understand why the brain is observing the medium stimulus to be moving while it is a stationary stimulus.

Additionally, research in the neurobiological field would be useful as it seems that an energy demand caused by either an increase in metabolism or mitochondrial dysfunction in which not enough energy is produced in occipital, may be the underlying cause of the hyperexcitable response to PG stimuli resulting in VS, migraine and, in more severe cases, epilepsy. Research in modeling the CSD and in vivo research on animal brains or iEEG and single cell recording research may shed more light on the subject than this research project was able to, given the limitations of scalp EEG electrode recordings.

5.14 Conclusion

Overall, the results of the three analyses both support existing findings in this field and also reveal hitherto undiscovered effects. The theta effect in Chapter 4 and the headache and discomfort effects in Chapters 2 and 3, operating at different times in terms of stimulus presentation and on different components, are potentially important new discoveries. Additionally, by observing effects present for onset 2:8, but not onset 1, this thesis has provided supporting evidence that visual stress (and by extension, migraine, and perhaps epilepsy) is driven by a failure to habituate, with this failure observable in the time-domain (missing N1) and the frequency domain (theta and gamma effects). These findings add to the body of existing knowledge and ultimately may contribute to the further development of clinical interventions in this area.

LIST OF REFERENCES

Adjamian, P., Holliday, I. E., Barnes, G. R., Hillebrand, A., Hadjipapas, A., & Singh, K. D. (2004). Induced visual illusions and gamma oscillations in human primary visual cortex. *European Journal of Neuroscience*, *20*(2), 587-592.

Adjamian, P. (2014). The application of electro-and magneto-encephalography in tinnitus research–methods and interpretations. *Frontiers in neurology*, *5*, 228.

Aldrich, A., Hibbard, P., & Wilkins, A. (2019). Vision and hyper-responsiveness in migraine. *Vision*, *3*(4), 62.

Allen, M. (Ed.). (2017). *The SAGE encyclopedia of communication research methods*. Sage Publications.

Ambrosini, A., & Schoenen, J. (2006). Electrophysiological response patterns of primary sensory cortices in migraine. *The journal of headache and pain*, *7*(6), 377-388.

Aurora, S. K., & Wilkinson, F. (2007). The brain is hyperexcitable in migraine. *Cephalagia*, *27*(12), 1442-1453.

Atkinson Jr, A. J., Colburn, W. A., DeGruttola, V. G., DeMets, D. L., Downing, G. J., ... & Spilker, B. A. (2001). Biomarkers and surrogate endpoints: preferred definitions and conceptual framework. *Clinical pharmacology & therapeutics*, *69*(3), 89-95.

Badawy, R. A., Loetscher, T., Macdonell, R. A., & Brodtmann, A. (2012). Cortical excitability and neurology: insights into the pathophysiology. *Functional neurology*, *27*(3), 131.

Bar, M. (2009). Predictions: a universal principle in the operation of the human brain.

Bauer, E. P., Paz, R., & Paré, D. (2007). Gamma oscillations coordinate amygdalo-rhinal interactions during learning. *Journal of Neuroscience*, *27*(35), 9369-9379.

Berger, H. (1929). Über das elektrenkephalogram des menschen. *Archiv für psychiatrie und nervenkrankheiten*, *87*(1), 527-570.

Bickford, R. G., Daly, D., & Keith, H. M. (1953). Convulsive effects of light stimulation in children. *AMA American journal of diseases of children*, *86*(2), 170-183.

Bickford, R. G., & Klass, D. W. (1964). Eye movement and the electroencephalogram. *The oculomotor system*, 293-302.

Bickford, R. G., Klass, D. W., Jasper, H. H., Ward, A. A., & Pope, A. (1969). Basic mechanisms of the epilepsies. *Little, Brown, Boston*, 543-564.

Bjørk, M. H., Stovner, L. J., Nilsen, B. M., Stjern, M., Hagen, K., & Sand, T. (2009). The occipital alpha rhythm related to the "migraine cycle" and headache burden: a blinded, controlled longitudinal study. *Clinical neurophysiology*, *120*(3), 464-471.

Braithwaite, J. J., Broglia, E., Bagshaw, A. P., & Wilkins, A. J. (2013). Evidence for elevated cortical hyperexcitability and its association with out-of-body experiences in the nonclinical population: new findings from a pattern-glare task. *Cortex*, *49*(3), 793-805. 445.

Brodal, P. (2004). *The central nervous system: structure and function*. Oxford University Press.

Bryson, S. E., Clark, B. S., & Smith, I. M. (1988). First report of a Canadian epidemiological study of autistic syndromes. *Journal of Child Psychology and Psychiatry*, *29*(4), 433-

Carlson, N. R. (2007). Physiology of behavior. 9th. *Needham Heights, MA: Paramount Publishing*, *88*, 91.

Campbell FW, Robson JG. Application of Fourier analysis to the visibility of gratings. Journal of Physiology. 1968;197:551-66.

Cialdella, P., & Mamelle, N. (1989). An Epidemiological Study of Infantile Autism in a French Department (Rhône): Research Note. *Journal of Child Psychology and Psychiatry*, *30*(1), 165-175.

Clarke, C. E., MacMillan, L., Sondhi, S., & Wells, N. E. (1996). Economic and social impact of migraine. *Qjm*, *89*(1), 77-84.

Clifford, C.W.G., Wenderoth, P., & Spehar, B. (2000). Proceedings of the Royal Society of London B, 267, 1705-1710.

Conlon, E. (2000). Visual perceptual problems in reading: Their relationship to reading disability and neural processing. In *6th Irlen International Conference, Australia*.

Cornelissen, P., Richardson, A., Mason, A., Fowler, S., & Stein, J. (1995). Contrast sensitivity and coherent motion detection measured at photopic luminance levels in dyslexics and controls. *Vision research*, *35*(10), 1483-1494.

Coulombe, S., Tremblay, J. F., & Marchand, S. (2004). International Adult Literacy Survey. Literacy Scores Human Capital and Growth Across, 14.

Coutts, L. V., Cooper, C. E., Elwell, C. E., & Wilkins, A. J. (2012). Time course of the hemodynamic response to visual stimulation in migraine, measured using near-infrared spectroscopy. *Cephalalgia*, *32*(8), 621-629.

Den Ouden, H. E., Kok, P., & De Lange, F. P. (2012). How prediction errors shape perception, attention, and motivation. *Frontiers in psychology*, *3*, 548.

Deykin, E. Y., & MacMahon, B. (1979). The incidence of seizures among children with autistic symptoms. *The American journal of psychiatry*.

Dugué, L., Marque, P., & VanRullen, R. (2011). The phase of ongoing oscillations mediates the causal relation between brain excitation and visual perception. *Journal of Neuroscience*, *31*(33), 11889-11893.

Evans, B. J., Busby, A., Jeanes, R., & Wilkins, A. J. (1995). Optometric correlates of Meares–Irlen syndrome: a matched group study. *Ophthalmic and Physiological Optics*, *15*(5), 481-487.

Evans, B. J., Drasdo, N., & Richards, I. L. (1996). Dyslexia: the link with visual deficits. *Ophthalmic and Physiological Optics*, *16*(1), 3-10.

Evans, B. (2001). *Dyslexia and vision* (Vol. 5). Wiley.

Evers, S., Quibeldey, F., Grotemeyer, K. H., Suhr, B., & Husstedt, I. W. (1999). Dynamic changes of cognitive habituation and serotonin metabolism during the migraine interval. *Cephalalgia*, *19*(5), 485-491.

Field, D.J., Hayes, A., & Hess, R.F. (1993). Contour integration by the human visual system: evidence for a local "association field", Vision Research, 33, 173-193

Fila, M., Pawłowska, E., & Blasiak, J. (2019). Mitochondria in migraine pathophysiology–does epigenetics play a role? *Archives of medical science: AMS*, *15*(4), 944.

Friedman-Hill, S., Maldonado, P. E., & Gray, C. M. (1999). Temporal dynamics of neuronal activity in the striate cortex of alert macaque: I. Incidence and stimulus-dependence of oscillations. *J. Neuroscience.*

Fries, P., Reynolds, J. H., Rorie, A. E., & Desimone, R. (2001). Modulation of oscillatory neuronal synchronization by selective visual attention. *Science*, *291*(5508), 1560-1563.

Friston, K. (2005). A theory of cortical responses. *Philosophical transactions of the Royal Society B: Biological sciences*, *360*(1456), 815-836.

Frith, U. (2003). Autism: Explaining the enigma. *Blackwell Publishing.*

Gasparini, C. F., & Griffiths, L. R. (2013). The biology of the glutamatergic system and potential role in migraine. International journal of biomedical science: IJBS, 9(1), 1.

Gastaut, H., Tassinari, C. A., & Duron, B. (1966). Polygraphic study of the episodic diurnal and nocturnal (hypnic and respiratory) manifestations of the Pickwick syndrome. *Brain research*, *1*(2), 167-186.

Georgeson, M.A. & Sullivan, G.D. (1975) Contrast constancy: deblurring in human vision by spatial frequency channels. J. Physiol. (Lond.), 252, 627– 656.

Gerrard, P., & Malcolm, R. (2007). Mechanisms of modafinil: a review of current research. *Neuropsychiatric disease and treatment*, *3*(3), 349.

Goldberg, L. D. (2005). The cost of migraine and its treatment. *The American journal of managed care*, *11*(2 Suppl), S62-7.

Gough, P. B., & Tunmer, W.E. (1986). Decoding, reading, and reading disability. *Remedial and Special Education*, *7*, 6-10.

Hanslmayr, S., Aslan, A., Staudigl, T., Klimesch, W., Herrmann, C. S., & Bäuml, K. H. (2007). Prestimulus oscillations predict visual perception performance between and within subjects. *Neuroimage*, *37*(4), 1465-1473.

Haigh, S. M., Karanovic, O., Wilkinson, F., & Wilkins, A. J. (2012). Cortical hyperexcitability in migraine and aversion to patterns. *Cephalalgia*, *32*(3), 236-240.

Haigh, S. M., Cooper, N. R., & Wilkins, A. J. (2015). Cortical excitability and the shape of the haemodynamic response. *Neuroimage*, *111*, 379-384.

Haigh, S.M., Chamanzar, A., Grover, P. and Behrmann, M., 2019. Cortical Hyper-Excitability in Migraine in Response to Chromatic Patterns. *Headache: The Journal of Head and Face Pain*, *59*(10), pp.1773-1787.

Harriott, A. M., Takizawa, T., Chung, D. Y., & Chen, S. P. (2019). Spreading depression as a preclinical model of migraine. *The journal of headache and pain*, *20*(1), 1-12.

Hawkins, J., & Blakeslee, S. (2004). *On intelligence*. Macmillan.

House of Commons, (2010), Headache Disorders – not respected, not resourced. All-Party Parliamentary Group on Primary Headache Disorders.

House of Commons, (2014). Headache Services in England. All-Party Parliamentary Group on Primary Headache Disorders.

Huang, J., Cooper, T. G., Satana, B., Kaufman, D. I., & Cao, Y. (2003). Visual distortion provoked by a stimulus in migraine associated with hyperneuronal activity. *Headache: The Journal of Head and Face Pain*, *43*(6), 664-671.

Huang, J., Zong, X., Wilkins, A., Jenkins, B., Bozoki, A., & Cao, Y. (2011). fMRI evidence that precision ophthalmic tints reduce cortical hyperactivation in migraine. *Cephalalgia*, 31(8), 925-936.

Huang, J., & Zhu, D. C. (2017). Visually stressful striped patterns alter human visual cortical functional connectivity. *Human brain mapping*, *38*(11), 5474-5484.

Hutcheon, B., & Yarom, Y. (2000). Resonance, oscillation and the intrinsic frequency preferences of neurons. *Trends in neurosciences*, *23*(5), 216-222.

Hughes, J. R. (1964). Responses from the Visual Cortex of Unanesthetized Monkeys1. In *International review of neurobiology* (Vol. 7, pp. 99-152). Academic Press.

Irlen, H. (1983, August). Successful treatment of learning disabilities. In *91st annual Convention of the American Psychological Association, Anaheim, CA, USA*.

Irlen, H. (1991). Reading by the colours. *New York: Avery*.

Irlen, H. (1994). Scotopic sensitivity/Irlen syndrome: Hypothesis and explanation of the syndrome. *Journal of Behavioral Optometry*, *5*(62), 65-66.

Irlen, H. (1997). Reading problems and Irlen coloured lenses. *Dyslexia review*, *8*, 4-7.

Iwamoto, S., Tamura, M., Sasaki, A., & Nawano, M. (2021). Dynamics of neuronal oscillations underlying nociceptive response in the mouse primary somatosensory cortex. *Scientific reports*, *11*(1), 1-12.

James, S. L., Abate, D., Abate, K. H., Abay, S. M., Abbafati, C., Abbasi, N., ... & Briggs, A. M. (2018). Global, regional, and national incidence, prevalence, and years lived with disability for 354 diseases and injuries for 195 countries and territories, 1990–2017: a systematic analysis for the Global Burden of Disease Study 2017. *The Lancet*, *392*(10159), 1789-1858.

Jensen, O., Gips, B., Bergmann, T. O., & Bonnefond, M. (2014). Temporal coding organized by coupled alpha and gamma oscillations prioritize visual processing. *Trends in neurosciences*, *37*(7), 357-369.

Kafaligonul, H., Breitmeyer, B. G., & Öğmen, H. (2015). Feedforward and feedback processes in vision. *Frontiers in psychology*, *6*.

Kandel, E. R. (1991). Cellular mechanisms of learning and the biological basis of individuality. *Principles of neural science*, *3*, 1009-1031. Kandel, E. R. (1991). Cellular mechanisms of learning and the biological basis of individuality. *Principles of neural science*, *3*, 1009-1031.

Kraya, T., Deschauer, M., Joshi, P. R., Zierz, S., & Gaul, C. (2018). Prevalence of headache in patients with mitochondrial disease: a cross-sectional study. *Headache: The Journal of Head and Face Pain*, *58*(1), 45-52.

Kientz, M. A., & Dunn, W. (1997). A comparison of the performance of children with and without autism on the Sensory Profile. *American Journal of Occupational Therapy*, *51*(7), 530-537.

Klimesch, W. (1996). Memory processes, brain oscillations and EEG synchronization. *International journal of psychophysiology*, *24*(1-2), 61-100.

Klimesch, W., Sauseng, P., & Hanslmayr, S. (2007). EEG alpha oscillations: the inhibition–timing hypothesis. *Brain research reviews*, *53*(1), 63-88.

Kohn, A., & Movshon, J. A. (2003). Neuronal adaptation to visual motion in area MT of the macaque. *Neuron*, *39*(4), 681-691.

Kumar, S., Narayan, Y., & Amell, T. (2003). Power spectra of sternocleidomastoids, splenius capitis, and upper trapezius in oblique exertions. *The Spine Journal*, *3*(5), 339-350.

Lamme, V. A., Super, H., & Spekreijse, H. (1998). Feedforward, horizontal, and feedback processing in the visual cortex. *Current opinion in neurobiology*, *8*(4), 529-535.

Leao, A. A. (1944). Spreading depression of activity in the cerebral cortex. *Journal of neurophysiology*, *7*(6), 359-390.

Leviant I., (1981) Enigma.

Leviant, I. (1996). Does' brain-power' make Enigma spin?. *Proceedings of the Royal Society of London B: Biological Sciences*, *263*(1373), 997-1001.

Lehmkuhle, S., Garzia, R. P., Turner, L., Hash, T., & Baro, J. A. (1993). A defective visual pathway in children with reading disability. *New England Journal of Medicine*, *328*(14), 989-996.

Livingstone, M., & Hubel, D. (1988). Segregation of form, color, movement, and depth: anatomy, physiology, and perception. *Science*, *240*(4853), 740-749.

Livingstone, M. S., Rosen, G. D., Drislane, F. W., & Galaburda, A. M. (1991). Physiological and anatomical evidence for a magnocellular defect in developmental dyslexia. *Proceedings of the National Academy of Sciences*, *88*(18), 7943-7947.

Llinás, R. R. (1988). The intrinsic electrophysiological properties of mammalian neurons: insights into central nervous system function. *Science*, *242*(4886), 1654-1664.

Logothetis, N. K., Pauls, J., Augath, M., Trinath, T., & Oeltermann, A. (2001). Neurophysiological investigation of the basis of the fMRI signal. *Nature*, *412*(6843), 150.

Lovegrove, W. (1991). Spatial frequency processing in dyslexic and normal readers. *Vision and visual dysfunction: vision and visual dyslexia*, *13*, 148-153.

Lovegrove, W., Martin, F., & Slaghuis, W. (1986). A theoretical and experimental case for a visual deficit in specific reading disability. *Cognitive Neuropsychology*, *3*(2), 225-267.

Luck, S. J. (2005). An introduction to event related potentials and their neural origins. *An introduction to the event related potential technique*, *11*.

Ludlow, A. K., Wilkins, A. J., & Heaton, P. (2006). The effect of coloured overlays on reading ability in children with autism. *Journal of Autism and Developmental Disorders*, *36*(4), 507-516.

Maclachlan, A., Yale, S., & Wilkins, A. (1993). Open trial of subjective precision tinting: a follow-up of 55 patients. *Ophthalmic and Physiological Optics*, *13*(2), 175-178.

Maldonado, P. E., Friedman-Hill, S. R., & Gray, C. M. (1999). Temporal dynamics of neuronal activity in the striate cortex of alert macaque: II. Short and long-range temporally-correlated activity. *J. Neurosci.*

Mears, O. (1980). Figure/background brightness/contrast and reading disability. *Visible Language*, *15*, 13-29.

Meyer, Y., & Flandrin, P. (1999). Time-Frequency/Time-Scale Analysis. *Wavelet Analysis and its applications*.

Millichap, J. G., Bickford, R. G., Klass, D. W., & Backus, R. E. (1962). Infantile spasms, hypsarhythmia, and mental retardation. A study of etiologic factors in 61 patients. *Epilepsia*, *3*(2), 188-197.

Mitchell, D. (2014). *What really works in special and inclusive education: Using evidence-based teaching strategies*. Routledge.

Monger, L. J., Wilkins, A. J., & Allen, P. M. (2015). Pattern glare: the effects of contrast and color. *Frontiers in psychology*, *6*, 1651.

Monger, L., Allen, P., Evans, B., & Wilkins, A. (2016). Pattern Glare. Optician Select, 9(145695-1).

Montagna, P., Pierangeli, G., & Cortelli, P. (2010). The primary headaches as a reflection of genetic darwinian adaptive behavioral responses. *Headache: The Journal of Head and Face Pain*, *50*(2), 273-289.

Mulleners, W. M., Chronicle, E. P., Palmer, J. E., Koehler, P. J., & Vredeveld, J. W. (2001). Suppression of perception in migraine evidence for reduced inhibition in the visual cortex. *Neurology*, *56*(2), 178-183.

Muthukumaraswamy, S. D., Evans, C. J., Edden, R. A., Wise, R. G., & Singh, K. D. (2012). Individual variability in the shape and amplitude of the BOLD-HRF correlates with endogenous GABAergic inhibition. *Human brain mapping*, *33*(2), 455-465.

Muthukumaraswamy, S. (2013). High-frequency brain activity and muscle artifacts in MEG/EEG: a review and recommendations. *Frontiers in human neuroscience*, *7*, 138.

Nakayama, K., He, Z. J., & Shimojo, S. (1995). Visual surface representation: A critical link between lower-level and higher-level vision. *Visual cognition: An invitation to cognitive science* (*2)*, 1-70.

Naudé, W. A. (2004). The effects of policy, institutions and geography on economic growth in Africa: an econometric study based on cross-section and panel data. *Journal of International Development*, *16*(6), 821-849.

Nyrke, T., Kangasniemi, P., & Lang, H. (1990). Alpha rhythm in classical migraine (migraine with aura): abnormalities in the headache-free interval. *Cephalalgia*, *10*(4), 177-181.

Olesen, J., Gustavsson, A., Svensson, M., Wittchen, H. U., Jönsson, B., CDBE2010 Study Group, & European Brain Council. (2012). The economic cost of brain disorders in Europe. *European journal of neurology*, *19*(1), 155-162.

Olman, C. A., Ugurbil, K., Schrater, P., & Kersten, D. (2004). BOLD fMRI and psychophysical measurements of contrast response to broadband images. *Vision research*, *44*(7), 669-683.

Ornitz, E. M. (1973). Childhood autism—A review of the clinical and experimental literature. *California Medicine*, *118*(4), 21.

Ottman, R., & Lipton, R. B. (1994). Comorbidity of migraine and epilepsy. *Neurology*, *44*(11), 2105-2105.

O'Hare, L., Menchinelli, F., & Durrant, S. J. (2018). Resting-State Alpha-Band Oscillations in Migraine. *Perception*, *47*(4), 379-396.

Palva, S., & Palva, J. M. (2007). New vistas for α-frequency band oscillations. *Trends in neurosciences*, *30*(4), 150-158.

Perfetti, C. A. (1985). *Reading ability*. New York, NY: Oxford University Press.

Pfurtscheller, G. (2001). Functional brain imaging based on ERD/ERS. *Vision research*, *41*(10-11), 1257-1260.

Pfurtscheller, G. (2003). Induced oscillations in the alpha band: functional meaning. *Epilepsia*, *44*, 2-8.

Ray, W. J., & Cole, H. W. (1985). EEG alpha activity reflects attentional demands, and beta activity reflects emotional and cognitive processes. *Science*, *228*(4700), 750-752.

Ramus, F., Rosen, S., Dakin, S. C., Day, B. L., Castellote, J. M., White, S., & Frith, U. (2003). Theories of developmental dyslexia: insights from a multiple case study of dyslexic adults. *Brain*, *126*(4), 841-865.

Rees, T., Tempesta., A., Bowman., H., (2020). Visually evoked DC shifts? An investigative study into the electrophysiology of visual stress, *University of Birmingham,* Unpublished.

Ren, J., Xiang, J., Chen, Y., Li, F., Wu, T., & Shi, J. (2019). Abnormal functional connectivity under somatosensory stimulation in migraine: a multi-frequency magnetoencephalography study. *The journal of headache and pain*, *20*(1), 1-10.

Reyngoudt H, Achten E, Paemeleire K (2012) Magnetic resonance spectroscopy in migraine: what have we learned so far? *Cephalalgia 32*:845–859 28.

Robinson, D. A. (1992). Implications of neural networks for how we think about brain function. *Medicine, Baltimore*, *1500*, 21287.

Russo, A., Silvestro, M., Tedeschi, G., & Tessitore, A. (2017). Physiopathology of migraine: what have we learned from functional imaging?. *Current neurology and neuroscience reports*, *17*(12), 1-11.

Rutter, M. (1970, November). Autistic children: infancy to adulthood. In *Seminars in psychiatry* (Vol. 2, No. 4, p. 435).

Sarchielli, P., Tarducci, R., Presciutti, O., Gobbi, G., Pelliccioli, G. P., Stipa, G., ... & Capocchi, G. (2005). Functional 1H-MRS findings in migraine patients with and without aura assessed interictally. *Neuroimage*, *24*(4), 1025-1031.

Schoenen, J. (1992). Clinical neurophysiology studies in headache: a review of data and pathophysiological hints. *Functional neurology*, *7*(3), 191-204.

Schoenen, J. (1996). Deficient habituation of evoked cortical potentials in migraine: a link between brain biology, behavior and trigeminovascular activation?. *Biomedicine & pharmacotherapy*, *50*(2), 71-78.

Semyanov, A., Walker, M. C., & Kullmann, D. M. (2003). GABA uptake regulates cortical excitability via cell type–specific tonic inhibition. *Nature neuroscience*, *6*(5), 484.

Shapiro, R. E., & Goadsby, P. J. (2007). The long drought: the dearth of public funding for headache research.

Shepherd, A. J. (2005). Colour vision in migraine: selective deficits for S-cone discriminations. *Cephalalgia*, *25*(6), 412-423.

Singleton, C., & Trotter, S. (2005). Visual stress in adults with and without dyslexia. *Journal of Research in Reading*, *28*(3), 365-378.

Skalicky, S. E. (2016). The Lateral Geniculate Nucleus. In *Ocular and Visual Physiology* (pp. 201-206). Springer, Singapore.

Smith, J. M., Bradley, D. P., James, M. F., & Huang, C. L. H. (2006). Physiological studies of cortical spreading depression. *Biological Reviews*, *81*(4), 457-481.

Snowling, M. J. (2000). *Dyslexia.* Oxford: Blackwell.

Solman, R. T., Cho, H. S., & Daint, S. J. (1991). Colour-mediated grouping effects in good and disabled readers. *Ophthalmic and Physiological Optics*, *11*(4), 320-327.

Solman, R. T., Dain, S. J., Lim, H. S., & May, J. G. (1995). Reading-related wavelength and spatial frequency effects in visual spatial location. *Ophthalmic and Physiological Optics*, *15*(2), 125-132.

Stanovich, K. E. (1991). Word recognition: Changing perspectives. In R. Barr, M.L. Kamil, P. Mosenthal, & P.D. Pearson (Eds.), New York: Longman. *Handbook of reading research* (2), 418-452.

Steffenburg, S., &Gillberg, C. (1986). Autism and autistic-like conditions in Swedish rural and urban areas: a population study. *The British Journal of Psychiatry*, *149*(1), 81-87.

Stein, J. (2001). The magnocellular theory of developmental dyslexia. *Dyslexia*, *7*(1), 12-36.

Stein, J., & Talcott, J. (1999). Impaired neuronal timing in developmental dyslexia—the magnocellular hypothesis. *Dyslexia*, *5*(2), 59-77.

Stein, J., & Walsh, V. (1997). To see but not to read; the magnocellular theory of dyslexia. *Trends in neurosciences*, *20*(4), 147-152.

Steiner, T. J., Scher, A. I., Stewart, W. F., Kolodner, K., Liberman, J., & Lipton, R. B. (2003). The prevalence and disability burden of adult migraine in England and their relationships to age, gender and ethnicity. *Cephalalgia*, *23*(7), 519-527.

Steiner TJ et al. Migraine: the seventh disabler. *The Journal of Headache and Pain 2013*, 14:1.

Steiner, T. J., Stovner, L. J., & Birbeck, G. L. (2013). Migraine: the seventh disabler. *Headache: The Journal of Head and Face Pain*, *53*(2), 227-229.

Stockman, A., & Sharpe, L. T. (2000). The spectral sensitivities of the middle-and long-wavelength-sensitive cones derived from measurements in observers of known genotype. *Vision research*, *40*(13), 1711-1737.

Stromquist, N. P. (2005). The Political Benefits of Adult Literacy. Paper Commissioned for the EFA Global Monitoring Report 2006, *Literacy for Life.*

Stovner, L. J., & Andrée, C. (2008). Impact of headache in Europe: a review for the Eurolight project. *The journal of headache and pain*, *9*(3), 139-146.

Sullivan, A., & Brown, M. (2013). Reading for pleasure puts children ahead in the classroom. *Institute of Education, London, UCL*.

Takano, T., Tian, G. F., Peng, W., Lou, N., Lovatt, D., Hansen, A. J., ... & Nedergaard, M. (2007). Cortical spreading depression causes and coincides with tissue hypoxia. *Nature neuroscience*, *10*(6), 754-762.

Tanoue, Y., Oda, S., Asano, F., & Kawashima, K. (1988). Epidemiology of infantile autism in southern Ibaraki, Japan: differences in prevalence in birth cohorts. *Journal of Autism and Developmental Disorders*, *18*(2), 155-166.

Tatum IV, W. O. (2014). *Handbook of EEG interpretation*. Demos Medical Publishing.

Tempesta, A. J., Miller, C. E., Litvak, V., Bowman, H., & Schofield, A. J. (2021). The Missing N1 or Jittered P2: Electrophysiological Correlates of Pattern-Glare in the Time and Frequency Domain. *European Journal of Neuroscience*.

Todorovic, A., van Ede, F., Maris, E., & de Lange, F. P. (2011). Prior expectation mediates neural adaptation to repeated sounds in the auditory cortex: an MEG study. *Journal of Neuroscience*, *31*(25), 9118-9123.

Treisman, A. (1996). The binding problem. *Current opinion in neurobiology*, *6*(2), 171-178.

Uhlhaas, P. J., & Singer, W. (2006). Neural synchrony in brain disorders: relevance for cognitive dysfunctions and pathophysiology. *neuron*, *52*(1), 155-168.

Van Hooff, J.C., Dietz, K.C., Sharma, D., & Bowman, H. (2008). Neural correlates of intrusion of emotion words in a modified Stroop task, *International Journal of Psychophysiology*, *67*, 23-34.

Van Gelder, N. M. (1987). Calcium mobility and glutamic acid release associated with EEG abnormalities, migraine and epilepsy. *Migraine and Epilepsy. Boston: Butterworths*, 367-378.

Vazquez, A. L., & Noll, D. C. (1998). Nonlinear aspects of the BOLD response in functional MRI. *Neuroimage, 7*(2), 108-118.

Vellutino, F.R. (1979). *Dyslexia: Theory and research*. Cambridge, MA: MIT Press.

Vellutino, F.R. (1987). *Dyslexia. Scientific American*, March, 1, 34-41.

Vellutino, F. R., Fletcher, J. M. Snowling, M. J. & Scanlon, D. M. (2004). Specific reading disability (dyslexia): what have we learned in the past four decades? *Journal of Child Psychology & Psychiatry, 45*(1), 2-40.

Vellutino, F. R., Scanlon, D. M., & Chen, R. (1995). The increasingly inextricable relationship between orthographic and phonological coding in learning to read: Some reservations about current methods of operationalizing orthographic coding. In V. Berninger (Ed.), *The varieties of orthographic knowledge II: Relationships to phonology reading, and writing* (pp.47-111). Dordrecht: The Netherlands.

Vellutino, F. R., Scanlon, D.M., Sipay, E. R., Small, S. G., Ptratt, A., Chen, R. S., & Denckla, M.B. (1996). Cognitive profiles of difficult to remediate and readily remediated poor readers: Early intervention as a vehicle for distinguishing between cognitive and experiential deficits as basic causes of specific reading disability. *Journal of Educational Psychology, 88,* 601-638.

Vellutino, F.R., Scanlon, D.M., & Tanzman, M. S. (1994). Components of reading ability: Issues and problems in operationalizing word identification, phonological coding, and orthographic coding. In G.R. Lyon (Ed.), Frames of reference for the assessment of learning disabilities: New views on measurement issues (pp. 279-324). Baltimore, MD: Paul H. Brooks.

Vidyasagar, T. R. (2004). Neural underpinnings of dyslexia as a disorder of visuo-spatial attention. *Clinical and Experimental Optometry*, *87*(1), 4-10.

Vollono, C., Primiano, G., Della Marca, G., Losurdo, A., & Servidei, S. (2018). Migraine in mitochondrial disorders: prevalence and characteristics. *Cephalalgia*, *38*(6), 1093-1106.

Wallace, D. J., Fitzpatrick, D., & Kerr, J. N. (2016). Primate thalamus: more than meets an eye. *Current Biology*, *26*(2), R60-R61.

Wagner, D., Manahilov, V., Loffler, G., Gordon, G. E., & Dutton, G. N. (2010). Visual noise selectively degrades vision in migraine. *Investigative ophthalmology & visual science*, *51*(4), 2294-2299.

Welch, K. M., D'andrea, G., Tepley, N., Barkley, G., & Ramadan, N. M. (1990). The concept of migraine as a state of central neuronal hyperexcitability. *Neurologic clinics*, *8*(4), 817-828.

White, B. B., & White, M. S. (1987). Autism from the inside. *Medical hypotheses*, *24*(3), 223-229.

Whitham, E. M., Pope, K. J., Fitzgibbon, S. P., Lewis, T., Clark, C. R., Loveless, S., ... & Willoughby, J. O. (2007). Scalp electrical recording during paralysis: quantitative evidence that EEG frequencies above 20 Hz are contaminated by EMG. *Clinical neurophysiology*, *118*(8), 1877-1888.

Wing, L., & Gould, J. (1979). Severe impairments of social interaction and associated abnormalities in children: Epidemiology and classification. *Journal of autism and development.*

Wilkins, A. J., Darby, C. E., & Binnie, C. D. (1979). Neurophysiological aspects of pattern-sensitive epilepsy. *Brain*, *102*(1), 1-25.

Wilkins, A., Nimmo-Smith, I. A. N., Tait, A., McMANUS, C., Sala, S. D., Tilley, A., ... & Scott, S. (1984). A neurological basis for visual discomfort. *Brain*, *107*(4), 989-1017.

Wilkins, A. (1986). Intermittent illumination from visual display units and fluorescent lighting affects movements of the eyes across text. *Human Factors*, *28*(1), 75-81.

Wilkins, A. J. (1995). *Visual stress* (No. 24). Oxford University Press.

Wilkins, A. J. (2003). Reading Through Colour: How Coloured Filters Can Reduce Reading Difficulty. *Eye Strain, and Headaches*.

Wilkins, A. (2016). A physiological basis for visual discomfort: Application in lighting design. *Lighting Research and Technology*.doi:10.1177/1477153515612526.

Wilkins, A.J., Binnie, C.D. (1980) Visually induced seizures *Prog. Neurobiol., 15*, 85-117.

Wilkins, A. J., Darby, C. E., & Binnie, C. D. (1979). Neurophysiological aspects of pattern-sensitive epilepsy. *Brain*, *102*(1), 1-25.

Wilkins, A. J., & Evans, B. J. W. (2001). Pattern glare test instructions. London, UK: IOO Sales Ltd.

Williams, M. C., LeCluyse, K., & Rock-Faucheux, A. (1992). Effective interventions for reading disability. *Journal of the American Optometric Association*.

Williams, D. (1998). *Like colour to the blind: Soul searching and soul finding*. Jessica Kingsley Publishers.

World Health Organization. (2016). Headache Disorders. Fact Sheet No 277 (2007).

Wright, J. J., Robinson, P. A., Rennie, C. J., Gordon, E., Bourke, P. D., Chapman, C. L., ... & Alexander, D. (2001). Toward an integrated continuum model of cerebral dynamics: the cerebral rhythms, synchronous oscillation and cortical stability. *Biosystems*, *63*(1-3), 71-88.

Wu, T., Fan, J., Chen, Y., Xiang, J., Zhu, D., Zhang, J., ... & Jiang, T. (2018). Interictal abnormalities of neuromagnetic gamma oscillations in migraine following negative emotional stimulation. *Frontiers in behavioral neuroscience*, *12*, 169.

Yang, W., Chu, B., Yang, J., Yu, Y., Wu, J., & Yu, S. (2014). Elevated audiovisual temporal interaction in patients with migraine without aura. *The journal of headache and pain*, *15*(1), 44.

Younis S, Hougaard A, Vestergaard MB, Larsson HBW, Ashina M (2017) Migraine and magnetic resonance spectroscopy: a systematic review. Curr Opin Neurol 30:246–262.

Zanker, J. M., & Walker, R. (2004). A new look at Op art: towards a simple explanation of illusory motion. *Naturwissenschaften*, *91*(4), 149-156.

Zeki, S., Watson, J. D. G., & Frackowiak, R. S. (1993). Going beyond the information given: the relation of illusory visual motion to brain activity. *Proceedings of the Royal Society of London B: Biological Sciences*, *252*(1335), 215-222.

Zeki, S. (1983). Colour coding in the cerebral cortex: the reaction of cells in monkey visual cortex to wavelengths and colours. Neuroscience, 9(4), 741-765.